

Winter 2003

Bedrock geology of the seacoast region of New Hampshire, United States

Jose Cruz Escamilla-Casas
University of New Hampshire, Durham

Follow this and additional works at: <https://scholars.unh.edu/dissertation>

Recommended Citation

Escamilla-Casas, Jose Cruz, "Bedrock geology of the seacoast region of New Hampshire, United States" (2003). *Doctoral Dissertations*. 190.
<https://scholars.unh.edu/dissertation/190>

This Dissertation is brought to you for free and open access by the Student Scholarship at University of New Hampshire Scholars' Repository. It has been accepted for inclusion in Doctoral Dissertations by an authorized administrator of University of New Hampshire Scholars' Repository. For more information, please contact nicole.hentz@unh.edu.

BEDROCK GEOLOGY OF THE SEACOAST REGION OF NEW HAMPSHIRE, U.S.A.

BY

JOSE CRUZ ESCAMILLA-CASAS

Ingeniero Geólogo

Universidad Autónoma de San Luis Potosí, S. L. P.

México, 1986

DISSERTATION

Submitted to the University of New Hampshire

in Partial Fulfillment of

the Requirements for the Degree of

Doctor of Philosophy

in

Earth Sciences - Geology

December, 2003

UMI Number: 3111503

INFORMATION TO USERS

The quality of this reproduction is dependent upon the quality of the copy submitted. Broken or indistinct print, colored or poor quality illustrations and photographs, print bleed-through, substandard margins, and improper alignment can adversely affect reproduction.

In the unlikely event that the author did not send a complete manuscript and there are missing pages, these will be noted. Also, if unauthorized copyright material had to be removed, a note will indicate the deletion.

UMI[®]

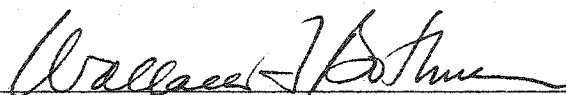
UMI Microform 3111503

Copyright 2004 by ProQuest Information and Learning Company.

All rights reserved. This microform edition is protected against unauthorized copying under Title 17, United States Code.

ProQuest Information and Learning Company
300 North Zeeb Road
P.O. Box 1346
Ann Arbor, MI 48106-1346

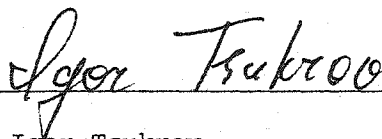
This dissertation has been examined and approved.



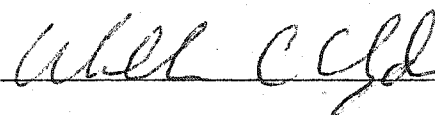
Dissertation Director, Dr. Wallace A. Bothner
Professor of Geology



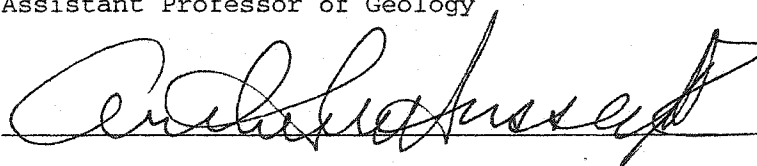
Dr. Jo Laird
Associate Professor of Geology



Dr. Igor Tsukrov
Associate Professor of Mechanical Engineering



Dr. William C. Clyde
Assistant Professor of Geology



Dr. Arthur M. Hussey II, Professor Emeritus of
Geology, Bowdoin College, Brunswick, Maine

December 3, 2003
Date

ACKNOWLEDGEMENTS

I want to dedicate this work to my parents. Special thanks to my colleague A. Piñán-Llamas, who has been there with immense encouragement, support, inspiration, and faith. A grateful thank you is extended to Dr. W. A. Bothner, Dr. Igor Tsukrov, Dr. J. Laird, Dr. W. C. Clyde, and Dr. A. M. Hussey II for their constructive criticism.

I would like to extend my profound gratitude to Dr. W. A. Bothner and his wife for their incommensurable help, support, and understanding. Finally I'm grateful to the many friends, co-workers, colleagues, and specially, to the people of the seacoast region of New Hampshire. This research was supported in part by the scholarship # 110769 from CONACyT (Consejo Nacional de Ciencia y Tecnología) from México and by the USGS-EDMAP Program 1999-2001.

TABLE OF CONTENTS

	ACKNOWLEDGEMENTS -----	iii
	LIST OF TABLES -----	ix
	LIST OF FIGURES -----	x
	ABSTRACT -----	xv
CHAPTER		PAGE
I.	INTRODUCTION -----	1
	Scope of this Research -----	1
	Geologic Setting -----	1
	Lithotectonic Units -----	1
	Intrusive Bodies -----	5
	Major Faults -----	5
	Tectonic Setting -----	6
	Methods of Analysis -----	8
	Fieldwork, Rock Sampling, and Data Collection -----	8
	Geologic Mapping -----	8
	Fourier Series Analysis -----	10
	Petrography and Microstructural Analysis -----	18
	Finite Element Analysis and Computer Modeling -----	19
II.	FOLDS -----	21
	Introduction -----	21
	Degree of Asymmetry, Shape, and Attitude -----	21
	Results -----	21

Discussion -----	24
Fold Mechanisms -----	31
Results -----	32
Discussion -----	34
Superposed Folding -----	45
Results -----	45
Discussion -----	45
III. FINITE ELEMENT ANALYSIS OF PYRITE CRYSTAL DEFORMATION ---	49
Introduction -----	49
Sample Preparation -----	51
Description of Finite Element Models and Load	
Cases -----	53
Processing of Numerical Simulation Results -----	53
Results -----	60
Discussion -----	61
IV. MICROSTRUCTURAL ANALYSIS -----	64
Introduction -----	64
Area # 1 - Rye Complex -----	67
Sample Description -----	70
Sample MGJ-506 -----	70
Sample GC-1 -----	73
Sample GC-3 -----	75
Sample GC-4 -----	78
Sample GC-5 -----	79
Sample GC-6 -----	81

Sample GC-7 -----	82
Sample GC-8 -----	82
Sample GC-110 -----	84
Sample 480 -----	85
Sample 520 -----	85
Sample 530 -----	87
Results -----	89
Discussion -----	90
Area # 2 - Rye Complex -----	91
Sample Description -----	93
Sample 0725-1 -----	93
Discussion -----	93
Area # 3 - Rye Complex -----	95
Sample Description -----	95
Sample NH-61 -----	95
Sample NH-62 -----	96
Discussion -----	96
Area # 4 - Merrimack Group -----	98
Sample Description -----	98
Sample P-1 -----	98
Sample P-2 -----	98
Discussion -----	101
V. STRATIGRAPHY OF THE MERRIMACK GROUP -----	102
Introduction -----	102
Kittery Formation -----	107
Stratigraphy -----	107

	Evidence of Biogenic Structures -----	111
	Eliot Formation -----	115
	Stratigraphy -----	115
	Suspect Biogenic Structures -----	120
	Stratigraphic Contacts -----	122
	Transition Eliot - Kittery -----	122
	Results -----	130
	Discussion -----	131
	Transition Eliot - Berwick -----	132
	Structures -----	137
VI.	GEOLOGY OF THE RYE COMPLEX IN NORTH HAMPTON NEW HAMPSHIRE	143
	Introduction -----	143
	Mineral Assemblages -----	145
	Graphical Representation of Mineral Assemblages -----	147
	Correlation -----	151
	Metamorphism -----	154
	Discussion -----	154
VII.	INTERPRETATION AND CONCLUSIONS	157
	Introduction -----	157
	Geologic Map -----	158
	Theoretical Aspects -----	160
	Fourier Series Analysis -----	160
	Finite Element Analysis -----	162
	Geologic Interpretation -----	163
	Stratigraphy -----	163

Interpretation of Folds -----	166
Interpretation of Faults -----	174
Tectonic Model-----	184
REFERENCES CITED	189
APPENDIX I Derivation of Formulas and Program in BASIC --	196
APPENDIX II. Anticlastic Bending -----	205
APPENDIX III. Strain Analysis of the Generation of Cleavages in Folds -----	209
APPENDIX IV. Results From Finite Element Analysis -----	215
PLATE 1 BEDROCK GEOLOGIC MAP OF THE EXETER AND HAMPTON 7.5' QUADRANGLES	

LIST OF TABLES

1.1	Fold classification based on profile symmetry -----	18
1.2	Ratio of first and third harmonic coefficients -----	18
2.1	Summary of results of the Fourier Series Analysis -----	24
2.2	Types of interference patterns according to the current classifications -----	47
3.1	Summary of microphotographs -----	54
3.2	Material properties of pyrite and quartzite -----	55
3.3	Pyrite crystals and models for FEA -----	56
3.4	Summary of the results of the numerical simulations -----	58
4.1	Characteristics of the three regimes of dynamic recrystallization -----	66
4.2	Summary of results from the microstructural analysis -----	89
5.1	Settings summary of the Siemens D 500 diffractometer -----	130
6.1	Visual estimation of modes in samples from study area 3 -----	148
7.1	Summary of radiometric ages in the seacoast region of New Hampshire -----	185

LIST OF FIGURES

1.1	Simplified geologic map -----	2
1.2	Six USGS 7.5 minute quadrangles -----	9
1.3	Photograph and scheme of folded surfaces -----	13
1.4	3D representation of the two limbs of a fold -----	14
1.5	b_1 Vs b_3 plot -----	16
1.6	Cartesian plot of the b_3 Vs b_1 harmonic coefficients -----	17
2.1	Folds showing the "long-short-long" limb pattern -----	22
2.2a	Classification of fold shapes -----	25
2.2b	Three dimensional plot of the first three odd terms -----	25
2.3	Sample location map -----	28
2.4	Fold shapes in the MG -----	29
2.5a	Stereograms and outcrop photos at location 8 -----	30
2.5b	Stereograms and outcrop photos at location 9 -----	30
2.6	Quartz and calcite "slickensides" -----	33
2.7	The upper section of the graphic representation of boudinage -----	35
2.8a	Undulations oblique to the fold axis -----	37
2.8b	View from top -----	37
2.8c	Stereographic projection of the axial planes -----	37
2.8d	Strong foliation and boudins -----	37
2.9	Structures in the MG -----	39
2.10	Graphic representation of folding -----	40
2.11	Plots in an x-y space of ideal chevron fold profiles -----	41
2.12	Graphic representation of the results of the strain analysis of chevron folds -----	43

2.13	Interference patterns in the study area -----	48
3.1	Map showing sample location -----	51
3.2a	General view of the folded structure -----	52
3.2b	Fold limb -----	52
3.2c	Sample for thin sectioning -----	52
3.3	View of spreadsheet -----	60
3.4	Representation of unit volumes containing pyrite crystals --	62
4.1	Location map -----	68
4.2	Map showing sample location -----	69
4.3	Sample MGJ-506 Serrated boundaries -----	71
4.4	Sample MGJ-506 Quartz subgrains -----	72
4.5	Sample MGJ-506 Crystal plastic deformation -----	72
4.6	Sample GC-1 -----	73
4.7	Sample GC-1 Quartz grains -----	74
4.8	Sample GC-1 Pinning structure -----	74
4.9	Sample GC-1 Garnet porphyroblasts -----	75
4.10	Sample GC-3 New and original grains -----	76
4.11	Sample GC-3 Pinning structure -----	76
4.12	Sample GC-3 Shear band (S-C fabric) -----	77
4.13	Sample GC-3 K-spar porphyroblasts -----	77
4.14	Sample GC-4 Shape preferred orientation -----	78
4.15	Sample GC-4 Shear band -----	79
4.16	Sample GC-5 Main foliation -----	80
4.17	Sample GC-5 Shear bands -----	80
4.18	Sample GC-6 Quartz subgrains -----	81
4.19	Sample GC-6 Garnet sigma grains -----	82
4.20	Sample GC-7 Shear bands -----	83
4.21	Sample GC-8 Recrystallized and original quartz grains -----	83

4.22	Sample GC-110 Shear band -----	84
4.23	Sample GC-110 Garnet Porphyroblasts -----	85
4.24	Sample 480 Quartz grains -----	86
4.25	Sample 520 Recrystallized quartz grains -----	86
4.26	Sample 520 Crystal plastic deformation -----	87
4.27	Sample 530 Characteristic cauliflower structure -----	88
4.28	Sample 530 Crystal plastic deformation -----	88
4.29	Spatial distribution of the deformation regimes -----	91
4.30	Map of Area #2 -----	92
4.31	Crenulation lineation -----	93
4.32	Mylonitic texture -----	94
4.33	Garnet porphyroblast -----	94
4.34	Map of Area #3 -----	95
4.35	Sample NH-61 Polygonal texture -----	96
4.36	Sample NH-61 Quartz grains -----	97
4.37	Sample NH-62 Sigma grain -----	97
4.38	Map of Area #4 -----	99
4.39	Pervasive slickenfiber lineation -----	99
4.40	Illustration of a thin pseudotachyllite vein -----	100
4.41	Sample P-1 Recrystallized quartz grains -----	100
4.42	Sample P-2 Flow banding in a pseudotachyllite vein -----	101
5.1	Topographic map of Great Bay -----	105
5.2	Topographic map showing study locations -----	106
5.3	Geologic map showing the three subdivisions -----	108
5.4	Sedimentary structures in SOka subunit -----	109
5.5	Example of SOkb subunit -----	110
5.6	Example of SOkc subunit -----	111
5.7a	Close view photograph of the 0.9in long object -----	113

5.8b	Photograph revealing the relief of the object -----	113
5.7c	General view of the block -----	114
5.8	Close up of the suspect bioturbation -----	115
5.9	Geologic map of the Town of Madbury new fire station -----	117
5.10	Stratigraphic column of the Eliot Formation -----	118
5.11	Illustration showing the trace of the stratigraphic section	119
5.12	Suspect biogenic structure -----	121
5.13	Illustration of a piece of core from NR-1 -----	124
5.14	Basal conglomerate -----	125
5.15	Photomicrograph of the basal conglomerate -----	126
5.16	Stratigraphic style in the Bellamy River -----	128
5.17	Topographic map of the Lee Five Corners Area -----	129
5.18	QPP (quartz, plagioclase, and pelite) ternary diagram -----	131
5.19a	Decimeter-scale kinematic indicator -----	133
5.19b	Undulations associated with boudinage and "bookshelf" structure -----	134
5.19c	Undulations associated with boudins and mega sigma grains --	134
5.19d	Folds with attenuated limbs -----	135
5.20	Aspect of compositional layering -----	136
5.21	Quartz veins and buckling folds -----	136
5.22	Structural map of the contact zone between the SOe and SOb -	138
5.23	Composite stereogram -----	140
5.24	Illustration of the intersection of foliation planes with a faulting plane -----	141
5.25	Slickensides associated with brittle faulting -----	141
5.26	Fold in the north block -----	142
5.27	Difference in the orientation between the axial planes and fold axes -----	142

6.1	Topographic map showing the areas for correlation -----	144
6.2	Map showing the trace of the Great common Fault Zone, sample locations, and projections -----	146
6.3	Alteration texture of biotite to chlorite -----	147
6.4	Sample GC-110 Staurolite surrounded by andalusite -----	149
6.5	Sample GC-5 Equilibrium assemblage -----	149
6.6	Topographic map of New Castle Island -----	150
6.7	Microphotograph of Sample GC-110 -----	152
6.8	P-T grid -----	156
7.1	3-dimensional representation of chevron refolded folds -----	161
7.2	Projection of a Type 3 interference pattern -----	162
7.3	3-dimensional representation of the "short-long-short" limb fold pattern -----	167
7.4	Graphical representation of a fold and a pyrite crystal -----	168
7.5	Graphic representation of anticlastic bending -----	170
7.6	Map showing the deflected attitude of the mean direction of the fold planes -----	171
7.7	Geometrical 3-D representation of a refolded surface -----	173
7.8	3-D representation of the folding style observed in the study area -----	175
7.9	Digital elevation model of the ten 7.5 min quadrangles -----	181
7.10	Digital elevation model composite map -----	182
7.11	Schematic representation of the tectonic evolution of the seacoast region of New Hampshire -----	188

ABSTRACT

BEDROCK GEOLOGY OF THE SEACOAST REGION OF NEW HAMPSHIRE, U.S.A.

By

José C. Escamilla-Casas

University of New Hampshire, December 2003

The seacoast region of New Hampshire is underlain by two lithotectonic belts: the Rye Complex (RC), and the eastern portion of the Merrimack Group (MG). The Rye Formation and the Breakfast Hill member constitute the RC; the Kittery, Eliot, and Berwick Formations, the MG. The stratigraphic order interpreted in this study places the Kittery Formation transitionally above the Eliot, and identifies the contact between the Berwick and the Eliot Formations as a fault.

Study of folds using a variant of the Fourier series analysis indicates that the degree of asymmetry and shape of folds in the MG and the RC are similar. Besides documenting the folding event that affected the RC and the MG simultaneously (Acadian Orogeny), the method has proven its effectiveness as an educational tool.

Occurrence of pyrite crystals in MG rocks permitted the application of Finite Element Analysis. It consisted of numerical simulation of a set of controlled load cases applied to models of distorted pyrite crystals to reconstruct their assumed regular square shape. Results suggest that deformation of the crystals is related to folding that affected the host rock and not to the emplacement of a nearby Mesozoic dike.

Fieldwork, microstructural analysis, and digital elevation models, provide refinement of the traces of the Calef, Nannie Island,

Portsmouth, and Great Common Fault Zones; and the identification of the brittle "Exeter Fault". Petrographic and microstructural analyses document the temperature of deformation in the south block of the Great Common Fault Zone, and support the correlation of these rocks with outcrops on New Castle Island and to the northeast on Gerrish Island, ME.

A proposed transpressional tectonic model involving a continuum from the late Silurian through early Paleozoic suggests that folding, magmatic intrusion(s), and ductile followed by brittle faulting affected the seacoast. In this model, after juxtaposition, simultaneous folding of the MG and RC was followed by northeast-trending, right lateral ductile shear. Later, right lateral, normal, northeast-trending, and east-west trending brittle faulting occurred affecting most Paleozoic plutons. The emplacement of Mesozoic mafic dikes is associated to the opening of the Atlantic Ocean.

CHAPTER I

INTRODUCTION

Scope of This Research

The geology of the seacoast region of New Hampshire has proven challenging to study for several reasons. (1) There is little stratigraphic control due to the lack of identified fossils and the presence of few stratigraphic markers. (2) The presence of intrusive bodies and faults interrupts the continuity of the stratigraphic column. Some of these faults presumably have large displacements and in most cases, their traces are inferred. (3) Multiple (?) deformations of this long-lived orogen makes structural analysis and tectonic interpretation difficult. (4) There is poor control on the timing of metamorphism, and locally the rocks are poly-metamorphosed. (5) The extensive cover of glacial and younger deposits makes correlation between scarce rock outcrops difficult.

This research attempts to 1) clarify the stratigraphic sequence in the Merrimack Group. 2) Establish the relative chronological order of events, crustal level of formation, and dynamics of the Portsmouth Fault Zone as a boundary between two blocks, the Merrimack Group in the west and the Rye Complex in the east. 3) Establish the dynamics and stages of deformation of the Great Common Fault zone within Rye Complex lithologies.

Geologic Setting

Lithotectonic Units - The seacoast region is located in the extreme southeast corner of the State of New Hampshire, USA. Tectonostratigraphically, the region includes the Rye Complex and the

eastern portion of the Merrimack Group (fig. 1.1).

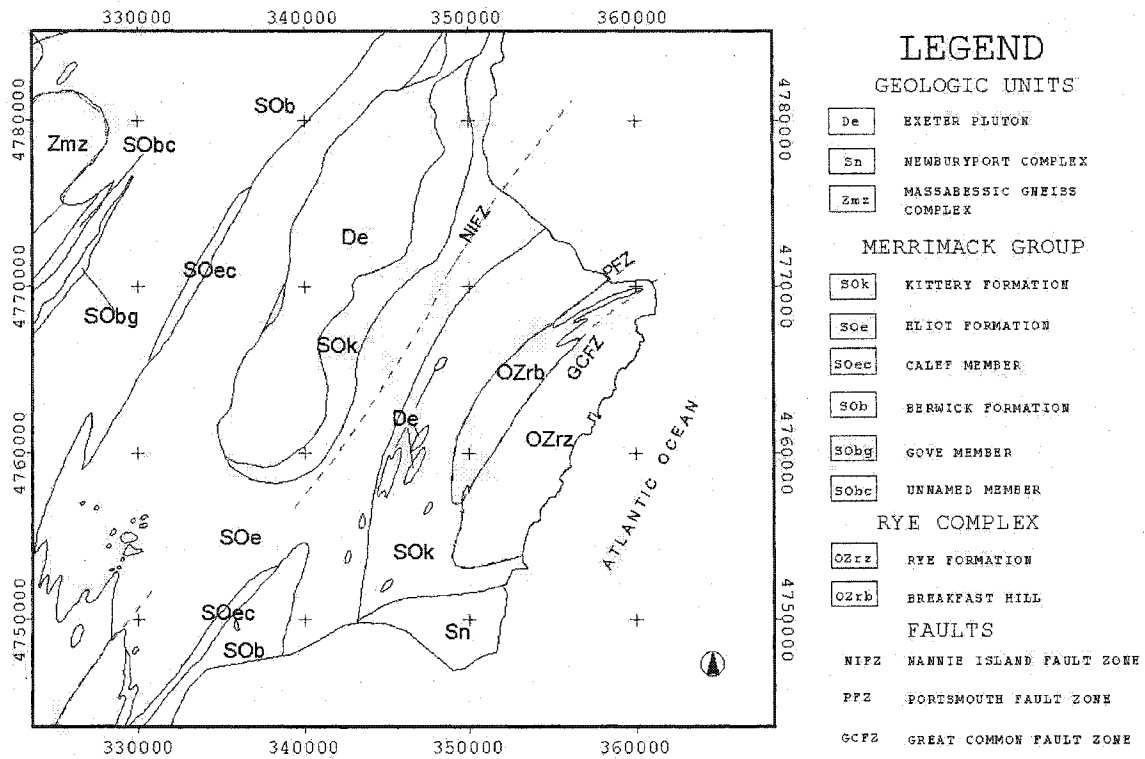


Figure 1.1 - Simplified geologic map of southeastern New Hampshire showing the principal structural and stratigraphic elements (projected in UTM coordinate system; adapted from Lyons et al., 1997).

The relation with the proximal 623 ± 8 Ma (U/Pb, zircon) Massabessic Gneiss Complex (Aleinikoff and Walter, 1995) and the ages of the crosscutting 406 ± 1 Ma (U/Pb, zircon) Exeter Pluton and the 418 ± 1 Ma (U/Pb, zircon) Newburyport Complex (Bothner et al., 1993 in Lyons et al., 1997) imply a Silurian-Ordovician age assignment for the Merrimack Group (MG). The MG is a thick sequence of calcareous turbidites, and its stratigraphic subdivision consists of three formations, the Kittery, Eliot, and Berwick (Katz, 1917; Billings, 1956; Bothner et al., 1984). The Kittery Formation (Kittery Quartzite of Katz, 1917; Novotny, 1969; Billings, 1956; and Hussey, 1968) is primarily a thin-bedded feldspathic calcareous metasiltstone and metasandstone. Hussey (1968, 1985) defined this unit as a variably thick to thin bedded, tan-weathering, fine-grained calcareous and feldspathic metasandstone with usually thin

interbeds of dark gray to black, often sulfidic phyllite. The fine-grained rocks are thin-bedded to laminated, whereas the thicker beds show cross lamination, flame structures, and graded bedding. A detailed study by Rickerich (1983) suggests that primarily turbidity currents deposited this unit in a submarine fan environment.

The Eliot Formation consists primarily of thin to thick tabular and lenticular beds of calcareous metasiltstone and metasandstone. It generally consists of thin-bedded alternations of tan-gray weathering, turbiditic calcareous metasandstone, and silvery dark gray phyllite. Its contact with the Kittery Formation is gradational (Hussey, 1985), but the stratigraphic order remains ambiguous (Lyons et al., 1989; Bothner and Hussey, 1999).

Freedman (1950) mapped a black, graphitic phyllite along the western margin of the Eliot Formation as the Calef Member. Bothner and Hussey (1999) interpreted this highly sheared rock type as a phyllonite. Schulz and Loveless (2001) redefine the Calef Member as a well-crenulated, rusty-maroon weathering, gray graphitic phyllonite with discontinuous quartz stringers that marks a major shear zone separating the Eliot Formation from the generally higher-grade Berwick Formation to the west.

The Berwick Formation (Katz, 1917) consists of three sub-units (Lyons et al., 1997). The first sub-unit is described as a purplish biotite-quartz-feldspar granofels with interlayers or boudins of calc-silicate granofels and rusty, sulfidic metapelites. The second sub-unit, the Gove member (Freedman, 1950, Loveless and Schulz, 2002) consists of silvery garnet-staurolite-biotite schist. It contains abundant porphyroblasts of garnet, and, depending on the metamorphic grade, staurolite, and/or sillimanite. The upper member (Siramadas 1966; Lyons and Bothner, 1989) and lately redefined as the Unnamed

Member (Lyons et al., 1997) contains more calc-silicate (15%) than the remainder of the formation (5%).

The Gove and the Unnamed (upper) members constitute the western half of the Berwick Formation. Allard (1998) and Allard et al., (1998) identify the "Watson Hill" member (a silvery gray pelitic unit) and the "Transition Zone" (a moderately to highly migmatized unit) as two separate lithologies within the Unnamed Member.

The Rye Formation is a major lithotectonic sequence in this area, so named by Billings (1956) from its excellent exposures in Rye, New Hampshire. It was interpreted as the oldest of the metasedimentary units exposed in the seacoast region and maybe is one of the oldest formations to be seen in the state.

Billings (1956) recognized two important divisions, a lower metasedimentary member (feldspathic mica-schist) and an upper metavolcanic member (amphibolite and mica schist). Both members are rather coarse-grained and distinctly banded. Within the Rye Formation, Novotny (1969) mapped the Breakfast Hill Granite, which is a 0.5 km² elliptical, per-aluminous, highly foliated pluton with massive foliated pegmatite. Hussey (1980) studied the Rye Formation in Gerrish Island, and concluded that the originally interpreted metavolcanic rocks are injected and migmatized material resembling bedding.

Hussey (1980) and Hussey and Bothner (1993) redefined the Rye Formation as an association of variably metamorphosed calcareous and non-calcareous metasandstone and metasilstone with migmatized and non-migmatized metapelite. It includes minor discontinuous but mappable units of rusty weathering sulfidic graphitic phyllite, marble, and amphibolite. Semi-concordant granitic and tourmaline-bearing pegmatitic layers (porphyroclastic augen gneisses) are abundant and share the same mylonitization history as their metasedimentary hosts. Bothner and

Hussey (1999) identified this unit as the most important ductile structure in New Hampshire and named it the Rye complex (RC).

Intrusive Bodies - Two major intrusions are present in the seacoast region of New Hampshire, the Exeter Pluton and the Newburyport Complex. Bothner et al. (in Lyons et al., 1997) reported U/Pb ages of 406 ± 1 and 418 ± 1 Ma, respectively. The Exeter Pluton is principally diorite in composition but exhibits local variations from gabbro to quartz monzonite (Billings, 1955, Novotny 1963, 1969, and Bothner, 1974). Other minor intrusive bodies are related lithologically and mapped to the east and southeast of Exeter Pluton (Novotny, 1969; Billings, 1956; and Escamilla-Casas, 2001).

Novotny (1963) described a medium to coarse grained, light colored rock as the Newburyport quartz diorite. This rock, as described by Zartman and Naylor (1984), is a medium to coarse-grained, porphyritic, and non-porphyritic granodiorite and quartz monzonite occupying a faulted block north of Newburyport in northernmost Massachusetts and adjacent New Hampshire.

Several northeast-trending diabase dikes intrude the MG and the RC and crop out in the study area. Based on whole rock ages (Ar^{40}/K^{39}) of 158 ± 6 to 191 ± 10 Ma, a Mesozoic age is assigned to these dikes (McHone, 1978).

Major Faults - The Norumbega Fault Zone (NFZ) has been locally described in mid-coastal Maine by Stewart and Wones (1974) and recently mapped regionally for about 450 km; from Casco Bay in southern Maine to central New Brunswick (Ludman and West, 1999). The NFZ probably extends into the seacoast region of New Hampshire as the Portsmouth Fault and the Great Common Fault zones, (PFZ) and (GCFZ). The PFZ is a 100 - 300 m wide, north - and northeast-trending, and northwest dipping structure

(Carrigan, 1984; Swanson and Carrigan, 1984; Hussey and Bothner, 1993, 1995; and Bothner and Hussey, 1999). The Merrimack Group and the Rye complex are in contact along the PFZ. Two different fabrics have been identified in this structure: (1) a ductile fabric represented by mylonitized rocks reveals a predominantly right-slip sense of shear and (2) brittle fault structures indicate a dip slip motion, northwest side down (Bothner and Hussey, 1999).

The Great Common Fault Zone (GCFZ) is a ~50 m wide fault zone which separates less migmatized lithologies of the Rye complex on the southeast from more migmatized lithologies on the northwest (Carrigan, 1984). The GCFZ also has an early ductile fabric and a later brittle fabric. Boeckeler (1994) obtained Rb/Sr whole rock ages from pseudotachylite of 298 ± 31 Ma that constrains the timing of a high velocity, dextral strike slip displacement in the GCFZ. These ages represent the last stage of movement in this mylonite zone so far recognized.

The Nanny Island phyllonite, as described by Bothner and Hussey (1999), is a poorly exposed narrow northeast-trending shear zone no more than 200 m wide, with predominantly dextral shear sense indicators. These indicators include isoclinal folds with the hinges lying parallel to phyllonitic foliation and limbs strongly attenuated and/or truncated. The extension of this phyllonite to the northeast and to the southwest is virtually impossible to follow due to the lack of exposure.

Tectonic Setting - Tectonically, the Siluro-Ordovician MG and the probably older RC of the seacoast region are associated with the tectonic evolution of the Northern Appalachians. Current tectonic interpretations consider collision and terrane accretion as the mechanisms responsible for the genesis of the Appalachian orogen as part of the Avalon and Laurentia convergence. Williams and Hatcher (1983)

and Keppie (1985, 1989), among others, recognize the Taconic (Ordovician), Acadian (Devonian), and Alleghanian (Carboniferous) orogenies as the three major tectonic events that affected the northern Appalachians during the Paleozoic.

Based on paleomagnetic and tectonostratigraphic data, Van der Pluijm et al., (1993) reported that during the Silurian the Appalachians record the closure of the Iapetus Ocean (a major ocean delimited by the Avalonian micro continent and the Laurentian craton). The main assumption for this model is that during Early Ordovician times, the Iapetus Ocean consisted of at least two basins, Iapetus I and Iapetus II. The tectonic sequence of their model establishes three main stages: (1) During the Early Ordovician, a volcanic arc, and a back-arc basin (Iapetus I Ocean) were located near the Laurentian margin. (2) During the Middle Ordovician, closure of Iapetus I occurred due to the convergence of Avalon and Laurentia by northward subduction. (3) The convergence continued through the Late Silurian when the closure of Iapetus II was completed. In this working hypothesis, the three major orogenic events (Taconic, Acadian, and Alleghanian) are considered as deformation peaks and as part of a continuous progressive deformation. This hypothesis also considers the extension of the Acadian orogeny into the early Silurian or the addition of an orogenic phase (Caledonian?) between the Taconic and the Acadian.

Bradley et al., (2000) reassessed the Acadian orogenesis in Maine based on U/Pb and (super 40) Ar/ (super 39) Ar ages of Acadian plutons, new conodont and palynomorph ages. The analysis shows that the Acadian deformation front migrated 240 km (present distance) from southeast to northwest from Late Silurian to Middle Devonian time (a span of about 40 million years). Robinson et al. (1998) and Robinson (2003) now extend an

"Acadian" through much of the middle and late Paleozoic (Silurian at least to Mississippian).

The Mesozoic tectonic setting of the seacoast region is interpreted as a predominantly extensional regime associated with the opening of the Atlantic Ocean. During that time, the MG and the RC were "welded" and together constituted the country rock into which the diabase dikes were intruded. The intrusions of this nature crosscut the probable contacts between the RC and the MG, but do not occur parallel to them. The northeast - preferred orientation of these dikes are often interpreted as the trend of extensional fractures (McHone, 1978, Swanson, 1992).

Methods of Analysis

Fieldwork, Rock Sampling, and Data Collection - The topographic base for geologic fieldwork consists of six adjacent USGS 7.5-minute quadrangles (fig. 1.2). The collection and representation of geological data for structural analysis and synthesis is based on the use of a Brunton compass, GPS, and computer-aided stereographic projection software (GEOrient V90; Holcombe, 2001).

Direct measurements on enlarged printouts of scanned photographs and/or digital images of folded surfaces give the parameters for the Fourier analysis. The petrographic and micro structural analyses rely on thin sections cut from representative and oriented hand specimens of rocks. A combination of thin sections, photomicrographs, and digitized maps from pyrite crystals constitute the materials for the Finite Element Analysis computing simulations.

Geologic Mapping - Three different sources provided the topographic information of the study area that constitutes the base of the overall geologic mapping. First, a set of paper copies of USGS 7.5 minute quadrangles was used for transferring data in the field (location of

outcrops, rock samples, and wells-to-bedrock) and to produce preliminary geologic maps. Second, detailed geologic maps were hand-drafted by using enlarged Topo-USA® software printouts as a topographic base then

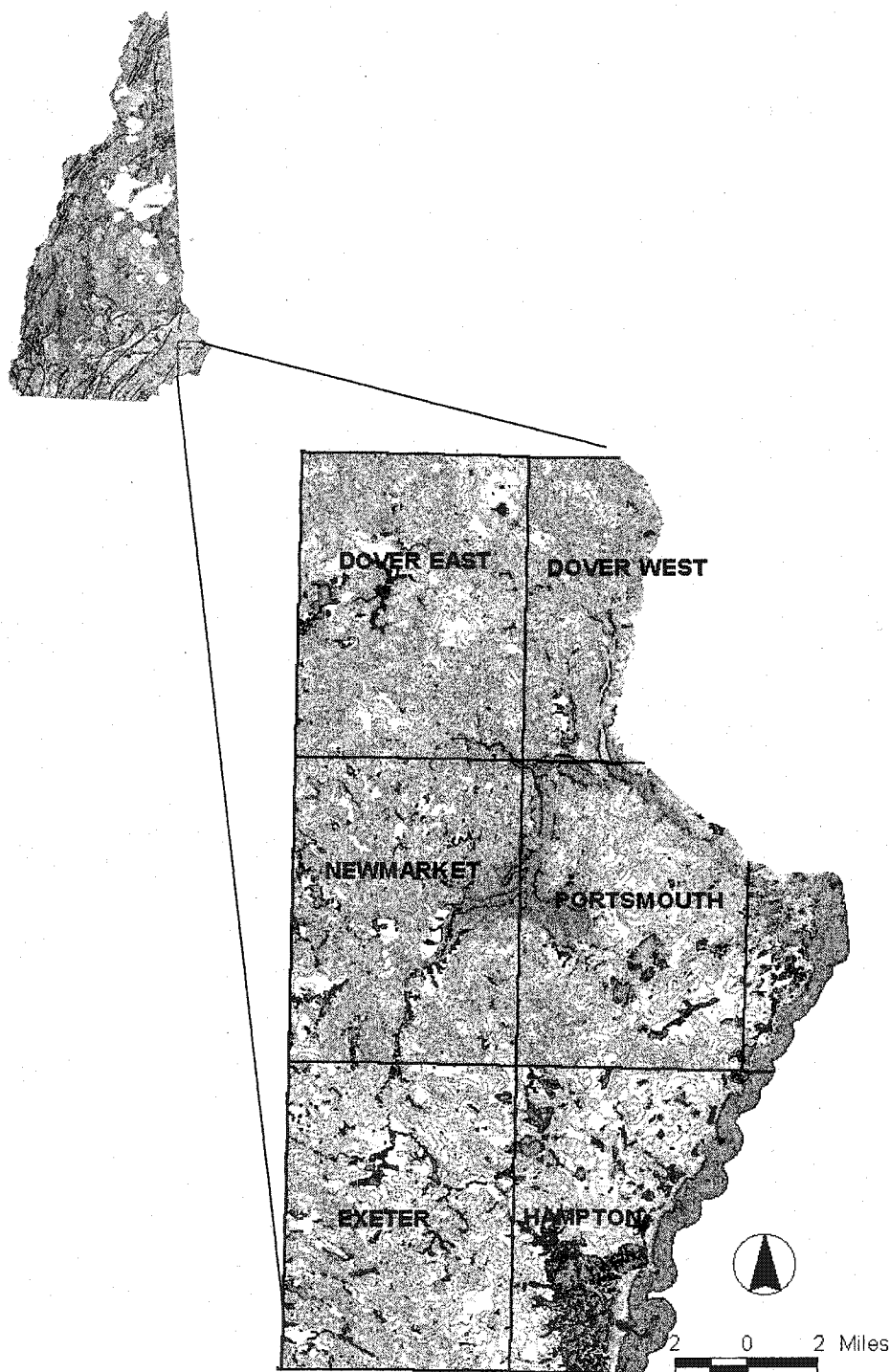


Figure 1.2 - The six USGS 7.5-minute quadrangles that constitute the topographic base of the study area.

scanned and converted into printable electronic images for insertion in this text. Third, downloaded files from the UNH-GRANITE Database World Wide Web site were re-projected into the NAD-27 coordinate system and updated with geologic information using the Geographic Information System (GIS) Arc-View[®] software. The last source was fundamental to produce the general geologic map of the Exeter and Hampton 7.5 min quadrangles with GIS specifications (Plate 1).

Fourier Series Analysis - Except along the coast and recent road cuts, rock exposures are scarce in the seacoast region. Where it is found, very often, the structures cannot be studied in three-dimensions; in many cases, folds are only seen on planar surfaces. Consequently, the acquired structural data are approximate and often insufficient. In this variant of the Fourier series analysis, folds are treated as three-dimensional waves that are represented by the sum of an infinite number of harmonics of sine and cosine waves of decreasing amplitudes. Such a representation can describe waves (folds) of any shape and the formulas for the amplitudes are provided, for example, in Greenberg (1978).

Several researchers applied Fourier series to the analysis of folds. Huddleston (1972) used the first two odd sine harmonics for a visual interpretation. Ramsay (1967) and Ramsay and Huber (1987) used two harmonics to perform a quantitative study of the geometry of folded surfaces.

In this research, the Fourier series analysis quantitatively characterizes fold patterns by assessing their shape and degree of asymmetry by using the first three harmonics. This characterization compares folds from different localities, and helps to develop numerically based three-dimensional graphic representations of folded rocks.

Represented mathematically, the Fourier series can be:

$$f(x, y) = a_0 + \sum_{n=1}^{n=\infty} [a_n \cos(n\theta) + b_n \sin(n\theta)] \quad (1.1)$$

where a_0 = constant of position, a_1, a_2, \dots, a_n ; b_1, b_2, \dots, b_n = amplitudes, and $\theta = 2\pi x/\lambda$ in which λ is the wavelength and x is a distance. Successive coefficients in this series become smaller and, in mathematical terms, the series converges.

To compare fold patterns in terms of shape and asymmetry, half of an antiform is considered as a "quarter" wavelength. Placing the antiform with an inflection point (limb) at the origin of the coordinate system, all cosine terms, even-numbered sine terms, and the constant a_0 become zero (eq. 1.2). Consequently, the Fourier series can be reduced to a curve defined by only three terms, the first, third, and fifth sine harmonics, for matching the shape of the fold.

$$f(x, y) = b_1 \sin \theta + b_3 \sin 3\theta + b_5 \sin 5\theta \quad (1.2)$$

Potential errors are introduced because the axial trace and the inflection points are selected visually from the image. The amount of inaccuracy and error is comparable to the use of a Brunton compass to measure a strike and dip, for example, on an uneven bedding surface (approximately $\pm 5^\circ$).

The view direction of the images can be oblique to the axis of the fold. An oblique image of a fold profile distorts both limbs in the same proportion. Therefore, the difference in both limbs remains the same, and the results in this analysis are not affected.

Measurements and tracing of construction lines are made directly on enlarged printouts of digital images and/or photographs of the folded surfaces (fig. 1.3). To make the measurements three lines are drawn. One represents the trace of the axial surface and the other two are perpendicular to the first and intersect the selected inflection point at either side of the antiform. These perpendicular lines represent the

wave base (W) of each limb. Thereafter, values of three amplitudes at either limb (d_1 , d_2 , and d_3) are measured at 30° intervals. For correction and scale elimination purposes, all d_n values are multiplied by $\pi/2W$, and Y_n values result from the expression:

$$Y_n = d_n \frac{\pi}{2W} \quad (1.3)$$

where the d_n values are the amplitudes, and W is the length of a quarter wave base.

The combination of the first three terms of the series in equation (1.2) with Y_n values generates a system of three simultaneous equations:

$$Y_1 = b_1 \sin 30^\circ + b_3 \sin 90^\circ + b_5 \sin 150^\circ \quad (1.4)$$

$$Y_2 = b_1 \sin 60^\circ + b_3 \sin 180^\circ + b_5 \sin 300^\circ \quad (1.5)$$

$$Y_3 = b_1 \sin 90^\circ + b_3 \sin 270^\circ + b_5 \sin 90^\circ \quad (1.6)$$

Solving for b_1 , b_3 , and b_5 (see Appendix 1 for derivations) yields:

$$b_1 = \frac{Y_3 + Y_1}{3} + \frac{Y_2}{2 \sin 60^\circ} \quad (1.7)$$

$$b_3 = \frac{2Y_1 - Y_3}{3} \quad (1.8)$$

$$b_5 = \frac{Y_3 + Y_1}{3} - \frac{Y_2}{2 \sin 60^\circ} \quad (1.9)$$

To evaluate folds the first three odd (sine) coefficients of the series are taken from equations (1.7), (1.8), and (1.9). First, the two-dimensional analysis proposed by Stabler (1968) is followed. A point on a b_1 vs. b_3 Cartesian coordinate system represents the shape of a limb (quarter wave sector) of the folded surface. Therefore, the relative position of two points, a point for each limb, on a b_3/b_1 graph represents the difference in shape of the two limbs. Hypothetically, if

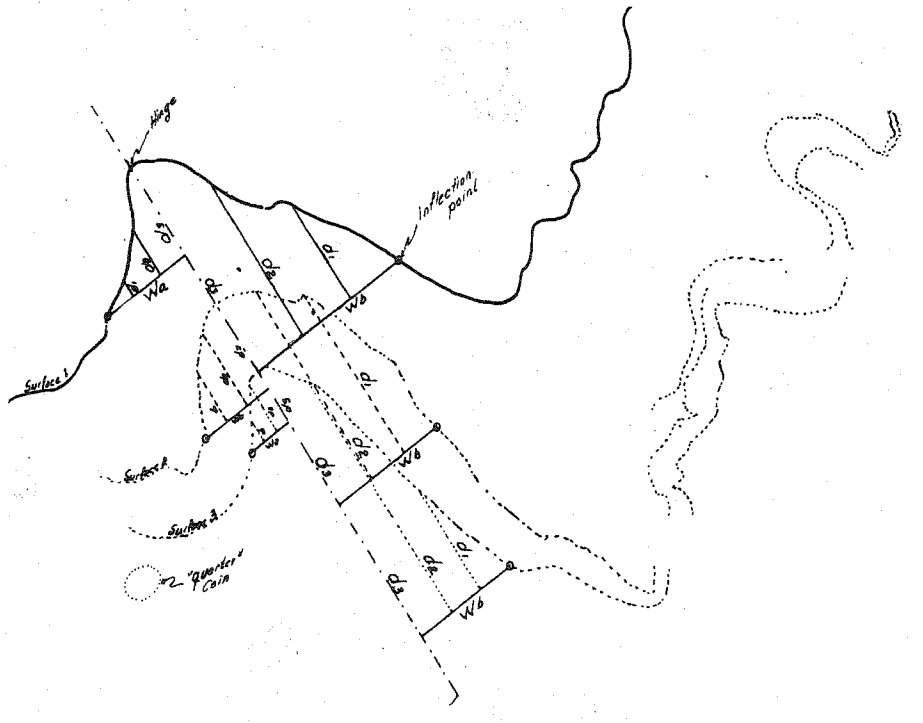


Figure 1.3 - Photograph and scheme of folded surfaces from Lee Five Corners (Eliot Formation type locality), the scheme shows the parameters considered in this analysis. The direction of view is to the north; a quarter dollar coin was used for scale.

the two points have identical b_1 and b_3 coordinates, the limbs would have identical shape.

Second, to analyze folds in terms of asymmetry, the same principles are applied and a third dimension added. Therefore, b_1 , b_3 , and b_5 define the three-dimension coordinate system.

Figure 1.4 shows two points A and B with b_1 , b_3 , and b_5 coordinates as (b_{1A}, b_{3A}, b_{5A}) and (b_{1B}, b_{3B}, b_{5B}) , respectively. These two points are defined as vectors of position in the three-dimensional coordinate system.

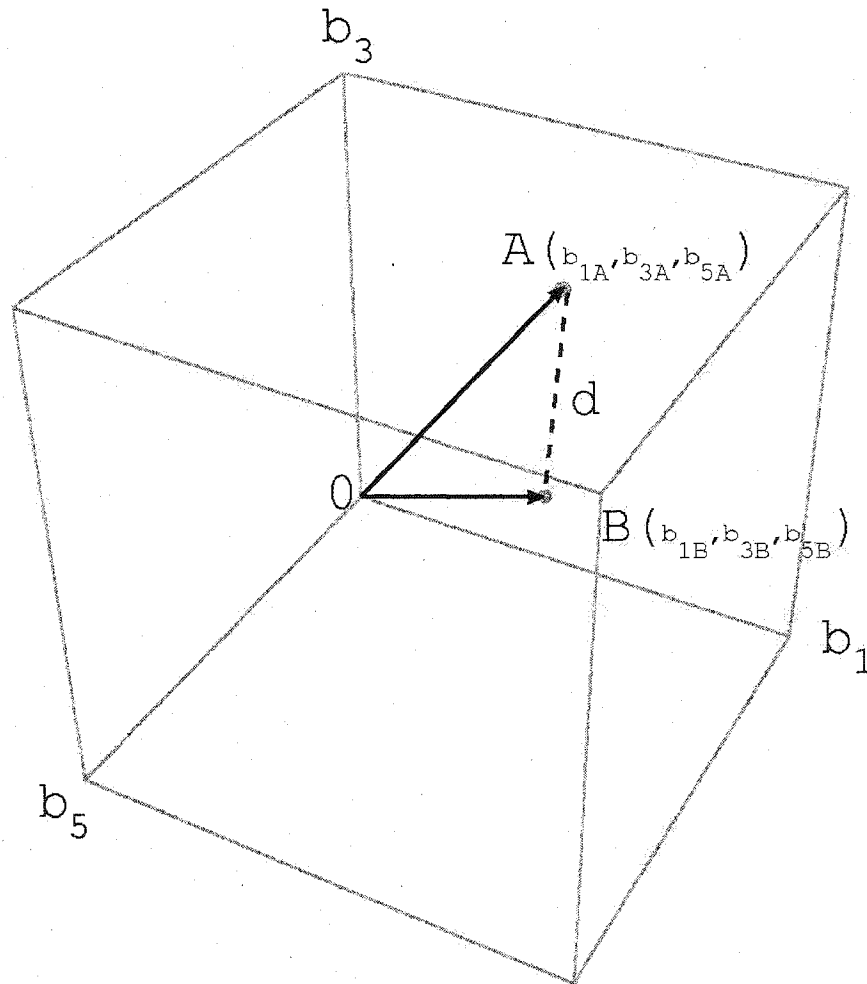


Figure 1.4 - A three dimensional representation of the two limbs of a fold, A and B are vectors of position, with coordinates (a_1, a_2, a_3) and (b_1, b_2, b_3) . The segment "d" is the distance between them.

The difference in amplitude can be calculated by solving for the magnitude of each vector ($|a|$ and $|b|$) and the distance (d) between them. This distance represents the difference in size (amplitude) of the two limbs from the origin. The measure of the difference in the amplitude of the two limbs (Δ_{size}) may be defined as:

$$\Delta_{size} = \left| \frac{d}{|a|} - \frac{d}{|b|} \right| \quad (1.10)$$

On the b_3/b_1 plane, the angles that the lines OA and OB make with the b_3 axis are given as:

$$\alpha_1 = \tan^{-1} \left(\frac{b_{1A}}{b_{3A}} \right) \quad (1.11)$$

$$\alpha_2 = \tan^{-1} \left(\frac{b_{1B}}{b_{3B}} \right) \quad (1.12)$$

The difference in shape of the two limbs is represented as the angle between the lines joining them to the origin (fig. 1.5). The shape component (Δ_{shape}) can thus be defined as:

$$\Delta_{shape} = |\alpha_1 - \alpha_2| \quad (1.13)$$

As defined earlier, the degree of asymmetry (DA) of a folded surface is a function of two variables, that is, the shape component (Δ_{shape}) and the size component (Δ_{size}), and expressed mathematically as follows:

$$DA = \Delta_{shape} + \Delta_{size} \quad (1.14)$$

DA is compared with the classification shown in Table 1.1.

The b_3/b_1 points can be plotted on the Cartesian classification consisting of six categories of folded surfaces proposed by Huddleston (1972) (fig. 1.6 and Table 1.2). The use of the FOURIER.BAS program (compiled in BASIC) facilitates a quick calculation of the ratios and parameters for this analysis (Appendix 2).

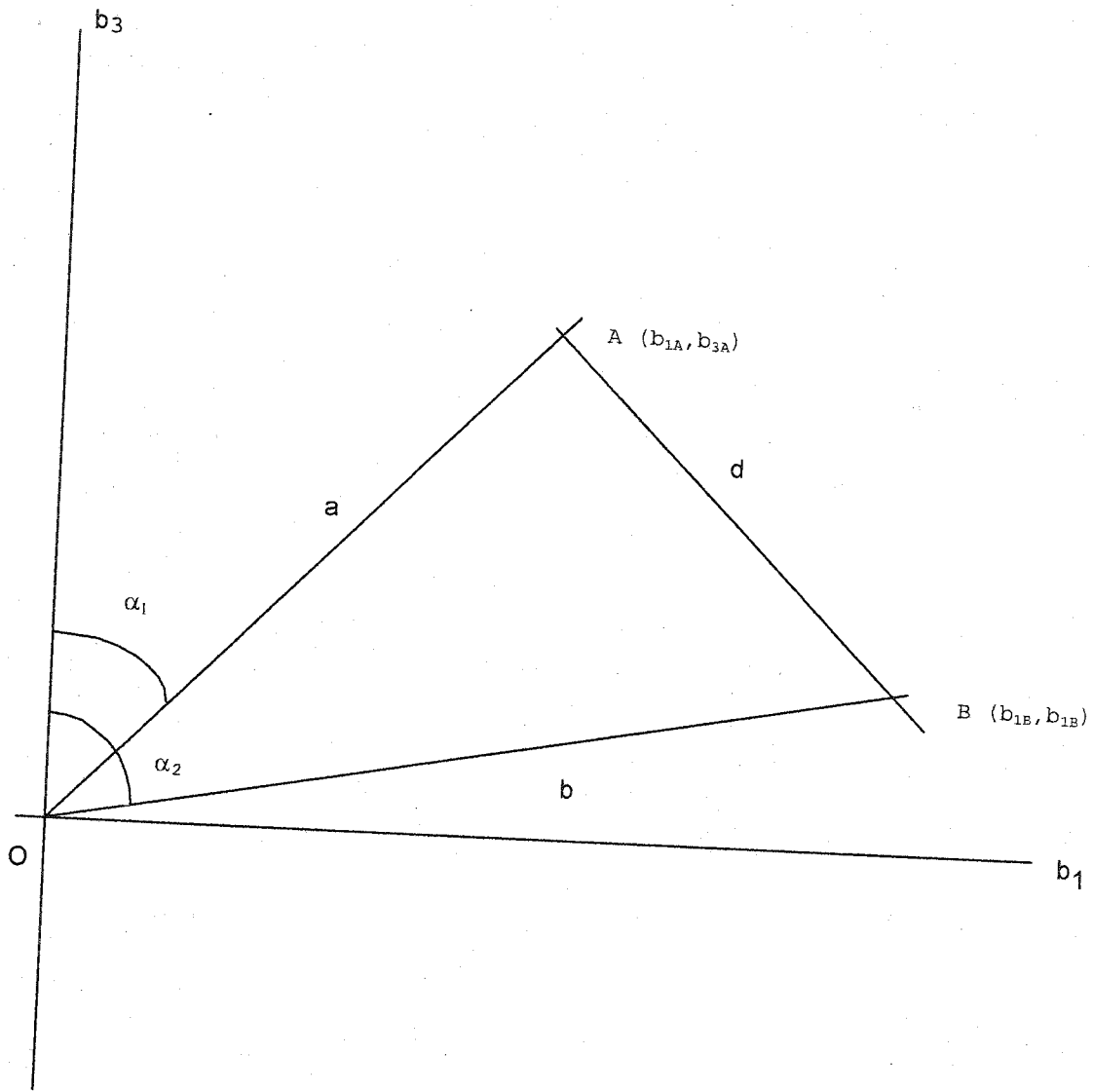


Figure 1.5 - b_1 Vs b_3 plot. Points A and B represent the two limbs, and α_1 α_2 represent the shape of each limb.

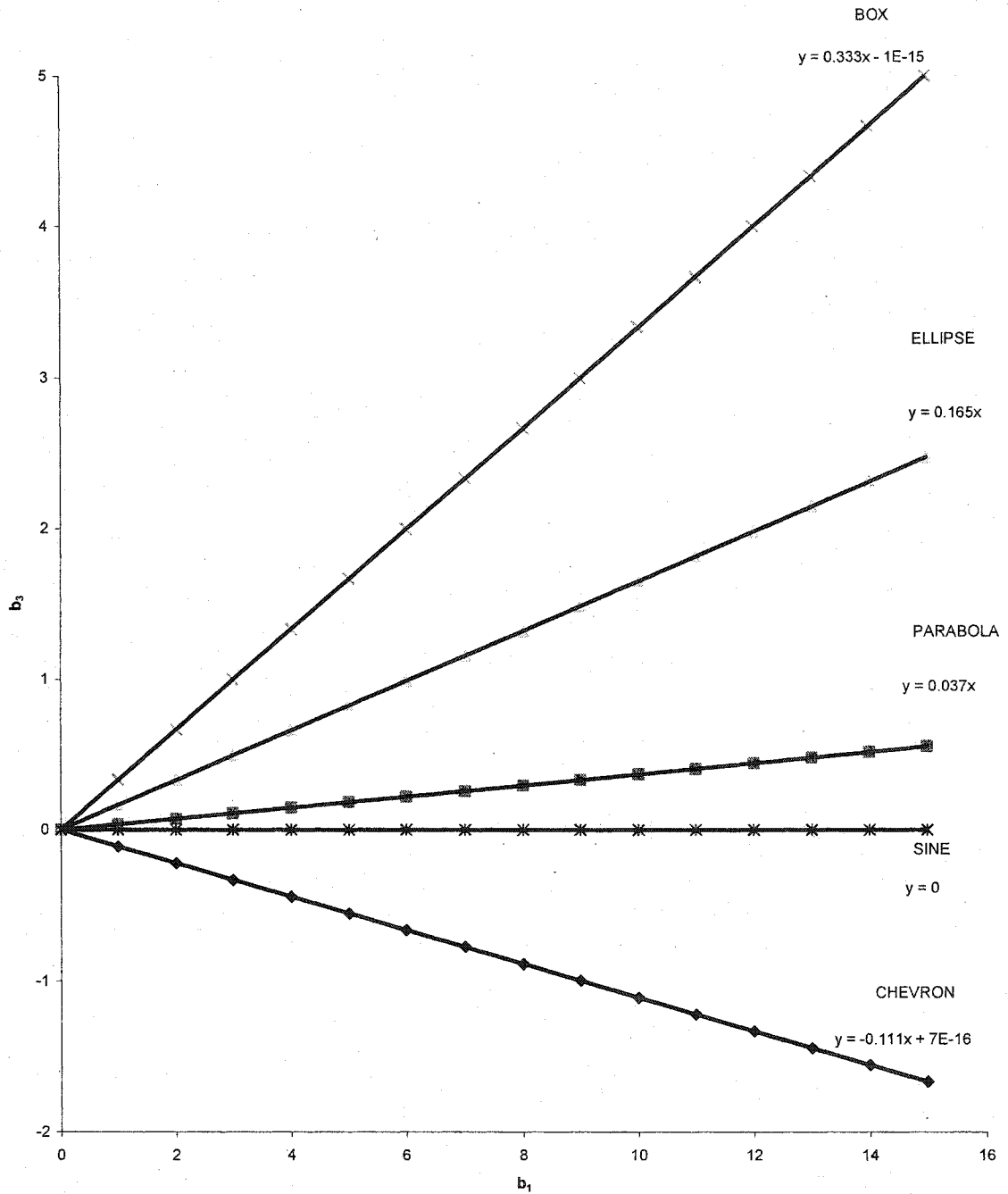


Figure 1.6 - A Cartesian plot of the third b_3 and first b_1 harmonic coefficients. The radiating lines from the origin are equal "shape lines" of the fold classes (adapted from Huddleston, 1972).

Degree of Asymmetry	Shape
DA = 0	Symmetrical
0 < DA < = 4	Sub-symmetrical
4 < DA < = 8	Asymmetrical
8 < DA < = 12	Highly asymmetrical
12 < DA	Extremely asymmetrical

Table 1.1 - Fold classification based on profile symmetry.

Function type	b_3/b_1
Chevron	-0.111
Sine wave	0.0
Parabola	0.037
Semi-circle	0.165
Semi-ellipse	0.165
Box	0.333

Table 1.2 - Ratio of third and first harmonic coefficients for ideal functions (Huddleston, 1972).

The use of this method has three main objectives: 1) Interpret numerically the shape and degree of asymmetry of folds. 2) Extract all possible morphological information of folded rocks exposed on flat surfaces. 3) Compare and recognize the similarities among the folding styles of the MG and the RC. Preliminary results identify a major folding event that affected rocks of the MG and the RC simultaneously, presumably during the Acadian Orogeny (Escamilla-Casas, 2002). The combination of this method with the structural analysis might help to determine and describe the sequence of events that constitute the deformation history of the study area.

Petrography and Microstructural Analysis - The petrographic study of rock samples starts with the proper identification and determination of the mineral assemblages. The chemography and topology are generated qualitatively. Finally, an appropriate projection describing the

metamorphic character of the rocks and the chemical reactions explaining their metamorphism are hypothesized.

A detailed study of micro fabrics in thin sections from oriented samples, the interpretation of kinematic indicators, and identification of deformation mechanisms constitute the core of the microstructural analysis. The description of the deformation mechanisms is based on intracrystalline deformation structures.

Finite Element Analysis and Computer Modeling - The basic materials for this analysis are thin sections from oriented samples containing pyrite crystals embedded in a quartzitic matrix, microphotographs, and digitized maps of the crystals. First, a microphotograph from a thin section is taken and the contour of the pyrite crystal is digitized from the photograph. The digitized map provides a set of coordinates that define the boundaries between the crystal and host rock to be used in the model. The Finite Element analysis (FEA) follows a series of steps (Chandrupatla and Belegundu, 1997; and Ramsay and Lisle, 2000) summarized as follows:

1. The main concept of the FEA relies on the discrete partition; this is the division of the complex model into a large number of smaller parts or elements with simple geometry and mechanical properties. These elements are linked to their adjacent elements at points called nodes. Besides the geometry, the boundary conditions of the model are also divided.

2. The next stage derives, for each particular element, the relationships between applied forces and displacements that define the stiffness of the element. Mathematically, it is a matrix that contains the coefficients of the set of simultaneous equations that relate the displacements to forces at the nodes of the finite element.

3. The calculation of the global stiffness matrix includes the combination of the stiffnesses of all the elements.

4. The setting of the boundary conditions modifies the global stiffness matrix. This stage modifies and simplifies the global stiffness matrix because the boundary conditions restrict the freedom of the body to deform.

5. Calculation of displacements, strains, and stresses. The solution of the global stiffness matrix gives the unknown nodal displacements. Once this is completed, strains and stresses within each element can be found from the differential displacements of nodes.

Rocks from the MG have deformed pyrite porphyroclasts embedded in a fine-grained rock mass. This characteristic can be used to clarify the stages of deformation of these rocks: 1) if the crystals were formed at some time before the last folding event, then the crystals will reflect similar deformation as the folds. 2) If the origin of the crystals is related to the intrusion of Mesozoic dikes, presumably the deformation of the crystal represents the result of the forces and displacements that prevailed at that time.

Computer models reproduce the distribution of displacements and strains in microscopic geological bodies composed of materials with known mechanical properties by numerical simulations of the various deformation stages. The advanced computer-modeling tool of the computational solid mechanics - Finite Element method- will be used for this purpose.

The numerical simulations will try to restore the deformed pyrite crystal into a regular square shape by applying several load cases (combination of tension, compression, and shear). Based on these simulations, a possible deformation history can be assessed.

CHAPTER II

FOLDS

Introduction

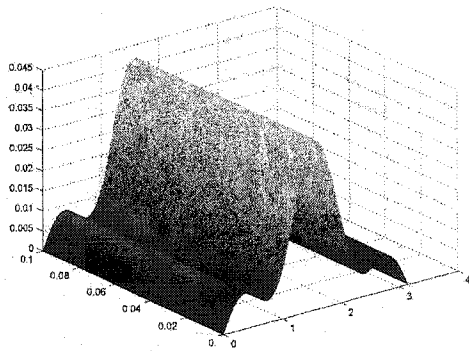
The study of folds involves geometric, structural, and strain analyses, and identifies close similarities in the folded structures along the seacoast region of New Hampshire. This chapter contains the results from the analysis of orientation, shape and asymmetry, the strain analysis of cleavages, and other genetic structures associated with folds and folding in the study area.

The interpretation of these results supports the hypothesis of the existence of a major folding event. It is probable that the folding event occurred during the Acadian Orogeny, and simultaneously affected the RC and the MG. The analysis of the regional geology in Chapter VII discusses the above-mentioned hypothesis in detail and its implication in the regional geology of the seacoast of New Hampshire.

Degree of Asymmetry, Shape, and Attitude

Results - In spite of the different lithology and the mechanical properties of the rocks, the folds in the seacoast region of New Hampshire have topological and structural similarities. A visual description of the fold profiles ranges from tight chevron to sinusoidal folds, and a combination of these two forming a "long-short-long limb" asymmetric pattern (fig. 2.1).

This research uses a variant of the Fourier series analysis (FSA) as a method to analyze numerically the folding style in terms of shape and degree of asymmetry. The FSA gives the coefficients that are necessary to plot three-dimensional representations of the folds.



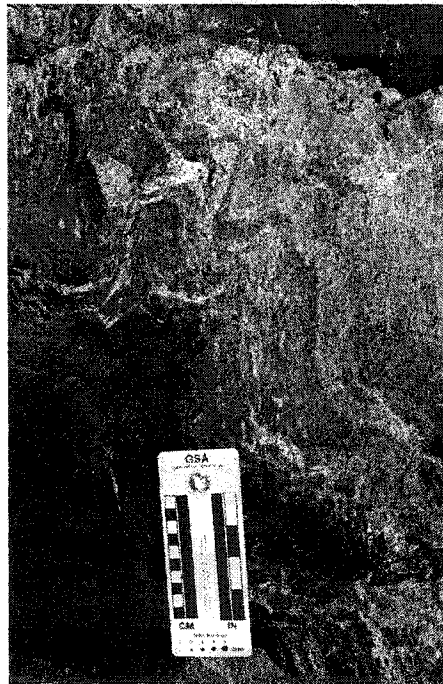
a)



b)



c)



d)

Figure 2.1 - Folds showing the predominant "long-short-long" limb pattern. a) Three dimensional representation; b) folds in the RC; c) and d) folds in the MG. Figure 1.3 and c) are the same.

The MATLAB (Version 6.0) computer program is a useful tool to plot and compare the three dimensional graphics. The application of different approaches (Fourier series, strain, and structural analyses) to the study of folds in the seacoast region recognizes the similarities among them.

The analysis of the fold-shapes in the FSA follows the six categories of Hudleston's classification (1972), which uses b_3 vs. b_1 graphs to plot the shape of each limb of a fold. This study evaluates five to ten folded surfaces for each fold to obtain the values of shape and degree of asymmetry as an average, and uses the FOLDS.BAS program (compiled in BASIC, Appendix 1) to perform the calculations. The distribution of fold samples for testing relies on the occurrence and accessibility to the folds in the field.

Figure 2.2a illustrates a Cartesian plot (b_3 vs. b_1) that groups the fold-samples according to the lithological unit, and following Hudleston's classification; Figure 2.2b represents the folds in a three dimensional space in which the first three harmonics (b_1 , b_3 , and b_5) constitute the coordinate axes. For comparison and classification purposes, Table 2.1 shows the distribution of fold-samples according to the rock unit where they occur, attitude, the results of the FSA (shape and degree of asymmetry), attitude of the axial plane, and vergence.

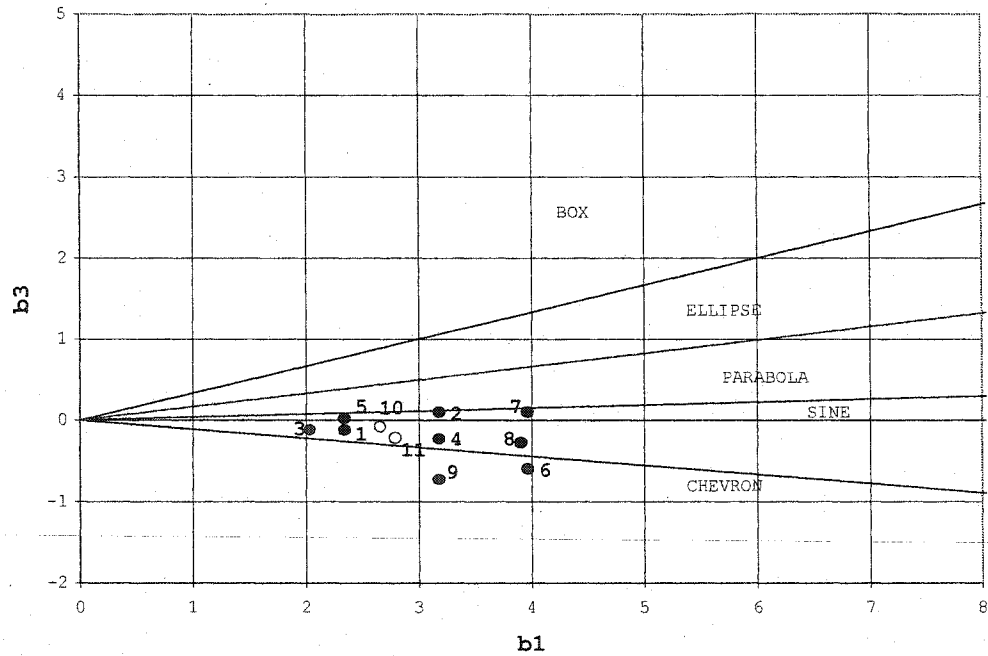
The map in Figure 2.3 displays the stereograms with the attitude of the axial planes and the location of the fold-samples. It is evident that the orientation of the fold axes changes along the study area. The orientation changes drastically from sample location 1 to 8 in the MG, and from 9 to 19 in the RC.

LOCATION (Refer to fig. 8)	UNIT	SHAPE	ASYMMETRY	STANDARD DEV.	No. of SURFACES	ATTITUDE A. PLANE	VERGENCE
Madbury	MG	Sine	4.86	.064	8	218,58	SE
North Hampton	MG	Sine	4.01	.099	6	078,86	SE
Islands G. Bay	MG	Sine	2.56	.097	38	277,54	SW
Scammel B. (N)	MG	Sine	3.78	.332	12	245,50	SE
Scammel B. (S)	MG	Sine	1.49	.035	4	104,89	SW
Adams Point	MG	Chevron	2.98	.045	39	092,90	SW
Furber Point	MG	Chevron	1.95	.032	5	232,73	SE
Fox Point	MG	Sine	2.88	.035	15	092,49	NE
Towle Road	MG	Sine	3.45	.088	75	219,39	SE
Coastline South of Rye Beach	RC	Sine	4.25	.038	58	048,81	NW
Golf Course, N Hampton	Rc	Sine	4.32	.094	39	193,51	SE

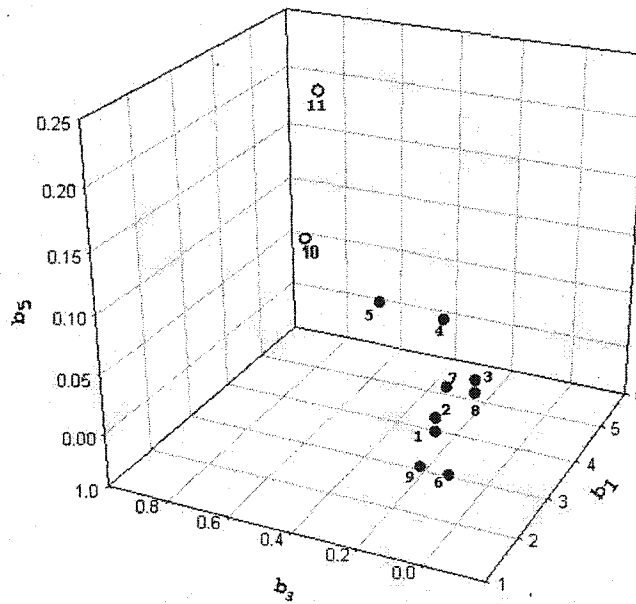
Table 2.1 - Summary of results of the Fourier Series Analysis. Refer to Table 1 in Chapter I for the significance of the shape and degree of asymmetry. The attitude of the axial plane expresses the average value and follows the right hand rule (strike and dip). The vergence expresses the predominant lean direction.

Discussion - The degree of asymmetry varies from sub-symmetrical ($0 < DA < 4$) to asymmetrical ($4 < DA < 8$). The changes in values are due to the amplitude and wavelength of the folds. These parameters are smaller eastwards, where the RC crops out.

The relative amount of competent rocks with respect to the incompetent rocks controls the shape of the folds in the MG. The turbiditic sedimentation that is characteristic of the MG and the exposure of half wavelengths in the outcrops permit the estimation of the ratio of competent to incompetent rocks (n-value, Ramsay and Huber, 1987) along the area of influence of the folds.



a)



b)

Figure 2.2 - a) Classification of fold shapes according to Hudleston's classification. b) The three dimensional plot of the first three odd terms in the Fourier series representing the folds. The solid circles correspond to the MG, open circles to the RG. Refer to Figure 8 for locations. 1 Madbury, 2 North Hampton Beach, 3 Great Bay islands, 4 Towle Road, 5 Scammel Bridge (N), 6 Adams Point 7 Scammel Bridge (S), 8 Fox Point, 9 Furber Point, 10 Golf Course - North Hampton, 11 Coastline south of Rye Beach.

The shape of all the folds ranges from sinusoidal to chevron, and in the MG, particularly near the Scammel Bridge, at Adams Point, and at Fox Point the n-value is strongly related to the shape of the folds, the higher values (.35 - .25) correspond to the chevron folds, and the lower (.05 - .085) to sinusoidal folds (fig. 2.3, locations 2, 3, 4, and 6, and fig. 9).

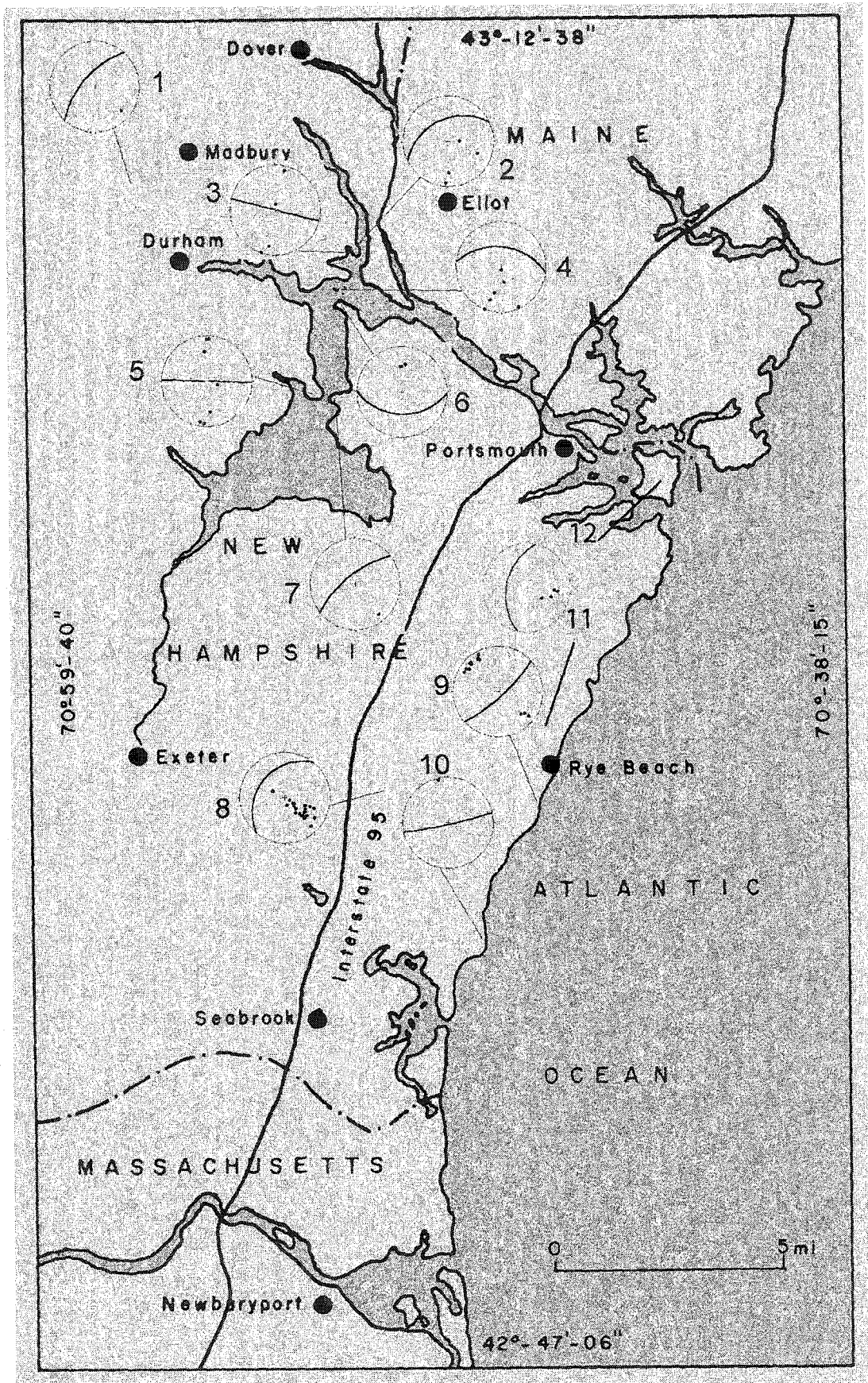
Folds at Towle Road (fig. 2.3, Location 8, MG outcrop) and at Rye Beach (Location 9, RC outcrop) are the best exposed folds in the area. The accessibility to the outcrops permits the study of the structures in three dimensions.

These locations are very important in terms of correlation of structures between the RC and the MG for three reasons: First, each location is representative of a unit. Second, the strong similarity in the attitude, shape, degree of asymmetry of the folds is remarkable. Third, the proximity to each other permits a reliable correlation of structures.

Besides the recognition of the similar topology of the folds in the MG and the RC, it is possible to identify linear structures such as crenulations and lineations parallel to the fold axes. The orientation of fold axes and associated lineations are predominantly parallel in both units (fig. 2.5).

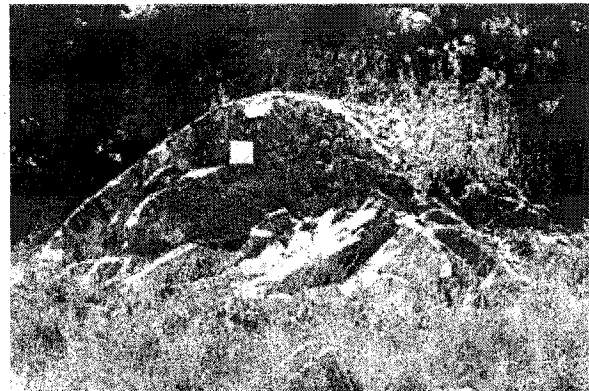
It is noticeable that the plunge of the axis and related lineations varies similarly in both units. The following two sections (Fold Mechanisms and Superposed folding) explain thoroughly the interpretation of the possible origin of this effect.

Figure 2.3 - Sample location map of folds showing the stereographic projection of the axial planes (points represent the poles to the axial planes (n), the great circle represents the mean direction of the planes). Single numbers represent locations. Locations are as follows: 1) Madbury, n = 2; 2) Scammel Bridge north, n = 4; 3) Scammel Bridge south, n = 4; 4) Islands in the Great Bay, n = 7; 5) Adams Point, n = 7; 6) Fox Point, n = 3; 7) Furber Point, n = 1; 8) Towle Road, n = 27; 9) Coastline south of Rye Beach, n = 15; 10) North Hampton Beach, n = 1; 11) Golf Course, N. Hampton, n = 5; 12) Gerrish Island.





a)



b)



c)

Figure 2.4 - Fold shapes in the MG; a) a chevron fold and c) a sinusoidal-chevron fold are from the Adams Point Area (location 5, fig. 2.3); b) is a sinusoidal fold from the south portion of the Scammel Bridge (location 2, fig. 2.3). Folds with shapes close to a sine wave have less incompetent layers. The direction of view in all the photographs points to the west. In b), an open field book was used for scale.

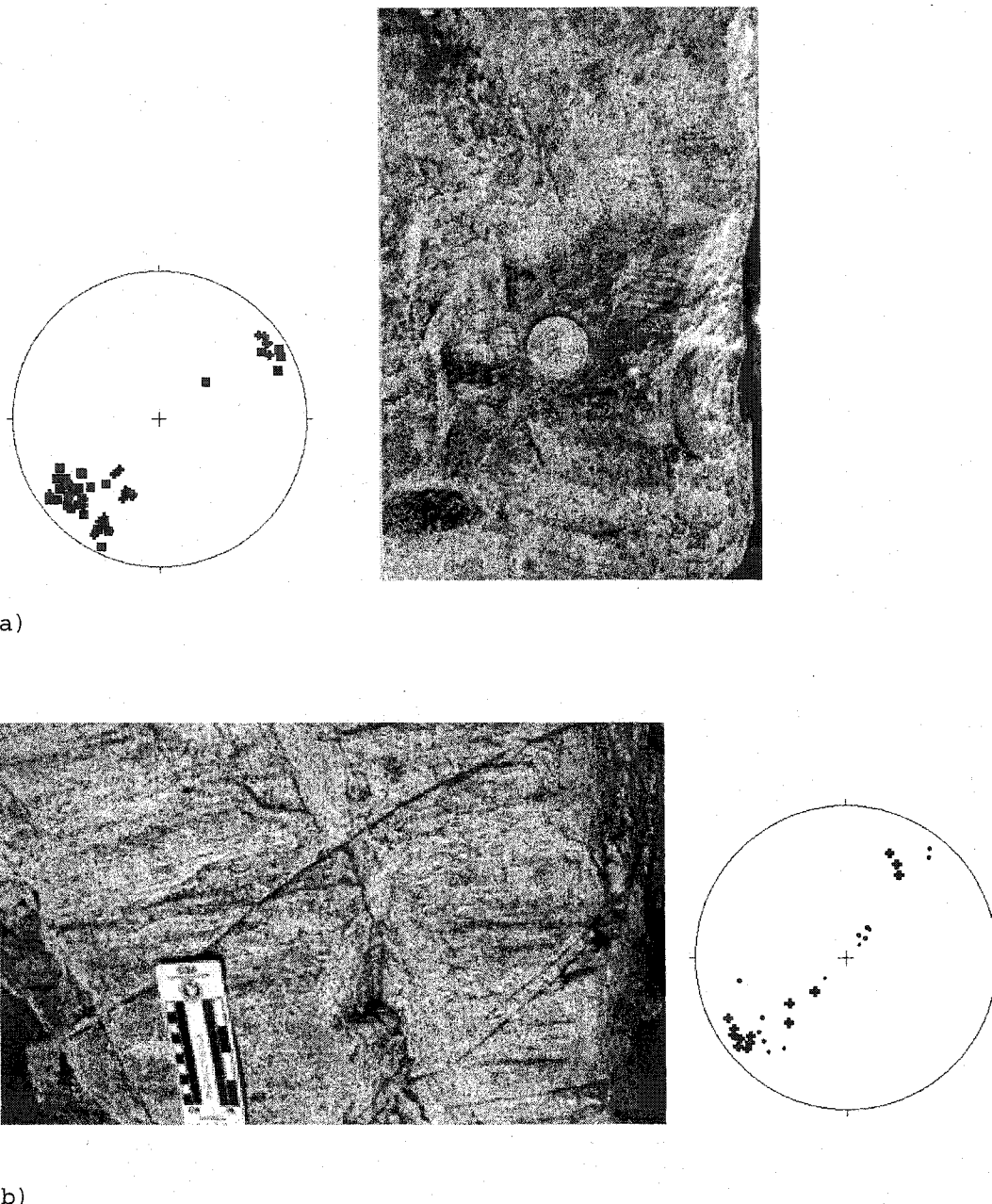


Figure 2.5 - Stereograms and outcrop photos at locations 8 (a) and 9 (b) in the MG and RC, respectively (see fig. 2.3 for locations). a) The stereogram at the left shows the attitude of fold axes and lineations (squares (n=28), and crosses (n=24), respectively). The photograph at the right shows a set of crenulations on a bedding plane in the MG, location 11. b) Photograph of lineations at location 9 (oldest structures) the stereogram at the right shows the attitude of the fold axes (n=20) and lineations (n=14), (dots and crosses, respectively).

Fold Mechanisms

Current theories of fold mechanisms consider four kinematic models to explain the tectonic folding of rocks in nature (Donath and Parker, 1964, Hudleston, 1991; Hudleston, et al., 1996, Stallard and Hickey, 2001). The mechanisms describe folding and related structures as they occur in a single layer, within the layers, between the layer planes, and in sequences of layers (multilayer fold). A brief description of these mechanisms follows:

The tangential-longitudinal strain model attributes the formation of folds to a body rotation of the limbs, and considers all the accumulation of the strain within the folded layer as coaxial. Ramsay (1967, p.397) defines this model as a pattern in which the axes of the strain ellipses on the fold profile are tangential and normal to the layers.

In this type of folding, the concentration of the maximum strain occurs at the hinge, and it is null at the inflection points (fold limbs). Furthermore, this mechanism applies extension to the outer arc and compression to the inner arc of the fold; it also generates a neutral surface that delimits the boundary between extension and compression. Along the fold hinge, the extension causes shortening, and likewise, compression causes extension. The combination of these mechanisms generates a flexure that is orthogonal with respect to the former fold.

The theory of solid mechanics explains this kind of effect in terms of stresses due to bending and denotes it as anticlastic bending. The geometry of a deformed cross section and the two curvatures are visible if a large rubber eraser is bent (fig. 3 - Appendix 2). A brief mathematical derivation that explains the orthogonal bending due to folding and its relation to Poisson's ratio is in Appendix 2.

The pure shear-folding model considers a pre-existing deflection, and it is the result of passive amplification by homogeneous coaxial shortening. This mechanism controls folding in areas where there is not a significant difference in the mechanical properties of the folded rock. Therefore, it is most likely to occur in rocks where the metamorphic grade is high.

The flexural slip-folding model involves the slip of upper beds over lower beds towards the anticlinal axis during folding of regularly bedded rock sequences (i.e., turbidites), and the distribution of simple shear is discontinuous along the fold. This model represents an important mechanism for the formation of chevron folds.

The flexural flow folding model considers a continuous distribution of simple shear along the fold. The maximum strain concentrates at the inflection points on the limbs and decreases towards the hinge. This folding mechanism takes place in mechanically very high anisotropic rock layers (i.e., with laminations, banding, mineral fabric). This model assumes no distortion in the plane of the folded layer.

Folded rocks may result as a combination of more than two mechanisms. The intensities of the mechanisms and the combination of them depend on the mechanical properties of the rocks and the external forces. Nevertheless, folding mechanisms may change as the fold develops.

Results - The MG crops out along the Great Bay where the accessibility to the outcrops permits the study in detail of beds, fold hinges, and limbs. Often, the mechanisms of folding imprint unique and characteristic structures on the rocks. Structures related to folds are less discernible along the coastline, where the RC dominates the outcrops, but some folding mechanisms are still distinguishable.

Chapter IV contains the description of the deformation mechanisms in the RC and the MG from microstructural point of view.

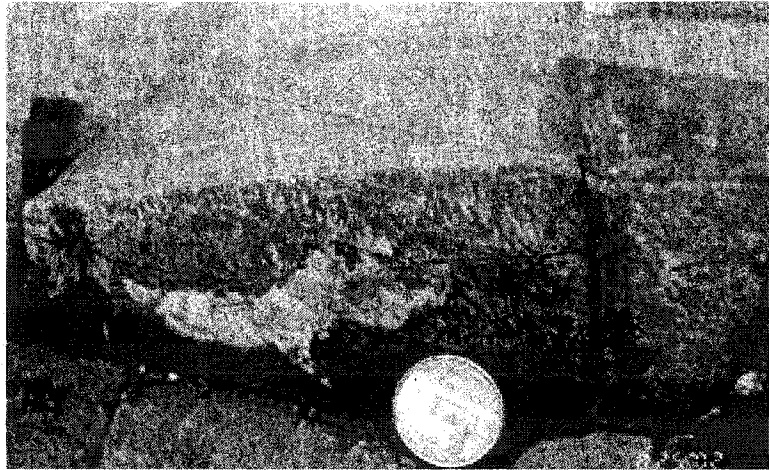


Figure 2.6 - Quartz and calcite "slickensides" revealing the relative displacement of the layers. Location 5, fig. 2.3.

Folds in the seacoast region present strong variations in the plunge direction of the fold axes. Rickerich (1983) and Willard (2000) observed the discontinuity of folds along the fold axis and the merging of fold couplets in the plunge direction in the MG, in the Portsmouth area and at Adams Point, respectively. Escamilla-Casas (2002) reported a change in the plunge direction of the fold axes in the RC along the coastline, and in the MG at Towle Road, North Hampton (fig. 2.5a).

Willard (2000) illustrated the relative displacement of quartz veins across folded beds as structures associated with flexural flow folding at Adams Point, where the MG crops out (fig. 2.3, Location 4). In the same area, the author observes concentrations of quartz and calcite similar to slickensides, along bedding planes, that are commonly sub-perpendicular to the fold axes (fig. 2.6).

Cleavages in the Adams Point area are mostly axial planar, parallel to bedding, and oblique to bedding. The axial planar cleavage is present in most of the folds and it is the principal cleavage. The

cleavages that are parallel and oblique to bedding, where present, are mostly concentrated along the limbs, and in some folds it is difficult to make a distinction between the two. Willard (2000) also reported the presence of these cleavages.

Discussion - This study presents three possible explanations for the changes in the attitude of the fold axes; one might be the anticlastic bending due to tangential longitudinal strain (fig. 2 - Appendix 2). The second explanation attributes the formation of boudins after the development of folds due to the increasing compressional stresses (axial planar normal compression, fig. 2.7).

Hypothetically, if the same compressional stresses affected the RC and the MG, those stresses generated the boudins in the RC at a later stage; and some extensional features must exist in the MG. The presence of undulations on the fold limbs that are oblique to the general trend of the fold axes supports the hypothesis that extensional stresses affected the MG. Furthermore, the strike of the crosscutting planes along the short axes of the boudins in the RC, which is also oblique to the general main foliation, is mostly parallel to the strike of the axial planes of the undulations oblique to the fold axes in the MG (fig. 2.8).

A third explanation considers a combination of the previous two, and it is the most plausible. Before the formation of boudins takes place, an interruption in the continuity of the media must occur (Mandal et al., 2000).

At the beginning of the process, the anticlastic bending produces the interruption of the media. It later induces the formation of boudins as the compressional stresses increase, and the deformation progresses. The principal stresses were mostly coaxial through the

entire deformation event, this is, the folding process and the formation of boudins.

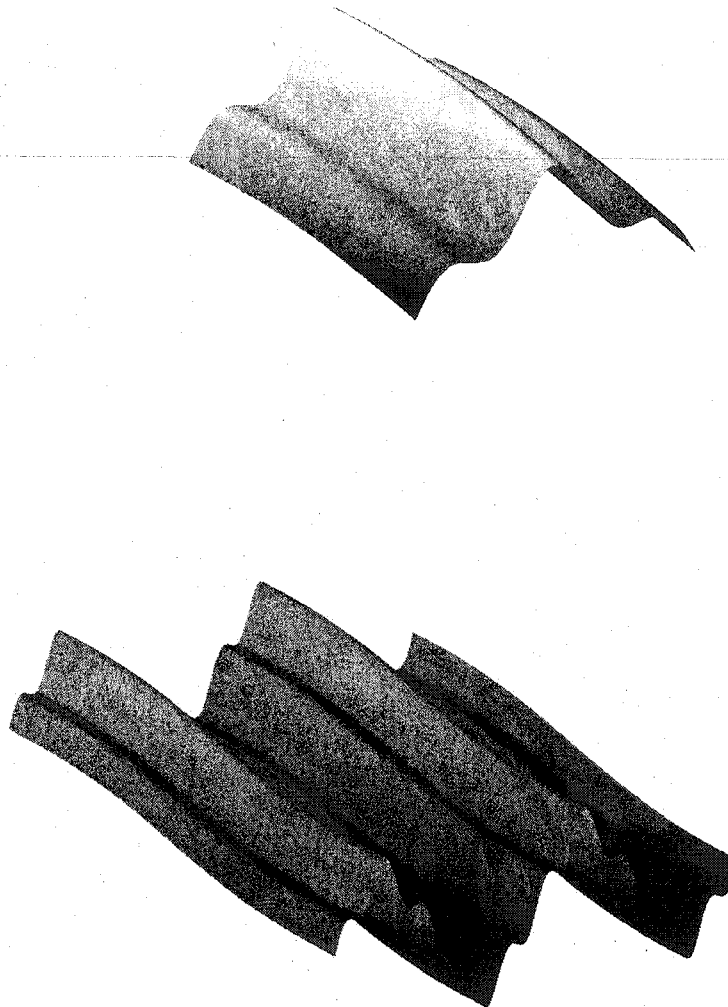
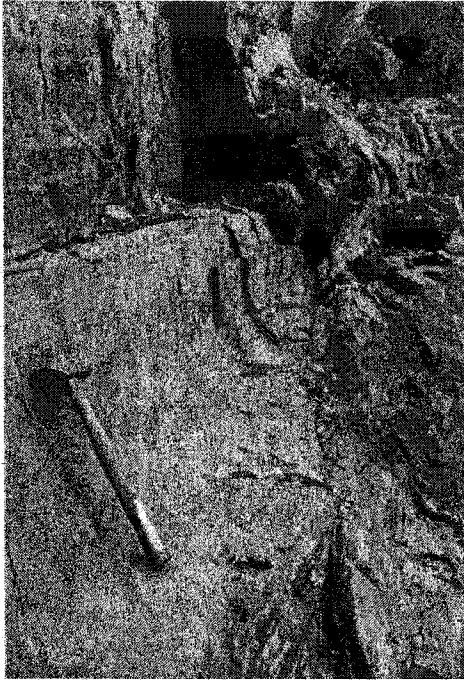
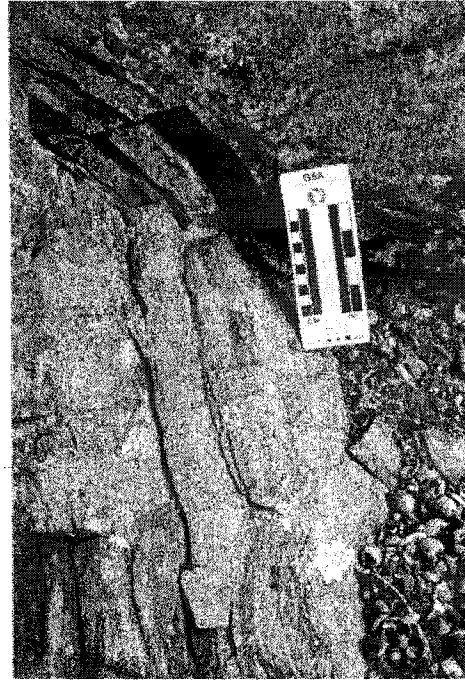


Figure 2.7 - The upper section of the graphic representation of boudinage after folding on a single layer fold (top) and a combination of anticlastic bending and boudinage after folding (bottom). The oblate shape in the top representation differs from the elongated shape in the bottom.

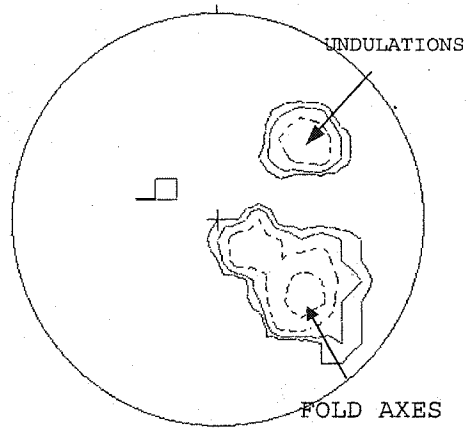
Figure 2.8 - Illustration a) shows the undulations oblique to the fold axes; b) is a view from top of the undulations; c) A stereographic projection of the axial planes of the folds and the axial planes of the undulations (poles) (location 8, fig. 2.3); d) shows the strong foliation and boudins in the RC (location 9, fig. 2.3). The axial planes of the undulations are almost perpendicular to the axial planes of the folds in the MG. In the RC the strike of the short axes of the boudins, make an angle of 80 - 90° with respect the strike of the main foliation.



a)



b)



c)



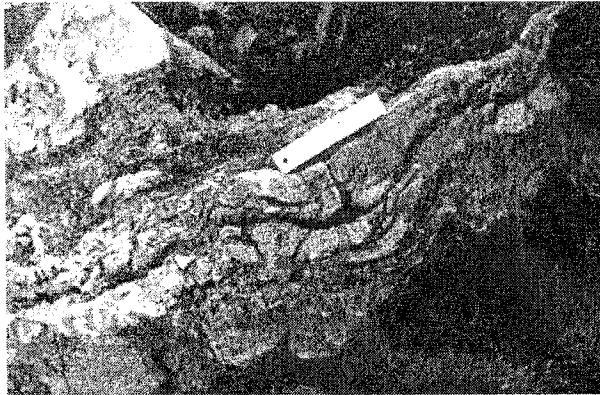
d)

The concentrations of calcite and quartz are structures that act as kinematic indicators that reveal the direction of the relative motion of the layers (flexural slip), and where the hinges are not exposed, they help to infer the location of the maximum amplitude of the fold. Where the hinges are observable, the relative displacement imprinted in the concentrations (as slickensides) coincide with the kinematics of the fold. Therefore, the structures of this kind are associated to folding.

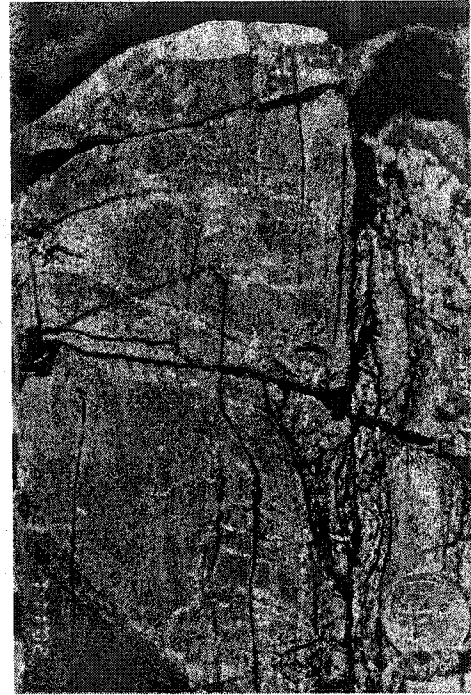
The combination of the flexural flow and the flexural slip is likely to be the principal folding mechanism in the MG at Adams Point. The combined mechanism possibly formed strong parallel-to-bedding cleavage and "accommodation" structures (fig. 2.9).

The presence of a cleavage parallel to bedding and an axial planar cleavage in the same fold suggest at least two different mechanisms. The following strain analysis illustrates this hypothesis (assuming the same type of rocks in each case): In Figure 2.10, the top illustration represents a sequence of layers before folding. The illustration at the bottom shows the finite deformation after folding. In Figure 2.11, the upper and lower illustrations represent the same sequence of rocks after folding; they have the same shape and degree of asymmetry (ideal chevron folds) but have a different deformation history as reflected by a different wave length.

The conditions of folding assumed for each case are: 1) the folds in the upper illustration are the result of deformation consisting of heterogeneous simple shear. 2) The folds in the bottom illustration resulted from a combination of heterogeneous simple shear and homogeneous plane strain, where the orientation of the principal strain directions is parallel and perpendicular to the axial planes.



a)



b)

Figure 2.9 - Structures in the MG related to the flexural flow and flexural slip mechanisms of folding. a) shows deformation of the incompetent beds, the direction of view points to the east. The scale is 10 cm long (location 7, fig. 2.3). In b), bedding strikes 265° and dips 85° . The axial plane of the upper fold of the box fold strikes 249° , dips 50° , the axis trends 255° , and plunges 12° . The direction of view is to the west (location 3, fig. 2.3).

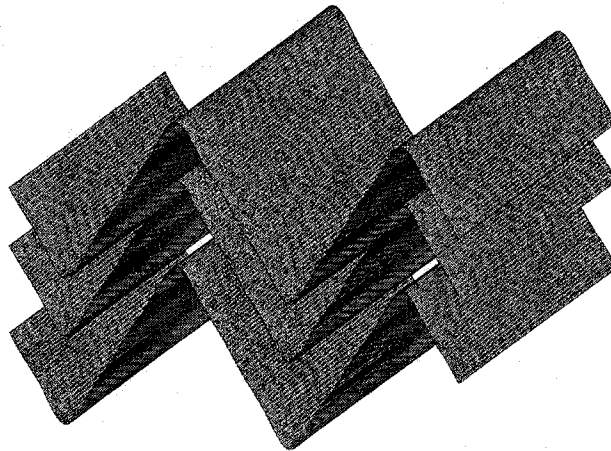
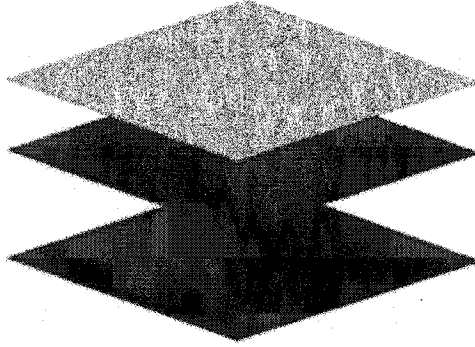
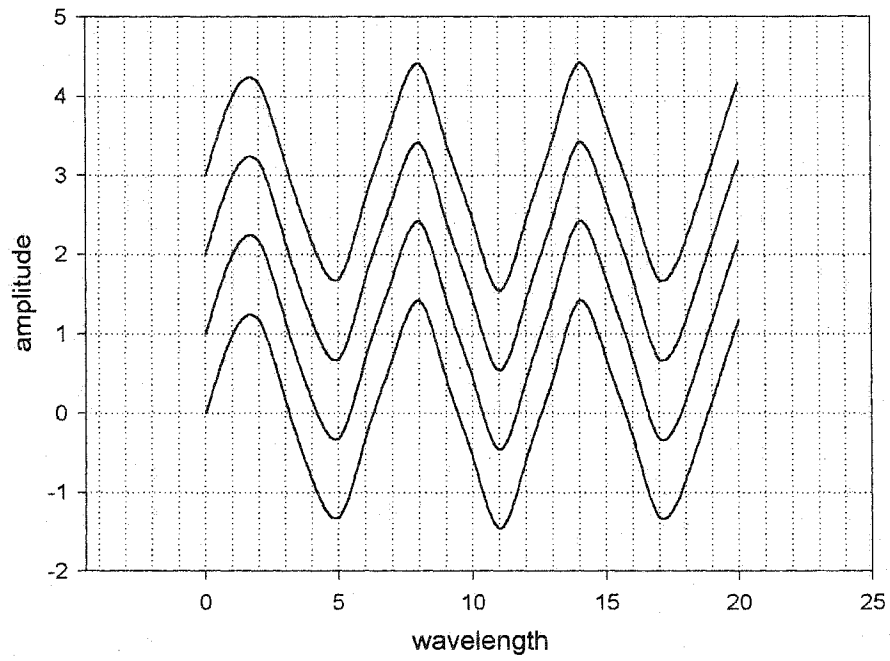


Figure 2.10 - Graphic representation of folding. The upper drawing shows a set of parallel planes representing layering. The lower illustration represents the same set of "layers" after folding. The shape of the folds corresponds to an ideal chevron fold.

Ideal Chevron Folds I



Ideal Chevron folds II

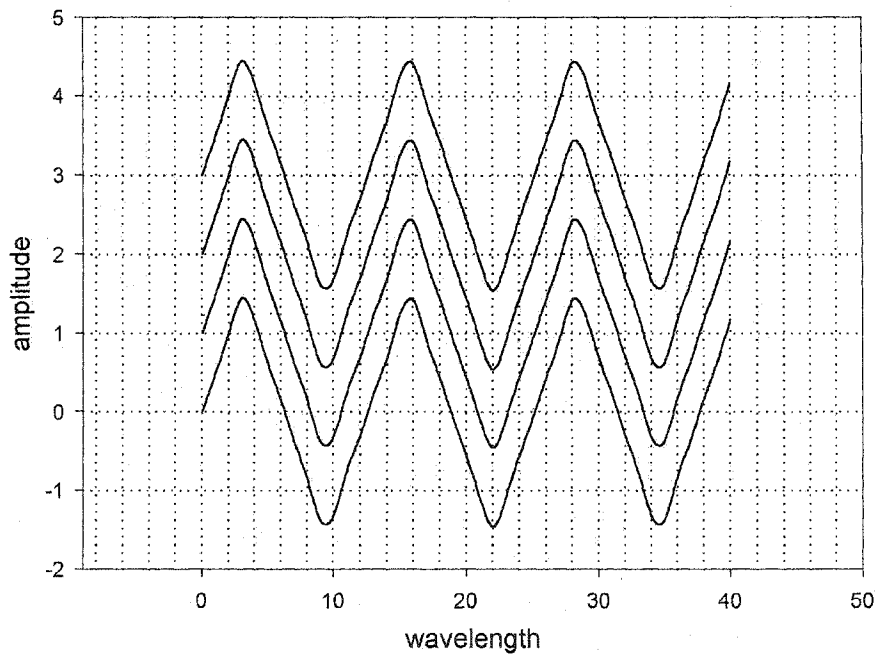


Figure 2.11 - Plots in an x - y space of ideal chevron fold profiles. Both fold-cases have similar shape and degree of asymmetry. Note change in horizontal scale.

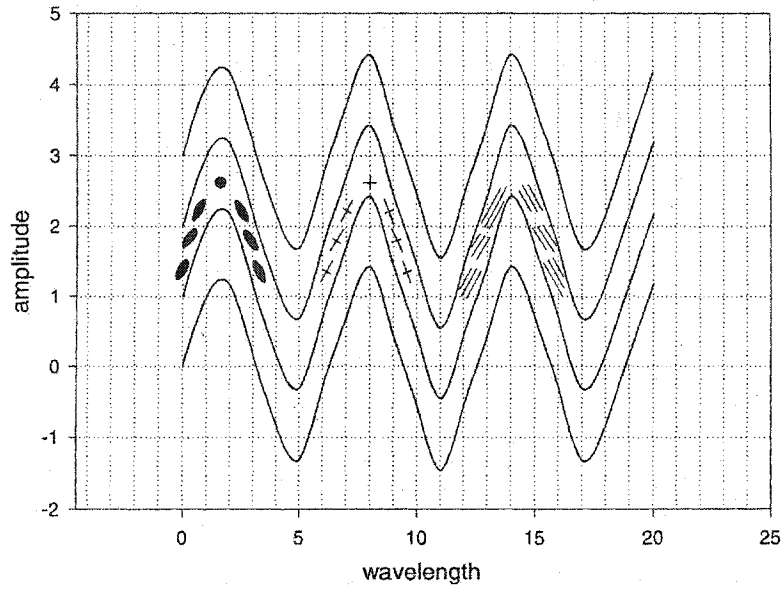
A plot of each fold profile in the x-y coordinate system with a reference grid provides the workspace for the geometrical analysis. Before folding, a set of coordinates defines the intersection of the bedding planes with the grid lines parallel to the y-axis. After folding, a new set of points defines the intersections.

The transformation of coordinates is necessary to evaluate the net displacement (displacement gradient matrix) of the points after folding. There are two ways to calculate the displacement. One considers the final set of coordinates as a frame of reference, and the other uses the initial set, they are the Lagrangian and Eulerian transformations, respectively.

Ramsay (1982) explained a method to calculate the strain data. The mathematical procedure that illustrates the strain direction field for each fold-case essentially follows Ramsay's method. Appendix 3 describes the calculations step-by-step. Figure 2.12 shows the orientation of the strain direction field (strain ellipses), the strain trajectories (intersections of the short and long axes of the ellipses), and the direction and concentration of cleavage along the fold.

The upper illustration shows the formation of one cleavage under heterogeneous simple shear as a mechanism of folding, and it is parallel to the long axis of the strain ellipses. The development of the cleavage occurs mostly in the limbs where it is subparallel to the bedding planes and shows a fanning structure. The same figure has a circle on the hinge where there is no strain in such location of the fold.

Ideal Chevron Folds I



Ideal Chevron Folds II

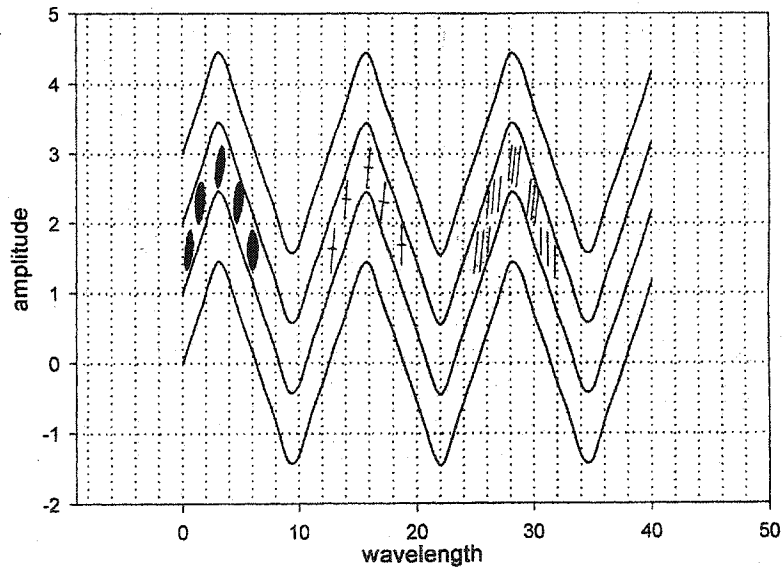


Figure 2.12 - Graphic representation of the results of the strain analysis of chevron folds. In each fold case, the first positive half wave-length represents the orientation of the strain ellipses, the second the principal axes, and the third the orientation of the resulting cleavages. Horizontal scales same as Figure 2.11.

The combination of heterogeneous simple shear and homogeneous plane strain produces a strong cleavage that is almost parallel to the axial plane of the fold (lower illustration in fig. 2.12). In spite of the same shape and degree of asymmetry, the two different types of cleavages reveal a different sequence and conditions of deformation for each set of folds.

In nature, depending on the intensities of the stresses, the mechanical properties of the rocks, and in time, the two cleavages may occur in the same fold. It is also possible that the later mechanism will deform or eventually erase the first cleavage.

The above example allows for the possibility that the deformation of an initial cleavage is not necessarily the result of a later folding event. Multiple cleavages may result from a single folding event in which the mechanisms of folding changed as it developed. These cleavages may be the consequence of a set of folding mechanisms possibly acting in a similar way as illustrated in the previous example.

Due to the scarce outcrop and the lack of a strict stratigraphic control of the units in the MG, it is difficult to establish a rigorous cleavage correlation. Consequently, it is valid to consider that all the deformation mechanisms may be part of the same folding event.

This research considers two assumptions regarding folds. First, that a folding mechanism is a discrete component of a folding event. Second, a folding event is an independent deformation that has its own distinctive genetic mechanisms including the orientation of stresses, folding style, and related structures.

These assumptions contribute to the integration of a model that explains tentatively the sequence and mechanisms of deformation of the

major folding event. The discussion of this model constitutes part of Chapter VII regarding the overall conclusions.

Superposed Folding

This study recognizes structures related to the mechanisms of a strong deformation that produced a similar folding style in the MG and the RC. Reasonably, the mechanisms are part of a progressive deformation, which may involve folding of initial buckled layers and/or primitive folds as it evolved. Hypothetically, the occurrence of two or more folding events acting in the same set of rocks will cause some degree of interference pattern.

Geometric models of interference patterns of folded folds consider two sets of folds with constant shapes and, in some cases, similar types of folding. The orientation of the initial set of folds with respect to the second strongly influences the geometry of the pattern in two and in three dimensions. There are two current classifications of interference patterns (Ramsay, 1962, 1967; Thiessen and Means, 1980); one is subdivided into three categories and the other five.

Results - Table 2.2 summarizes the field observations of interference patterns and relates them to the two current classifications. In general, the interference patterns are often troublesome to identify especially if the topologies of the two sets of folds are almost parallel to each other (coaxial folds).

Discussion - Only three locations display interference patterns, and their geometry reveals that they are the product of a coaxial deformation where the orientation of the second set of folds is parallel to the first (fig. 2.13). It is unlikely to have two strong folding events with a parallel orientation with respect to each other reflected on the resulting finite deformation and at a regional scale.

Such deformation implies the same orientation of stresses for the two folding events. If the amount of time between the first and the second stages of deformation is great, then the mechanical properties of the rock might change after the first event, and the orientation of stresses is unlikely to be the same for both events.

Furthermore, the preservation of primary sedimentary structures in the rocks of the MG containing interference patterns suggests that a restricted later deformation (not folding) deflected the first set of folds. Besides these few locations (see Table 4) no other place has an observable pattern in the remainder of the study area. The presence of interference patterns with coaxial geometry supports the hypothesis of the existence of a main folding event that experienced a subsequent local deformation.

A viable explanation of the genesis of the patterns is that they are the product of a later deformation that locally deformed the folds, and it is feasible that it is not related to a later folding event in a strict sense. It is possible that the deflection of the original folds resulted as part of the shearing inherent to a regional faulting (perhaps attributable to the Norumbega Fault?).

The model in Figure 2.12d illustrates the above-mentioned idea, and represents a folded surface with a strong variation in the orientation of the fold axes. According to this model, after folding, the folds were deformed along a strike slip displacement with a relative minor vertical component (mostly shear).

The separated blocks containing the folds with initially parallel axes, are displaced relatively to each other along discrete shear bands. The deflection is stronger nearest the zone of maximum of strike slip displacement, and it is less noticeable towards the middle of the shear bands, as it occurs in natural shear zones.

RAMSAY CLASSIFICATION	GEOMETRIC CHARACTERISTICS OF THE PATTERN	LOCATION
TYPE 1	Domes and basins	Not found
TYPE 2	Crescent mushroom and tree like forms	Not found
TYPE 3	Hook pattern	2, 11, and 12

THIESSEN & MEANS CLASSIFICATION	GEOMETRIC CHARACTERISTICS OF THE PATTERN	LOCATION
Type 0-1	$\alpha = \beta = \gamma = 90^\circ$	Not found
Type 0-2	$\beta = \gamma = 90^\circ$; $\alpha \neq 90^\circ$; noticeable changes in the amplitude and wavelength	1,3,4,5,6,7,8,9, 10.
Type 1	$\gamma + \alpha = 90^\circ$; basin and dome	Not found
Type 2	$\alpha = 90^\circ$; $\beta = 0^\circ = \gamma$; repeated sine wave	Not Found
Type 3	$\gamma = 90^\circ$; hook pattern	2, 11, and 12

Table 2.2 - Types of interference patterns according to the current classifications (Ramsay 1962, 1967; Thiessen and Means, 1980). The column in the extreme right gives the locations in the study area (refer to fig. 2.3).

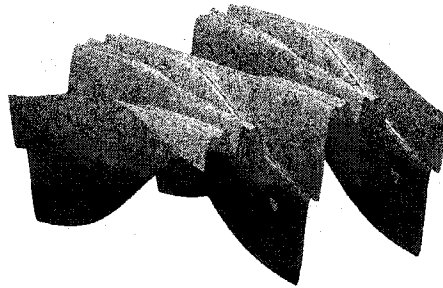
The results of the analyses of folds in this area reveal that there is one major folding event (responsible for the generation of similar types of folds in the MG and the RC) and that at least two stages of deformation with horizontal shear components are attributable to the GCFZ and the PFZ. The combination of mechanisms constitute a transpressional regime; this is, folding by compression and strike slip faulting.



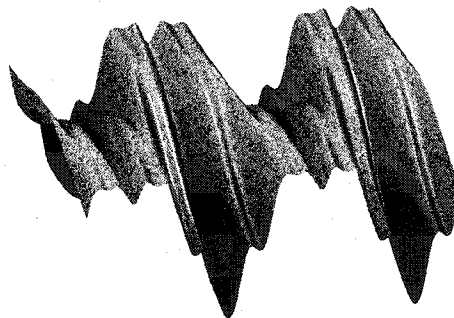
a)



b)



c)



d)

Figure 2.13 - Interference patterns in the study area; a) corresponds to location 12, b) to location 11 of Figure 8. c) and d) is a set of graphic representations of folding and shearing along discrete "shear bands" mimicking folds in a).

CHAPTER III

FINITE ELEMENT ANALYSIS OF PYRITE CRYSTAL DEFORMATION

Introduction

The Finite Element Analysis (FEA) is a numerical technique that helps engineers and scientists to design and analyze mechanical and physical systems involving solid mechanics, fluid mechanics, electromagnetic flux, and heat transfer. During the past decade, the application of FEA has been extended to solve geologic problems (e.g. Ramsay and Lisle, 2000).

In this study, FEA is used to test two working hypotheses: (1) to investigate if the deformation history recorded in pyrite crystals is associated with the fold that contains them (transpressional regime), and (2) that the deformation of pyrite crystals is related to the emplacement of later diabase dikes (extensional regime).

The area chosen contains both folds that are part of the major folding event, that affected the rocks of the Merrimack Group and the Rye complex (discussed in Chapter 2), and crosscutting Mesozoic dikes. Furthermore, the application of FEA will provide a test of its effectiveness in extracting critical information on the deformation of rocks at a micro-scale in making regional interpretations.

The cubic crystallographic form is the most common crystal shape of pyrite crystals. This study assumes regular cubes as the crystal shape of the pyrites before deformation. The above-mentioned assumption allows the attempt to simulate the possible deformation

path by the reconstruction of deformed crystal shapes into regular squares (sections of the regular cube).

The objective of the FEA simulations is to define the stages in the deformation history that resulted in the deformed shapes of pyrite crystals. The inverse approach to this problem is chosen: a set of controlled load cases is applied to the distorted crystal in order to reconstruct the regular squared shape.

The applied forces are modeled as combinations of shear, compression, and extension. The numerical simulations were performed using *MSC.Marc/Mentat* computer program (www.marc.com). This commercially available finite element package is widely used to model deformation of solids under various loading conditions, as well as to analyze other physical phenomena. The finite element models of deformed crystals were developed in *MSC.Mentat* using data obtained from microphotograph processing.

In the analysis, inherent geometric features of regular squares are used as parameters for comparison and evaluation of the models. These features are the eccentricity e , and "squareness" s :

$$e = \frac{L_1 + L_2}{L_{s1} + L_{s2}} \quad (3.1)$$

where L_1 and L_2 are the long sides, and L_{s1} and L_{s2} are the short sides of the quadrilateral;

$$s = \sqrt{\frac{1}{4} \sum_{n=1}^4 (\alpha_n - 90)^2} \quad (3.2)$$

where α is the internal angle of each corner of the quadrilateral expressed in degrees. Note that $e=1$, $s=0$ corresponds to a perfectly squared shape. Thus, any deviation from these values characterizes deformation of the crystals.

Sample Preparation

This study analyzes nine micro crystals embedded in a dark brown rusty weathering metasandstone from the south limb of an asymmetric anticlinal fold at Towle Road, North Hampton (fig. 3.1). Slicing out the external surface of the sample was performed to avoid the effects of weathering in the analysis.

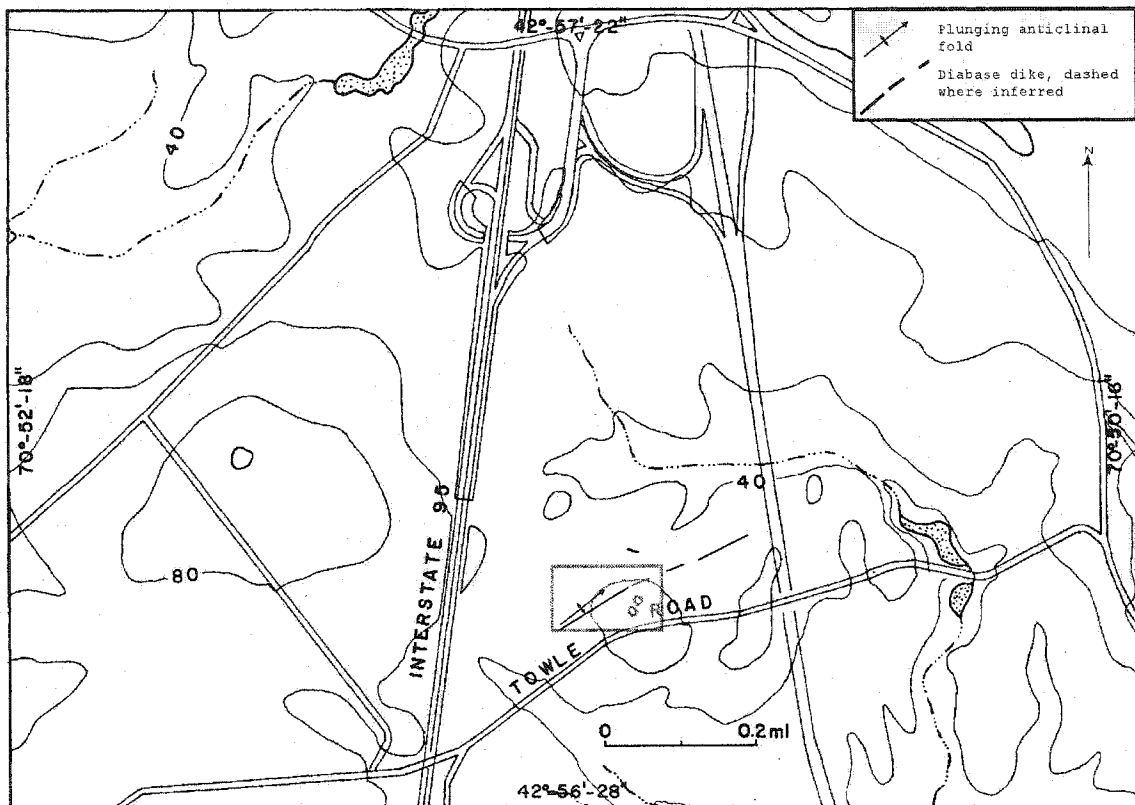


Figure 3.1 Map showing the sample location (area in square).

Figure 3.2 represents the relative position of the exposed fresh surface where the blanks for thin sections were obtained. The fresh surface strikes 28° and dips 84° to the south (parallel to the attitude of the fold limb).

The preparation of the thin sections follows the traditional method in petrography, except that the thickness is greater than 30 microns. The

extra thickness protects the pyrite crystals from over grinding and polishing.

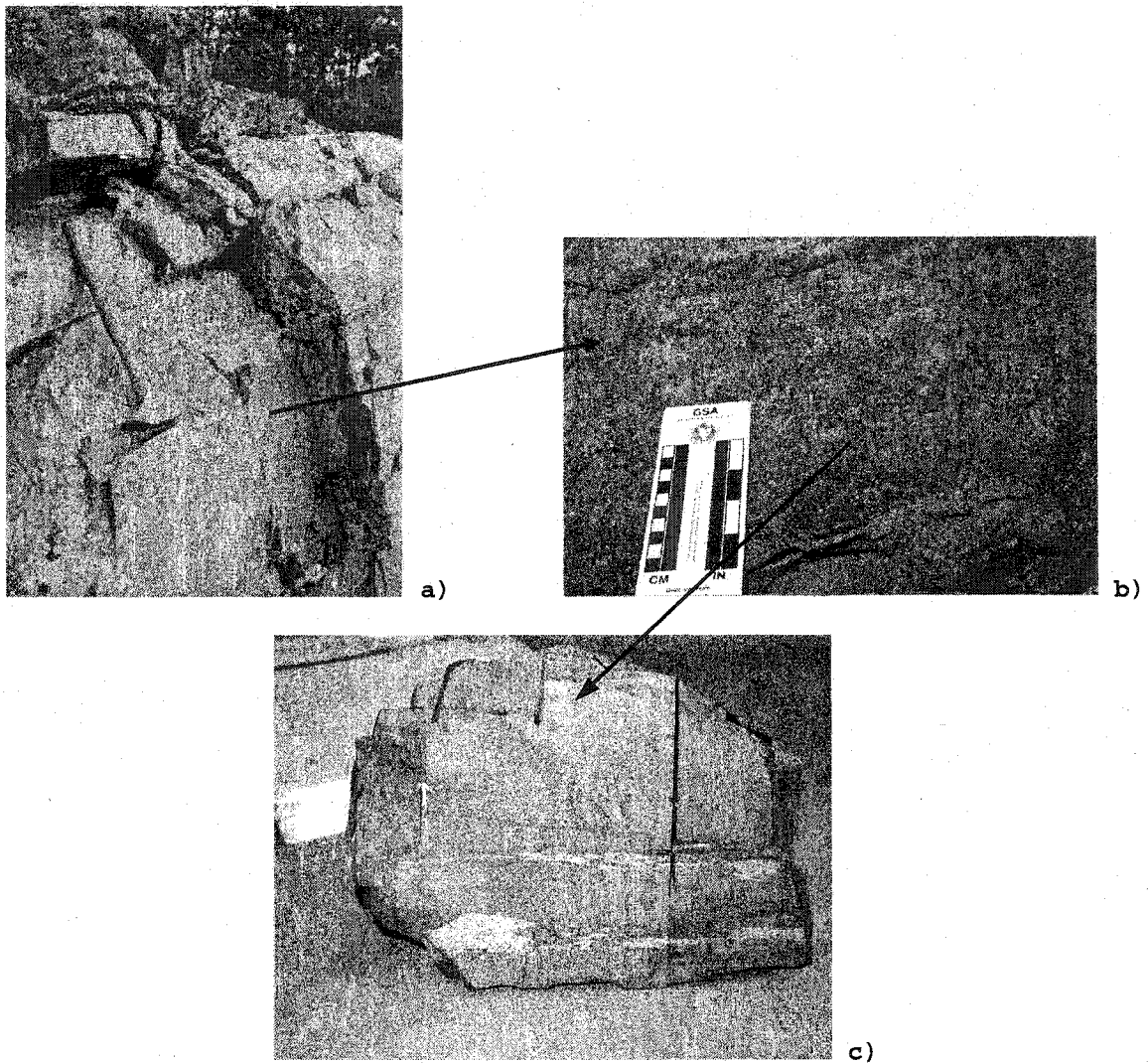


Figure 3.2 Illustrations showing a) general view of the folded structure, b) the limb from where the sample was obtained, and c) the sample for thin sectioning. The hammer is about 40 cm long and the sample has an area of 30 cm² approximately.

Microphotographs of the thin sections and a digitizing table were used to obtain the set of coordinates that define the contour of the crystals and their orientations. The set of coordinates is critical to define the geometric center of the model, the configuration of the finite element mesh, and the relative dimensions of the model crystal

to host rock. For orientation purposes, the upper edge of all models coincides with the upper surface of the sample. The direction of view of the photographs and the models points to the north. In all cases, the microphotographs were taken under plane polarized light (Table 3.1).

Description of Finite Element Models and Load Cases

The graphical user interface program *MSC.Mentat* provides the software tools for setting the models of the crystals. For simplification purposes, the small imperfections along the edges of the crystals were omitted. Such a simplification of the models is valid and does not generate a significant amount of error (Jasiuk, 1995). In each model, a sufficiently large domain of host rock is chosen to surround the crystal (approximately three times the diameter of the crystal, according to Tsukrov and Novak, 2002).

One out of eight crystals is twinned. Careful visual estimation allowed the geometrical separation of the twinned crystals for analysis as separate entities. Table 3.1 shows the microphotographs of the pyrite crystals.

The finite element models use two-dimensional quadrilateral elements with eight degrees of freedom. Table 3.2 shows the material properties of the pyrite crystals and the host rock. All models assume plane strain deformation. FEA Models of each crystal embedded in the host rock are presented in Table 3.3

Processing of Numerical Simulation Results

Any state of stress in a solid can be represented as a combination of tension/compression and shear. Three sets of load cases have been chosen to model the possible deformation paths: compression in y-direction, x-y (dextral) shear, and combination of compression and shear.

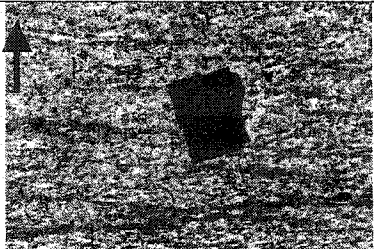
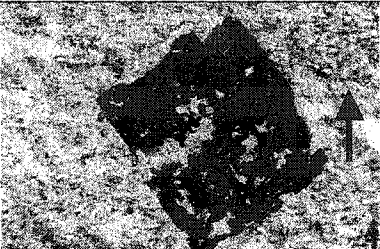
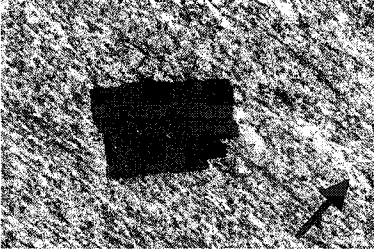
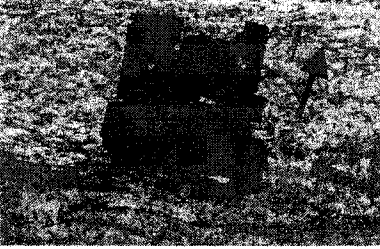
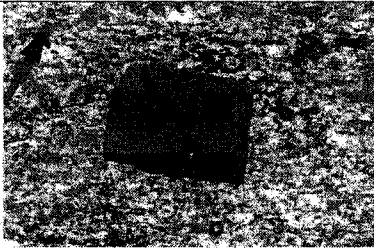
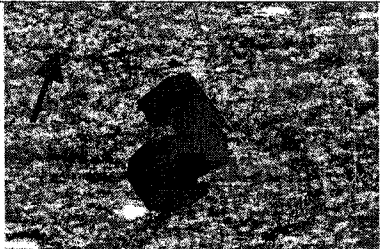
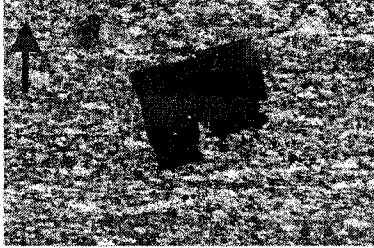
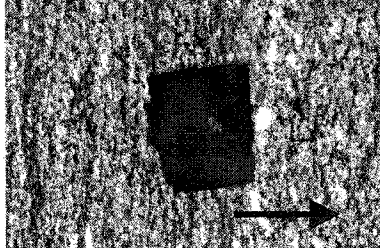

MODEL	PHOTOMICROGRAPH	MODEL	PHOTOMICROGRAPH
1		6	
2		7	
3		8	
4		9	
5			

Table 3.1 - Summary of microphotographs of the crystals in this analysis. Models 4 and 5 correspond to twinned crystals (left and right) from the same specimen. The arrow points to the upper part of the sample. In all microphotographs, the direction of view points to the north.


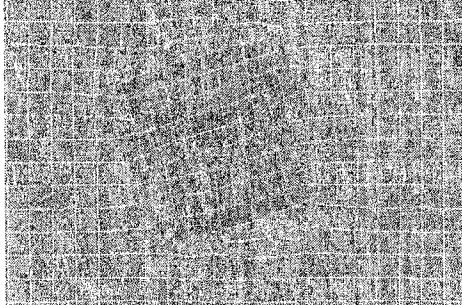
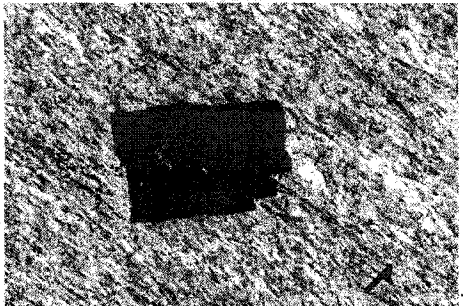
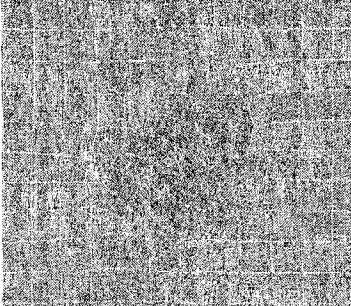
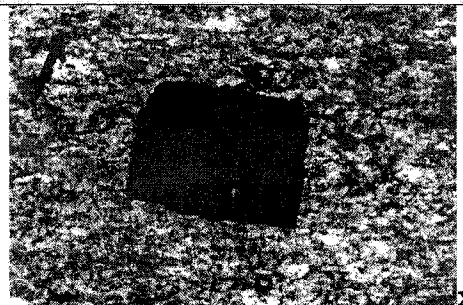
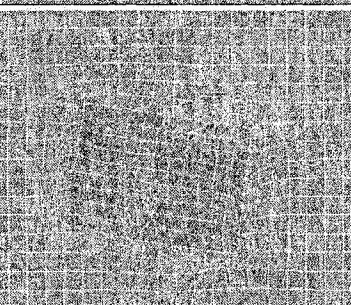

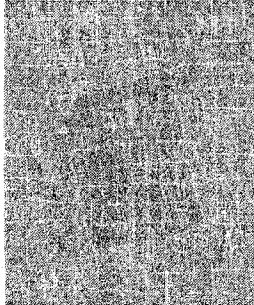
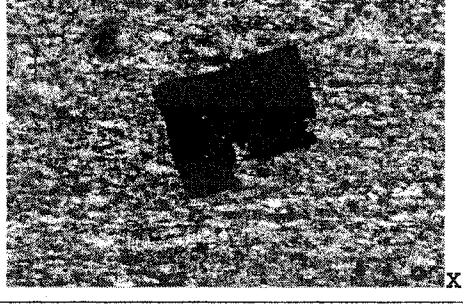
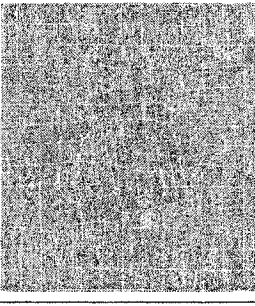
MATERIAL PROPERTIES	PYRITE	QUARTZITE
Young's Modulus (Pa)	1.649X10 ¹¹	6.205X10 ¹⁰
Poisson's Ratio	0.14	0.175

Table 3.2 Material properties of pyrite and quartzite (host rock) adapted from Birch, 1966.

The goal of the simulations is to solve the inverse problem of solid mechanics, i.e. to find the combination of forces that transforms the original geometry (deformed crystal shape) into a new geometry that is as close to a perfect square as possible. This is monitored by the change in the values of parameters e and s , introduced in the first section of this Chapter by equations (3.1) and (3.2). Parameters e and s are calculated based on new positions of the corners, which are, in turn, found from the finite element simulations. Data processing procedure is organized as follows:

1. Displacements of the corners are taken from the *MSC.Marc* output file.
2. Those displacements are added to initial corner coordinates to obtain the restored crystal geometry.
3. The values of angles and diagonal lengths are calculated.
4. Parameters e and s are found using formulas (3.1) and (3.2).
These parameters are then used to evaluate how close the restored shape is to a perfect square.

This procedure is implemented in the Microsoft Excel® spreadsheet as shown in Figure 3.3, which also includes graphs of the original and restored crystal shapes that are useful to compare and to identify possible errors in data capturing.

CRYSTAL SHAPE	FEA MODEL
 <p data-bbox="753 585 786 607">X4</p>	
 <p data-bbox="753 901 786 923">X4</p>	
 <p data-bbox="753 1218 786 1240">X4</p>	
 <p data-bbox="753 1535 786 1557">X10</p>	
 <p data-bbox="753 1852 786 1873">X10</p>	

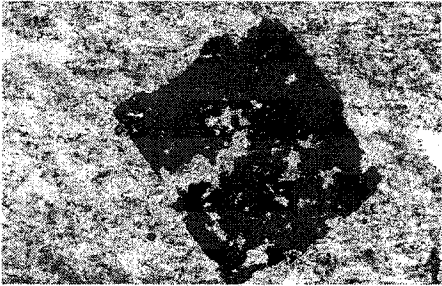
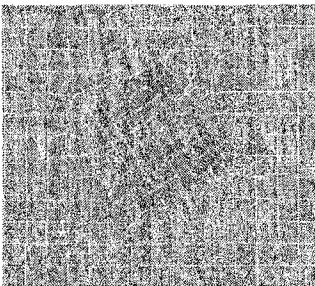
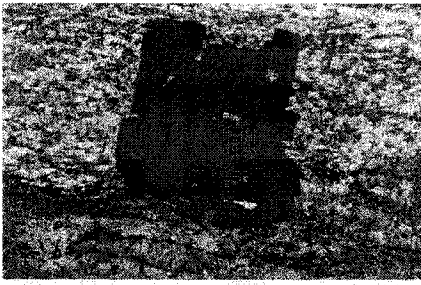
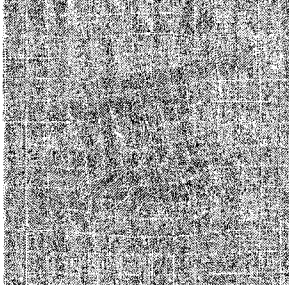
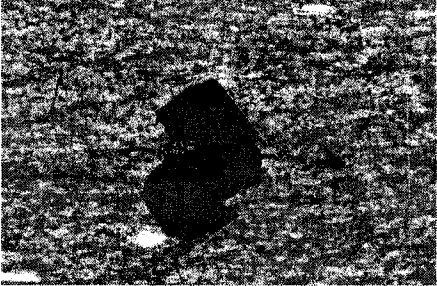
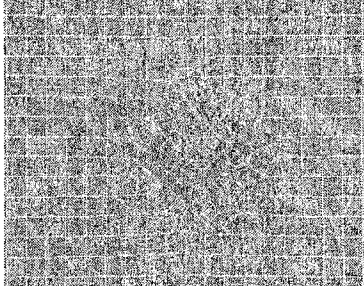
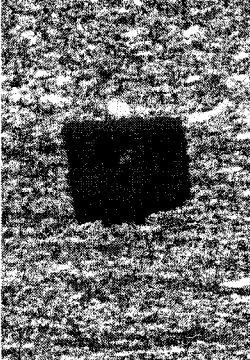
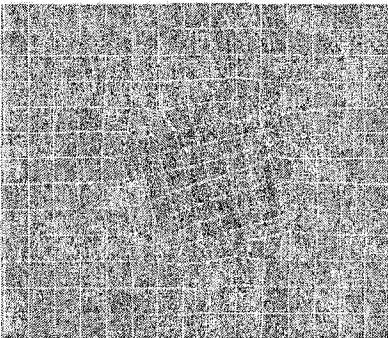
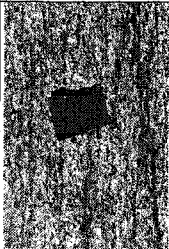
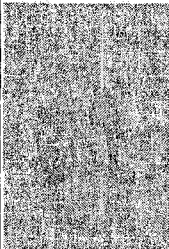
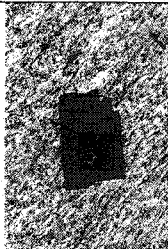

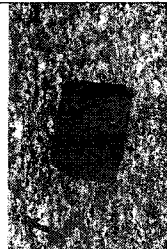
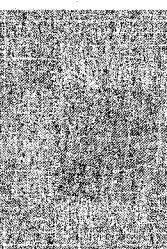
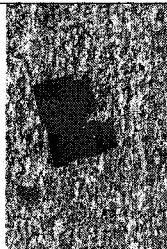
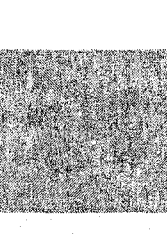
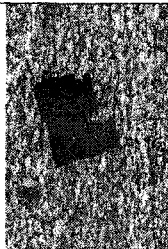
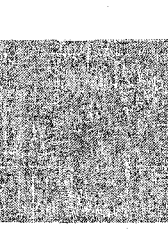
CRYSTAL SHAPE	FEA MODEL
 <p>X4</p>	
 <p>X10</p>	
 <p>X10</p>	
 <p>X10</p>	

Table 3.3 Pyrite crystals for FEA analysis. The right column contains the FEA models before reconstruction. The objective used in each microphotograph is indicated, all microphotographs were taken in plane polarized light.

CRYSTAL SHAPE	RECONSTRUCTED SHAPE	DEFORMED		LOADCASE 1 (6.5e8)		LOADCASE 2 (4e8)		LOADCASE 3 (1+2)	
		e	s	e	s	e	s	e	s
		1.135122	5.723417	1.128031	5.631681	1.46253	5.77806	1.02808	3.44087
		0.650566	17.31076	0.645725	17.11804	.658961	17.1994	.860276	10.8405
		1.380036	2.634683	1.377441	2.407633	1.38421	3.48383	1.19328	0.96308
		0.718944	4.511946	0.721259	5.193011	.945321	1.23104	.905133	2.08991
		1.151897	7.708562	1.154302	7.708562	1.1443	9.29754	0.97120	3.00903


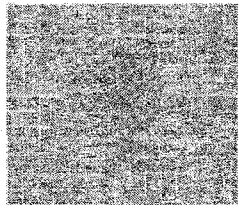
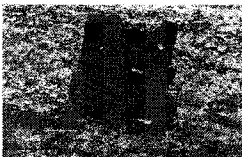
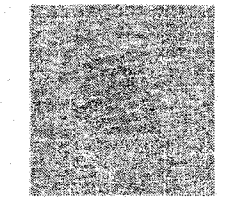

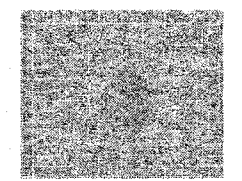

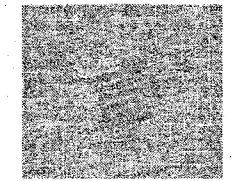
CRYSTAL SHAPE	RECONSTRUCTED SHAPE	DEFORMED		LOADCASE 1 (6.5e8)		LOADCASE 2 (4e8)		LOADCASE 3 (1+2)	
		e	s	e	s	e	s	e	s
		.875943	2.644535	.860149	3.633247	.887633	1.38813	.957956	1.06284
		.868642	13.19678	.869643	13.11027	1.05819	8.8207	.892422	8.3786
		1.01361	6.598716	1.015592	6.138322	1.19708	4.54294	1.00356	2.21453
		1.151897	7.08562	1.175617	6.641626	1.11987	2.9918	1.10235	9.0356
<u>AVERAGE DEVIATION FROM SQUARE</u>		0.190940	7.490558	0.194911	7.509155	0.20825	6.08149	0.08225	4.55944

Table 3.4 - Summary of the results of numerical simulations for the three load cases.

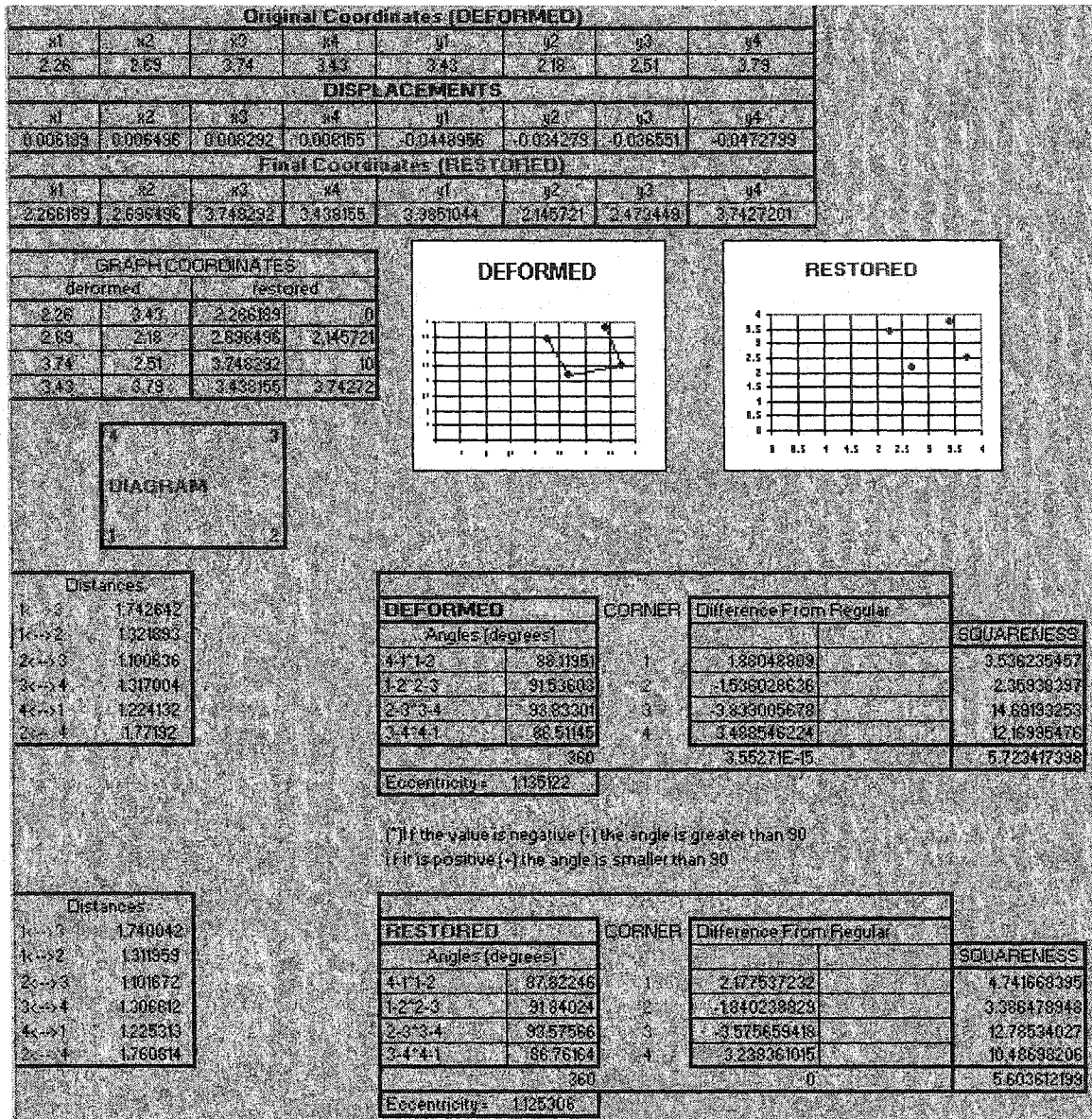


Figure 3.3 - View of the spreadsheet that calculates and summarizes the results after the simulation.

Results

For each crystal, three load cases were studied: compression, shear, and a combination of the first two. Numerical simulations were performed in a broad range of possible loads. The considered load cases and the corresponding displacements are provided in Appendix 4.

Table 3.4 summarizes the best results of the simulations. In the last row, the average deviation of eccentricity from value $e=1$ for a

perfect square is calculated as $\frac{1}{9} \sum_{i=1}^9 |1 - e^{(i)}|$. The average squareness is found as $\frac{1}{9} \sum_{i=1}^9 s^{(i)}$, where $e^{(i)}$ and $s^{(i)}$ are the eccentricity and the squareness of the i^{th} crystal.

The deformed shapes have an average deviation from the "perfect square" eccentricity equal to 0.190940, and an average squareness value of 7.490558. The simulations of load case 1 (compression) did not improve the eccentricity or the squareness. In load case 2 (shear), only the squareness was improved (1.409 units). The simulations that correspond to load case 3 (load case 1 + load case 2, last two columns of Table 3.4) improve the shapes of most crystals significantly. After the reconstruction by load case 3, the value of average deviation from the perfect square is 0.08225 and the squareness averages 4.55944. This represents an improvement of .109 units for the average deviation from the perfect square and of 2.936 units in the average squareness.

Discussion

Figure 3.4 represents a unit volume subjected to the analyzed load cases. Figure 3.4a, shows the same unit volume with the pyrite crystals and arrows representing the possible orientation of forces as in load case 1 (shear). Figure 3.4b represents the same unit volume with arrows oriented as in load case 2 (extensional regime), and figure 3.4c represents the combination of compression and shear as in load case 3 (transpressional regime).

Based on the results from the simulations, load cases 1 and 2 independently cannot be responsible for the deformation of the crystals to their actual shape. It can be speculated that only the combination

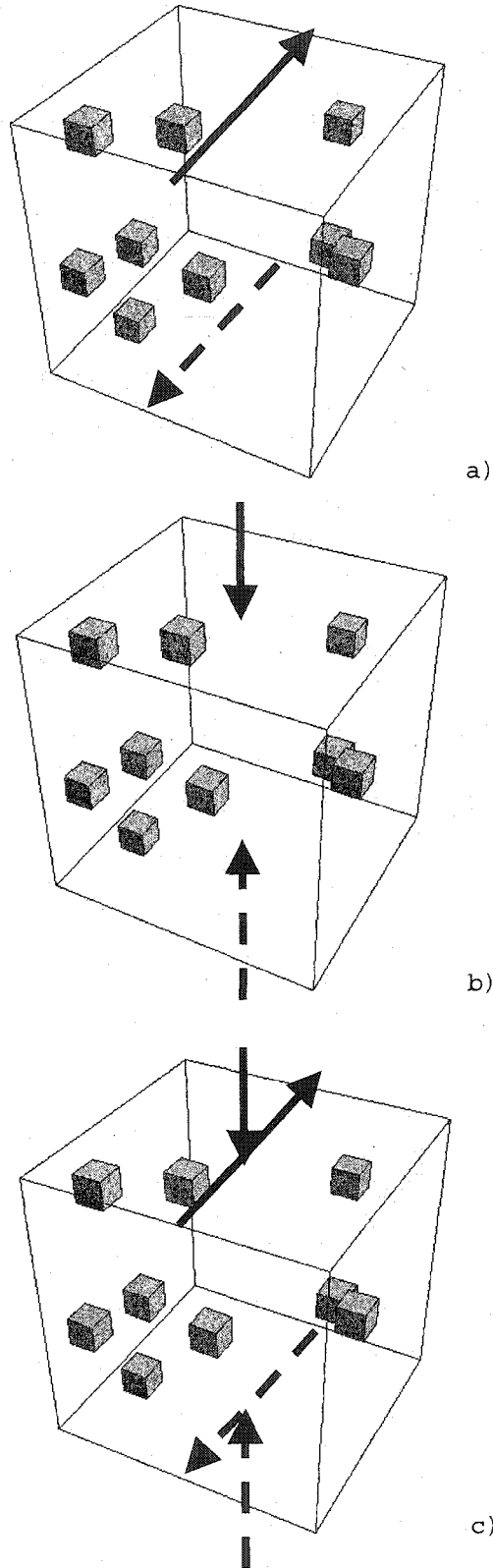


Figure 3.4 - Representation of unit volumes containing pyrite crystals, the arrows indicate the orientation of the loads. a) shear, b) extensional regime, and c) a transpressional regime.

of compression and shear can produce the observed deformation of the crystals. Even though the results provide a strong qualitative basis in the investigation of the deformation history in MG rocks at Towle Road, the following simplifying assumptions were considered in this analysis:

1. Two dimensional plane strain models were studied instead of three dimensional models.
2. Pyrite crystals are considered as isotropic.
3. For each model, the dimension of the host rock is equal to three times the diameter of the pyrite crystal. Consequently, only a portion of the host rock is modeled.
4. The crystal shape in each model is an approximation.

From the results obtained in Chapter 2, it can be stated that it is possible that the fold in Towle Road was formed by a combination of compression and shear. Such combination of loads is present in both, a transpressional regime and an anticlastic bending.

The combination of results from Chapter 2 and FEA, eliminate the possibility of an extensional regime as responsible for the deformation of the analyzed pyrite crystals. These results (Chapter 2 and FEA) support the hypothesis that the combination of shear and compression was involved in the folding mechanism of the Towle Road fold as well as in the deformation of the pyrite crystals.

CHAPTER IV

MICROSTRUCTURAL ANALYSIS

Introduction

The description of deformation microstructures and the determination of the mechanisms that created them are the most important fundamentals of the micro structural analysis. In nature, deformed rocks in shear zones often contain relatively strong megacrystals preserved in a finer grained recrystallized fabric (mylonites and ultra-mylonites), and the resulting geometry (porphyroclast system) records information regarding the deformation history of the rock (e.g., Ghosh and Ramberg, 1976).

Additionally, during shear, dislocation creep occurs as a viscous deformation over a wide range of physical conditions (temperature, differential stress, strain rate, and water content) and significantly alters the texture of the rock. Dislocation creep induces crystal plastic deformation in quartz grains and consequently imprints the latest chapter of the deformation history on them (e.g., Zulauf, 2001; Stipp et al., 2002).

Simpson and Schmid (1983) and Simpson (1986) introduced valuable criteria for the deduction of the sense of shear in mylonites, which at present, constitute the current, and widely accepted basis for the interpretation of shear zones. This study follows the criteria and the techniques of the above-mentioned authors. For the classification of porphyroblasts, it uses the study of porphyroclast systems by Passchier and Simpson (1986) as a guide.

White (1976, 1977), Urai et al. (1986), and Stipp et al. (2002) observed changes in the microstructure of quartz grains in samples from natural shear zones. Hirth and Tullis (1992) conducted experimental studies to document the dislocation creep regimes in quartz grains and identified three dislocation regimes for quartz grains. The study of microstructures in quartz grains became more accepted and the correlation between those three regimes and the textures in natural deformed rocks is now widely applied (e.g. Dunlap et al., 1997; Blenkinsop, 2000; Zulauf, 2001; Stipp et al., 2002).

This research focuses on the study of kinematic indicators (i.e. shear bands, asymmetric porphyroclasts, etc.) and on the texture development of quartz grains (crystal plastic deformation) in mylonitic rocks and in fault zones. It applies standard optical methods of micro fabric analysis to obtain qualitative results from five areas of small extent, three in the Rye Complex and two in the Merrimack Group (fig. 4.1). Because of the nature of the Rye Complex, the micro-structural analysis in that unit is the most exhaustive of all.

Experimental results state that the crystal plastic deformation structures in quartz grains are restricted to a series of conditions in terms of strain ratio, temperature, and dislocation density (Poirier, 1985; Hirth and Tullis, 1992). The interpretation of microstructures in quartz grains is reliable if it is restricted to a small area, and if the assumption of studying quartz grains of the same generation is valid. Table 4.1 summarizes the regimes in quartz and their characteristics so far recognized by other authors (Hirth and Tullis, 1992; Passchier, 1998, among others).

It is important to note that the temperature values and characteristics given in each regime depend on variables that cannot be calculated (e.g. strain rate, confining pressure, etc.). Nevertheless,

the correlations between microstructures and temperature serve, in the studied areas, as a guide and as a reliable estimator.

	<u>TEMP.</u>	<u>Strain Ratio</u>	<u>Differen- tial stress</u>	<u>Micro- structures in quartz</u>	<u>Mechanisms</u>
<u>Regime</u> <u>1</u>	Low 250°C (± 50)	High	High	1) Original grains are irregularly deformed. 2) Some equant grains may be present. 3) Chess-board undulatory extinction.	Grain boundary migration by bulging.
<u>Regime</u> <u>2</u>	Medium 350 - 400°C (± 50)	Medium	Medium	1) Original grains highly flattened. 2) Sweeping undulatory extinction. 3) Sub grains, core and mantle structure. 4) Recrystallized grains ≈ size of subgrains. 5) Lower dislocation density in original grains and in recrystallized grains. 6) Deformation lamellae. 7) Low to medium LPO and SPO	Subgrain Rotation
<u>Regime</u> <u>3</u>	High 450 - 550 °C (± 50) Higher in the migma- tite field	Low	Low	1) Subgrains, core and mantle structure. 2) Recrystllized grains > size of subgrains. 3) Recrystallized grains define a planar fabric. 4) High proportion of recrystallized grains. 5) Strong LPO.	Subgrain rotation Grain boundary migration

Table 4.1 - Characteristics of the three regimes of dynamic recrystallization (adapted from Hirth and Tullis, 1992; Blenkinsop, 2000; Zulauf, 2001; Stipp et al., 2002). LPO = Lattice Preferred Orientation; SPO = Shape Preferred Orientation.

The term dynamic recrystallization refers to the formation of new grains in a rock during solid-state deformation (Bates and Jackson, 1987). The planes of the microphotographs are parallel to the main lineation and perpendicular to the main foliation; unless, it is indicated otherwise in the captions.

Area # 1 - Rye Complex

The micro structural analysis in the Rye Complex (Area #1, fig. 4.1) has two objectives: 1) to investigate the deformation of the Great Commons Fault Zone, and 2) to identify and correlate the microstructures within both units, the Rye Formation and the Breakfast Hill (Plate 1).

The Rye Complex is a unit mostly dominated by mylonitic rocks that were probably deformed by transpression. Previous studies recognize strike slip and vertical displacements in the west contact of that unit (Carrigan, 1984; Hussey, 1980). To the west, the Great Commons Fault Zone, which is a shear fault with a ductile component, separates the Rye Formation from the Breakfast Hill (Carrigan, 1984).

Sampling in this area covers most of the (at present) accessible outcrops from the shoreline inland towards where the Breakfast Hill lithologies crop out (fig. 4.2). The main foliation in the Rye Formation trends 220 - 232° and dips 20 - 55° (NW), and it is parallel to the main crenulation lineation. Likewise, the crenulation lineation is parallel to the hinges of the tight asymmetric folds (fig. 2.5 and Plate 1).

The main foliation that defines the schistosity of the Breakfast Hill unit is subvertical and it trends 200 - 215°. The foliation defines undulations with wavelengths of no more than five to ten centimeters (Plate 1).

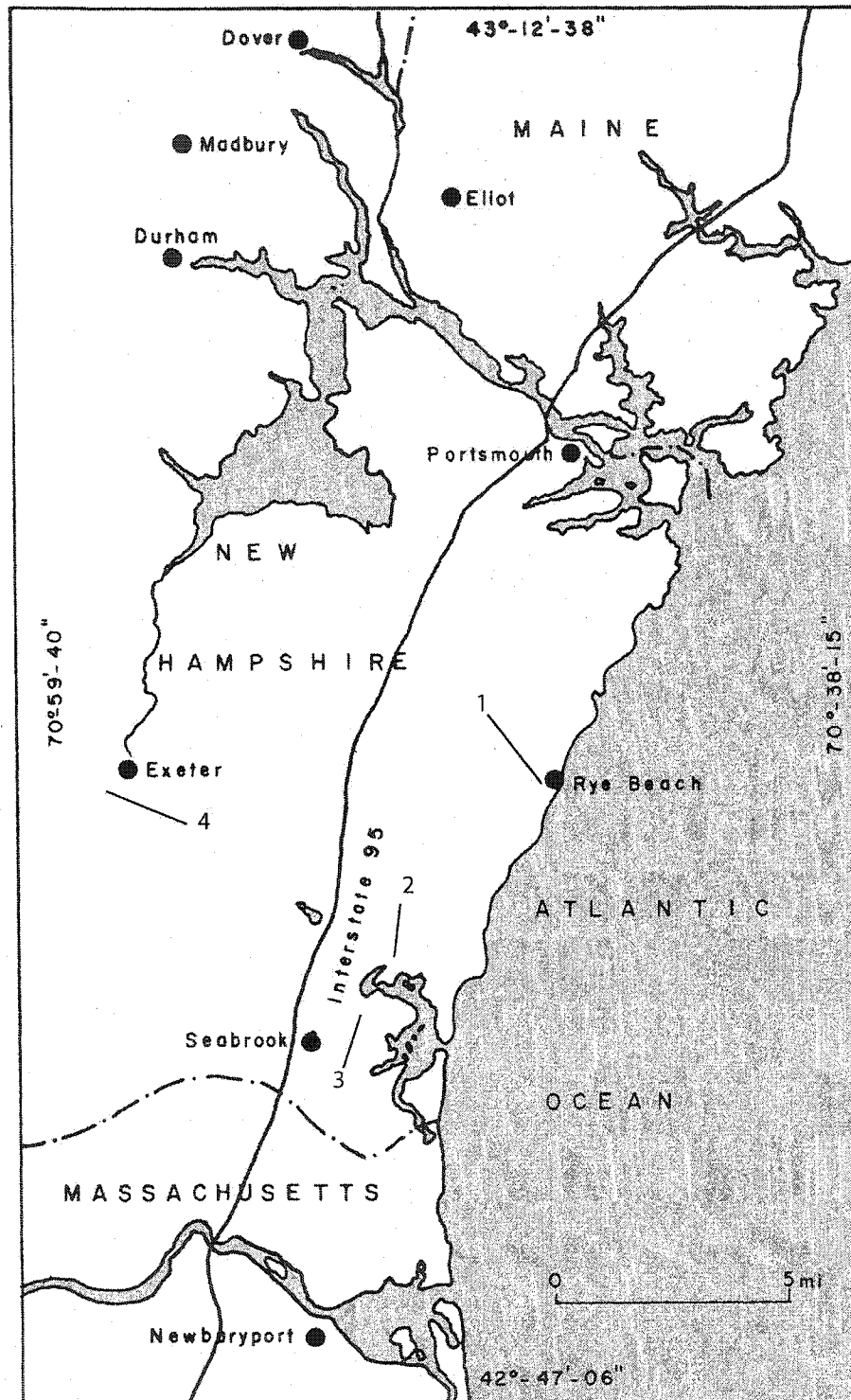


Figure 4.1 - Location map showing the areas where the microstructural analysis was conducted: 1) Golf Course, 2) Lafayette Road / Route 101, 3) Dodge Ponds, and 4) Exeter River.

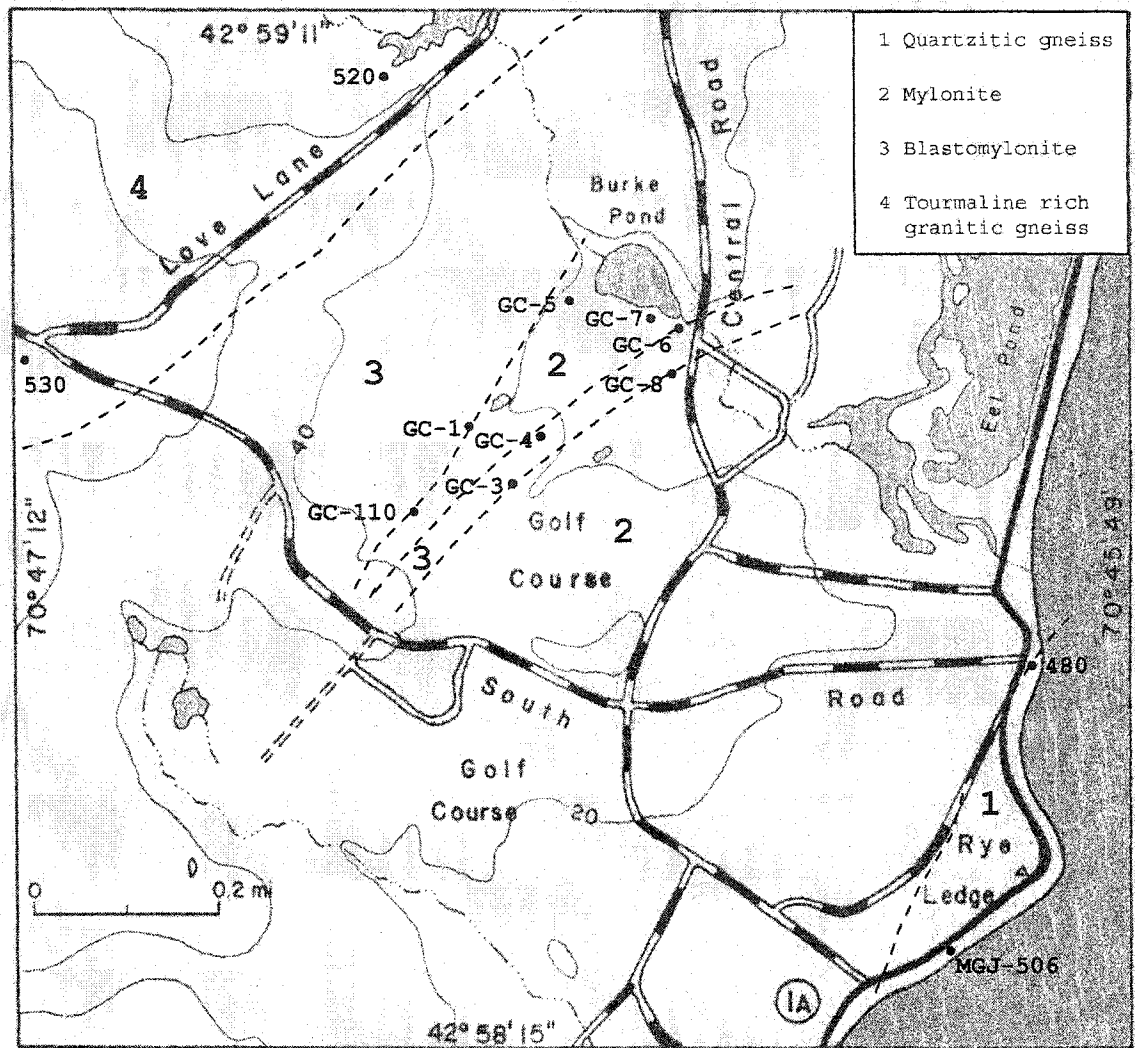


Figure 4.2 - Map showing the sample location and rock types of Area # 1, topographic contours at every 20 ft.

The author collected all samples for thin section analysis, except sample 520 and 530 collected by Novotny (1963); Carrigan (1982) collected sample MGJ-506a. At present, these samples belong to the thin section collection of the Earth Sciences Department at the University of New Hampshire. Unfortunately, the samples collected by Novotny and Carrigan were not oriented.

Sample Description

Sample MGJ-506 - Quartz grains in the three thin sections from this sample have a combination of irregular "serrated" boundaries (grain boundary migration by bulging), "chessboard" undulatory extinction, and few new dynamically recrystallized strain-free grains. All these structures are characteristic of the Regime 1 in Table 4.1 (fig. 4.3, 4.4, and 4.5).

In fig. 4.3, the grain boundary migration is clear, and the grain boundary rotation is incipient making the boundary between crystals irregular (serrated). Subgrains are beginning to form, and migration occurs towards the edges (white crystals with no undulatory extinction).

A set of microfractures is still observable and displays a weak conjugate pattern. The micro-fractures are relicts of a previous fragile deformation; it is likely that some of them underwent bending by ductile deformation (upper right corner). The quartz crystals display a weak undulatory extinction, and are optically oriented in different directions.

The quartz grain in the center of fig. 4.4 displays strong grain boundary migration by bulging (serrated boundaries). The grain in the left-hand-side preserves vestiges of the conjugate micro-fractures. On the right, the grain displays "chessboard" undulatory extinction. The subgrain patches become increasingly mis-oriented with respect to the surrounding lattice, and eventually (after a lattice misfit of about 15° or more), the boundary between a subgrain and its surroundings becomes a new grain boundary.

The grains on the left of fig. 4.5 display kink bands. In the lower part, the formation of a subgrain is occurring by separation from the main grain that contains micro-fractures. Three unstrained new

grains appear in the middle part. Their boundaries are irregular. Surrounding the large crystals are biotite, small quartz, and plagioclase anhedral crystals.

This sample contains several kinematic indicators mostly represented by pulled apart garnet grains displaying a "bookshelf" structure. There is no sense of shear interpretation because the orientation of the sample is not recorded.

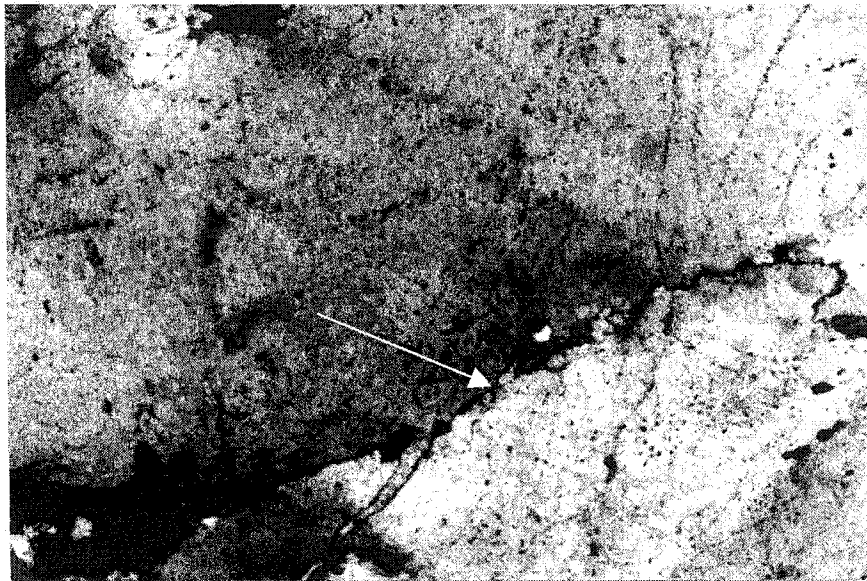


Figure 4.3 - Sample MGJ-506 - The arrow points to the serrated boundaries in quartz grains; the structure indicates grain boundary migration by bulging (XP, X10). The field of view is approximately 1.55 mm.

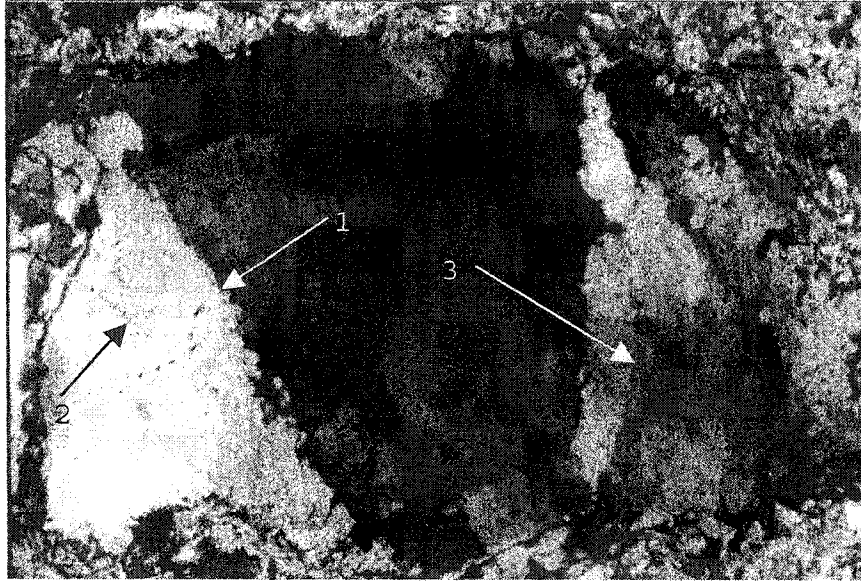


Figure 4.4 - Sample MGJ-506 - Quartz subgrains with serrated boundaries (1). To the left the subgrain preserves traces of fragile deformation as conjugate microfractures (2); to the right, the grain has "chess-board" undulatory structure (3); (XP, 40X). These structures are characteristic of Regime 1. The field of view is approximately 1.55 mm.

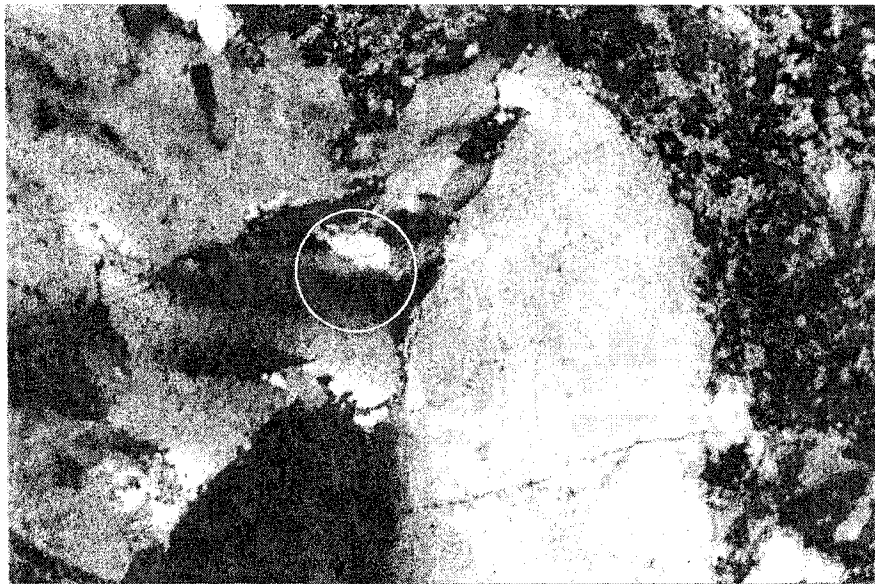


Figure 4.5 - MGJ-506 - In the center of the picture, a new strain-free grain "grows" with no undulatory extinction, circled (X4, XP). Crystal plastic recrystallization initiates. The field of view is approximately 2 mm).

Sample GC-1 - Original and new grains have approximately the same size, and a strong lattice and shape preferred orientation. Flat shape is predominant in most of the crystals, and defines a strong planar fabric parallel to the new foliation (fig. 4.6 and 4.7). The microstructures of this sample belong to Regime 3.

Crystal boundaries are almost straight, and the amount of new grains with respect to the original grains is almost the same. Biotite crystals define the new foliation, and are parallel to the planar fabric of quartz grains forming a 45° angle with the upper edge of the photograph (fig. 4.7).

Fig. 4.8 shows weak grain boundary pinning structure, where biotite grains have pinned the quartz grain boundaries. In the lower right corner of the microphotograph are a core and mantle structure and a concentration of new grains. The undulatory extinction is restricted to the few remaining original grains. Garnet porphyroblasts indicate a clear dextral sense of movement (Fig. 4.9).

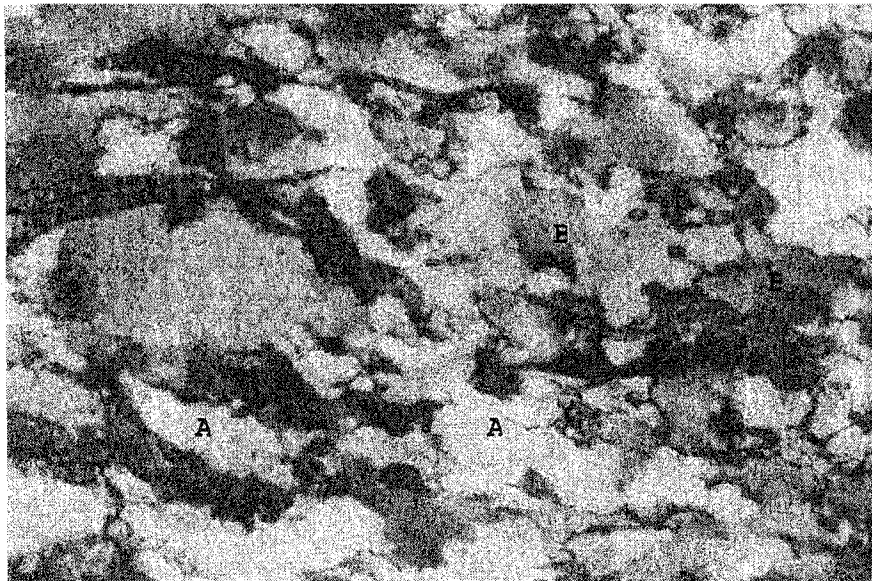


Figure 4.6 - Sample GC-1 - New grains (A) and original grains (B) have the same size. Crystal plastic deformation is the predominant rock texture. The field of view is approximately 1.55 mm (X10, XP).

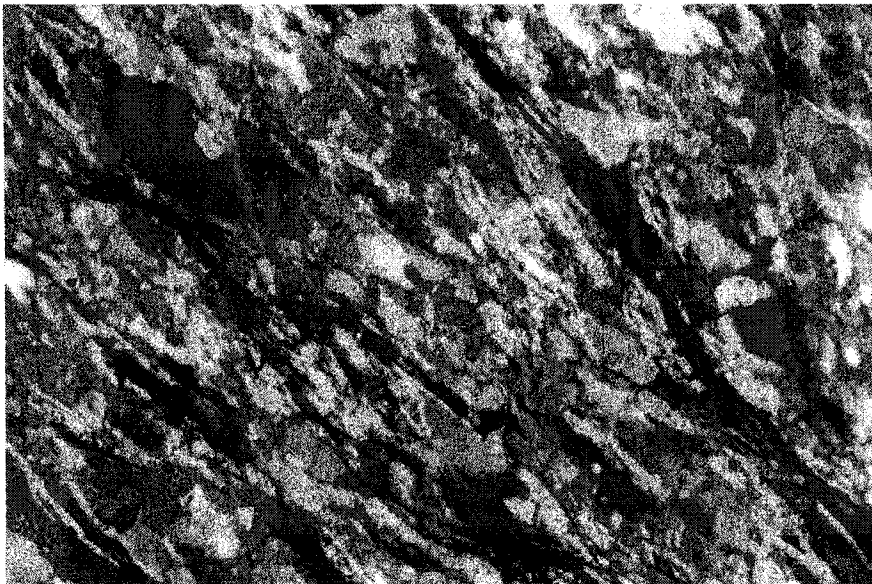


Figure 4.7 - Sample GC-1 - Quartz grains (original and recrystallized) form a strong shape and lattice-preferred orientation parallel to the developing foliation. The field of view is approximately 2 mm (X4, XP).

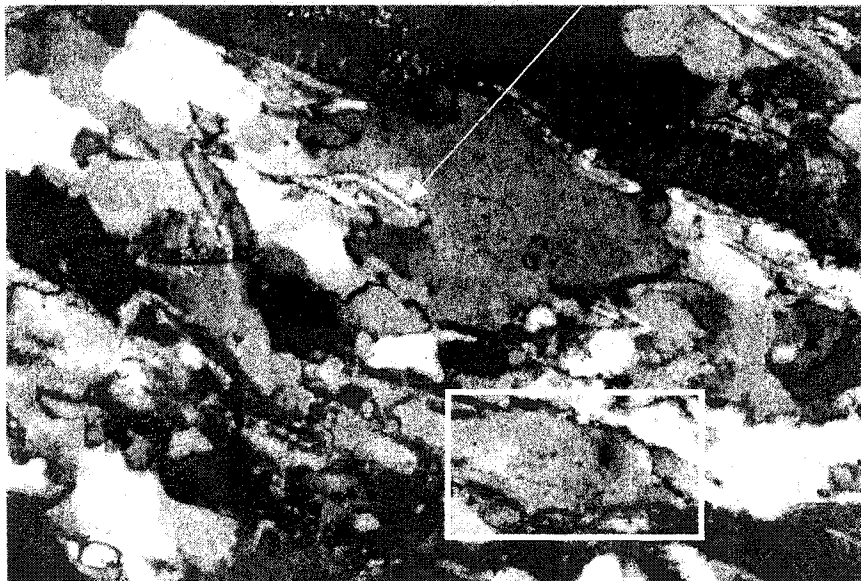


Figure 4.8 - Sample GC-1 - "Pinning" structure. The relicts of previously formed biotite crystals (B) "pin" the boundaries of the new grains of quartz. The inset shows the core and mantle structure. The field of view is approximately 1.55mm, (X10, XP).

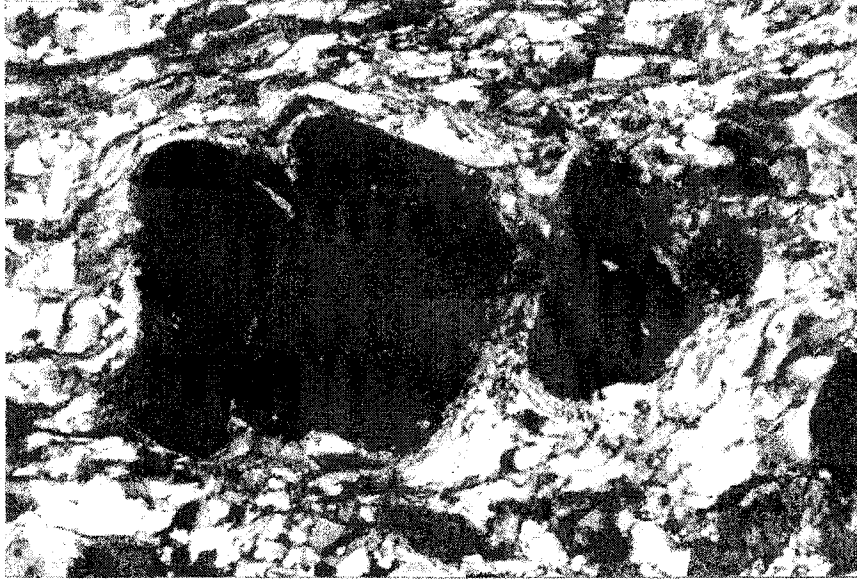


Figure 4.9 - Sample GC-1 - A garnet porphyroblast displaying a bookshelf structure. The sense of motion is dextral, and the field of view is approximately 2 mm (X4, XPL).

Sample GC-3 - This sample has structures that belong to the transition between Regime 1 and Regime 2 of Table 4.1. The boundaries of the new grains tend to be straight, and the "serrated" boundaries attenuated. The original grains have undergone flattening and grain size reduction (fig. 4.10).

Reorientation of the biotite crystals into the new foliation initiated (lower left corner of fig. 4.10). A previous foliation was likely to be parallel to the biotite crystals that crosscut the new foliation (lower half). If the reorientation of grains continues, the boundaries of the new quartz grains could trap lath-shaped biotite crystals, and then the "pinning" structure will result (Fig. 4.11).

The presence of kinematic indicators in this sample reveals a dextral sense of motion. The kinematic indicators are few monoclinic systems of K-spar porphyroblasts and shear bands (porphyroblasts systems terminology defined by Passchier and Simpson, 1986). The shear

bands certainly define a dextral sense of motion (Fig. 4.12), and in the monoclinic systems, the sense of motion is ambiguous (Fig. 4.13).

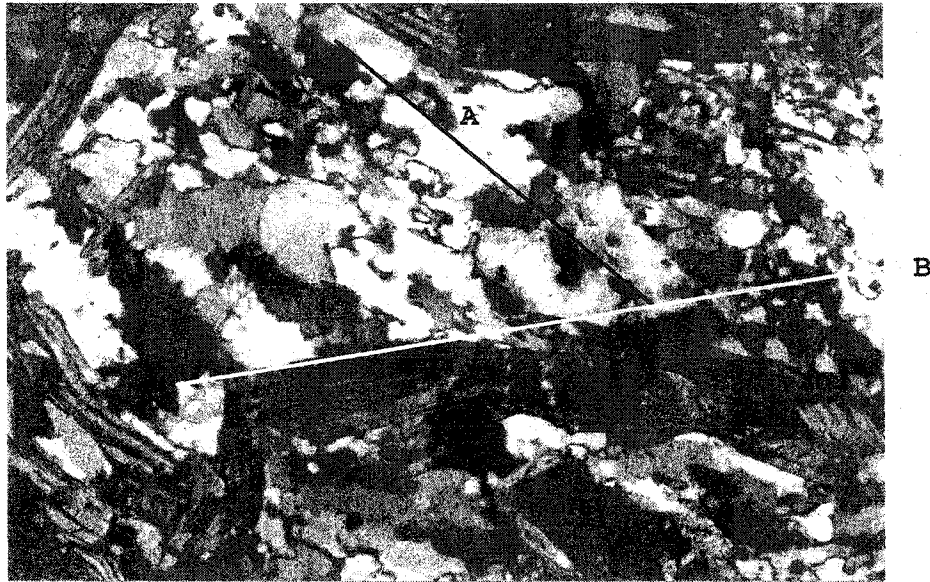


Figure 4.10 - Sample GC-3 - New and original grains define a preferred orientation parallel to the developing new foliation forming an acute angle with the upper border of the illustration (A). The old foliation is transverse to the former (B) (X10, XP). The field of view is approximately 1.55 mm.

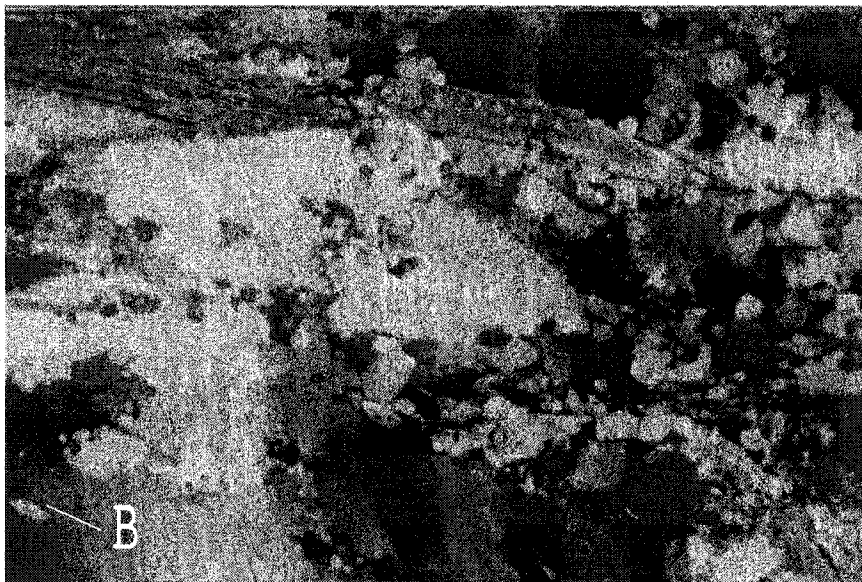


Figure 4.11 - Sample GC-3 - Initiation of the pinning structure. In the lower left corner there is a small biotite grain (B) surrounded by quartz. Eventually the biotite will pin the new quartz grains boundaries (X10, XP). The field of view is approximately 1.55 mm.

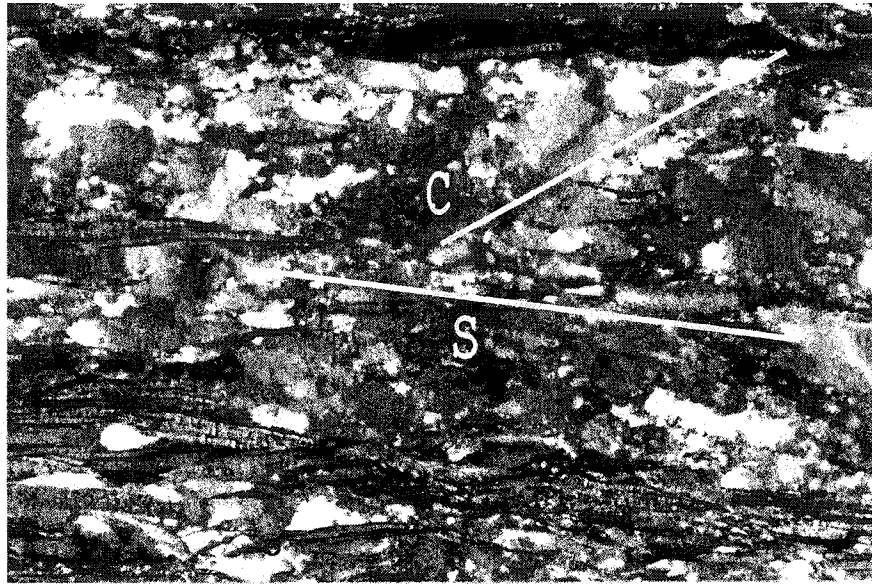


Figure 4.12 - Sample GC-3 - Shear band (S-C fabric). The biotite lath-shaped and flattened quartz crystals define the schistosity; the deflections in the biotite crystals and the orientation of quartz grains define the shear planes, as indicated (X10, XPL). The sense of shear is dextral; the field of view is about 1.55 mm.

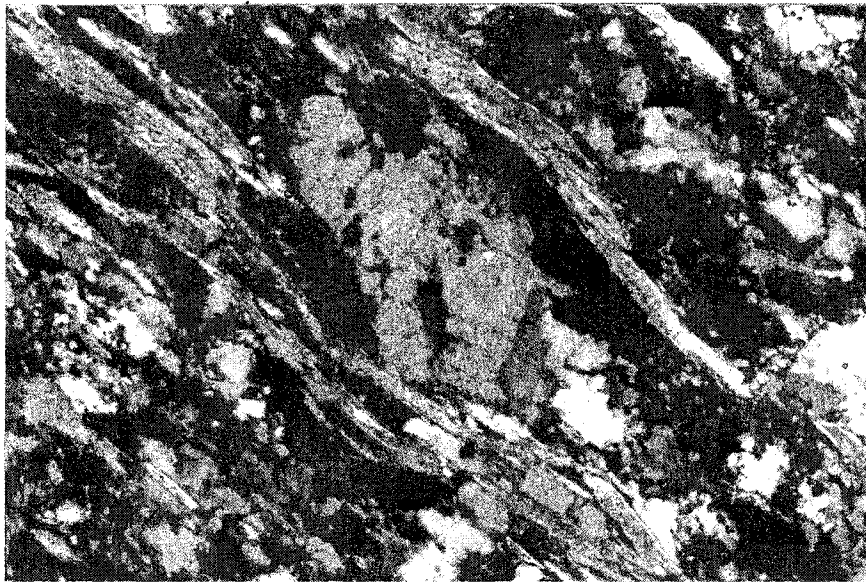


Figure 4.13 - Sample GC-3 - A K-spar porphyroblast and recrystallized quartz crystals clustered at the tails (pressure shadows) defining a monoclinic porphyroblast system. The sense of rotation is ambiguous; the field of view is approximately 1.55 mm (X4, XPL).

Sample GC-4 - Original quartz grains in this sample are slightly flat, display parallel undulatory extinction, and form a core and mantle structure in combination with the small subgrains (fig. 4.14). Subgrain rotation took place and the new grains developed a weak foliation (sub-parallel to the upper and lower edges of the illustration). The new grains have approximately the same size as the original grains, and tend to develop straight boundaries. In general, the microstructures in this sample correspond to the Regime 2 (Table 4.1).

The kinematic indicators are mostly garnet porphyroblasts and shear bands of quartz and lath-shaped biotite crystals. Figure 4.15 shows a garnet sigma grain and a shear band. The overall sense of motion is dextral.

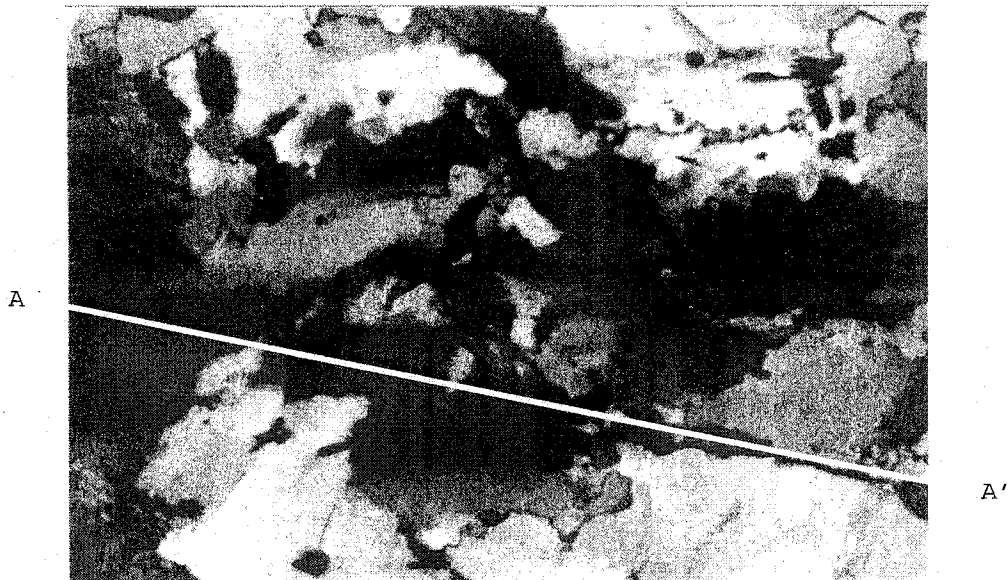


Figure 4.14 - Sample GC-4 - The shape preferred orientation of quartz grains (flattened boundaries) is parallel to the developing foliation (A-A'), and undulatory extinction is limited to the original grains (X10, XPL). The field of view is 1.55 mm.

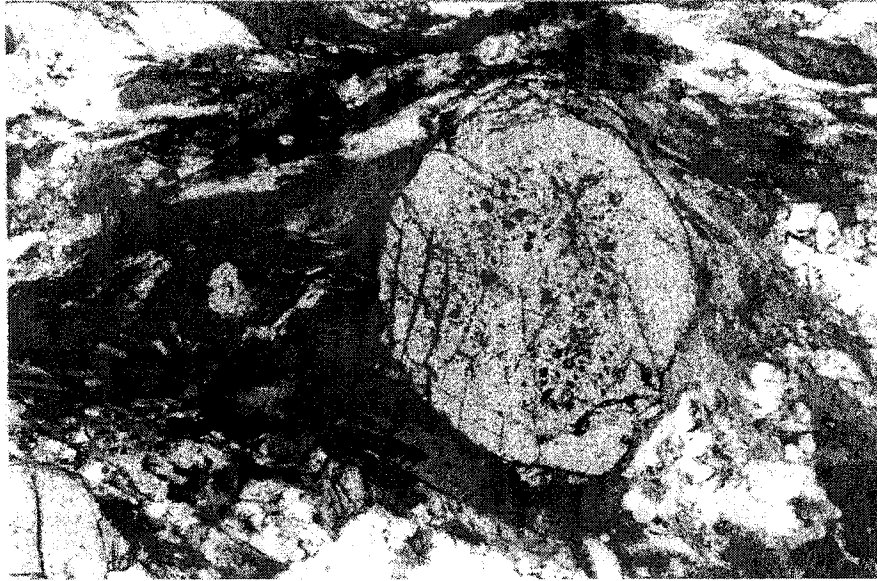


Figure 4.15 - Sample GC-4 - A shear band of lath-shaped biotite crystals (upper left) and a garnet sigma grain denote dextral sense of shear. The field of view is approximately 2 mm (X4, XPL).

Sample GC-5 - This sample has a high proportion of recrystallized quartz grains, and their size is larger than the few original grains that show undulatory extinction. Recrystallized grains have a strong lattice and shape-preferred orientation that define a planar fabric, which is parallel to the main foliation (fig. 4.16).

Figure 4.17 shows a set of shear bands that define a dextral sense of shear. Lath-shaped biotite crystals and flat recrystallized quartz grains define the new foliation.

There is no other evidence of a different type of kinematic indicators in this sample so far identified. The above-mentioned microstructures belong to Regime 3 of Table 4.1.

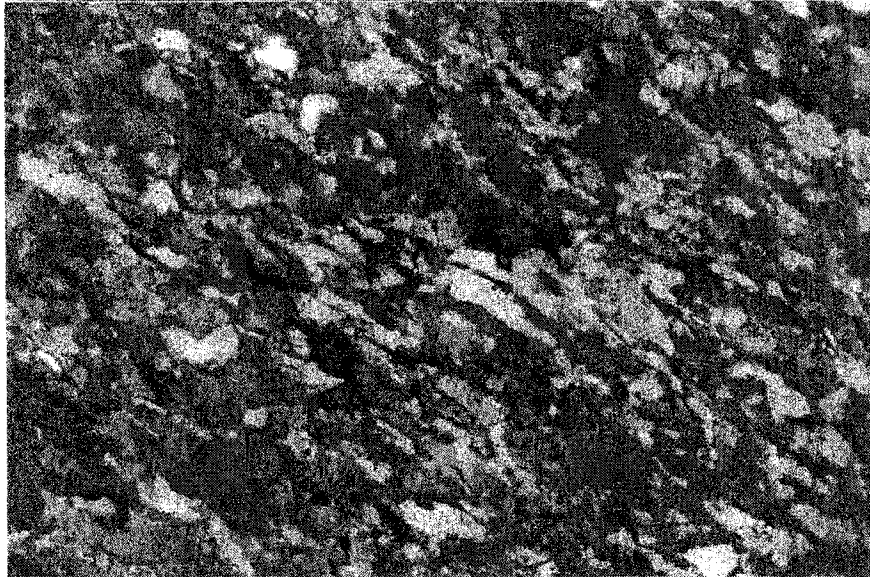


Figure 4.16 - Sample GC-5 - The main foliation forms an acute angle with the upper border of the photograph. The scarce original quartz grains appear illuminated. The field of view is approximately 2 mm (X4, XPL).

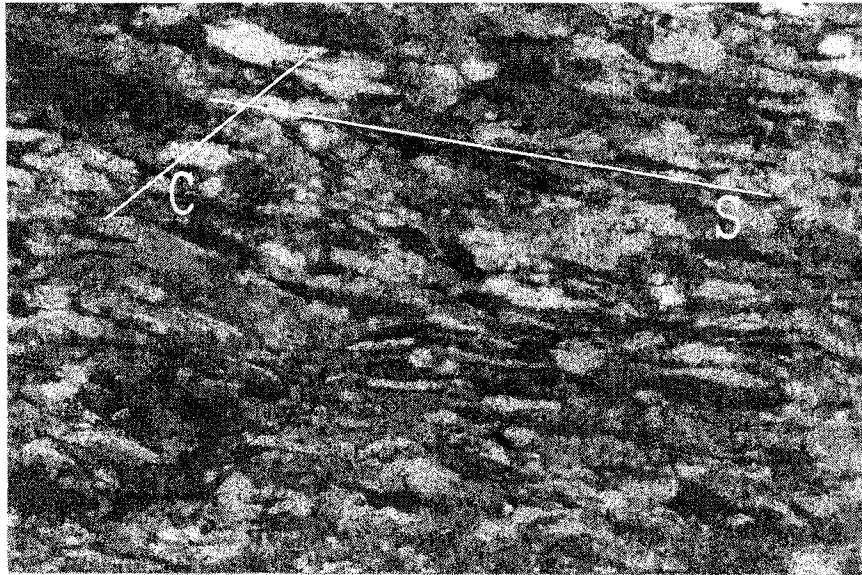


Figure 4.17 - Sample GC-5 - Shear bands defining a dextral sense of motion. The field of view is approximately 2 mm (X4, XPL).

Sample GC-6 - Recrystallized quartz grains and original grains have approximately the same size. Subgrains form core and mantle structures (subgrain rotation). The original grains have a strong undulatory extinction (fig. 4.18).

There is a weak shape and lattice preferred orientation that is parallel to the main foliation. Some original grains display deformation lamellae.

Kinematic indicators consist of sigma garnet grains (monoclinic porphyroblast system, Passchier and Simpson, 1986) and shear bands, and define a dextral sense of motion (fig. 4.19). The structures identified in this sample belong to Regime 2 of Table 4.1.



Figure 4.18 - Sample GC-6 - Quartz subgrains (illuminated) show core and mantle structure surrounded by garnet grains. Original grains have undulatory extinction (left). The field of view is approximately 2 mm (X4, XPL).

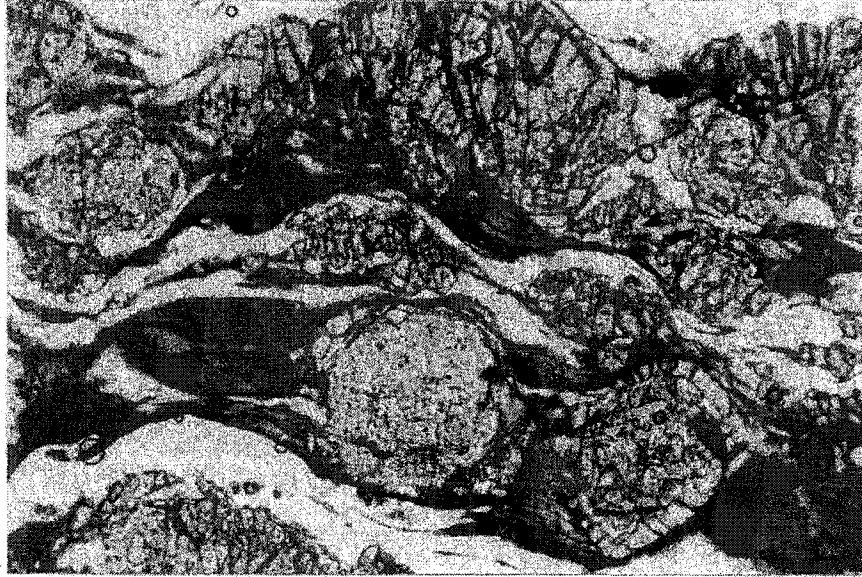


Figure 4.19 - Sample GC-6 - Garnet sigma grains and a set of shear bands define a dextral sense of shear. The field of view is approximately 2 mm (X4, PL).

Sample GC-7 - Subgrain rotation is evident in this sample; the original quartz grains show core and mantle structures and their size is about the same as the recrystallized grains. Original grains are flattened and have boundaries that are parallel to the main foliation; the boundaries between the grains are irregular.

The kinematic indicators are mostly shear bands defined by lath-shaped biotite crystals. The sense of motion is dextral (fig. 4.20). The structures in this sample point to Regime 2 of Table 4.1.

Sample GC-8 - The original and recrystallized grains have approximately the same size, and there is low dislocation density in the few large original grains. The recrystallized grains have lattice and shape-preferred orientation that defines a weak planar structure, and some of the remaining original grains display core and mantle structures (fig. 4.21).

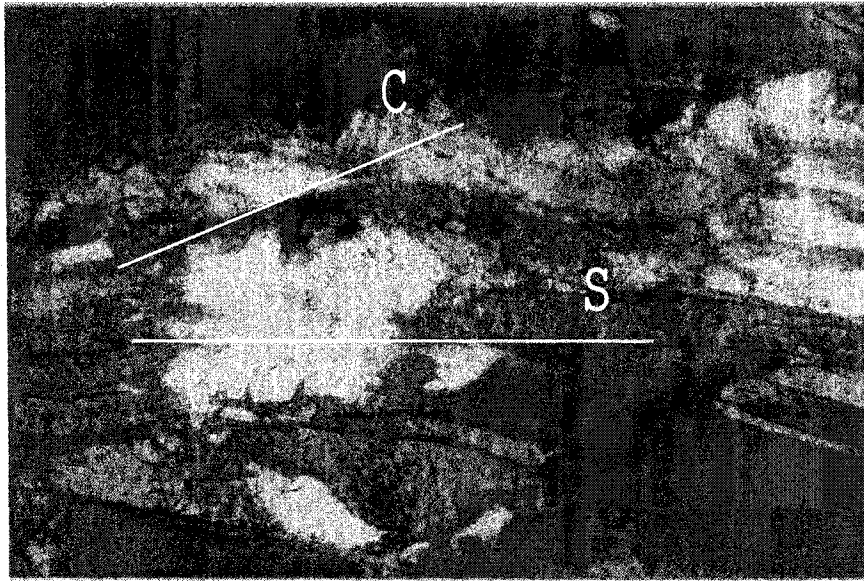


Figure 4.20 - Sample - GC-7 - Shear bands defining a dextral sense of motion. The long dimension of lath-shaped biotite crystals defines the planes of schistosity (S), and a crenulation developed in them define the shear planes (C). The field of view is approximately 2mm (X4, XPL).

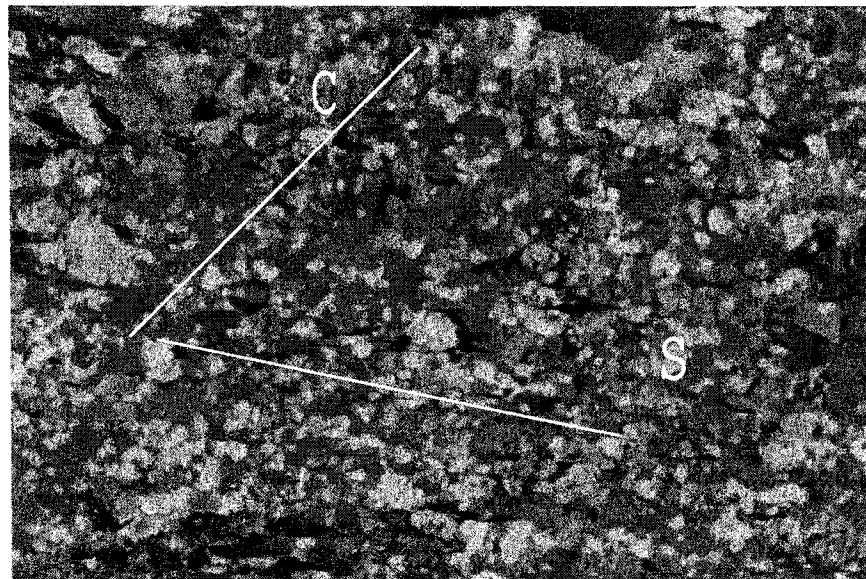


Figure 4.21 - Sample GC-8 - Recrystallized and original quartz grains have the same size. Shear bands consist of lath-shaped biotite crystals parallel to the "S" planes, and a weak crenulation in quartz grains define the "C" planes. The field of view is approximately 2 mm (X4, XPL).

The main foliation in this sample consists of small lath-shaped biotite crystals and by the flattened recrystallized grains of quartz. The boundaries between quartz grains are irregular.

The structures observed in this sample belong to Regime 2 of Table 4.1. The shear bands identified in this sample have a dextral sense of motion.

Sample GC-110 - In some areas of this sample, the recrystallized quartz grains are larger than the original quartz grains. Few original grains preserve core and mantle structures, and the recrystallized grains are flat. Recrystallized quartz grains and lath-shaped biotite crystals define a strong planar fabric. The identified microstructures belong to a transition between Regime 2 and 3 of Table 4.1. The kinematic indicators define dextral sense of shear (fig 4.22 and 4.23).

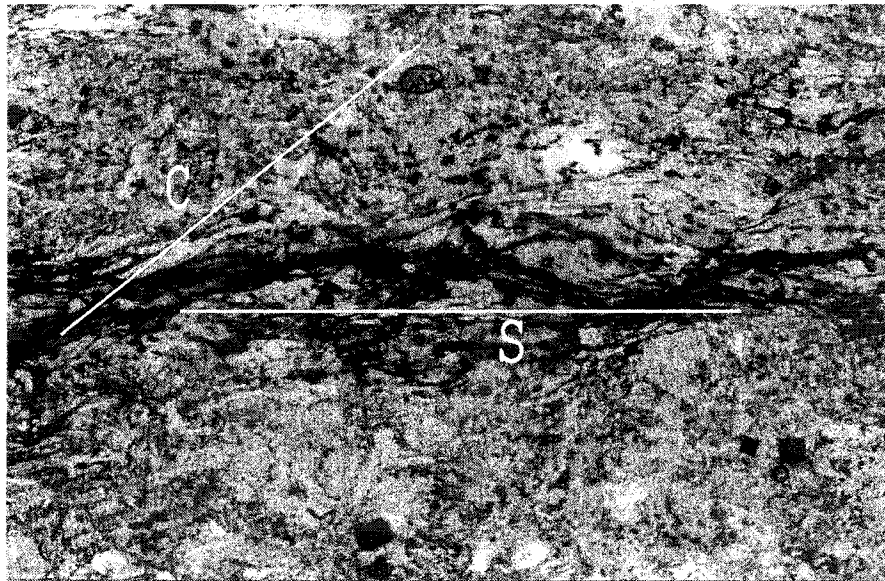


Figure 4.22 - Sample GC-110 - Shear band indicating a dextral sense of shear defined by the S and C fabric. The field of view is approximately 2 mm (X4, XPL).

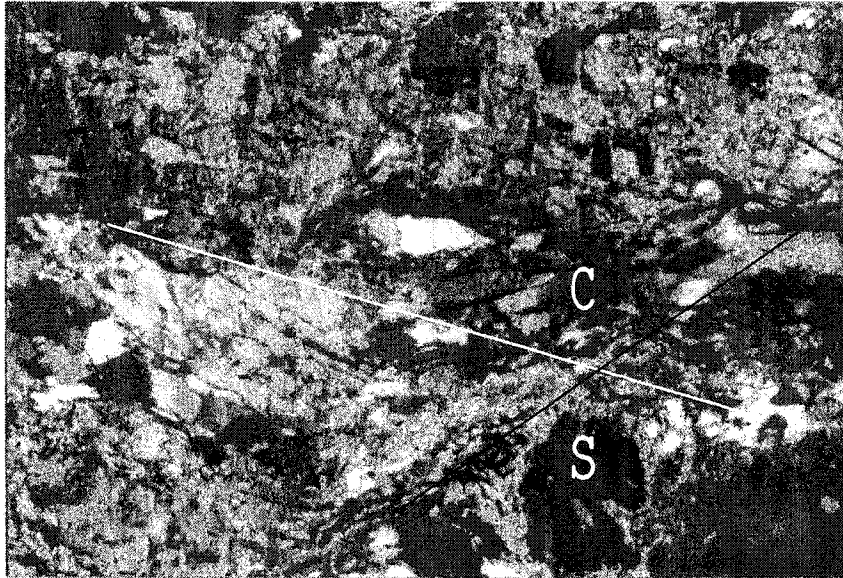


Figure 4.23 - Sample GC-110 - Garnet porphyroblasts and shear bands defining a dextral sense of motion. See text for discussion of C and S fabric. The field of view is approximately 2 mm (4X, XPL).

Sample 480 - This sample has a main foliation defined by quartz and K-spar ribbons. The quartz grains that constitute the bands have core and mantle structure and strong chess board undulatory extinction.

The equant grains between the ribbons have no lattice or shape preferred orientation, consequently do not define any planar structure. Kinematic indicators are present but the orientation of the sample is not available (fig. 4.24). The structures so far recognized point to a transition between Regime 1 and Regime 2 of Table 4.1.

Sample 520 - This sample has a high proportion of recrystallized grains of larger size than the original grains; few core and mantle structures are preserved in the original grains. The boundaries of the recrystallized grains are almost straight and tend to form triple junction boundaries (polygonal boundaries, fig. 4.25).

Flattened crystals define a planar structure, which is parallel to the foliation. Plagioclase crystals show crystal plastic deformation (fig. 4.26). There are kinematic indicators present in

this sample, but no orientation data are available. The microstructures in this sample are characteristic of Regime 3 of Table 4.1).

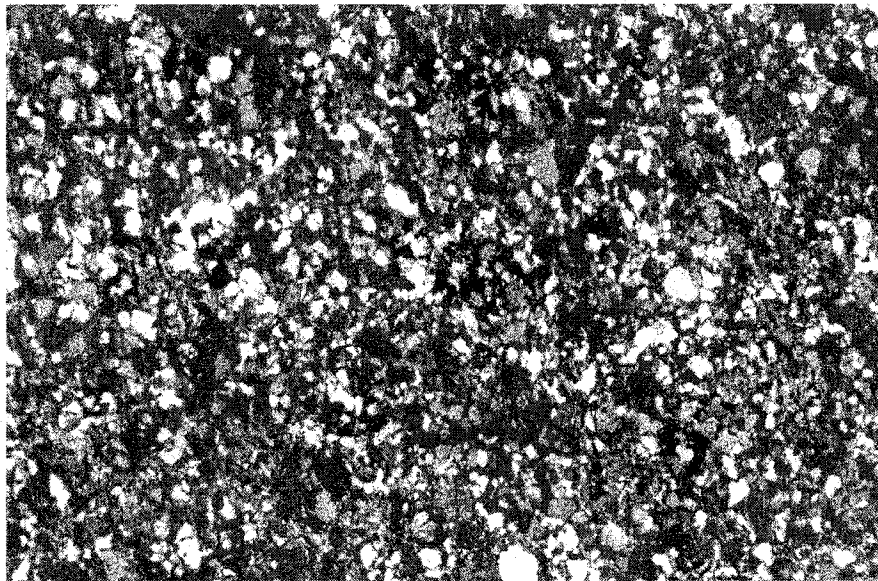


Figure 4.24 - Sample 480 - Quartz grains (original and recrystallized) are equant and define no planar structure. The field of view is approximately 2 mm (X4, XPL).



Figure 4.25 - Sample 520 - Recrystallized quartz grains tend to form triple junction boundaries (circles). The field of view is approximately 1.5 mm (X10, XPL).

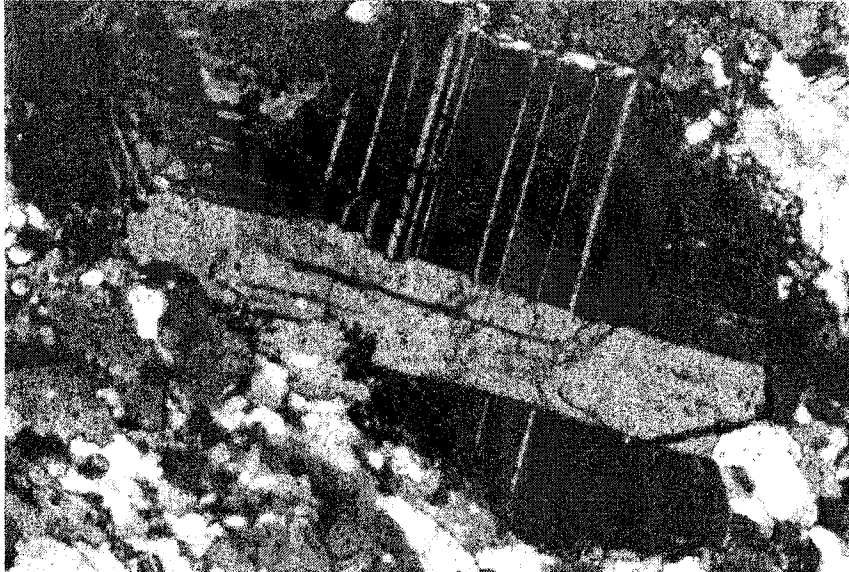


Figure 4.26 - Sample 520 - Crystal plastic deformations in plagioclase crystals. The field of view is approximately 0.8 mm (X20, XPL).

Sample 530 - This sample has a high proportion of recrystallized quartz grains and deformation in plagioclase crystals. The cauliflower structure characteristic of myrmekitic intergrowths is present. Crystal plastic deformation in plagioclase crystals is observable. The orientation of this sample has not been recorded. The microstructures in quartz grains of this sample are typical of Regime 3 of Table 4.1.

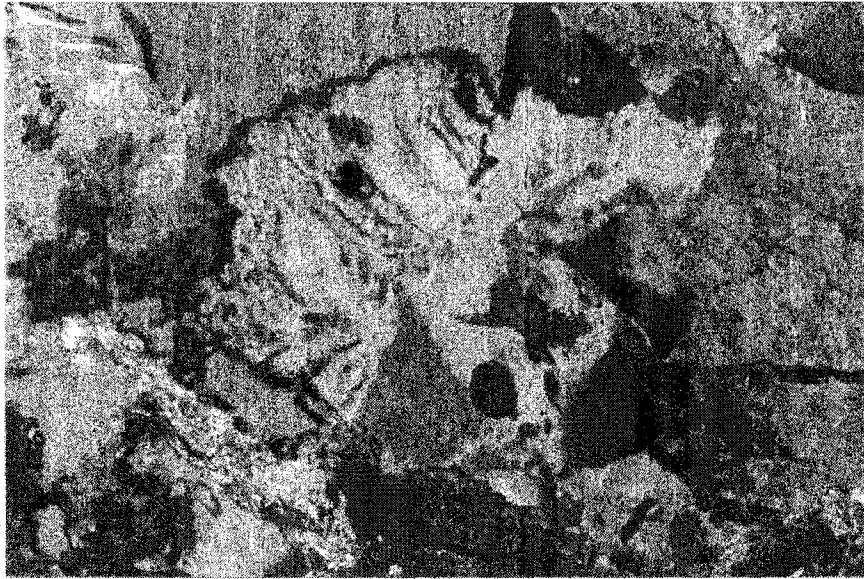


Figure 4.27 - Sample 530 - Characteristic cauliflower structures of myrmekite. The field of view is approximately 0.80 mm (X20, XPL).

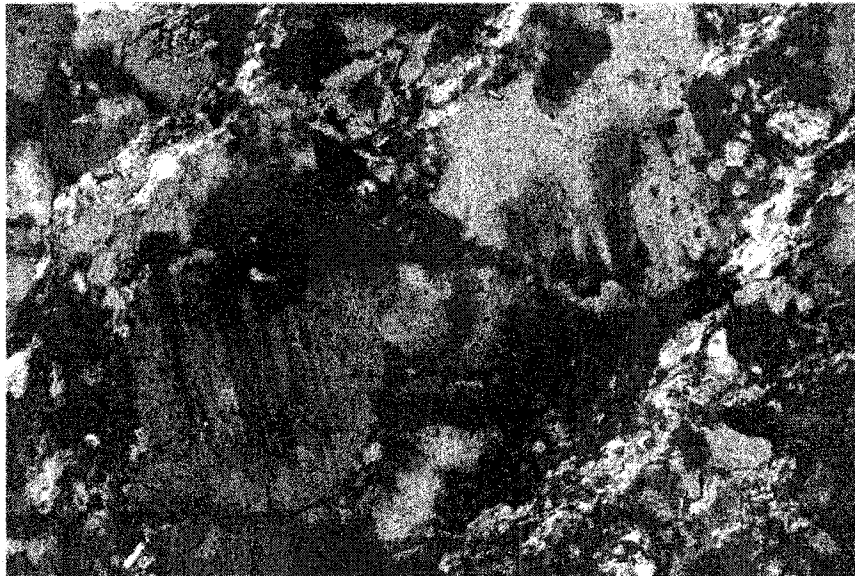


Figure 4.28 - Sample 530 - Crystal plastic deformation in plagioclase. The field of view is approximately 0.80 mm (X20, XPL).

Results - Table 4.2 summarizes the results of the microstructural analysis. Refer to Figure 4.29 for sample locations.

<u>SAMPLE</u>	<u>REGIME</u>	<u>SHEAR SENSE</u>
MGJ-506	Regime 1	Not recorded
GC-1	Regime 3	Dextral
GC-3	Regime 2	Dextral
GC-4	Regime 2	Dextral
GC-5	Regime 3	Dextral
GC-6	Regime 2	Dextral
GC-7	Regime 2	Dextral
GC-8	Regime 2	Dextral
GC-110	Transitional 2 - 3	Dextral
480	Transitional 1 - 2	Not obtained
520	Regime 3	Not obtained
530	Regime 3	Not obtained

Table 4.2 - Summary of results from the microstructural analysis in Area # 1.

Discussion - Table 4.1 contains the summary of microstructures of each crystal plastic deformation regime in quartz grains, and it has proven its usefulness to recognize and differentiate the regimes in Area # 1. In this area, the three regimes of deformation are present, and follow a remarkable spatial distribution. It is noticeable that the crystal plastic deformation in quartz grains increases from the southeast corner (Regime 1) towards the northwest corner (Regime 3).

Two out of twelve samples (GC-110 and 480) contain microstructures that belong to two regimes and are interpreted as transitional. Consequently, they represent the borders between adjacent regimes. For interpretation purposes, the boundary line for each regime is parallel to the attitude of the foliation.

Where observed, the kinematic indicators revealed a dextral sense of shear, which is consistent in all samples. This fact supports the validity of the analysis because of three reasons: 1) the kinematic indicators do not present bimodal sense of shear, indicating that they belong to the same generation. 2) Therefore, the imprinted crystal plastic deformation in quartz grains is attributable to the same deformation episode. 3) This study area has a short extent.

From this analysis, samples 520 and 530 differ from the rest of the samples lithologically. The increasing amount of plagioclase, quartz, and tourmaline, the absence of sillimanite and staurolite and a lesser amount of garnet suggests a metaigneous origin of these rocks.

Welch (1993) described the Great Common Fault Zone as a 20 ft wide strike slip fault that puts in contact a north block that consists of quartzo-feldspathic and amphibolitic gneisses, calc-silicates, and sheared pegmatites with a south block of pegmatites and pelitic schists. It is possible that the 20 ft (6m) wide Great Common Fault

Zone described by Carrigan (1984) occurs somewhere in the Regime 3 area. These differences in lithology will be addressed in Chapter VI.

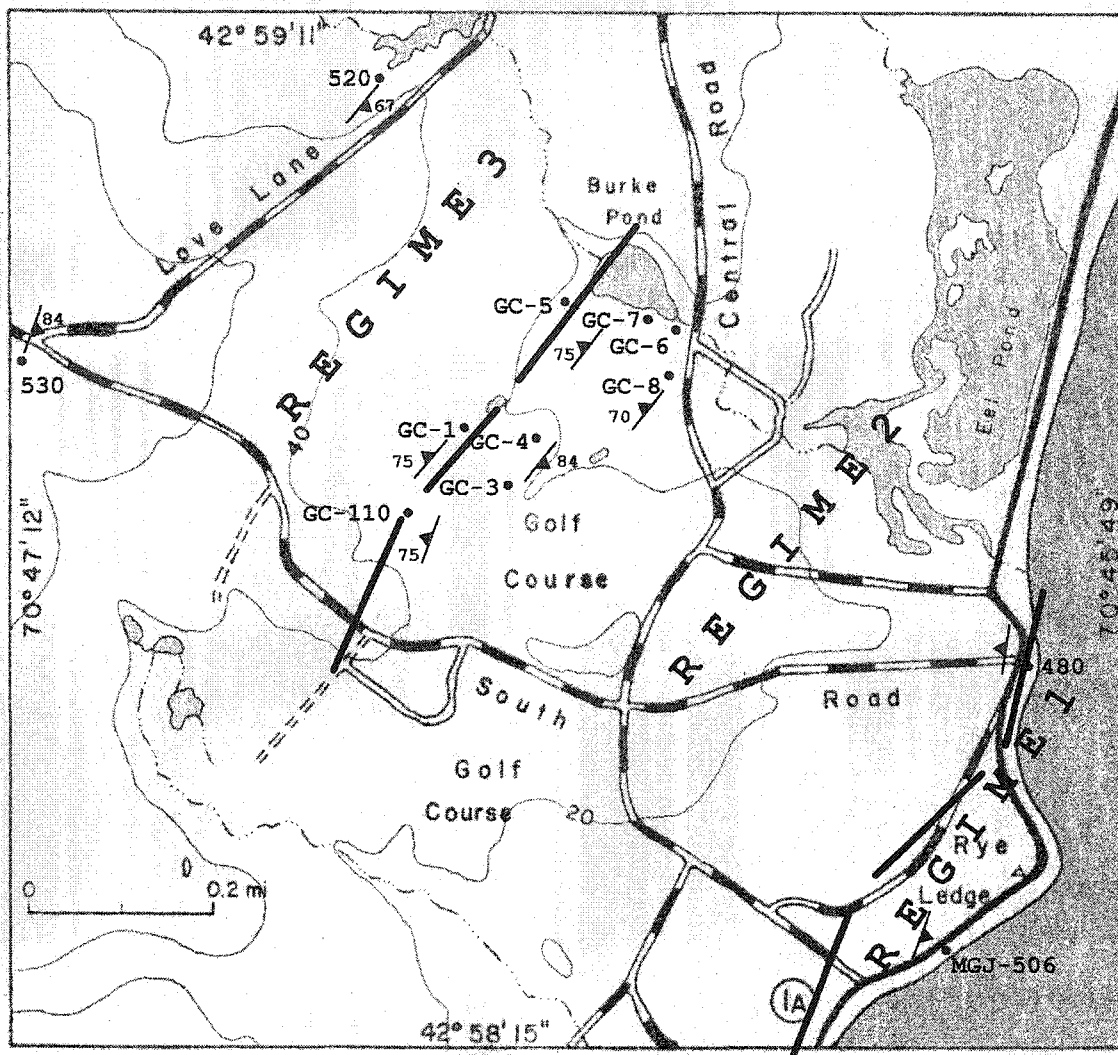


Figure 4.29 - Spatial distribution of the deformation regimes in Area # 1. The crystal plastic deformation increases towards the west.

Area # 2 - Rye Complex

Area #2 is located along the Hampton-Boston railroad close to the intersection of Lafayette Road and Route 101. It includes the outcrops around the electric substation of Hampton, New Hampshire

(Figures 4.1 and 4.30). In this locality, Lyons et al., (1997) showed the contact between the Rye Complex and the Merrimack Group which corresponds to the trace of the Portsmouth Fault Zone (Plate 1).

The objectives of the microstructural analysis in this area were to investigate the textures in quartz grains, and the shear sense along small outcrops of mylonite occurring along the railroad and close to the electric substation. Foliation in this locality strikes 057° and dips 58° (SE); on these planes a lineation that trends 233° and plunges 13° is present (fig. 4.31).

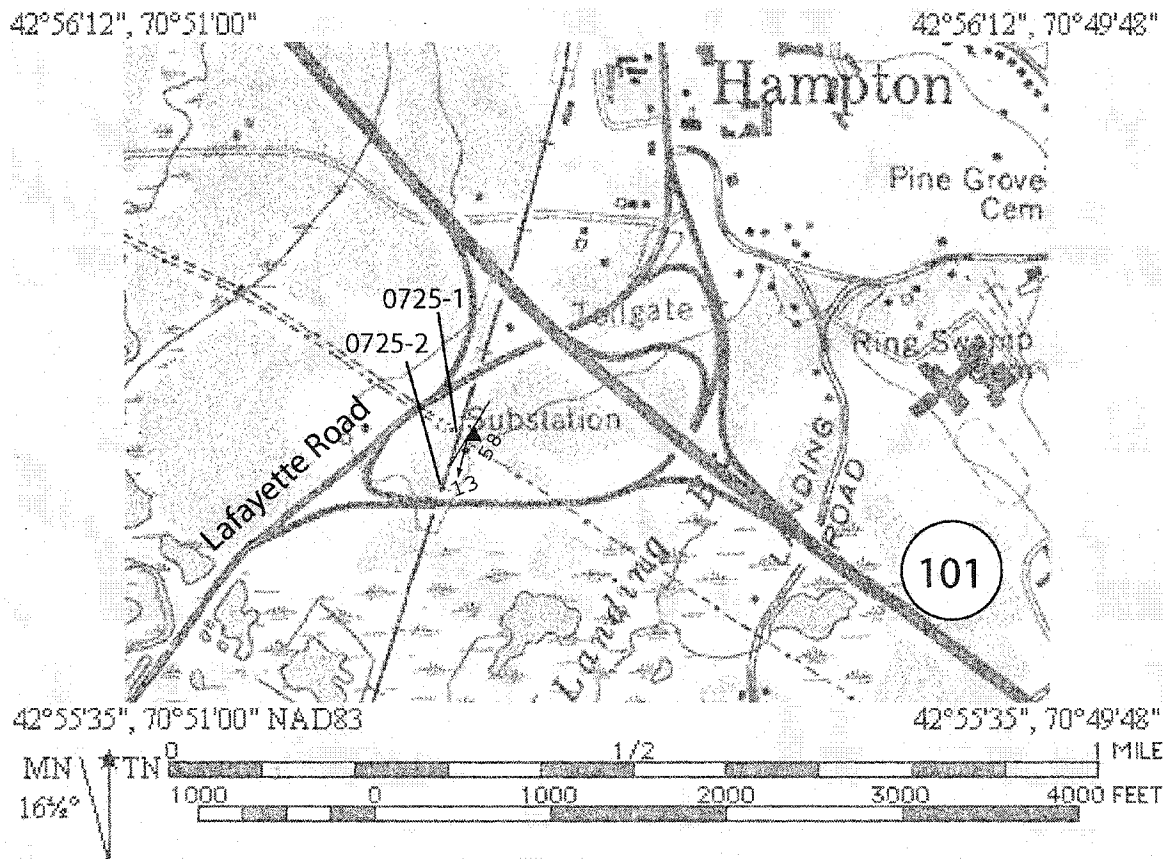


Figure 4.30 - Map of Area #2 showing sample locations. The strike and dip of the foliation is indicated, and the arrow shows the trend and plunge of the crenulation lineation.



Figure 4.31 - Crenulation lineation on a foliation plane of Area #2. The direction of view is to the northwest, a quarter dollar coin serves as scale.

Sample Description

Sample 0725-1 - Quartz grains in the two thin sections from this sample are equant, fine grained, and have polygonal texture (fig. 4.32). The amount of porphyroblasts (less than 10%) corresponds to a mylonitic type of rock. The few porphyroblasts present "bookshelf" structures and constitute systems with dextral sense of shear (fig. 4.33). The textures in quartz grains correspond to a transition between Regimes 2 and 3 of Table 4.1.

Discussion - The results of this analysis indicate that the dextral sense of motion is compatible with Area #1. Due to the on-strike location of this locality, it is plausible that the mylonitic rocks in these outcrops were affected by the Great Commons Fault Zone

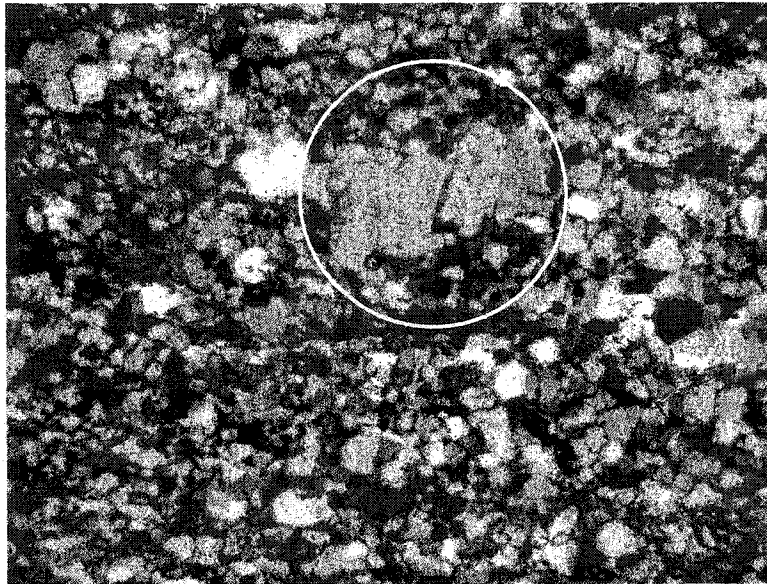


Figure 4.32 - Mylonitic texture in Sample 0725-1. A porphyroblast of K-spar has bookshelf structure indicating a dextral sense of shear (circled). The field of view is approximately 1mm (X10, XPL).

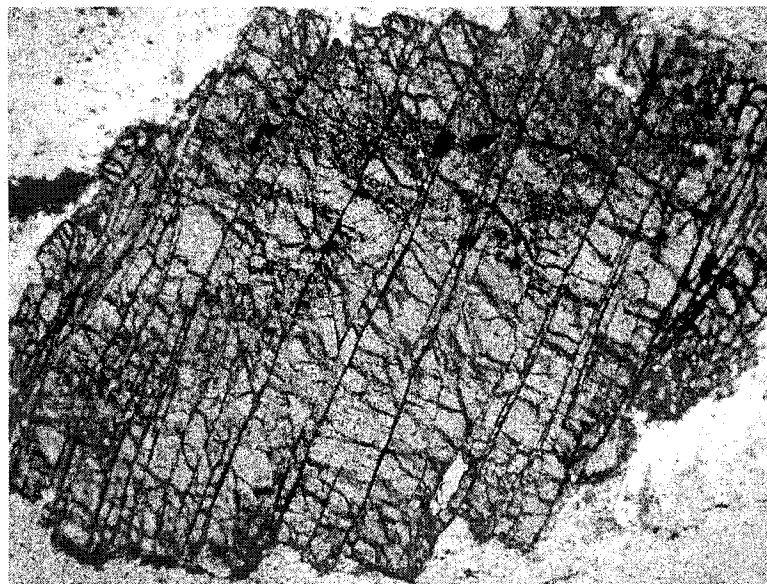


Figure 4.33 - Garnet porphyroblast in Sample 0725-1. The bookshelf structure indicates a dextral sense of motion. The field of view is approximately 3 mm (PPL, X4).

Area # 3 - Rye Complex

The microstructural analysis of the outcrops in Area #3 helped to identify a shear zone located under the bridge along Lafayette Road in the Dodge Pond area, close to Hampton Falls, New Hampshire (Figures 4.1, 4.34, and Plate 1). In this locality, the foliation strikes 075° and dips 50° (SE). A crenulation lineation that trends 120° and plunges 40° is occasionally present on the foliation planes.

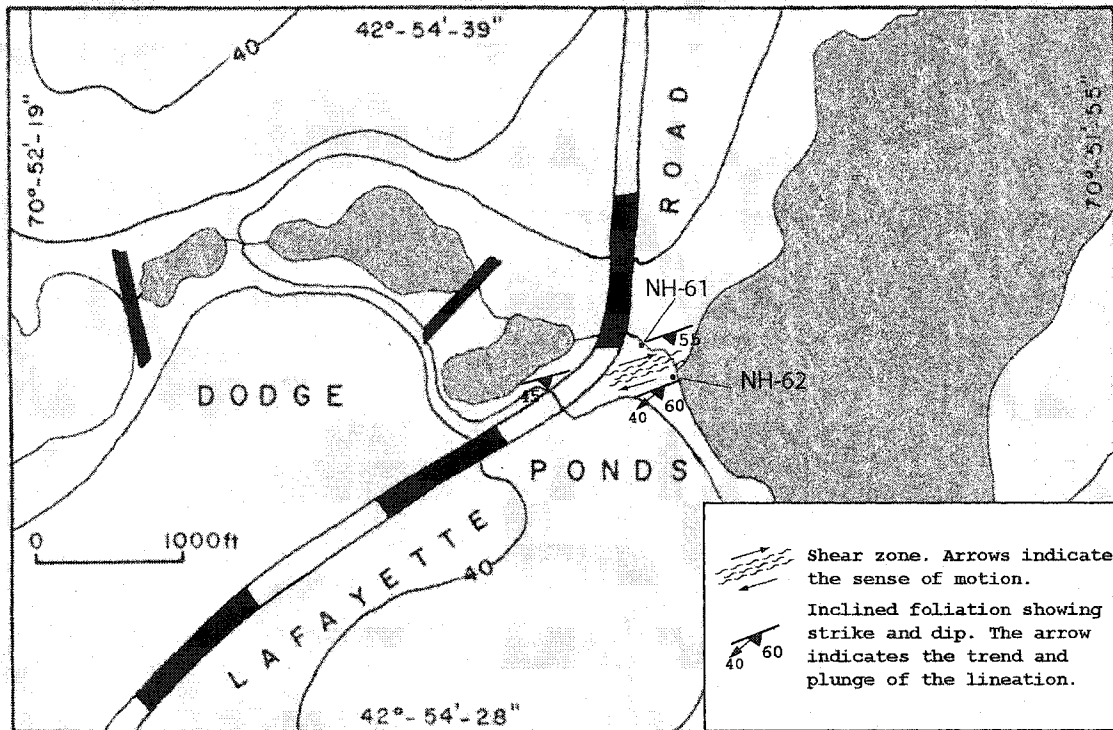


Figure 4.34 - Map of Area #3 showing the orientation of the shear zone, foliation, and location of samples NH-61 and NH-62, contouring at every 20 ft.

Sample Description

Sample NH-61 - In this sample of mylonitic rock, the boundaries of the quartz grains are flat and tend to form triple junctions (fig. 4.35). Recrystallized grains define a planar fabric, present a strong lattice, and shape preferred orientations parallel to the foliation (fig. 4.36).

The proportion of recrystallized quartz grains is higher than the original grains. Likewise, the size of the recrystallized quartz grains is larger than the original grains. The textures in this thin section correspond to Regime 3 of Table 4.1.

Sample NH-62 - This sample contains sigma grains of white mica pseudomorph of andalusite that define a dextral sense of shear (unimodal sense of motion). The blastomylonitic texture of the rock, the alteration, and the abundant lath shaped crystals of biotite that define the foliation around the porphyroblasts make the microstructures of quartz grains unclear.

Discussion - The results of this analysis indicate that the dextral sense of motion in Area #3 is compatible with Area #2, which is located about 2 miles farther to the northeast along Lafayette Road. These facts suggest that the two locations (Area #2 and #3) belong to the same structure. If true, then the Portsmouth Fault Zone is the structure that affected them.

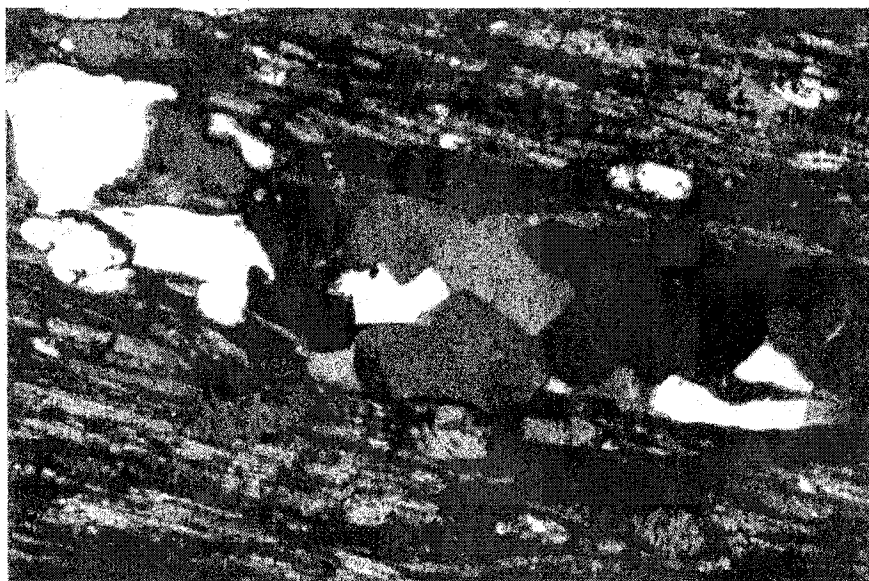


Figure 4.35 - Sample NH-61 - Polygonal textures in a quartz band parallel to the foliation. The boundaries of the subgrains are flat and tend to form triple junctions. The field of view is approximately 1.5mm (XPL, X10).

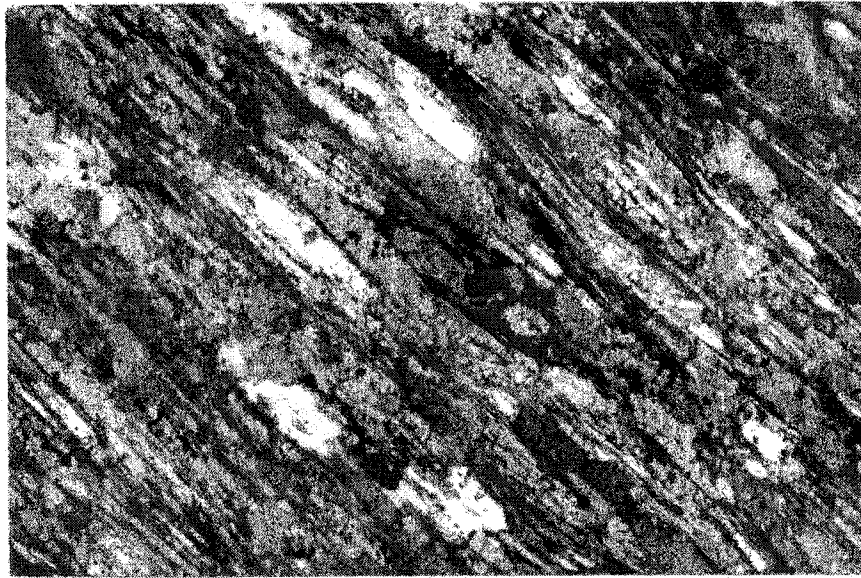


Figure 4.36 - Sample NH-61. Quartz grains show significant grain size reduction. The crystals are flat, their boundaries straight and parallel to the foliation, displaying shape and lattice preferred orientation. The field of view is approximately 2mm (XPL, X4).

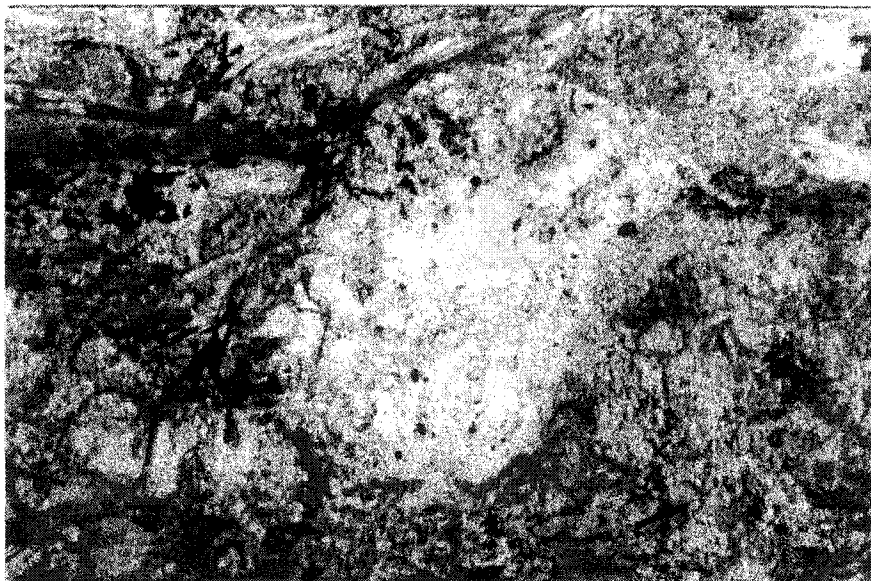


Figure 4.37 - Sample NH-62 - A sigma grain indicating a dextral sense of shear. The field of view is approximately 1.5 mm (PPL, X10).

Area # 4 - Merrimack Group

The microstructural analysis of the outcrops in Area #4 helped to identify an east-west trending ductile-brittle fault with the north block downthrown. The fault is located along the Exeter River, close to the intersection of Powder Mill Road and Juniper Ridge Road (fig. 4.1 and 4.38). In this locality, layering and foliation strike 259° and dip 40° (NW). A pervasive slickenfiber lineation that trends 047° and plunges 27° is present on the foliation-layering planes (fig. 4.39).

Veins of dark brown to black pseudotachylite of variable thickness occur in the P-2 sample location (fig. 4.40). In this locality, the outcropping rocks are not brecciated.

Sample Description

Sample P-1 - Recrystallized quartz grains tend to form triple junction boundaries with adjacent crystals. The straight boundaries are parallel to the foliation, which is defined by lath shaped biotite crystals (fig. 4.41). Quartz grains exhibit a low to medium shape and lattice preferred orientations. Textures in this thin section correspond to Regime 2 of Table 4.1.

Sample P-2 - This thin section belongs to a rock that contained a thin vein of black material (fig. 4.40). To investigate the presence of pseudotachylite in the rock, the plane of the thin section was cut parallel to the trace of the vein in the rock. The pseudotachylite vein with fragments of the host rock has no preferred orientation, branches along the area of the thin section, and has variable thickness. Fragments of the host rock, mostly quartz, occur along the flow banding of the vein. Where the vein narrows it is fine grained, where it widens it is glassy (fig. 4.42).

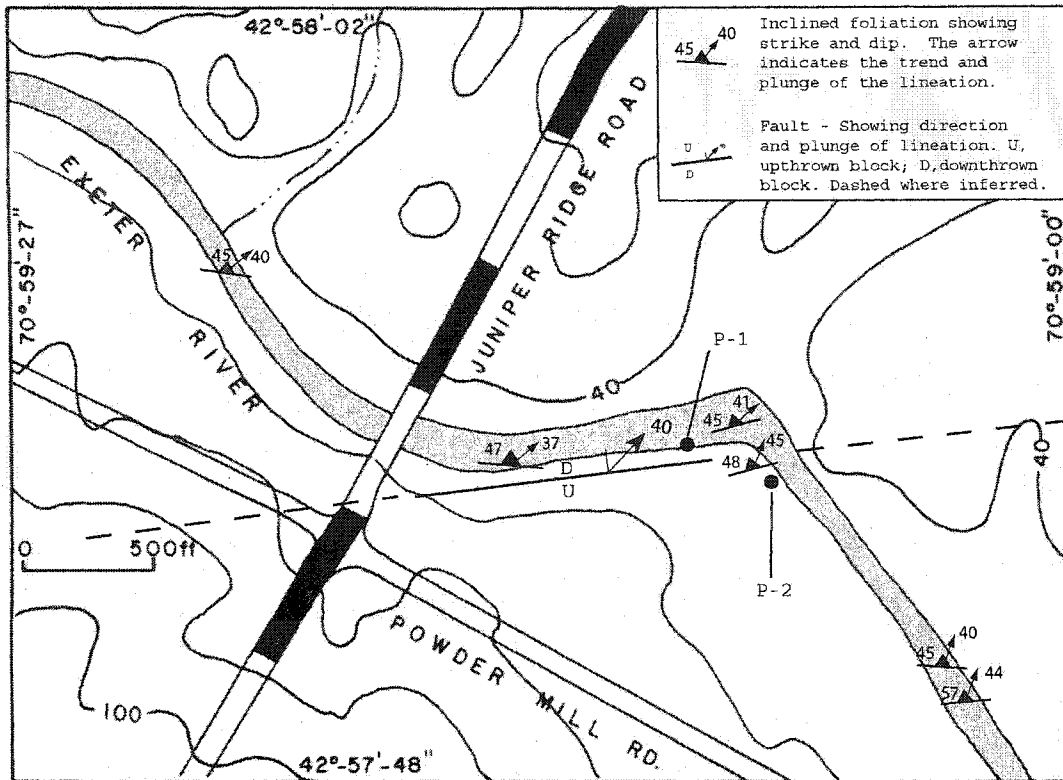


Figure 4.38 - Map of Area #4 showing the orientation of layering/foliation, fault, and sample locations, contouring at every 20 ft.

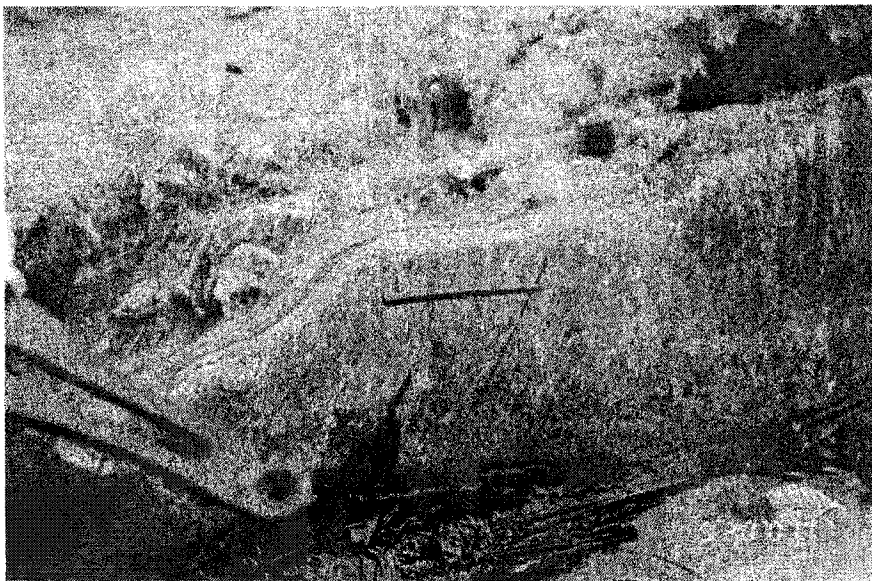


Figure 4.39 - Pervasive slickensided lineation on a layering plane. The strike of the layers is indicated by the black line. The large sight of the Brunton compass is 6.5 centimeters long, location P-2 in Figure 4.38.

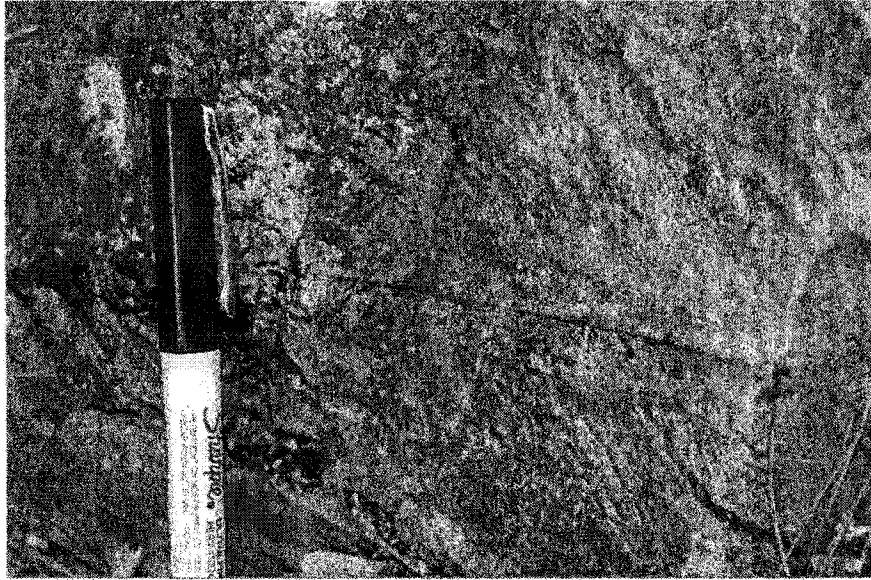


Figure 4.40 - Illustration of a thin pseudotachylite vein (2-3 mm thick). The cap of the marker is 5 cm long, location P-2 in figure 4.38.

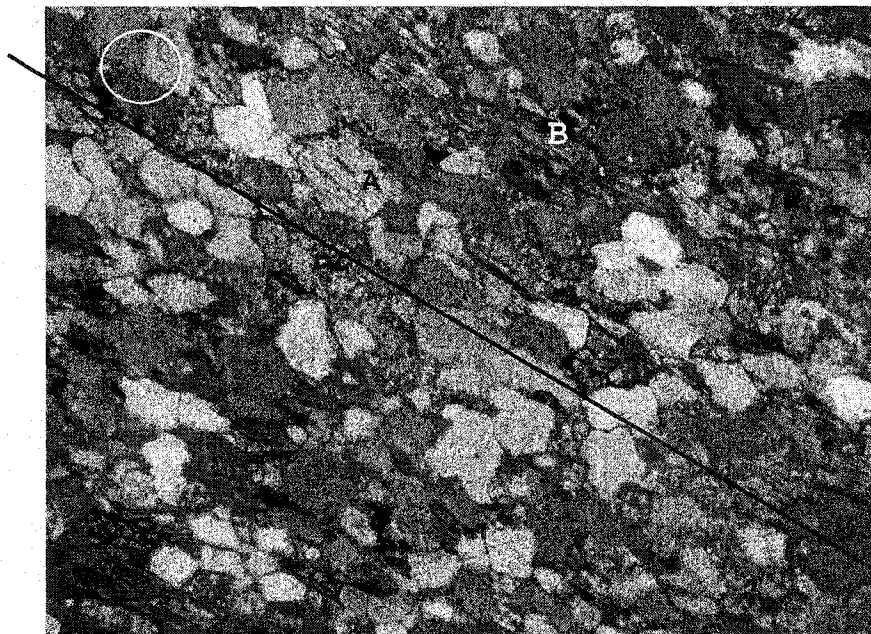


Figure 4.41 - Sample P-1 - Recrystallized quartz grains have straight boundaries parallel to the foliation (line), and tend to form triple junctions with adjacent crystals (circle). Lath-shaped biotite (B) and amphibole (A) crystals define the foliation. Original and recrystallized crystals present a medium shape and lattice preferred orientation. The field of view is 1.5 mm (XPL, 10X).

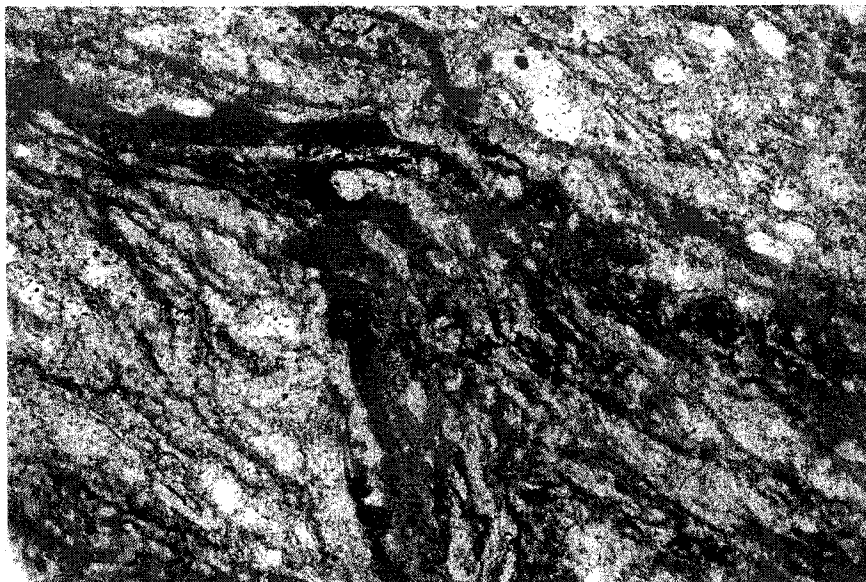


Figure 4.42 - Sample P-2 - Flow banding in a pseudotachylite vein with few isolated fragments of the host rock. The field of view is 1.5 mm (PPL, 10X).

Discussion - The presence of pseudotachylite and the pervasive slickensite lineation along layering and foliation planes provide evidence of ductile-brittle deformation in this area. From quartz slickensites, a principal vertical north block down combined with an eastwards horizontal movement is inferred. The trace of the suspect fault is almost east - west. The extension of this structure to the west of this area is discussed in Chapter VII.

CHAPTER V

STRATIGRAPHY OF THE MERRIMACK GROUP

Introduction

Previous authors defined the Merrimack Group as non-fossiliferous calcareous metasediments deposited by turbiditic currents (Rickerich, 1983; Bothner et al., 1984). The stratigraphic subdivision of the Merrimack Group, as originally defined by Katz (1917), includes the Kittery, Eliot, and Berwick Formations. However, the stratigraphic sequence of these formations remains ambiguous (Katz, 1917; Billings, 1956; Bothner et al., 1984). In the seacoast region, the Merrimack Group crops out predominantly in the Great Bay and in the Piscataqua River; in the remaining parts of the study area, it is present only in isolated outcrops (Novotny, 1963, 1969; Lyons et al., 1997); resulting in an intricate, and often difficult, correlation among units.

In an attempt to clarify the stratigraphy of the Merrimack Group, the author conducted a stratigraphic analysis of the Kittery and Eliot formations. The analysis focuses on the probable contacts between the Eliot - Kittery, and Eliot - Berwick formations. The analysis of the Berwick Formation is limited to the contact with the Eliot Formation in the Cocheco River (in Dover, NH). Recent structural and petrologic studies describe the nature of this unit (e.g., Allard, 1998). An ongoing study conducted by Schulz (Masters Thesis in progress) will shed more light on the understanding of this unit.

Escamilla-Casas (2002) subdivided the Kittery Formation to understand the present distribution of the unit in the study area, to identify the boundaries within the subdivisions and between adjacent stratigraphic units, and to provide keys for correlation. The Merrimack Group (more so the Kittery than the Eliot Formations) contains abundant and well-preserved primary sedimentary structures. These characteristics helped to identify the stratigraphic top in many outcrops.

In the fall of 1999, the USGS-Groundwater division drilled a series of boreholes along the Great Bay shore. The author studied the cores from well NR-1 (Fig. 5.1, Fabyan Point) and interpreted the contact between the Eliot and the Kittery formations as transitional, and tentatively placed the Kittery on top of the Eliot Formation. Because of the characteristics of the core and the lack of more evidence, the results were not conclusive.

During the summer of 2001, the Town of Madbury initiated construction of a new fire station (Fig. 5.2). The construction and blasting activities uncovered a wide area of Eliot Formation lithology. The pavement exposure of rocks allowed a detailed study of the folding style (discussed in Chapter 2) and of approximately 33m of, mostly continuous, stratigraphic column of this unit. A year later, the new building covered these rocks.

This chapter presents a discussion regarding recent findings of centimeter-scale structures in the Kittery and Eliot Formations, which suggest the presence of biogenic structures (e.g., burrows). Furthermore, a loose block of rock from Great Bay, presumably from the Kittery Formation, contains a reasonably well-preserved, three dimensional unidentified object that resembles a fossil (Location 1,

Fig. 5.1). At present, the identification of the suspect fossil, and the origin of the above-mentioned structures is still not confirmed.

In a later stage of this study, detailed geologic mapping, petrologic, and micro-structural analysis (discussed in Chapter 4) were conducted along certain accessible portions of the Bellamy and the Cocheco rivers, in order to describe the geologic characteristics of the probable Eliot - Kittery and Eliot - Berwick contacts (Fig. 5.2).

The study of the Kittery - Eliot transition includes detailed mapping and systematic sampling along the Bellamy River, as well as X-ray diffractometry. Results from these analyses favor the hypothesis that the Kittery Formation transitionally overlies the Eliot Formation.

Small scale (.5 - .3m) kinematic indicators such as boudins and attenuated folds are common structures under the Whittier Street bridge, over the Cocheco River, close to downtown Dover (fig. 5.2). Previous workers mapped the contact between the Eliot and Berwick formations close to this locality (e.g., Novotny, 1963; Lyons et al., 1997).

Field observations and detailed mapping of the deformational structures in the Cocheco River suggest that the contact between the Eliot and the Berwick Formations is not stratigraphic but an oblique dextral shear zone that affected the previously folded rocks. Superposed on the shear deformation is late brittle faulting. These observations support the hypothesis that the contact between the Eliot and the Berwick formations is a complex fault zone.

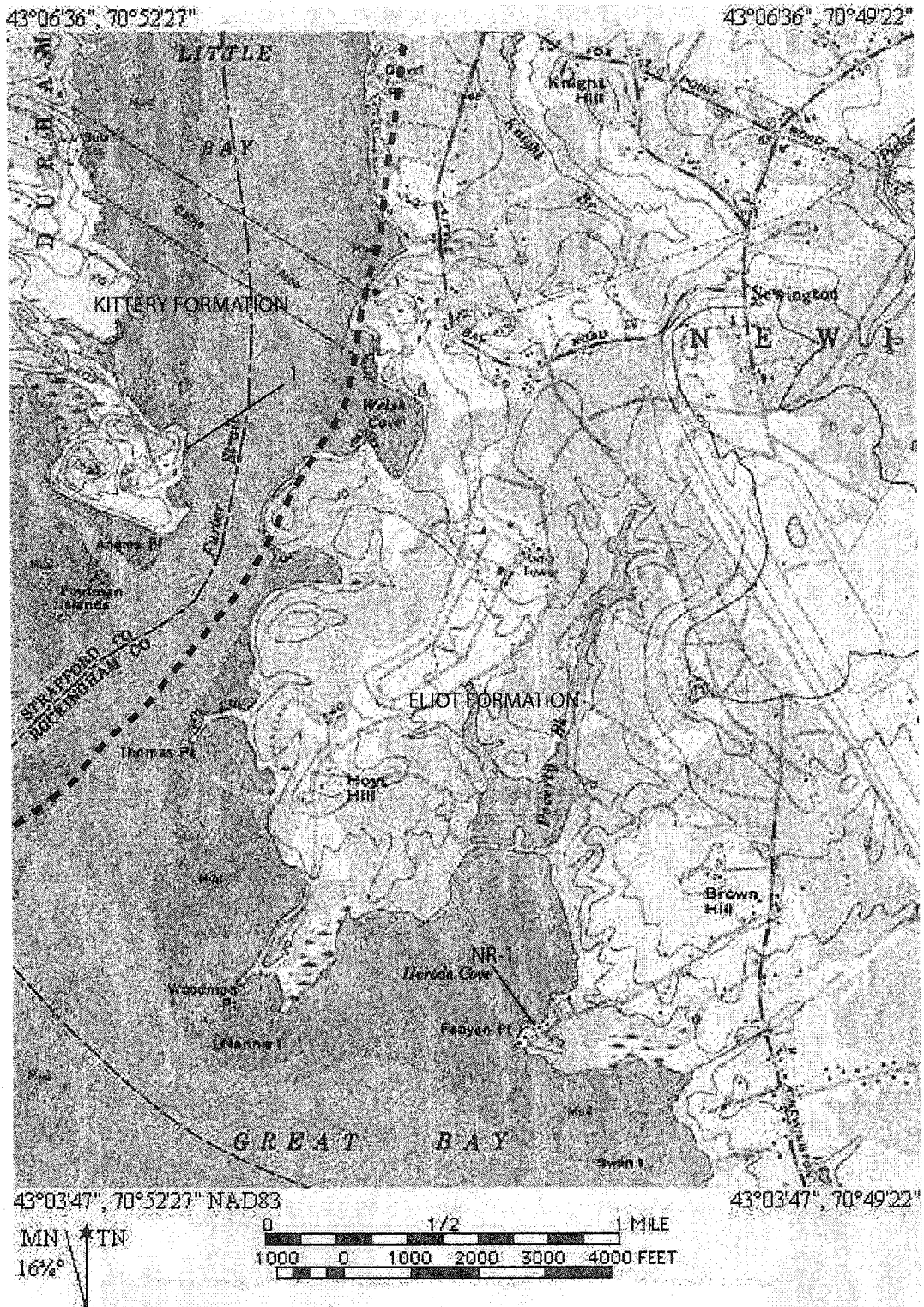


Figure 5.1 - Topographic map of Great Bay showing the location of the suspect biogenic structures (1), and the USGS drill-site at Fabyan Point (NR-1). The dashed line represents the contact between the Eliot (SOe) and the Kittery (SOk) Formations.

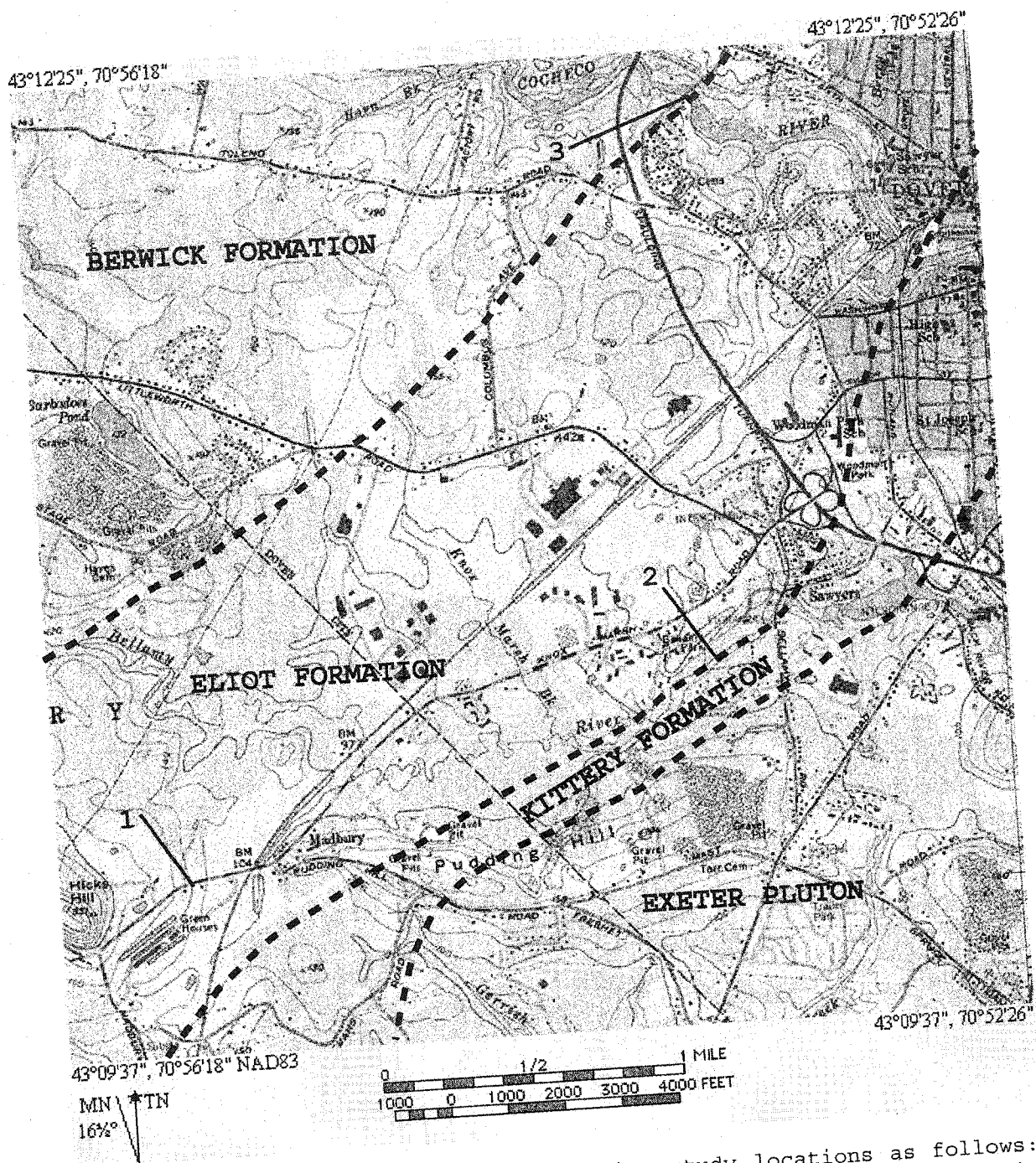


Figure 5.2 - Topographic map showing study locations as follows:
 1) Town of Madbury new fire station, 2) Bellamy River, and 3) is pointing to the intersection of Whittier St. an the Cocheco River.

Kittery Formation

Stratigraphy - Hussey (1968, 1985) defined this unit as a variably thick to thin bedded, tan-weathering, fine-grained calcareous and feldspathic metasandstone with usually thin interbeds of dark gray to black, often sulfidic phyllite. The thicker beds preserve cross lamination, flame structures, and graded bedding while the fine-grained rocks are thin-bedded, often laminae thick.

This study considers the relative abundance of metasandstone with respect to phyllite, local stratigraphic thickness, and the presence of sedimentary structures to subdivide this formation into three subunits (SOka, SOkb, and SOkc). In the Kittery Formation the more massive metasandstone layers consist mostly of quartz, feldspar, chlorite and/or biotite (depending on the metamorphic grade), and a variable content of carbonate minerals (about 10-20%). The rock weathers dark brown to dark gray and is rusty brown to medium gray/green (depending on the presence of chlorite) on fresh surfaces. Cross-beds are locally preserved in this type of rock.

Dark gray and gray phyllite layers are well foliated (predominantly parallel to the stratification), and weather reddish brown. They consist of fine-grained quartz, chlorite, or biotite, and are locally sulfidic. Metasandstone layers with flaser bedding and flame structures are often interlaminated with black thin layers of phyllites.

SOka - This subunit consists of light brown weathering metasandstone (10 - 60 cm thick) intercalated with light to dark brown phyllite (2 - 8 cm thick) with a ratio that ranges 2:1 to 3:2. Abundant primary sedimentary structures (i.e., cross-beds, flame

structures, graded bedding, and flaser beds) facilitate the recognition of the stratigraphic top in most of the outcrops.

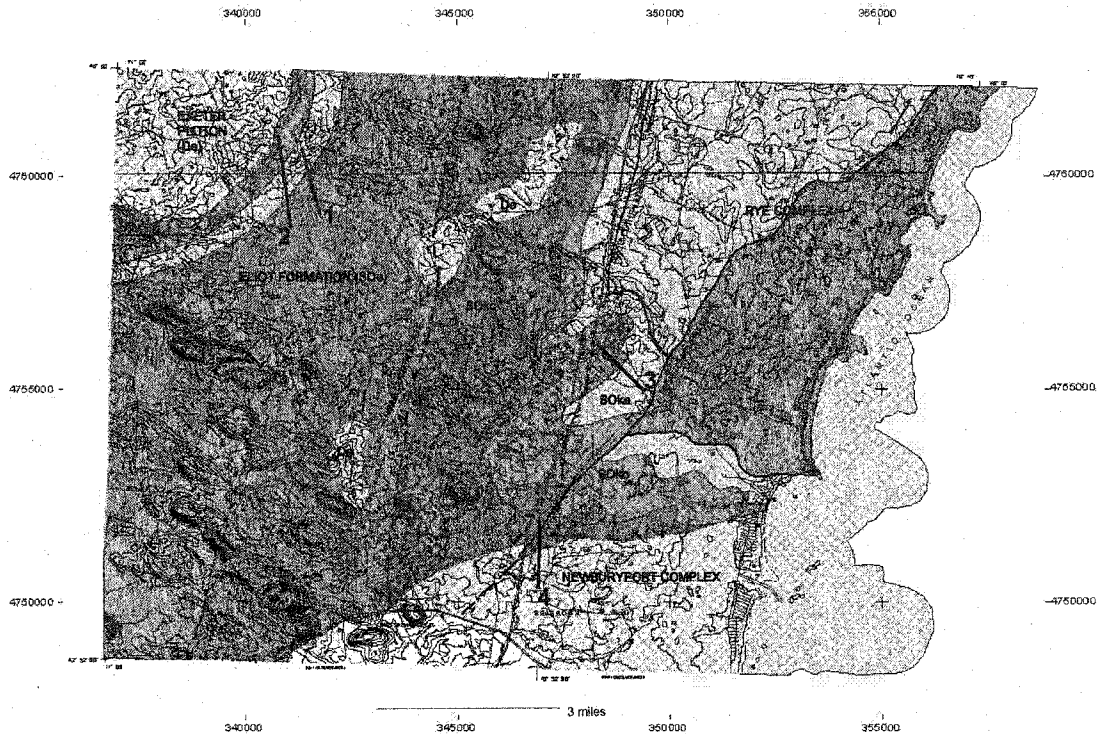


Figure 5.3 - Geologic map showing the three subdivisions of the Kittery Formation: SOka, SOkb, and SOkc (adapted from Escamilla-Casas, 2002, see Plate 1). The sampling location 1) corresponds to the bridge in Downtown Exeter, and 2) to the Exeter-Boston railroad.

Where the ratio changes to 3:2, subunit SOka is a massive quartz-feldspar-biotite granofels intercalated with dark brown to black phyllite layers (0.5 - 1 cm thick) and biotite schist layers are present. The identification of primary sedimentary structures is virtually impossible in this variant, but there is a clearly defined compositional layering.

The type locality of these rocks is the Exeter River, specifically in downtown Exeter, New Hampshire (Number 1 in fig. 5.3). The sample "Kittery - Bridge" for the X-ray analysis comes from this locality. Due to the characteristics of this subdivision, its

identification in other places along the study area is relatively easy. Figure 5.4 shows an example of sedimentary structures that are common to this subunit.

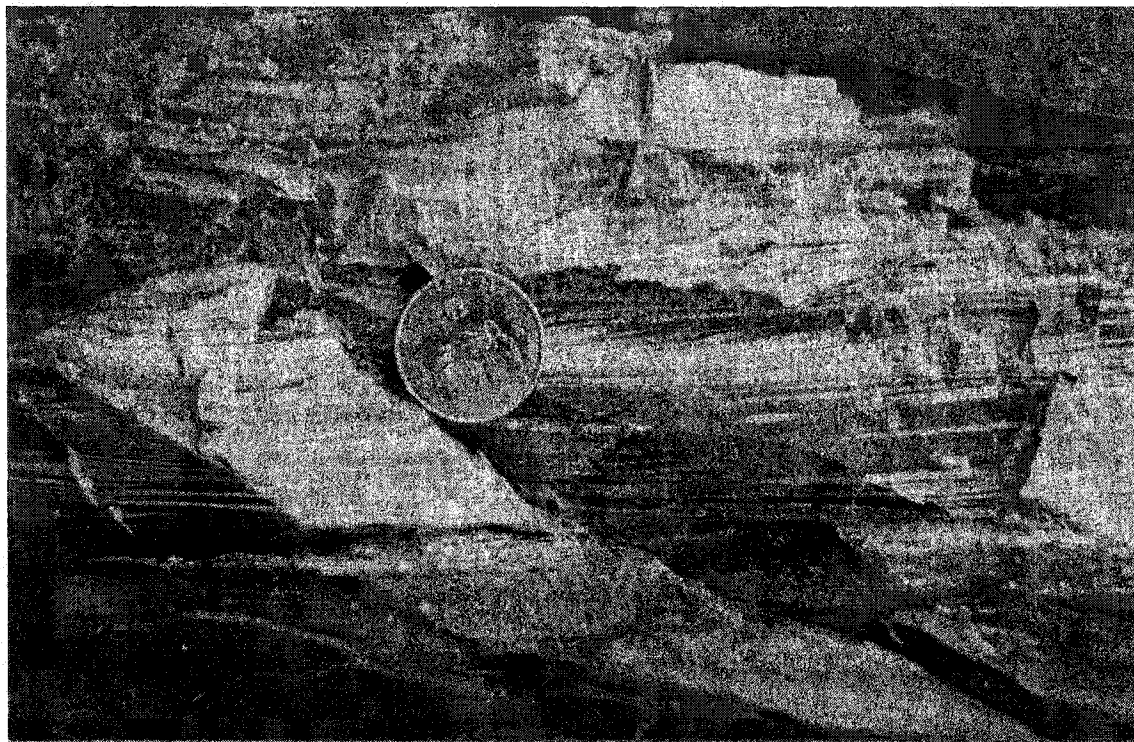


Figure 5.4 - Typical cross lamination in the SOka subunit. Location of this rock is the Exeter River in downtown Exeter, New Hampshire, quarter dollar coin for scale.

SOkb - This subunit consists of a light brown to light gray metasandstone (10 - 25 cm thick) and black to dark gray phyllite (1 - 3 cm thick) with a ratio of 3:1. The metasandstones are boudinaged and have undulatory bedding surfaces, in some cases containing buckled quartz veins. The contacts with phyllite layers are sharp, making the determination of stratigraphic tops difficult.

X-Ray diffractometry of a sample of this type of rock identified quartz, orthoclase, biotite, and chlorite as the principal components of the rocks in this subdivision (Sample Kittery - Railroad, number 2 of fig. 5.3). Figure 5.5 shows an example of this rock. At Towle Road

it crops out as a southwest-verging, asymmetric, variably plunging fold with associated crenulation-lineation on the limbs (number 3 in fig. 5.3).

SOkc - This subunit consists of a dark brown to light brown, fine grained, massive, slightly calcareous metasandstone (.85 - 1.0 m thick) intercalated with very thinly laminated phyllite (0.5 - 15 cm thick, when present) with a ratio of 4:1. The lack of primary sedimentary structures in this unit makes the identification of stratigraphic tops virtually impossible.



Figure 5.5 - Example of subunit SOkb. Important characteristics of this unit are the sharp contacts between the layers and the presence of probable sedimentary structures. The hammer is 30 cm long, approximately. The location of this outcrop is labeled as 3 in Figure 5.3.

This subunit crops out along the north portion of the Exeter River and Hampton Falls. Figure 5.6 shows a characteristic example of this subunit. It is probable that this subunit overlies the transition

with the Eliot Formation, and constitutes the lower stratigraphic member of the Kittery Formation.

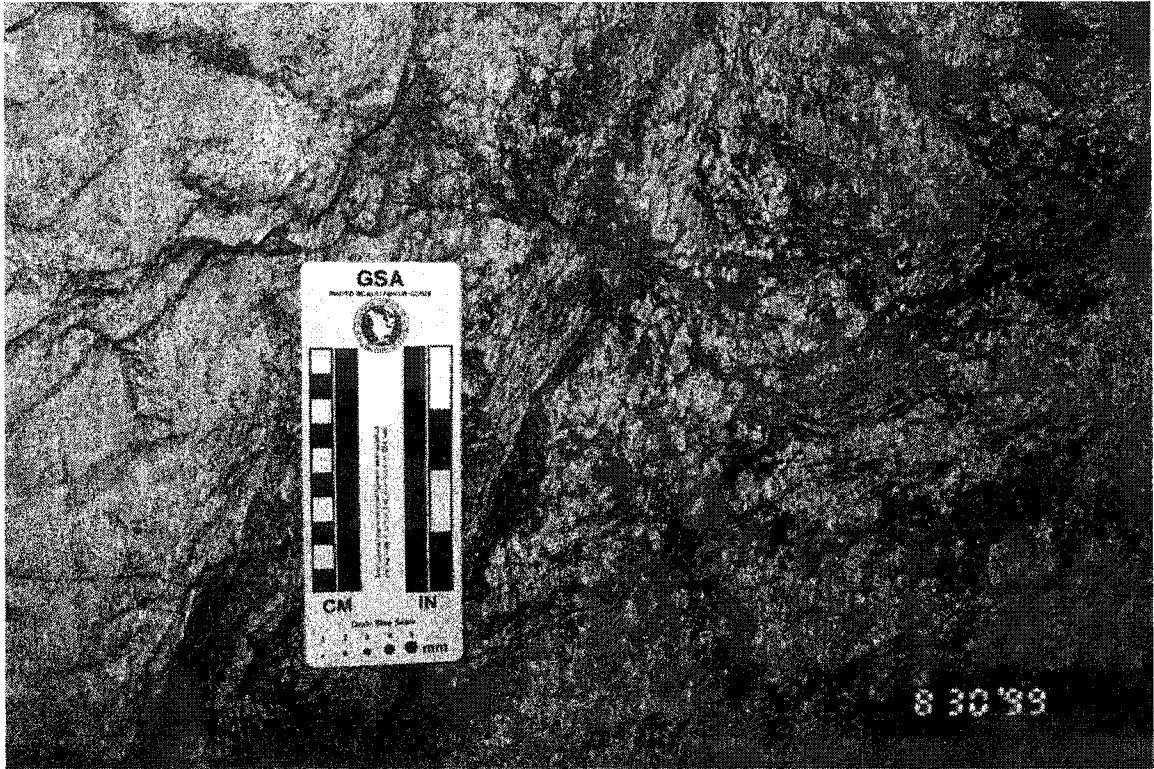


Figure 5.6 - Example of the S0kc subunit of the Kittery Formation. The location of this outcrop is labeled as 4 in Figure 5.3. A thin layer of pelite (where the scale is) separates two thick layers of metasandstone.

Evidence of Biogenic Structures - At the eastern end of Adams Point (north-west portion of Great Bay, fig. 5.1), a loose block of rock was found containing a reasonably well preserved three-dimensional unusual form. The block of light gray colored metasandstone is about 12 cm long, 8.5 cm wide and 5.5 cm thick. The preserved object is about 2.5 cm long. On the exposed section, the thickness ranges from 4 mm wide in one end to 1 mm in the opposite end (Figures 5.7 a, b, and c). The object projects out a few fractions of a millimeter from the flat

external surface of the layer that contains it. By simple visual inspection, the object resembles a fossil.

Efforts to identify the object are ongoing and local specialists at the University of New Hampshire as well as from other institutions have provided their insights in this regard. The following paragraphs summarize their comments:

Dr. William C. Clyde (UNH) thinks that the object resembles a fossil, but the conditions of preservation are not favorable enough for a positive identification. He insists that if a fossil is found then many more can be found. Dr. Herbert Tischler (professor emeritus, UNH) favors the hypothesis that the object is a fossil, and thought that the object resembles a section of a brachiopod based on its porous texture similar to bone.

Dr. Robert A. Gastaldo (Colby College) examined the specimen and considered that whatever was impressed in the sand it was three-dimensional when buried, and that the geometry of the object is difficult to determine.

He observed that silica replaced the material and that there is no organic matrix beneath the surface. He also identifies a coating with no cellular detail in it. The actual condition of the object is not well-enough preserved to make any identification, not even enough to discern if it is a piece of a plant or of an invertebrate.

Dr. Paul Strother (Boston College) observed the digital-images of the object (Figs. 5.7a-b) and thinks it is a piece of carbonaceous material that would have to be of terrestrial derivation. Based on the lithologic description of the rock, and from the primary sedimentary features in the metasandstone, he suggested that it belongs to a more proximal deposition than is typical for turbidites.

Dr. Strother suggests that it is necessary to identify another similar object, and states that it is very unusual for a fossil plant material to exist in isolation as a single specimen. Therefore, more than one specimen will facilitate a proper identification.

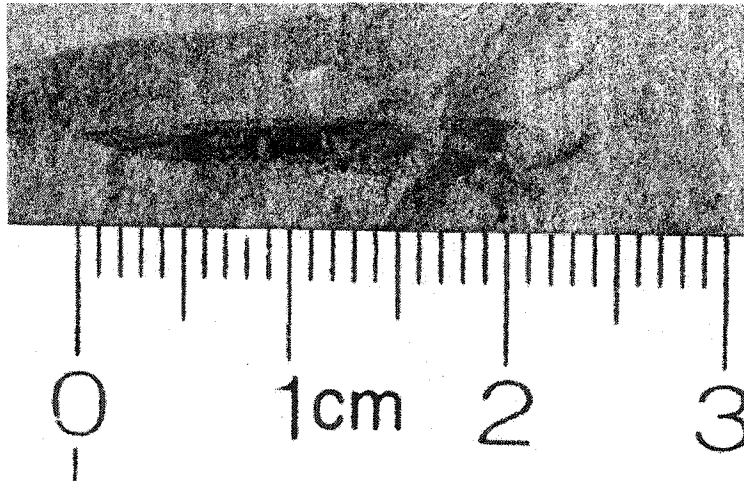


Figure 5.7a - Close-view photograph of the 0.9 in (2.3 cm) long object. A fracture filled with the unconsolidated sediment occurs in the right end. This fact reveals that the deposition of the object occurred during the sedimentation process.

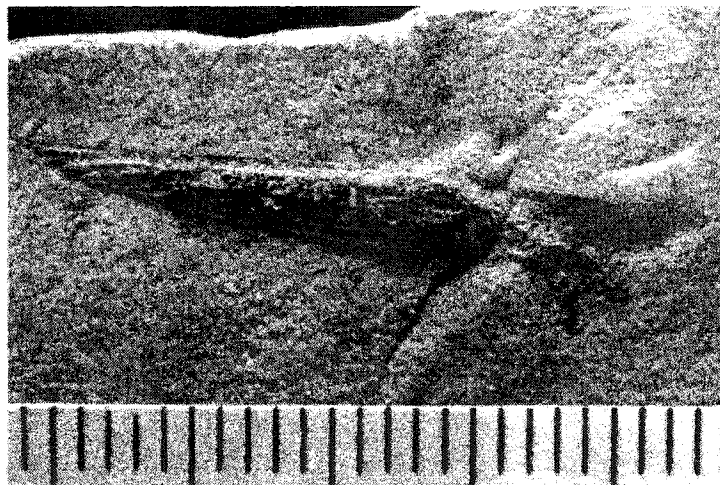


Figure 5.7b - The illumination of this photograph reveals the relief of the object. Twenty five subdivisions of the scale represent an inch.



Figure 5.7c - A general view of the block of host rock with the suspect object. The sample is from location 1 in Figure 5.1 (Kittery Formation).

Another of his suggestions is to look for organic matter in associated phyllites. This would yield clues as to provenance. Dr. Strother mentioned that the plant name given to simple organic axes similar to this form in the Devonian is "Hostinella".

Dr. Mark McMenamin (Mount Holyoke College) suggests that the object might be a spine from a possible Upper-Silurian (?) acanthodian fish. To support his opinion, Dr. McMenamin referenced Spjenldnaes (1967). Spjenldnaes (1967) described species of acanthodian fishes from the Siluro-Devonian beds of Ellesmere Island, Canada, as follows: "the fin-spines of the *Ischnacanthus* (?) *scheii* sp. nov. are fragmentary, and slightly curved to almost straight. In older specimens, the flanks are sculptured with fine, irregular longitudinal lines". The illustrations and descriptions in the above-mentioned work have strong similarities with the fossil-like object.

Furthermore, in subsequent visits to the same location, more evidence of biogenic structures was found in situ (Fig. 5.7). The layer with the suspect bioturbation is 10 ft (3m) far from the location where the loose block with the suspect fossil was found (Fig. 5.1).

The texture and color of both rocks are similar. The layer with the "bioturbation" is a light gray feldspathic metasandstone about 3 - 4 ft (1m) thick, delimited in the top by a dark gray metasandstone intercalated with laminae of dark gray, 12 to 15 cm thick phyllite.



Figure 5.8 - Close-up photograph of the suspect bioturbation in the Kittery Formation (Location 1, fig. 5.1). These cylindrical shaped structures are filled with material that is darker gray and finer grained than the host rock. The coin (American cent) has a diameter of about 3/4".

The layer contains well-preserved primary sedimentary structures, including cross beds and flame structures that are unequivocal indicators of the stratigraphic top. The layer at the bottom is black shale, 10 cm thick, which lacks stratigraphic top indicators. The sample described above will remain in the Department of Earth Sciences waiting future study.

Eliot Formation

Stratigraphy - The Eliot Formation consists primarily of thin to thick tabular and lenticular layers of calcareous metasiltstone and metashale with lesser amounts of metasandstone. It generally has thin-bedded alternations of tan-gray weathering, turbiditic calcareous metasilt, and silvery dark gray phyllite.

This section discusses the lithology of a 39 m long stratigraphic sequence measured during the initial stages of construction of the new fire station in the Town of Madbury. Figures 5.9 and 5.10 illustrate the geologic map and the stratigraphic sequence, respectively.

Plane table and alidade, measuring tape, Brunton compass, and a portable GPS unit were used to construct the geologic map. The identification of stratigraphic horizons facilitated the tracing of the bedding contacts on the map by using control stations (fig. 5.9). The trace of the stratigraphic column trends 42° . The "zero level" of the column coincides with the southwestern end of the trace line B-B', Figure 5.10.

The stratigraphic sequence does not satisfy the requirements of a stratigraphic section in a strict sense because the recorded thicknesses belong to a folded sequence (fig. 5.11). The stratigraphic column in Figure 5.9 displays the projected dimensions recorded at the ground surface on a 45° dipping plane that contains the fold axis.

The thicknesses of the layers in the stratigraphic column, consequently, may vary significantly from the real thicknesses. However, for documentation purposes the column is valid because the recordings of lithologic changes are direct observations of the exposed rocks, except in the intervals where the construction debris covered the rocks (less than 11%).

The sediments that constitute the protolith of these rocks are clay, silt, and fine to medium-grained sand; they were later metamorphosed to chlorite-biotite grade. The small grain size and the abundant pelitic to psammitic composition of these rocks indicate that low-density flows were responsible for the deposition and transport of the sediments.

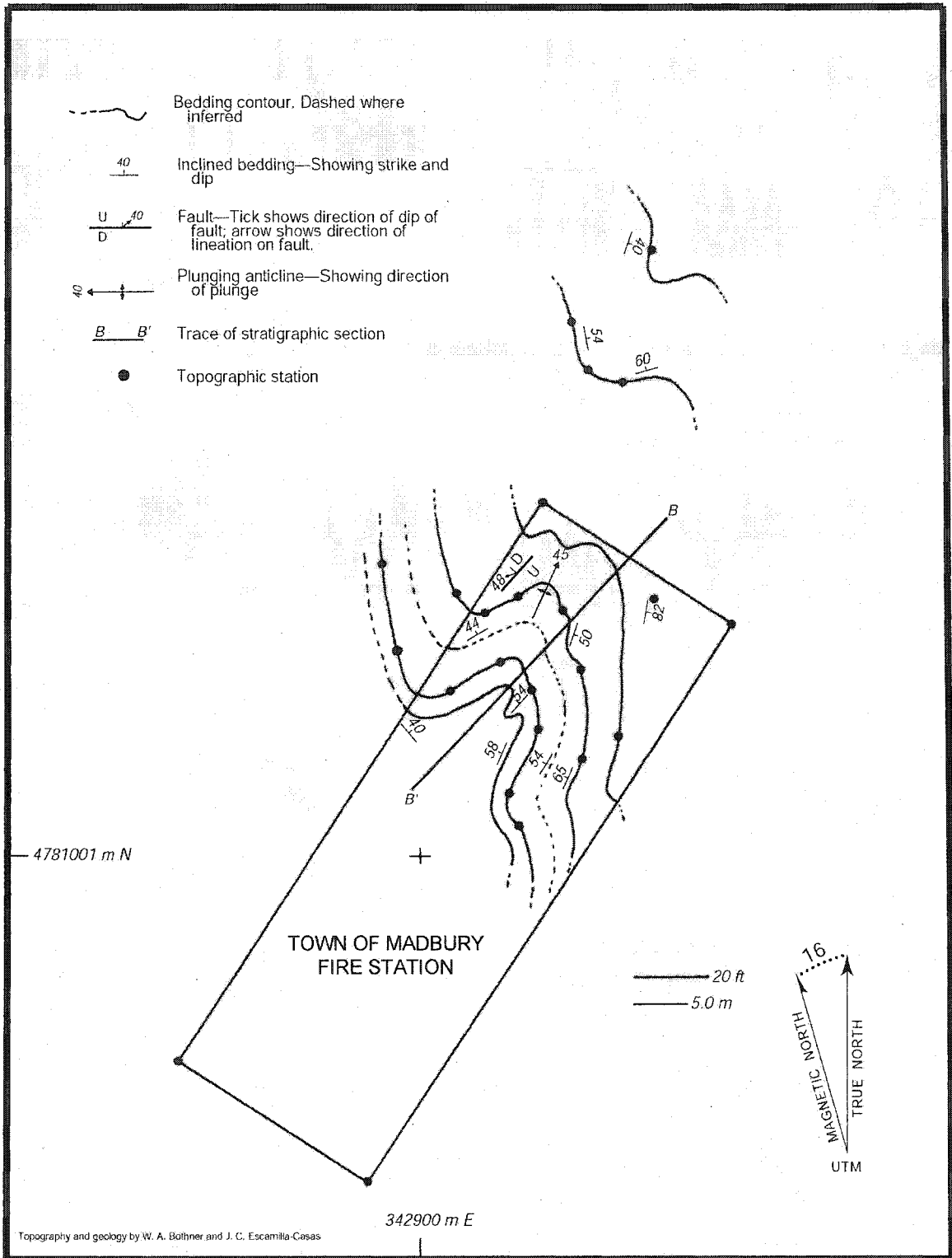


Figure 5.9 - Geologic map of the Town of Madbury new fire station. Line B - B' represents the trace of the stratigraphic section of Figure 5.10.

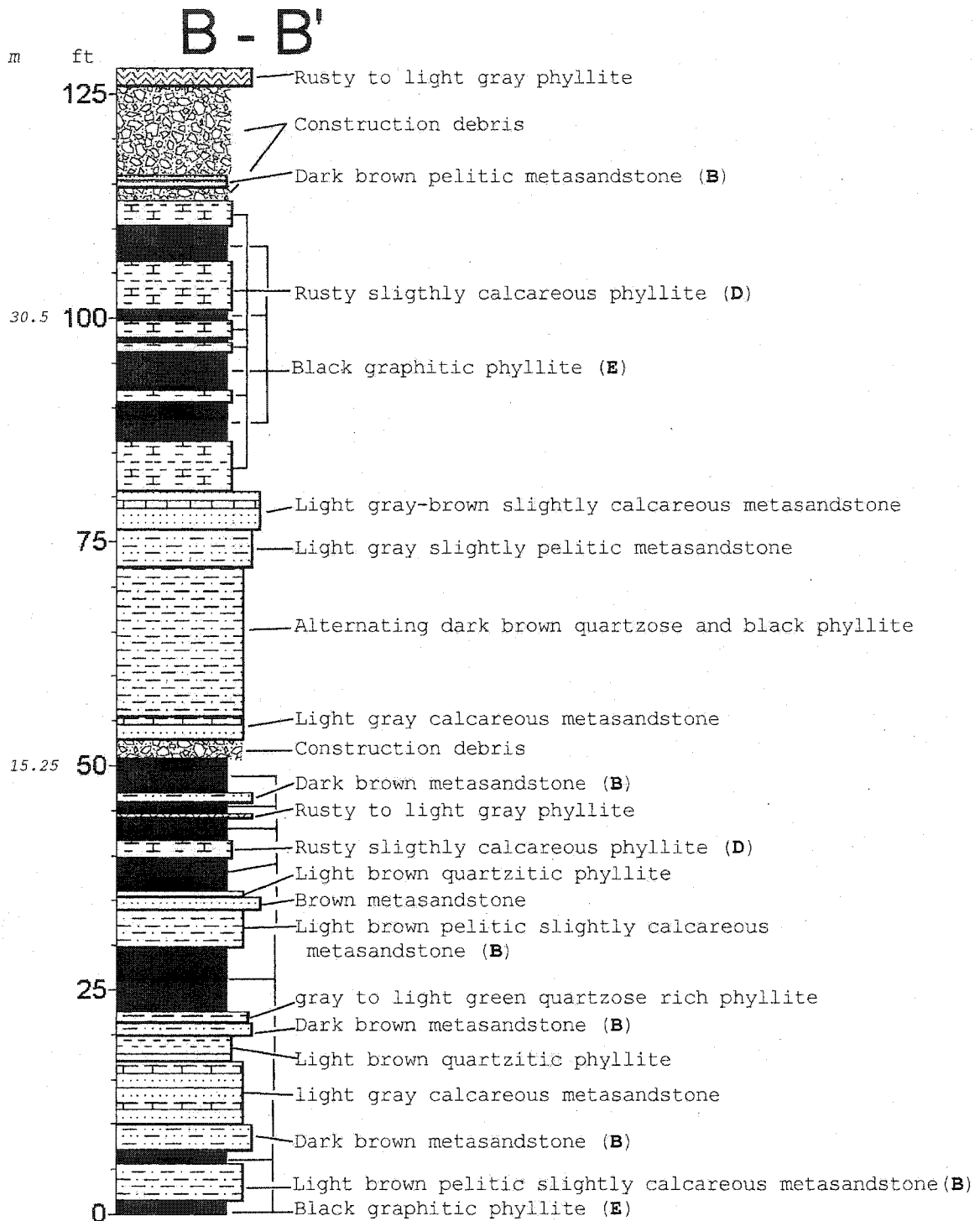


Figure 5.10 Stratigraphic column of the Eliot Formation at the Town of Madbury new fire station location. The bold capital letters in parenthesis indicate the corresponding structural unit of the Bouma sequence.

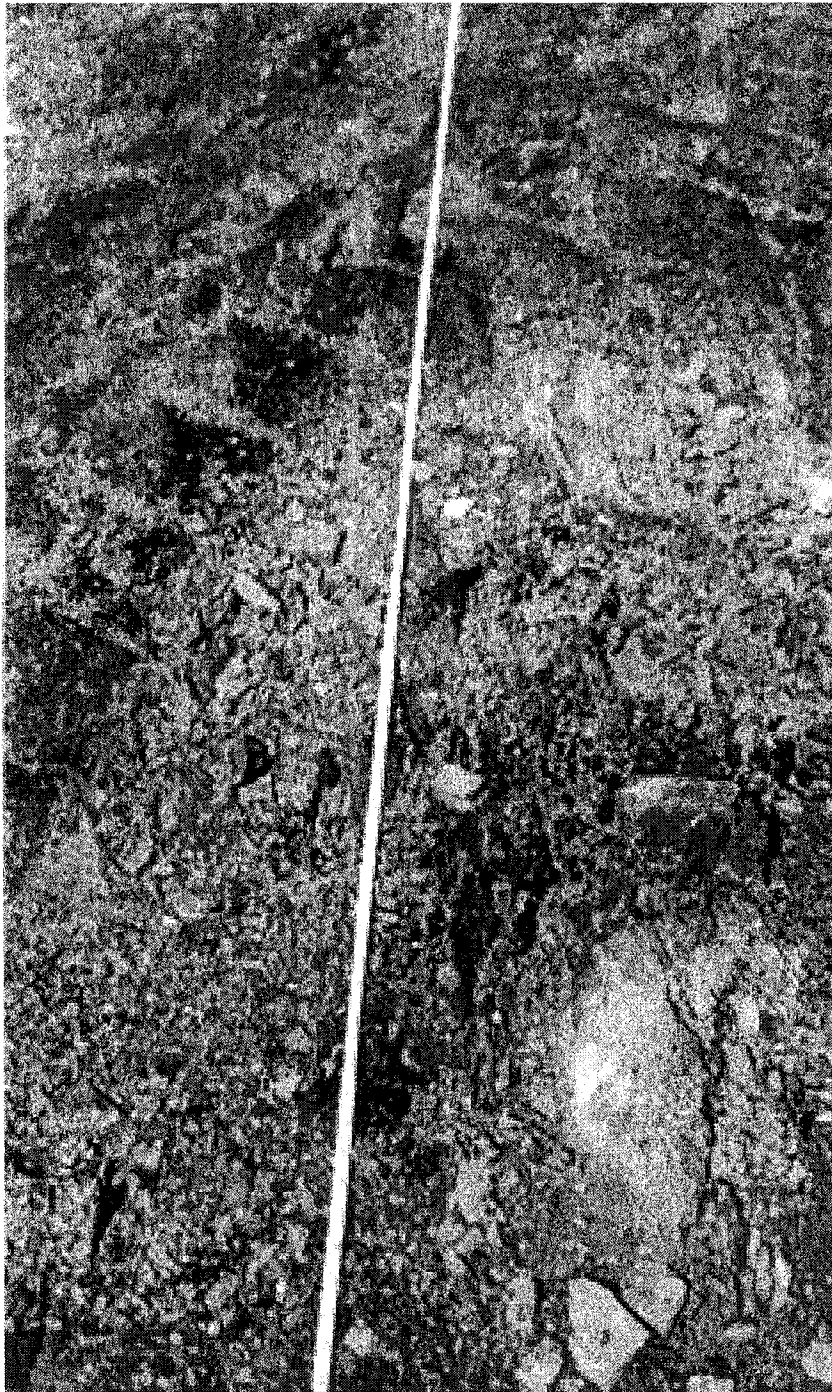


Figure 5.11 - This illustration shows the trace of the stratigraphic section and the folded structure in location 1, Figure 5.2. The length of the tape is about 1.20 m.

Bouma (1962) identified five units in an ideal turbidite sequence.

These units include characteristics of turbidites deposited from low-density flows as well as high-density flows.

The recorded data from the stratigraphic column (fig. 5.10) allows the identification of three structural units (B, D, and E) of the Bouma sequence. Unit E is the most persistent of all three, and it is present in the intervals of black graphitic phyllite. The intervals of light brown, pelitic, slightly calcareous metasandstone and the dark brown metasandstone constitute the structural units B. The structural unit D is present in the intervals of rusty, slightly calcareous phyllite.

Graded bedding in the intervals 80 - 120 and 20-30 ft define the polarity of the sequence. The stratigraphic tops clearly point to the northeast. Occasionally, in the remainder of the section, the stratigraphic top was unclear. However, an opposite polarity was not present in any segment of the section.

Suspect Biogenic Structures - The elongated structure, variably thick and 7 mm long, illustrated in the top illustration of Figure 5.12 belongs to a sample from the 29-30ft (9.7-10m) interval of the stratigraphic column. The bottom illustration of Figure 5.12 is the traced contour of the structure that facilitates visualization.

The structure has wave-shaped walls, and in both ends, it is tip-ended. The discovery of the structure occurred while cutting a blank for thin sectioning. Neither the blank nor the remainder of the rock preserves a counterpart of the structure due to the rock cutting process.

Inside the structure, the sediment is dark brown, slightly coarser than in the host rock, and the orientation of the grains is oblique with respect to the fine lamination in the host rock. The wave-shaped wall of the structure is a thin surface of extremely fine-grained black shaly material and may be carbonaceous (?). The long

axis of the structure is not perpendicular to the lamination, and the wave-shaped walls define ribs similar to chambers. The structure has a plane of symmetry along the longitudinal axis. The host rock is a dark brown, fine-grained, and finely laminated metashale.

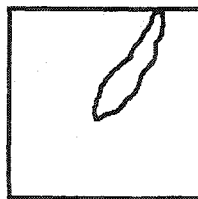
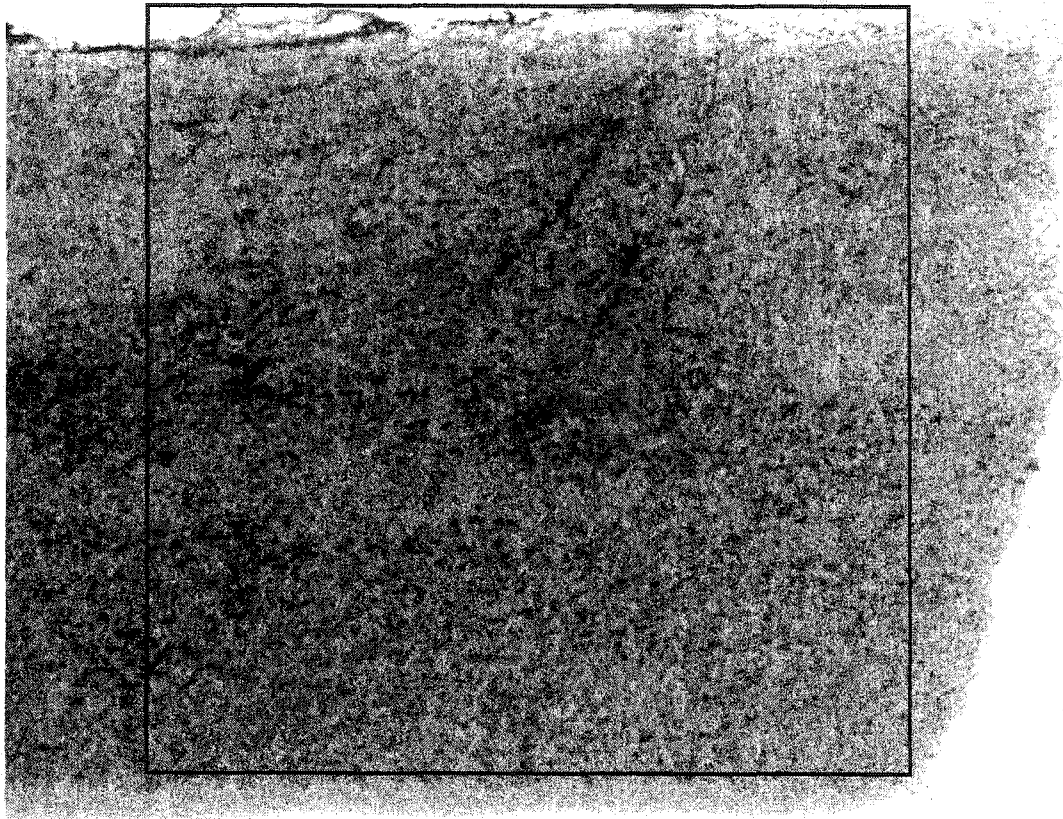


Figure 12 - Suspect biogenic structure from the segment 29-30 ft of the stratigraphic column from the Town of Madbury new fire station. The upper illustration shows the structure as it appears in thin section. The lower illustration is traced from the image above, the rectangular section is 9x7 mm.

In water-saturated sediments, fluidization structures may occur (e.g., sand dikes). The lack internal features except for some oriented mica flakes and other elongated particles that are commonly aligned parallel to their walls. The structure in question does not present any mineral orientation parallel to the walls.

The structure itself has few observable characteristics that may suggest a water-saturated sediment origin. On the other hand, the irregular shape of the walls and the non-parallelism of the sediments point to a biogenic origin. However, more evidence is necessary to clarify the origin and to make a proper identification of the structure.

Stratigraphic Contacts

Hussey (1985) interpreted a gradational contact between the Kittery and Eliot Formations with the Kittery being older. That stratigraphic order was reversed by Lyons and Bothner (1989) and later examined by Bothner and Hussey (1999). To clarify the stratigraphic order, a detailed examination of the core from well NR-1 and mapping across previously mapped contacts (e.g., Novotny, 1963; Lyons et al., 1997) of Kittery-Eliot (Bellamy River) and Eliot-Berwick (Coheco River) was conducted in this study.

Transitional Eliot- Kittery - A first stage in the attempt to clarify the stratigraphic order between the Kittery and Eliot formations took place while logging the segments of the core from well NR-1 in the fall of 1999. The identification of the probable contact between these two units occurs at 19.7ft (6m) deep. Megascopically, the rock above the 19.7 (6m) feet mark is a light green metasandstone, interlaminated with abundant black pelitic layers of 1-2in (2.5 - 5 cm) thick.

The strata dip 45° with respect to the longitudinal axis of the borehole, lack identifiable stratigraphic markers, and have a strong

crenulation cleavage (fig. 5.13). The minerals identified are quartz, plagioclase, biotite, chlorite, and disseminated carbonate. The accessory minerals are iron oxides and sulfides, zircon, and apatite. The relative abundance of biotite and chlorite is high. The crenulation cleavage in this core along the 15-19.7 ft (4.57-6 m) interval is critical for the identification of the contact.

The stratigraphic contact is 1-2 in (2-5 cm) thick horizon of probable basal conglomerate with slightly rounded clasts (fig. 5.14). The clasts are pieces of the cleaved rock included in a mass of quartzite. In thin section, the contact shows two important characteristics: one, the interruption of the crenulation cleavage, and two, the amount of biotite decreases towards the top of the borehole (fig. 5.15).

Below the 19.7 ft (6 m) mark, the rock consists of 2 - 8 in (5-20 cm) thick layers of light brown metasandstone interlaminated with layers of 0.5 - 1 in (1.2-2.5 cm) thick black shale. Primary sedimentary structures are abundant and define a stratigraphic top pointing towards the bottom of the borehole. The logging record indicates that the drill bit started cutting the bedrock at the 15 ft (4.572m) depth mark. The angle of intersection between the crenulation cleavage and the planes of stratification is 8 degrees.

Subsequent efforts to document the contact consisted of detailed mapping and systematic sampling along the Bellamy River. Field observations of the rocks in the Bellamy River are interpreted as a transition between the Eliot and the Kittery Formations.

Fieldwork indicates that the rocks in the west end of the Bellamy River traverse and the rocks in the Town of Madbury fire station have strong similarities. Likewise, the rocks in the middle part of the section are strongly similar to the rocks where the Kittery Formation

has been mapped (e.g., Adams Point, Downtown Exeter, NH, in Novotny, 1963, 1969; Lyons, 1997; among others). Along the Bellamy River traverse, the strike and dip of bedding are more or less persistent ($227^{\circ} - 44^{\circ}$).

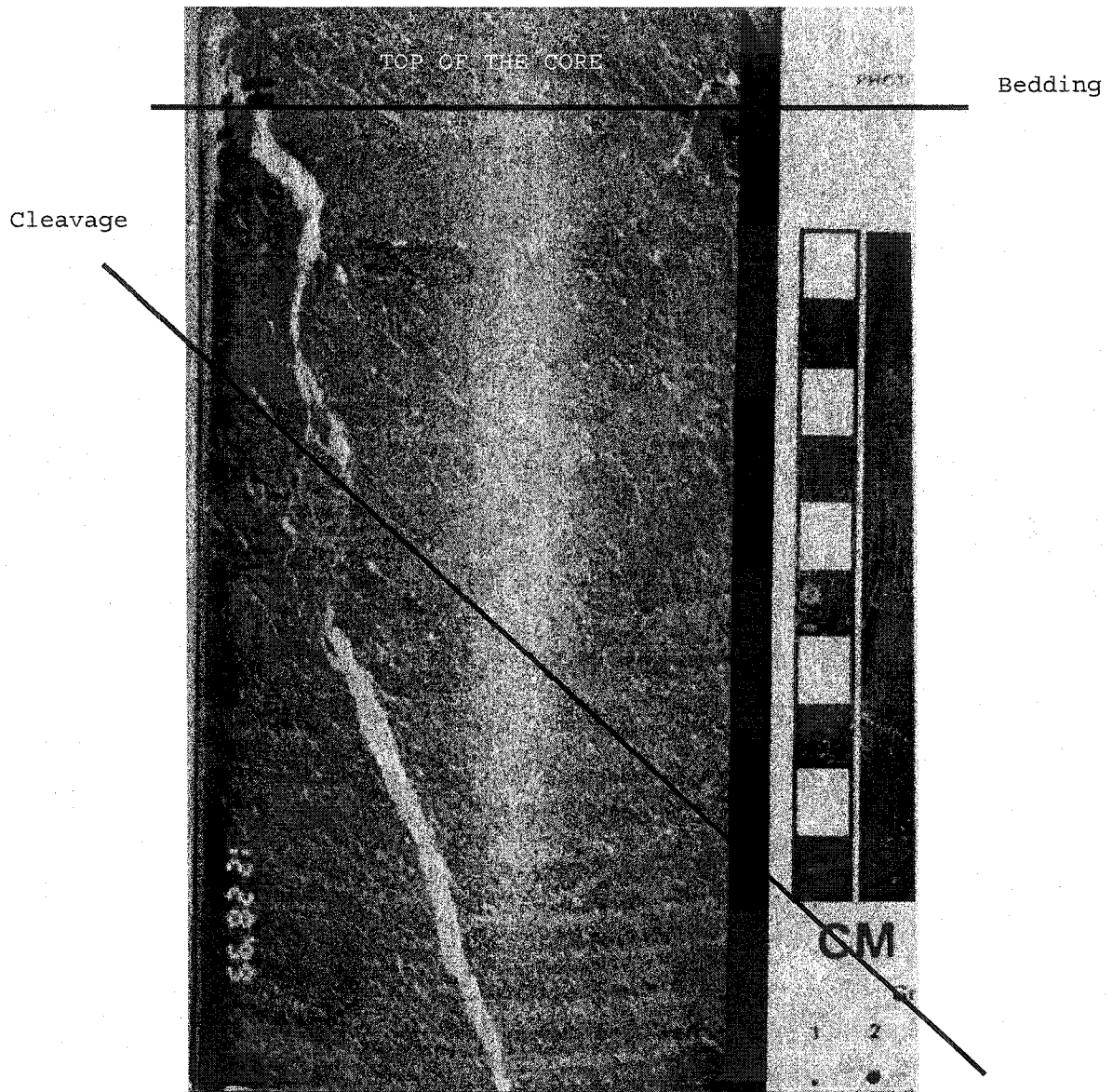


Figure 5.13 - Illustration of a piece of core from the NR-1 borehole. This segment shows the relation between bedding and crenulation cleavage, characteristic of the rock above the 19.7 ft (6m) mark (Eliot Formation lithology).

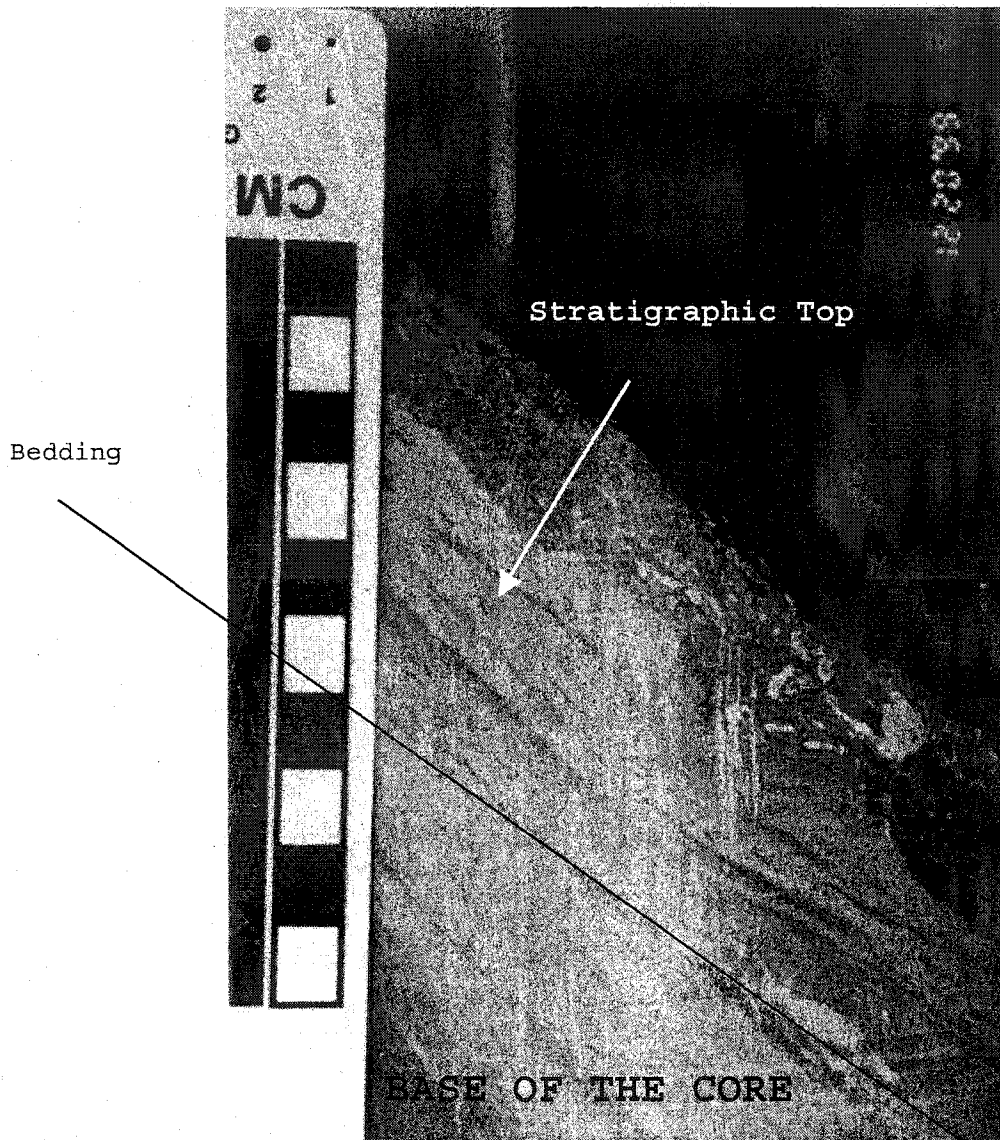


Figure 5.14 - The basal conglomerate that contains clasts of the rock with the crenulation cleavage embedded in the metasandstone with black laminae. The thickness of the conglomerate does not exceed 1 in (2.5 cm). The piece has been cut along the base of the conglomerate.

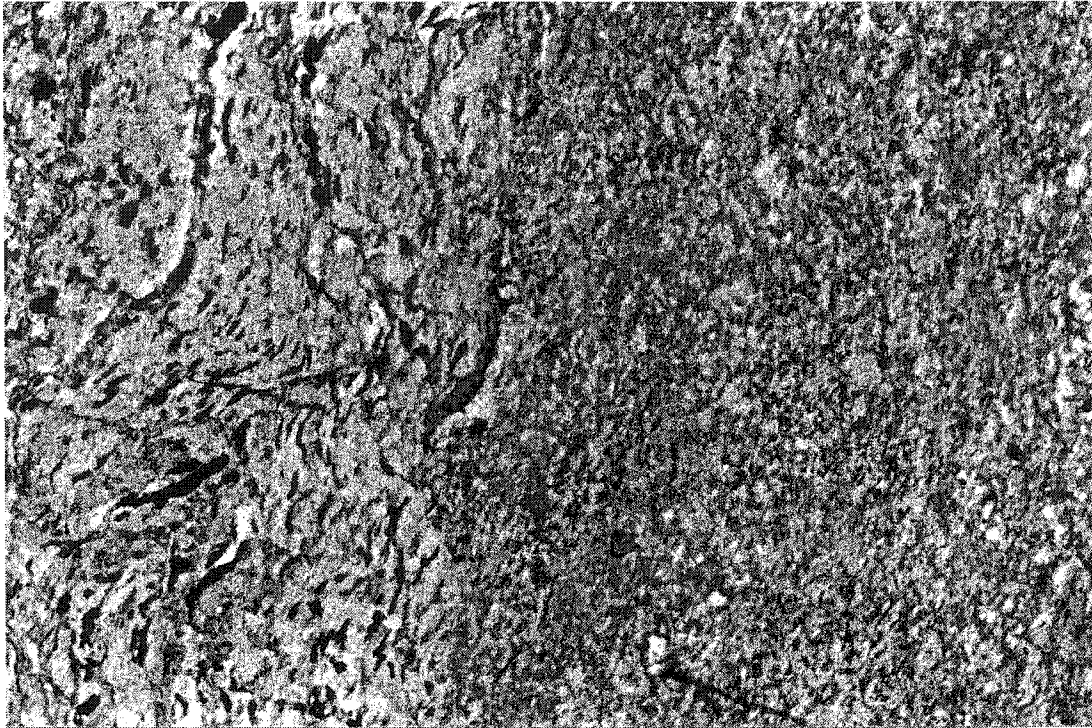


Figure 5.15 - Photomicrograph of the basal conglomerate. To the left of the illustration is a clast fragment with abundant biotite (black lath-shaped minerals). Biotite crystals define the crenulation cleavage. To the right of the illustration is the metasandstone, which is also the matrix of the conglomerate. The field of view is approximately 1.55 mm (XP, X10). The drilling direction points to the right.

The characteristics that established the similarities between the Eliot and Kittery Formations are the layer thickness, color (weathering and on fresh surface), and the stratigraphic style (fig. 5.16). Megascopically, to establish the mineralogical differences between the two types of rocks is difficult. The small grain sizes of these rocks lessen the effectiveness of the petrographic analysis.

Powder x-ray diffraction tested the above-mentioned hypothesis as an alternative approach. Whitmeyer et al. (1999) demonstrated the effectiveness of powder X-ray diffraction and described a methodology to estimate the mode of rocks using the 100% peaks of major minerals in

granitoids. For the study described here in the areas under the 100% peaks of quartz, albite, biotite, muscovite, and chlorite are measured using the same technique and software as Whitmeyer et al. (1999). The values were normalized and then plotted on a ternary diagram. The end members of the ternary diagram of Figure 5.18 are quartz, plagioclase, and pelite. The values for pelite resulted from the addition of the net values of alumina-silicate minerals (biotite, muscovite, and chlorite). Table 5.1 summarizes the settings of the Siemens D 5000 X-Ray diffractometer for the runs.

Three sets of two representative rock-samples were powdered and X-rayed. One set was representative of the Eliot-Kittery transition, a second set for the Kittery Formation, and a third set for the Eliot Formation.

The representative samples of the Eliot Formation are a black to dark gray, quartz rich, graphitic metashale from Snell Road (fig. 5.17), and a light brown pelitic metasandstone from the new Madbury fire station (location 1, fig. 5.2). The representative samples of the Kittery Formation are a dark gray pelitic metasandstone collected from the bridge in Downtown Exeter (S0ka), and a dark brown metasandstone from the Exeter-Boston railroad (S0kb), Locations 1 and 2 on Figure 5.3.

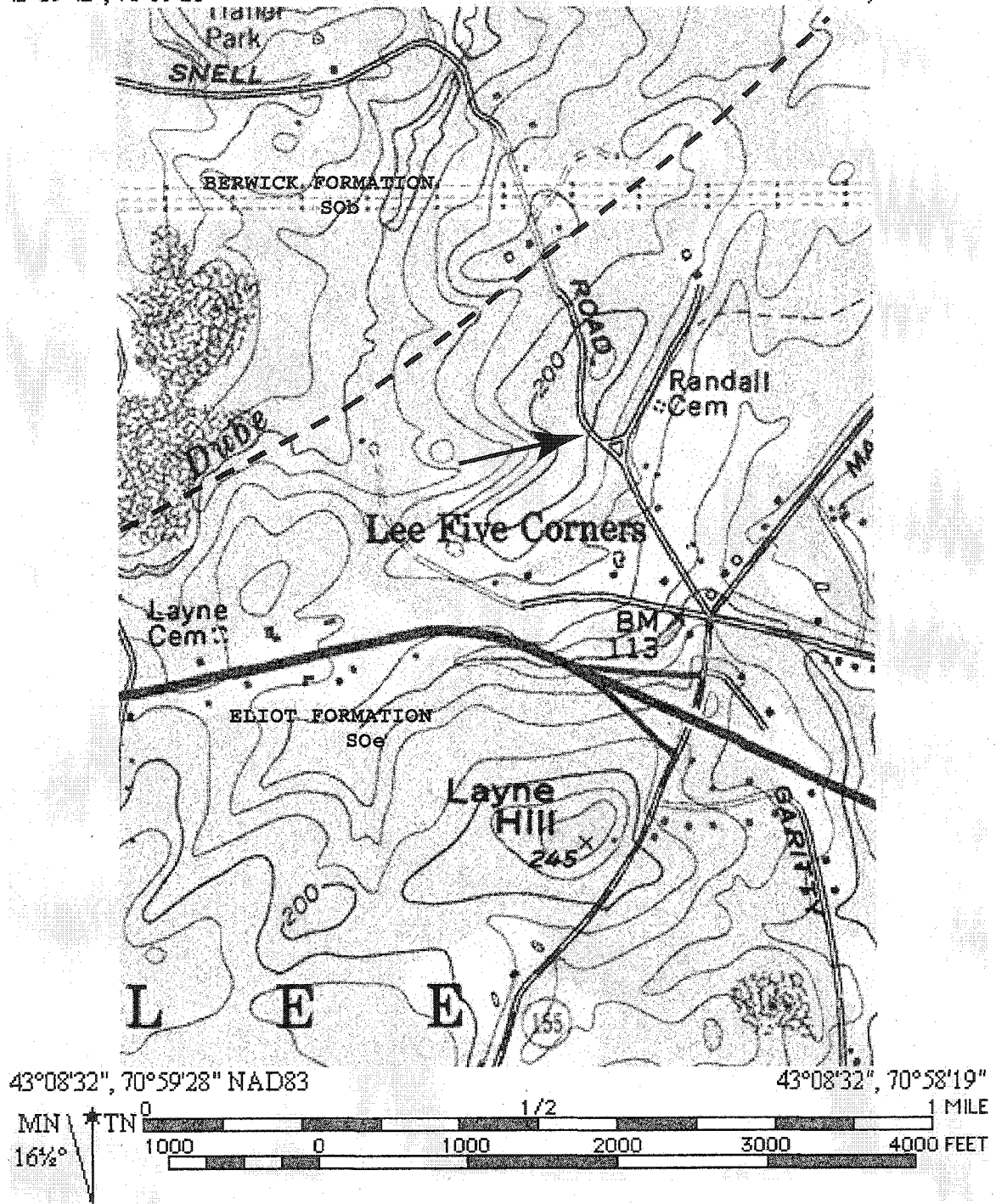
For the Bellamy River, one sample is a gray to light brown quartz-rich, slightly calcareous metashale, and the other is a dark brown, pelitic, metasandstone. The stratigraphic markers are more abundant and easier to identify in the middle than in the remainder of the section (fig. 5.16).



Figure 5.16 - Stratigraphic style in the Bellamy River. The illustration above (a) shows an example of the rock that contains more pelitic material than the rock in the illustration below (b).

43°09'42", 70°59'28"

43°09'42", 70°58'19"



43°08'32", 70°59'28" NAD83

43°08'32", 70°58'19"

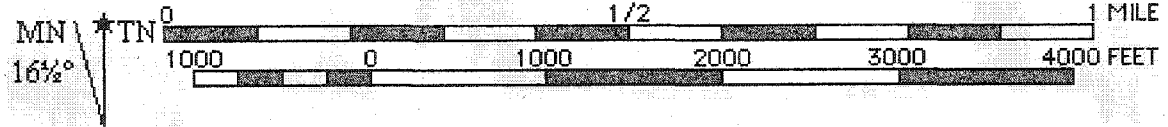


Figure 5.17 - Topographic map of the Lee Five Corners area. The arrow points to the location along Snell Road where Eliot Formation lithologies crop out. Sample Snell-1 comes from this location.

SAMPLE	RANGE 2 θ	STEP TIME	STEP SIZE
<u>Bellamy-2</u>	Range 1: 8-13.5°	3.0 sec	0.02°
	Range 2: 17-35°	3.0 sec	0.02°
<u>Bellamy-10</u>	6 - 36°	3.0 sec	0.02°
<u>Snell-1</u>	6 - 36°	3.0 sec	0.02°
<u>Madbury Fire Station</u>	6 - 36°	3.0 sec	0.02°
<u>Kittery Bridge</u>	7 - 65°	5 sec	0.02°
<u>Kittery Railroad</u>	7 - 65°	5 sec	0.02°

Table 5.1 - Settings summary of the Siemens D 5000 diffractometer. All samples were back-mounted. The constant arrangement of the slits is 2mm, 2mm, 0.1mm, 0.6mm.

Results - The ternary diagram in Figure 5.18 shows the estimated mode of each sample expressed in normalized percent values of quartz, pelite, and plagioclase. The rocks that represent the two locations of the Eliot Formation (Snell Road-1 and Madbury fire station) contain more pelite (about 38%) and less quartz (49 - 54%) than the rest of the samples. The percentage of plagioclase in these samples range between 4.5 - 12%.

Samples representing the Kittery Formation (Kittery - Bridge and Kittery Railroad) contain the greatest amounts of quartz (about 76%), and the smallest amount of pelite (8 - 18%) compared to the rest of the samples. Plagioclase ranges between 6 - 16%.

Samples from the Bellamy River are transitional and contain quartz ranging between 62 - 63%. Pelite and plagioclase percent values range between 22 - 24.5% and 12.5 - 15.6%, respectively. Sample Bellamy -2 belongs to the west end of the section, and sample Bellamy - 10 comes from the middle part of the section.

Discussion - A ternary diagram with end-members of quartz, plagioclase, and pelite facilitates the visualization of the differences in the mode of the three sets of samples (QPP diagram, fig. 5.18). The three end member minerals are present in all the samples. Therefore, the variations in percent values constitute a valid way to estimate the differences among them.

The Eliot and Kittery samples define isolated clusters when plotted on a QPP diagram. Likewise, the samples from the Bellamy River constitute a cluster that plots halfway between the other two. This observation provides more evidence to support the hypothesis that the rocks in the Bellamy River are transitional between the Eliot and the Kittery formations.

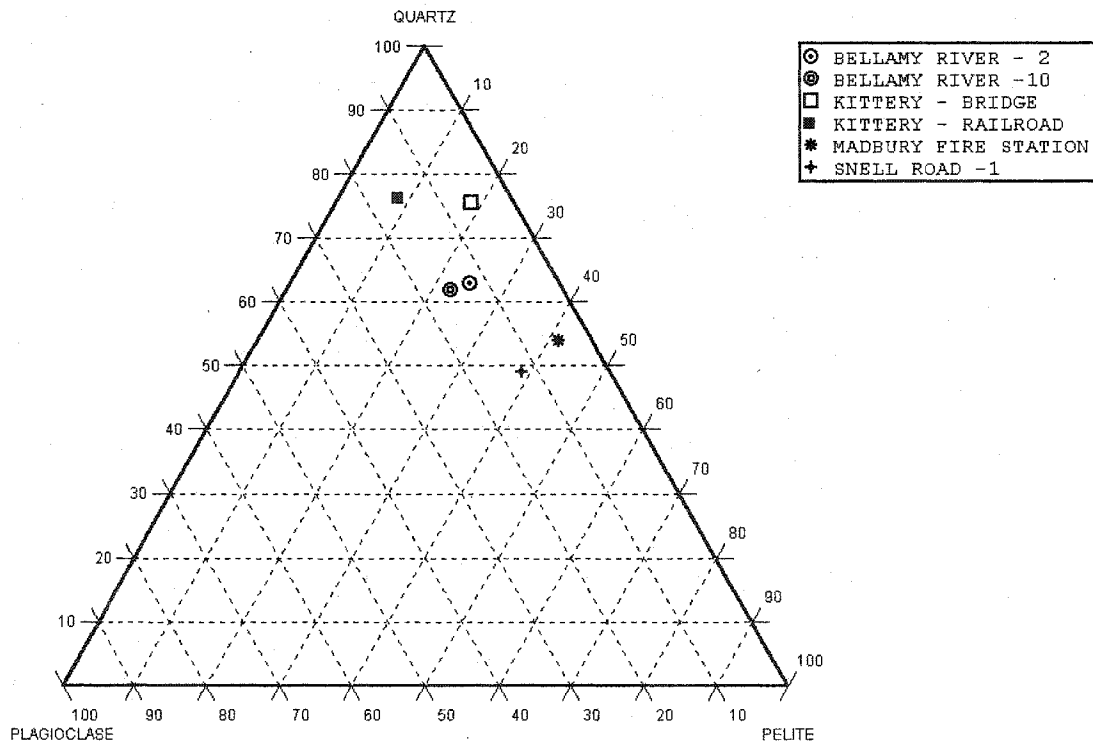


Figure 5.18 - QPP, quartz, plagioclase, and pelite (combined muscovite, biotite, and chlorite) ternary diagram. The sets define three separate clusters; the Kittery Formation has the greatest amount of quartz and the smallest amount of pelite. Samples from the Eliot Formation have the smallest amount of quartz and the highest amount of pelite. Rocks from the Bellamy River have an intermediate proportion of quartz and pelite.

Transition Eliot - Berwick - Previous workers defined the contact between the Eliot and Berwick formation as a northeast-southwest trending boundary that crops out in the Cocheco River. Novotny (1968) mapped the contact 0.6 miles to the southeast of the intersection of the Cocheco River and Whittier Street. Later, Lyons et al., (1997) showed the contact at this locality (fig. 5.2).

The outcrops under the Whittier Street bridge over the Cocheco River in Dover, NH preserve decimeter-scale kinematic indicators, associated boudinage, and transposed folds (fig. 5.19a, b, c, and d). Bothner and Hussey (1999) describe similar structures in the Nannie Island phyllonite. The mega-kinematic indicators clearly define a dextral sense of motion.

Pervasive slickenfibers are present on planes sub-parallel to the compositional layering. The slickenfibers reveal a sinistral oblique displacement (south block is the downthrown block).

Field observations indicate that the main lithologic difference between the northwestern and the southeastern portions in this site is the relative abundance of calcsilicate bands and metapelites. To the north, the compositional layering is thinner, the amount of metapelite diminishes, and the proportion of calcsilicate bands is greater.

In this locality, the rocks are dark brown-rusty weathering, often sulfidic, metapelites, and dark gray to green, quartz-feldspar-biotite, often calcareous, granofelsic rocks (fig. 5.20). Dark green to gray calcsilicate bands occur as intercalations. The compositional layering is often boudinaged and crosscut by abundant quartz veins, pods, and buckling folds (fig. 5.21).

Katz (1917) and Lyons and others (1997) described a similar type of rock as the first subunit of the Berwick Formation. On the other

hand, current definitions describe the Eliot Formation as an alternation of thin beds of calcareous metasandstone and dark gray and brown phyllite (Lyons et al., 1989; Bothner and Hussey, 1999). The difference between these units consists, based on these definitions, on the relative amount of calcsilicate and metapelite, and the increase of calcsilicate here supports the placement of the contact between the Eliot and the Berwick Formations at this locality.



Figure 5.19a - Decimeter-scale kinematic indicator. The megastigma quartz grain displays a dextral sense of movement defined by the "book shelf" structure inside the grain, and the step-up configuration of the tail. The top of the scale points to the south.



Figure 5.19b - Undulations associated with boudinage and "bookshelf" structure showing a dextral sense of motion. The upper side of the photo points to the south, a quarter dollar coin serves as scale.

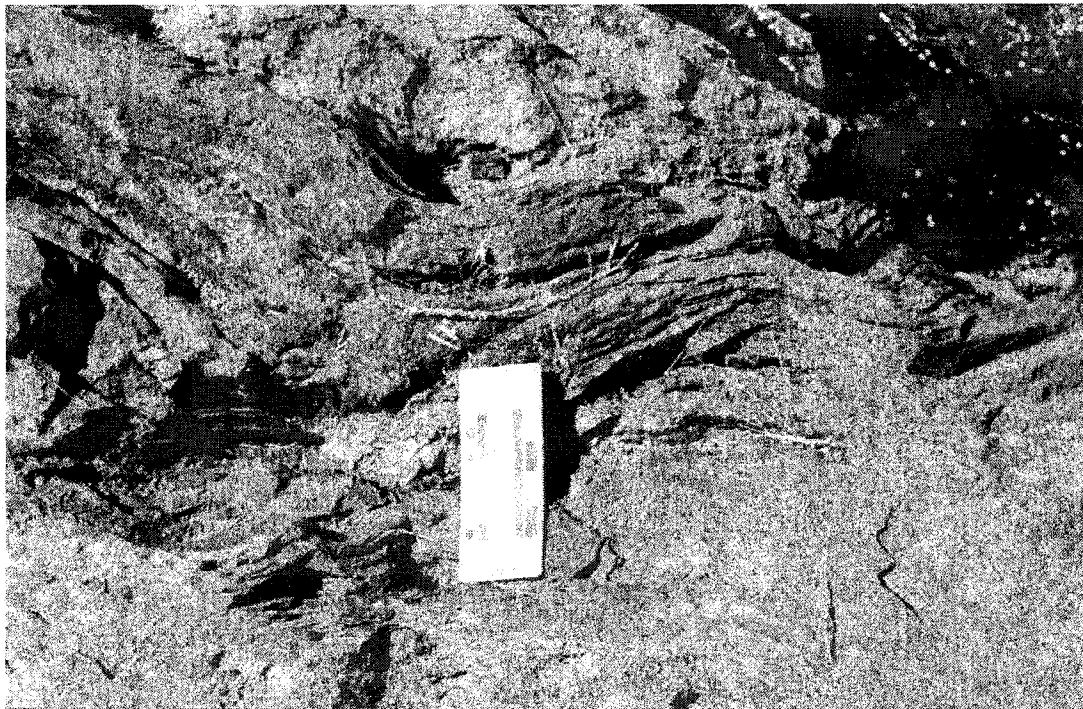


Figure 5.19c - Undulations associated with the boudins and megasigma grains. The upper end of the scale points to the south.

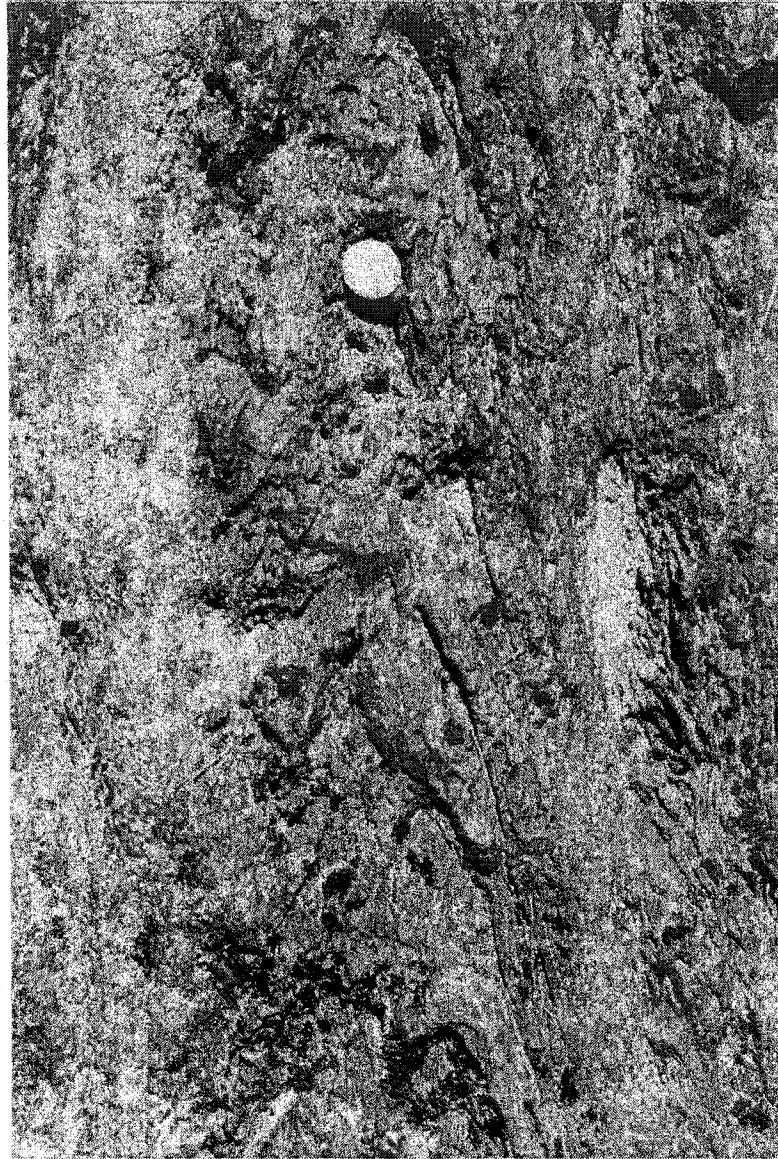


Figure 5.19d - The photo shows folds with attenuated limbs. The top of the illustration points to the west. A quarter dollar coin serves as scale.



Figure 5.20 - The illustration shows the aspect of the compositional layering. The direction of view is to the northeast. The ruler is 4 inches long.

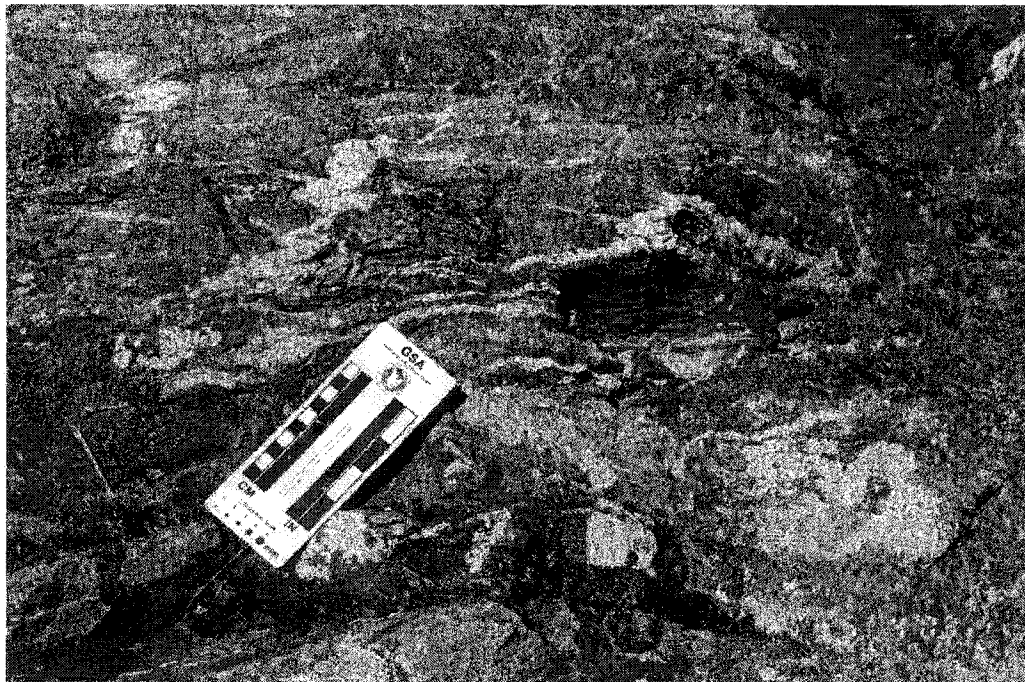


Figure 5.21 - Quartz veins and buckling folds crosscut a layer of calcsilicate between two metapelitic layers. The upper end of the scale points to the north.

Structures - Beneath the Whittier Street bridge, the general trend of the compositional layering is 216° , and the dip is 67° SW (fig. 5.22 and 5.23). Along planes that crosscut the compositional layering at an angle of about $10-15^\circ$, a pervasive mineral lineation that constitutes slickenfibers is present (fig. 5.24). The strike and dip of these planes is $212^\circ - 83^\circ$.

The trend of the slickenfibers is 17° and the plunge is 51° towards the north (fig. 5.23). The east-plunging slickenfibers and field observations suggest probable relative sinistral displacement of these two components (one minor vertical component that displaces the southeastern block up and a major horizontal component that displaces the south block to the east). This brittle deformation crosscuts the compositional layering.

The undulations that deflect the compositional layering have a wavelength of about three to five inches ($7.5 - 12.7$ cm), and contain boudines of quartz in the shape of mega sigma grains (fig. 5.21a and b). The axes of the undulations have an average trend of 262° and plunge of 35° W (fig. 5.23).

In the northwestern block the axis of a sinusoidal antiformal fold trends 340° and plunges 37° NE; the axial plane strikes 230° and dips 41° NW. A cleavage that strikes 270° and dips 45° N crosscuts the fold longitudinally. The north limbs strike 225° and dip 70° NW; the south limbs strike 20° and dip 54° SE (fig. 5.26).

In the southeastern block, tight, isoclinal folds occur with their limbs truncated by the planes of compositional layering. The trend of the fold axes is 120° and the plunge is 82° SE. The axial planes strike 315° and dip 82° NE (fig. 5.19d). The stereogram in Figure 5.27a shows the differences in structural attitude between the folds on the northwestern and southeastern blocks.

Discussion - Field observations at this locality confirm a relative change in lithology between the northwestern and southeastern block. There is more calcsilicate and less metapelite towards the northwest. Structural data indicate early folding followed by an intense ductile deformation that transposed and truncated the folds on the southeastern block (fig. 5.22).

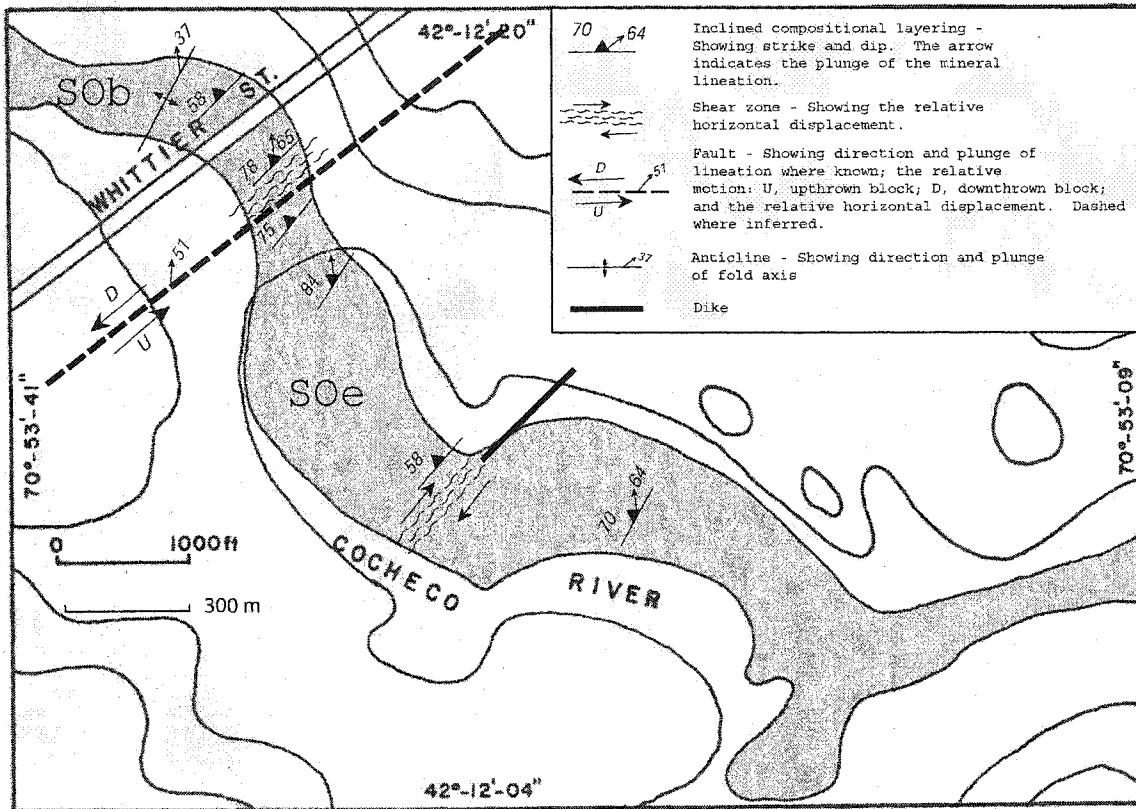


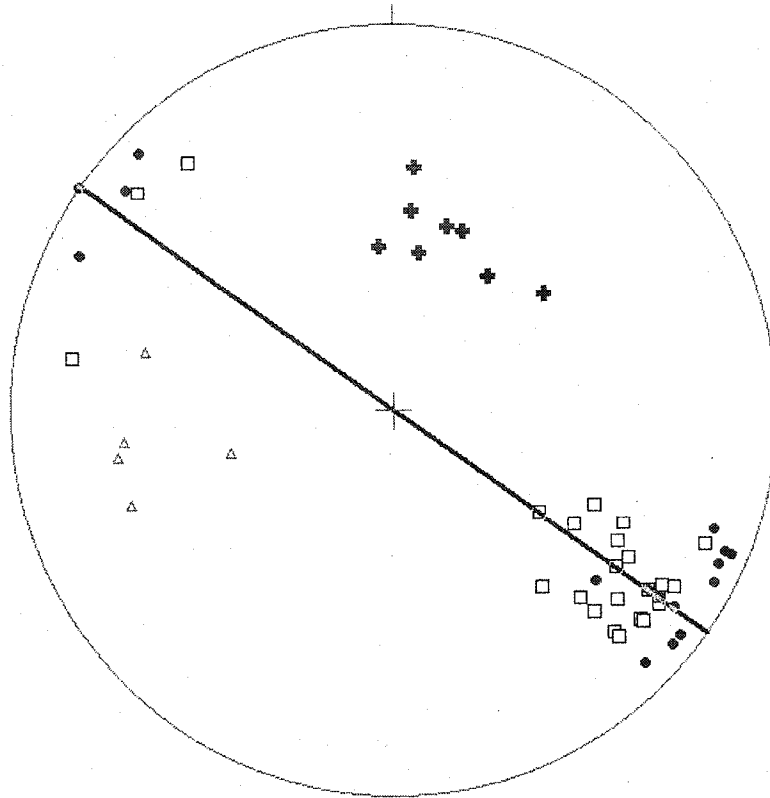
Figure 5.22 - Structural map of the contact zone between the Eliot (SOe) and Berwick (SOB) Formations (intersection of the Cocheco River and Whittier Street, Dover, NH).

The shear sense indicators (e.g., mega-sigma quartz grains) indicate a major right-lateral horizontal movement and a minor vertical component. The axis of rotation of such a mechanism has an orientation equivalent to the axes of the undulations (fig. 5.23).

Later brittle faulting affected these rocks and displaced the northwestern and southeastern blocks along a plane that is sub-parallel to the compositional layering. The faulting displaced the southeastern block up and to the northeast with respect to the northwestern block.

The stereogram in Figure 5.27b shows the attitude of fold axes of the northwestern and southeastern blocks. From this stereogram, the estimation of the net angular relative displacement between the two blocks is 45° , and along a plane which strikes 336° and dips 85° .

The above-mentioned results suggest that the nature of contact between the Eliot and the Berwick formations in this location cannot be explained with a high degree of certainty. The stratigraphic contact in a strict sense is not exposed, even though a lithologic difference between the northwestern and southeastern blocks is observable. Folding and faulting affected the rocks in this location resulting in a complex geologic history, because of these facts and for practical purposes, the contact between the Eliot and Berwick Formations can be considered as tectonic.



n = 24 So (squares)
 n = 17 fault planes (solid circles)
 n = 5 axes of undulations (triangles)
 n = 8 mineral lineations (crosses)
 Mean Orientation of So = 216-67
 Mean orientation of fault planes = 212-83
 Calculated girdle: 125-88

Figure 5.23 - Composite stereogram showing the orientations of the compositional layering, fault planes, undulations, and mineral lineation (slickenfibers). These structures crop out at the intersection of the Cochecho River and Whittier Street, Dover, NH.

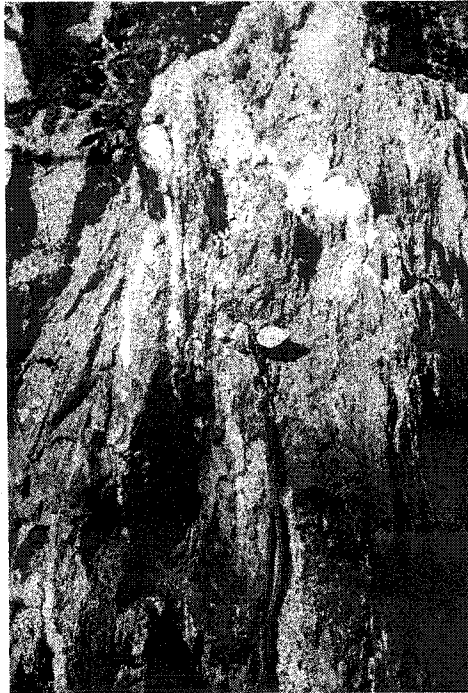


Figure 5.24 - The photo shows the intersection of the foliation planes (right side) with the faulting plane (left side). The hand lens is 0.5 in long (same locality as fig. 5.23).

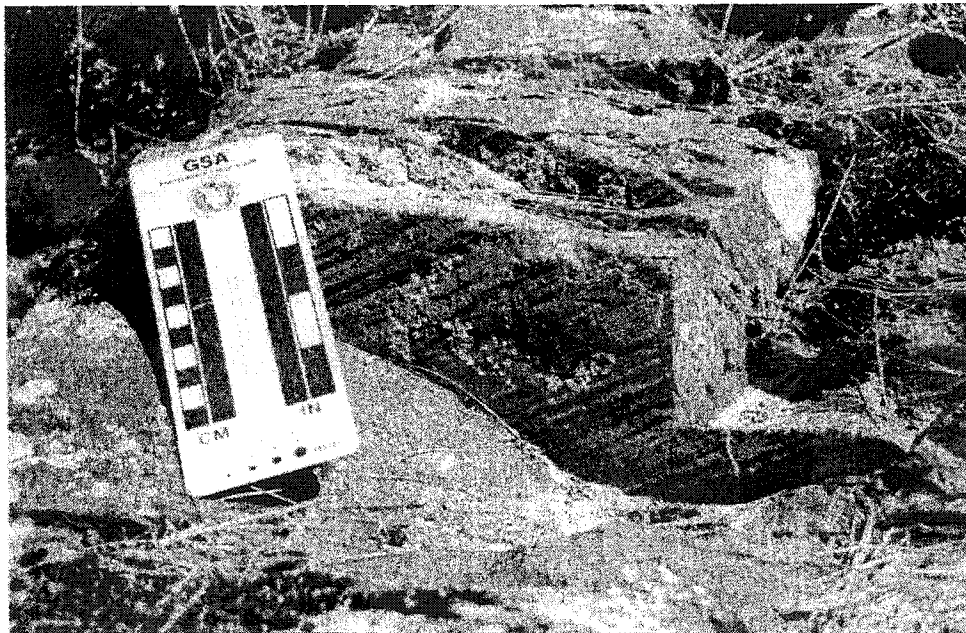


Figure 5.25 - The photo shows the slickenfibers associated with brittle faulting. The upper part of the scale points to the north (same locality as fig. 5.23).

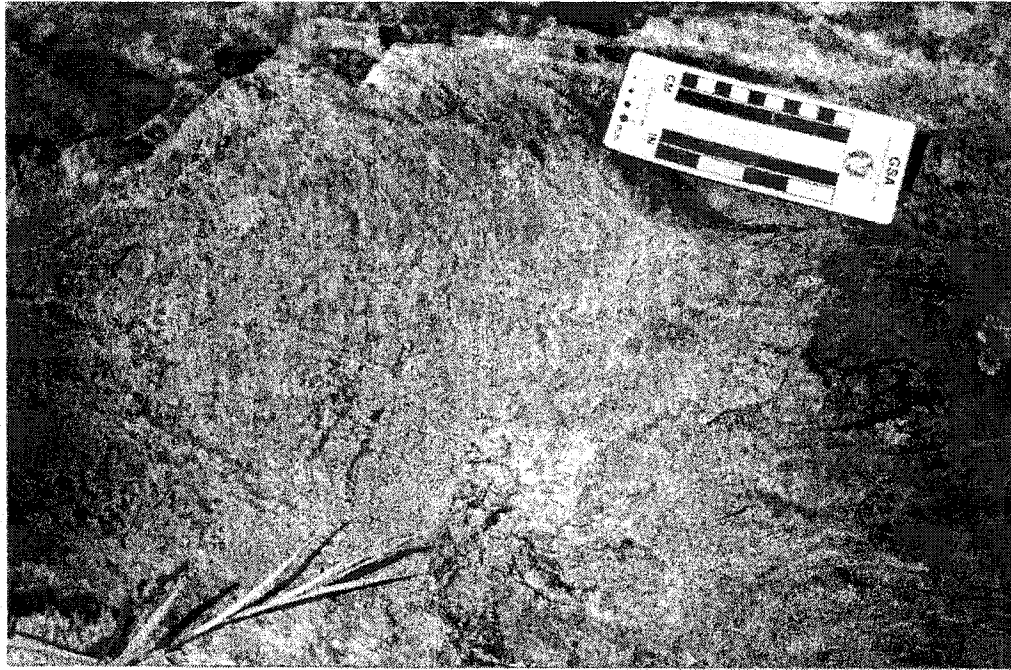


Figure 5.26 - Photograph of the fold in the north block showing the crosscutting cleavage. The upper part of the scale points to the east (same locality as fig. 5.23)..

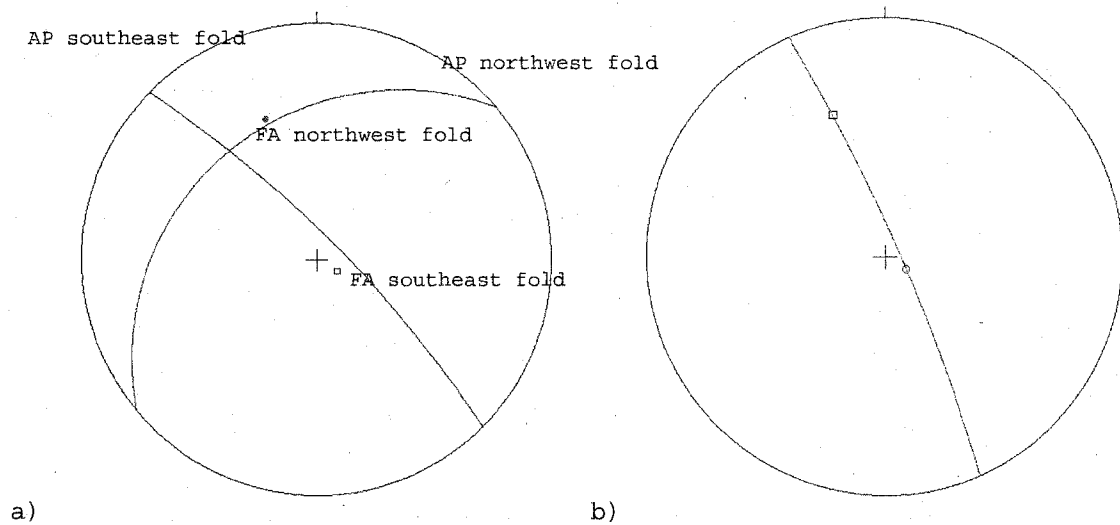


Figure 5.27 - a) Relative difference in the orientation between the axial planes (AP) and axes (FA) of the folds in the northwest and southeast blocks. b) An estimate of the probable net relative angular displacement of the fold axes is 45° along a plane equal to the calculated girdle (336-85). An open square represents the northwestern fold axis, and an open circle the southwestern fold axis (same locality as fig. 5.23).

CHAPTER VI

GEOLOGY OF THE RYE COMPLEX IN NORTH HAMPTON, NEW HAMPSHIRE

Introduction

Among others (e.g., Katz, 1917; Novotny, 1955, 1969) Billings (1956) mapped the Rye Formation as a southwest trending lithotectonic unit of about 7.5 km long and about 6.5 km wide. Billings subdivided the Rye into a lower metasedimentary member and an upper metavolcanic member (metamorphosed basalts, andesites, and soda-rhyolites). The Rye Formation is the lithotectonic unit that crops out in the easternmost portion of the seacoast region of New Hampshire.

Within the Rye Formation, Novotny (1969) mapped the Breakfast Hill Granite (a 0.5 km² elliptical, peraluminous, variably foliated granitic pluton with massive foliated pegmatite). Hussey (1980) and Lyons et al. (1997) included the Breakfast Hill Granite as the upper member of the Rye Formation. Later, Bothner and Hussey (1999) renamed the Rye Formation as the Rye Complex.

Hussey (1980) in his review of the interpretation of the Rye Formation of Gerrish Island, Kittery, Maine wrote, "These rocks, in particular the metapelites, are heavily migmatized and injected by layers of medium- to coarse-grained granite to granodiorite gneiss having a characteristic blastomylonitic fabric". Carrigan (1984), on New Castle Island, New Hampshire, identified metasedimentary (gray-green calc-silicate quartzites, dark brown pelitic schists, feldspathic quartzites, marble, and gray graphitic schist) and metaigneous rocks (gray metadiorite, light gray gneissic granites, dark green

amphibolite, and tourmaline-bearing pegmatite). These rocks are interpreted to constitute the continuation of the mappable units identified by Hussey (1990) on Gerrish Island, Maine.

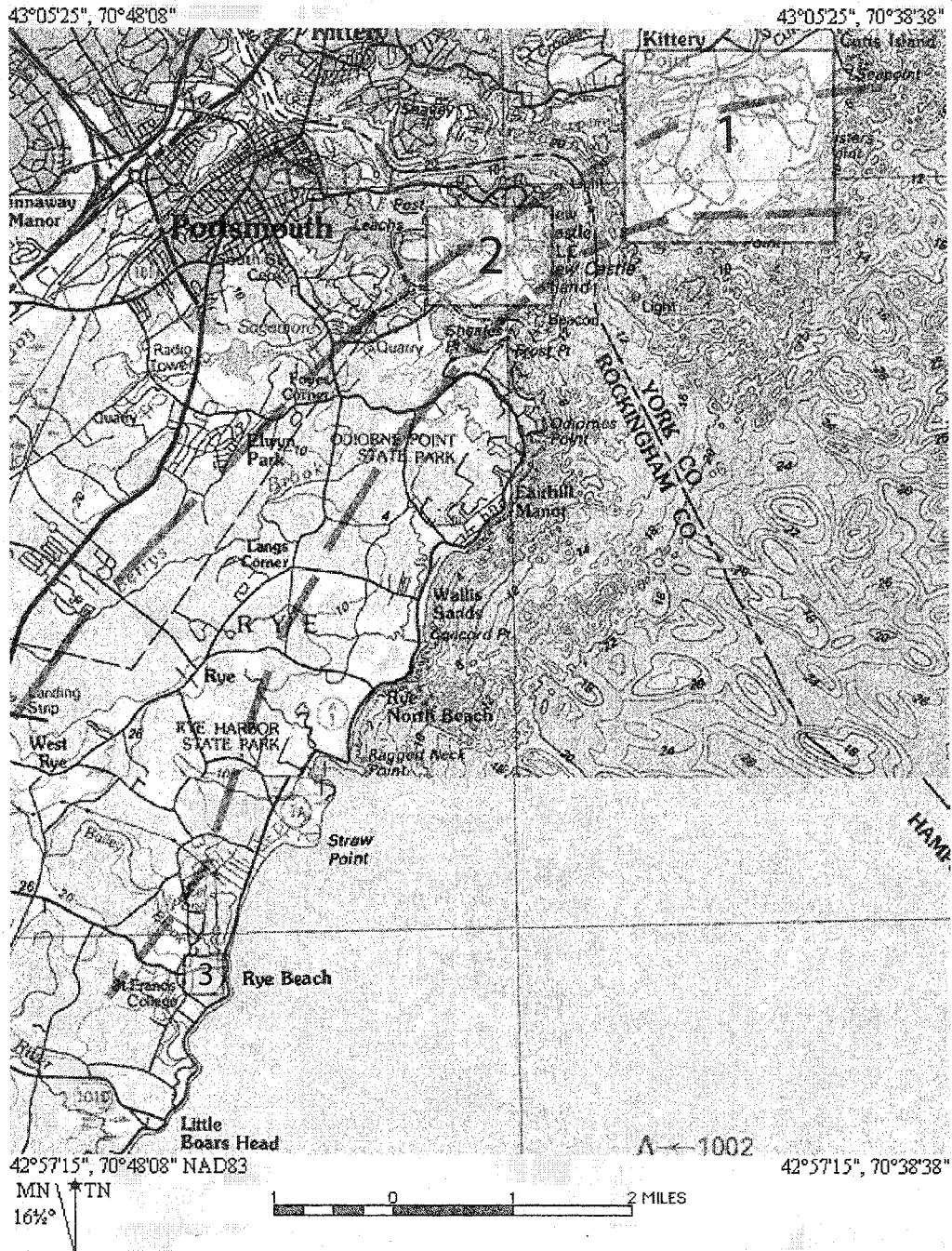


Figure 6.1 - Topographic map showing the areas for correlation. Areas are (1) Gerrish Island (Hussey, 1980), (2) New Castle Island (Carrigan, 1984), and (3) Golf Course Area in North Hampton, New Hampshire (this study).

In Portsmouth and on New Castle Island, Carrigan (1984) identified seven mappable lithologic zones within the Rye Formation. Mylonitization of variable intensity affected the Rye Formation and the Breakfast Hill. Hussey (1980) recognized ultra-mylonites in these rocks in Maine and in neighboring New Hampshire.

This study focuses on the metasediments of the Rye Formation in the Golf Course area, and has two objectives: first, to extend the subdivision proposed by Carrigan (1984) and to correlate the lithologies identified by Hussey (1980) to the south (Golf Course area). Second, to confirm the observations made in the microstructural analysis showing an increasing metamorphic grade from southeast to northwest across the Rye Complex.

Mineral Assemblages

Chapter IV discusses the identification of sheared structures and blastomylonitic textures identified in the rocks of the Golf Course area in North Hampton, New Hampshire. These textures and the presence of relict early formed minerals in some samples made the definition of the equilibrium mineral assemblage difficult (e.g., garnet with core and rim structures, chlorite as late alteration of biotite).

Bucher and Frey (1994, pp. 27-28) discussed the criteria that lead to the proper identification of the mineral assemblage of a metamorphic rock, and explained why some assemblages can be acceptable even though they cannot be considered as equilibrium mineral assemblages in a strict sense.

In this study, the determination of the mineral assemblage of the rocks is based on the visual estimation of the percentages of the minerals present in each rock. Not all the minerals may be in equilibrium. Figure 6.2 shows sampling locations and Table 6.1 lists the minerals identified.

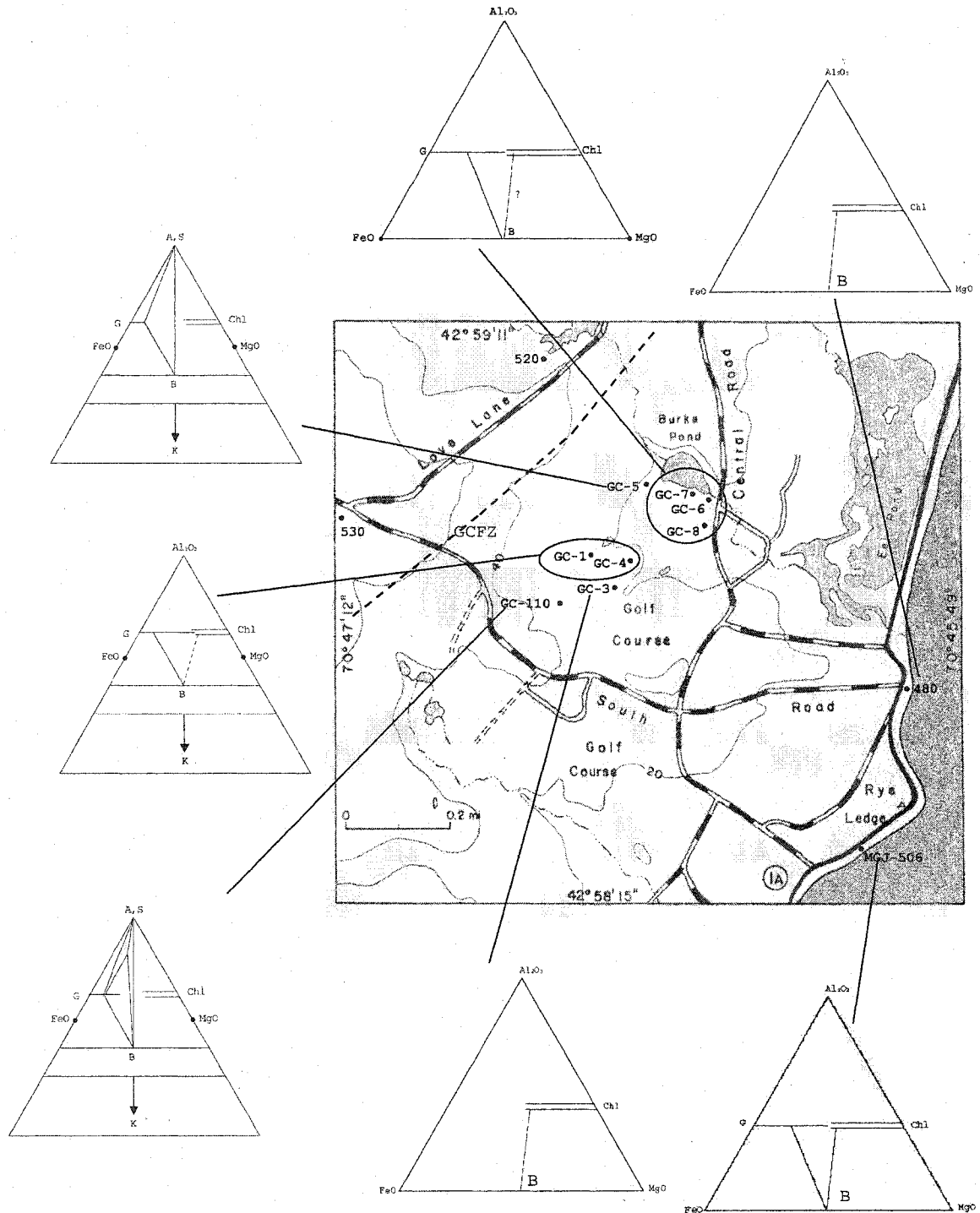


Figure 6.2 - Map showing the probable trace of the Great Common Fault Zone (GCFZ), sample locations, and Al_2O_3 -FeO-MgO projections of the mineral assemblages in area 3 of fig. 6.1. Samples GC-1 through 5 and GC-110 are projected from muscovite and quartz; while samples GC-7, 8; 480, and MGJ-506 are projected from potassium feldspar and quartz. Dashed lines represent the possible presence of chlorite in the original assemblage. See Table 6.1 for estimated modes and abbreviations.

Chlorite in all samples is considered magnesium rich ($(Fe + Mn + Cr) / (Fe + Mn + Cr + Mg) = 0.25 - 0.35$) based on the anomalous birefringence and the sign of elongation (Table 1 in Laird, 1988). Furthermore, based on the texture of chlorite and biotite, the presence of chlorite in all the samples is interpreted as a late alteration of biotite (Fig. 6.3).

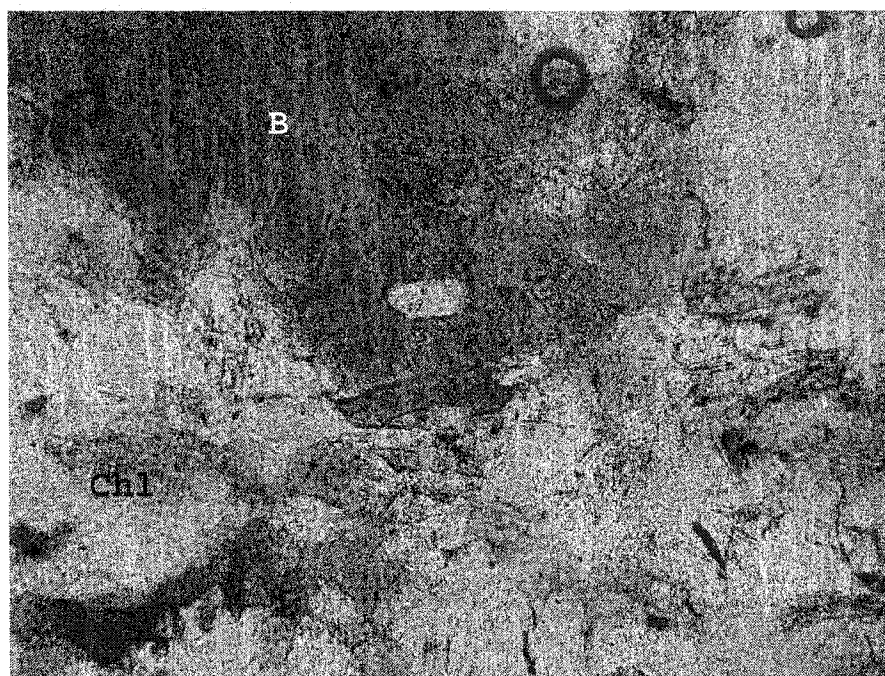


Figure 6.3 - Microphotograph showing the alteration texture of biotite (B) to chlorite (Chl). The field of view is approximately .18 mm (PPL).

Graphical Representation of the Mineral Assemblages

The presence of quartz and muscovite in samples GC-1 through 5 and GC-110 allows the projection of the mineral assemblages in each sample from muscovite and quartz onto AFM diagrams, according to the Thompson projection (1957). Mineral assemblages of samples GC-6 through GC-8, 480, and MGJ-506 do not include muscovite and are projected from potassium feldspar and quartz onto an AFM diagram (fig.

6.2). Muscovite and potassium feldspar occur in samples GC-1, GC-5, and GC-110.

	GC-1	GC-3	GC-4	GC-5	GC-6	GC-7	GC-8	GC-110	MGJ-506	480	520	530
Q	55	60	55	50	60	55	55	40	60	60	30	35
Pl	5	5	5	5		5	5	5		15	30	30
K	10			5		5	5	5		15	20	25
Mu	5	10	5	5				5				
B	5	15	10	5	10	8	10	5	10	5	10	10
Chl	5	5	5	5	5	5		5	5	5	10	5
G	10		15	15	20	20	25	10	20			
St								5				
A								15				
S				5				5				
Ac	Z, Op	Z, Op	Op	Tu, Op	Op	Z, Op		Ep, Op	Tu, Op			G, Tu

Abbreviations

A	Andalusite	Op	Opakes
Ac	Accessories	Pl	Plagioclase
Amp	Amphibole	Q	Quartz
B	Biotite	S	Sillimanite
Chl	Chlorite	Sp	Sphene
Ep	Epidote	St	Staurolite
G	Garnet	Tu	Tourmaline
K	Potassium Feldspar	Z	Zircon
Mu	White mica		

Table 6.1 - Visual estimation of modes in samples from study area 3. See Figure 6.2 for location of samples. According to the microstructural analysis of Chapter IV, samples GC-1 and GC-5 are in Regime 3, 480 and MGJ-506 are in Regime 1, AND the remainder of the samples are in Regime 2.

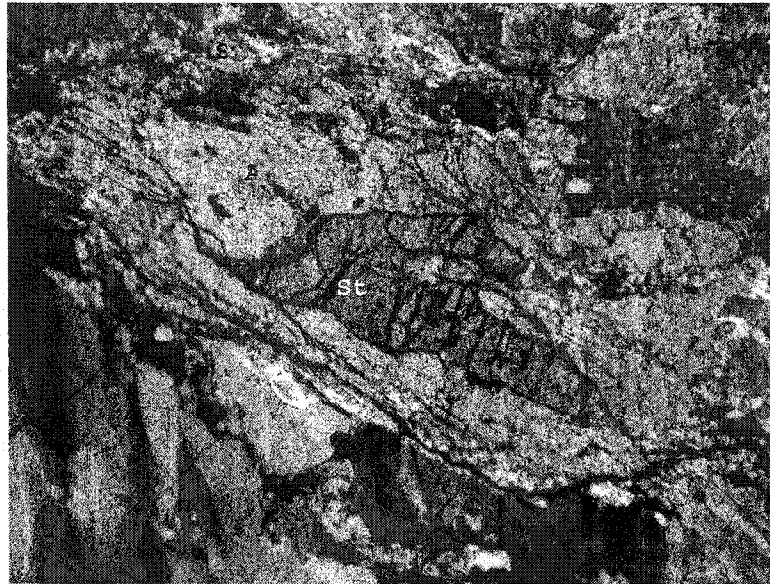


Figure 6.4 - Sample GC-110 - Staurolite (St) surrounded by andalusite (A). Biotite (B) and sillimanite (S) are present as lath shaped crystals. This texture represents the disequilibrium of staurolite in the rock. The field of view is approximately 0.8 mm long (XPL)

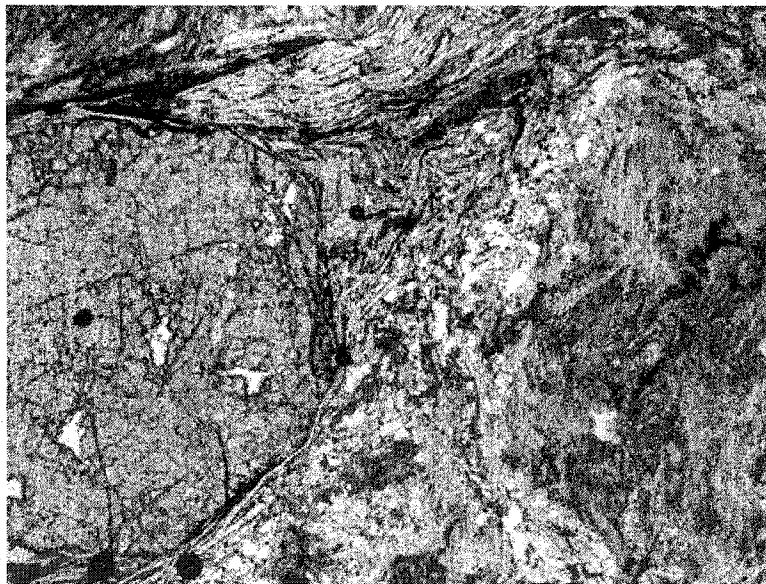


Figure 6.5 - Sample GC-5 - Equilibrium assemblage in Sample GC-5. To the left is garnet and to the right is a sillimanite pseudomorph of andalusite. Lath shaped crystals are biotite and muscovite. The field of view is .5 mm (PPL).

Samples GC-5 and GC-110 are different from the remainder of samples in that they contain minerals that are more aluminous than the garnet-chlorite (plus quartz and muscovite) tie line. Staurolite, andalusite, and sillimanite occur with garnet and biotite in GC-110 (fig.6.4). Sillimanite occurs with garnet and biotite in GC-5 (fig 6.5). It is possible that sillimanite in this sample occurs as a pseudomorph of andalusite. On New Castle Island, Carrigan (1984) reported the presence of andalusite porphyroblasts in Zone VII (fig. 6.6).

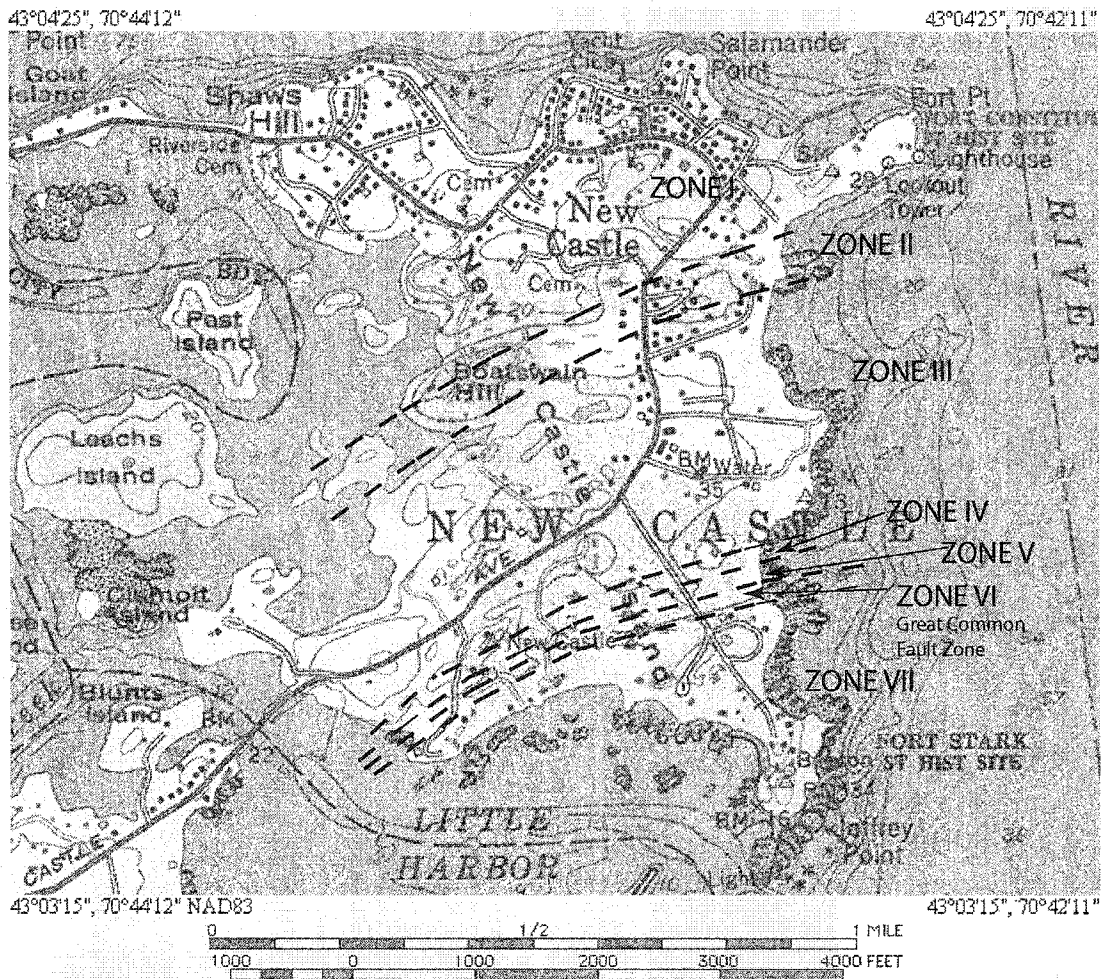


Figure 6.6 - Topographic map of New Castle Island showing the spatial distribution of the seven zones defined by Carrigan (1984).

Correlation

New Castle Island is located about 10.5 km to the northeast of the study area (fig. 6.1). In this locality, Carrigan (1984) identified seven zones in the Rye Formation (fig.6.6). The pelitic schist of Carrigan's Zone VII is characterized by its mylonitized texture and the presence of andalusite porphyroblasts. Occasionally, a fine to medium-grained feldspathic quartzite and a coarse grained, foliated white pegmatite with fractured tourmaline are present. Zone VII is mapped to the south of the Great Common Fault Zone, which constitutes Zone VI (fig. 6.6).

Based on the texture of the rocks, Carrigan (1984) identified two variants of mineral assemblages for Zone III and Zone VII, and referred to them as major and in equilibrium. The main difference between the major mineral assemblages in the metapelites of zones III and VII is the presence of andalusite and staurolite in Zone VII. He observed that staurolite occurs as a relict included in the andalusite porphyroblasts and that garnet, sillimanite, quartz, and biotite occur as independent grains in the matrix and as inclusions in andalusite.

The relict mineral assemblages of Zone VII are:

Quartz + Andalusite + Staurolite + Garnet + Biotite + Muscovite

Quartz + Sillimanite + Garnet + Muscovite + Biotite

In the study area, the predominant lithology is dark brown, fine-grained, micaceous pelitic schist with no well-preserved porphyroblasts. Feldspathic quartzites and pegmatite stringers are also present.



Figure 6.7 - Microphotograph of sample GC-110 showing an andalusite porphyroblast with inclusions of garnet (G) and biotite (B). The field of view is approximately 0.5 mm (PPL).

Porphyroblasts of andalusite present in sample GC-110 are pseudomorphosed in the Golf Course area. These pseudomorphs include staurolite (fig. 6.4) and garnet + biotite (fig. 6.7). Staurolite is present only as inclusions in andalusite. The mineral assemblage of sample GC-110 is:

*Quartz + Andalusite + Sillimanite + Staurolite + Garnet + Biotite +
Muscovite*

The observations in this analysis and the results reported by Carrigan (1984) are remarkably similar, and suggest that the rocks in the Zone VII of New Castle and the rocks in the Golf Course area correlatable. The facts that support this correlation are:

1) In New Castle and in the Golf Course area, the rocks are predominantly pelitic.

2) In both localities, porphyroblasts of andalusite occur with inclusions of staurolite and with inclusions of garnet + biotite.

3) The mineral assemblage of sample GC-110 and the relict mineral assemblage of Zone VII in Carrigan's study are equivalent.

Mineral assemblages of samples 520 and 530, collected by Novotny (1963), present differences with respect to the remainder of the samples in that they have a felsic rock character (Breakfast Hill lithologies). In addition, melting textures are present in sample 520 (figs. 4.38 and 4.29), and according to the microstructural analysis in Chapter IV, the textures in quartz grains reveal a Regime 3 of deformation, which implies temperatures in the range of 500-600 °C, the highest temperature of deformation in this locality.

From Novotny's field book (June, 1956, Bothner personal communication), the description of these samples is "520 - gray biotite gneiss, garnetiferous, close to a pegmatitic injection. 530 - Is garnetiferous and feldspathic, biotite gneiss." It is possible that these rocks represent the north block of the Great Common Fault Zone and may correspond to zone III described by Carrigan (1984). The investigation of the nature of these rocks and the explanation of the possible felsic character are beyond the scope of this study.

Hence, the correlation between Carrigan's Zone VII in New Castle Island and the pelitic rocks in the Golf Course area can be considered as viable. Samples 520 and 530 can be correlated with zone III (based on the felsic character of the rocks), and considered as Breakfast Hill lithologies.

On this basis, I mapped the Great Common Fault Zone at the northwest end of the Golf course area, separating the pelitic schist (Rye Formation) to the south, from the felsic gneiss (Breakfast Hill) to the north. The following section discusses the variation in the

temperature of metamorphism towards the northwest in the Golf Course area.

Metamorphism

The P-T grid in Figure 6.8 illustrates the possible metamorphic path of the metapelites in the Golf Course area. Garnet + chlorite occur together in location 1 of the diagram, but not at greater temperature.

The first appearance of staurolite in the mineral assemblage, location 2, occurs after the reaction *garnet + chlorite + muscovite = staurolite + biotite + H₂O*. In aluminous rocks, the first appearance of biotite occurs with this reaction. In location 3, andalusite + biotite is stabilized by the reaction *staurolite + chlorite = andalusite + biotite*.

The presence of muscovite and quartz is common in Samples GC-5 and GC-110. Sample GC-110 plots in location 4 (fig. 6.8) along the andalusite - sillimanite univariant line. Sample GC-5 plots in location 5 (fig. 6.8) beyond the reaction *staurolite + muscovite + quartz = sillimanite/andalusite + biotite + garnet + H₂O*.

Consequently, staurolite disappears from the ternary diagram diagram in location 5 (fig. 6.8). In the Barrovian sequence, the breakdown of staurolite occurs within the sillimanite-muscovite zone (Yardley, 1989).

Discussion

The P-T grid in Figure 6.8 displays the mineral assemblages present in the Golf Course area that correspond to locations 4 and 5, samples GC-110 and GC-5, respectively. The mineral assemblages of locations 1 to 3 are inferred according to the analysis of high Al-pelites by Spear (1993).

The P/T (pressure/temperature) path from field 4 to 5 is constrained to ~ 2.5 kb and above 600°C from the mineral assemblages and Figure 6.8. The consideration of prograde metamorphism in fields 1 through 3 of Figure 6.8 is based on the presence of chlorite. In this study, the presence of chlorite is considered as a late alteration. Therefore, the prograde metamorphism reflected in fields 1, 2, and 3 is uncertain.

From the microstructural analysis of Chapter IV, the deformation regime reflected in quartz textures increases towards the northwest (fig. 4.30). Quartz textures in Sample GC-5 belong to Regime 3 (higher temperature) and Sample GC-110 to the transition between Regimes 2 and 3 (lower temperature). According to Table 4.1, between Regime 2 and Regime 3, the temperature ranges from 450 to 600°C ± 50. Consequently, the two samples reflect an increase in the temperature of deformation towards the northwest. Likewise, between GC-110 and GC-5 the temperature of metamorphism increases. The highest temperature of deformation and metamorphism occurs in GC-5. Therefore, the Great Common Fault Zone is mapped closer to GC-5 than to GC-110. These two samples are located in the southeast block of the fault. Furthermore, the analysis of the Great Common Fault Zone by Welch (1993) identifies temperatures for the south block of the fault between 480 and 540°C.

The correlation between Zone VII of Carrigan (1984) and the Golf Course area, in addition to the increase in temperature of metamorphism and deformation towards the west in both localities, suggests that the Golf Course is part of the south block of the Great Common fault Zone. Furthermore, an increment in the temperature of metamorphism and deformation characterizes the proximity of the Great Common Fault Zone.

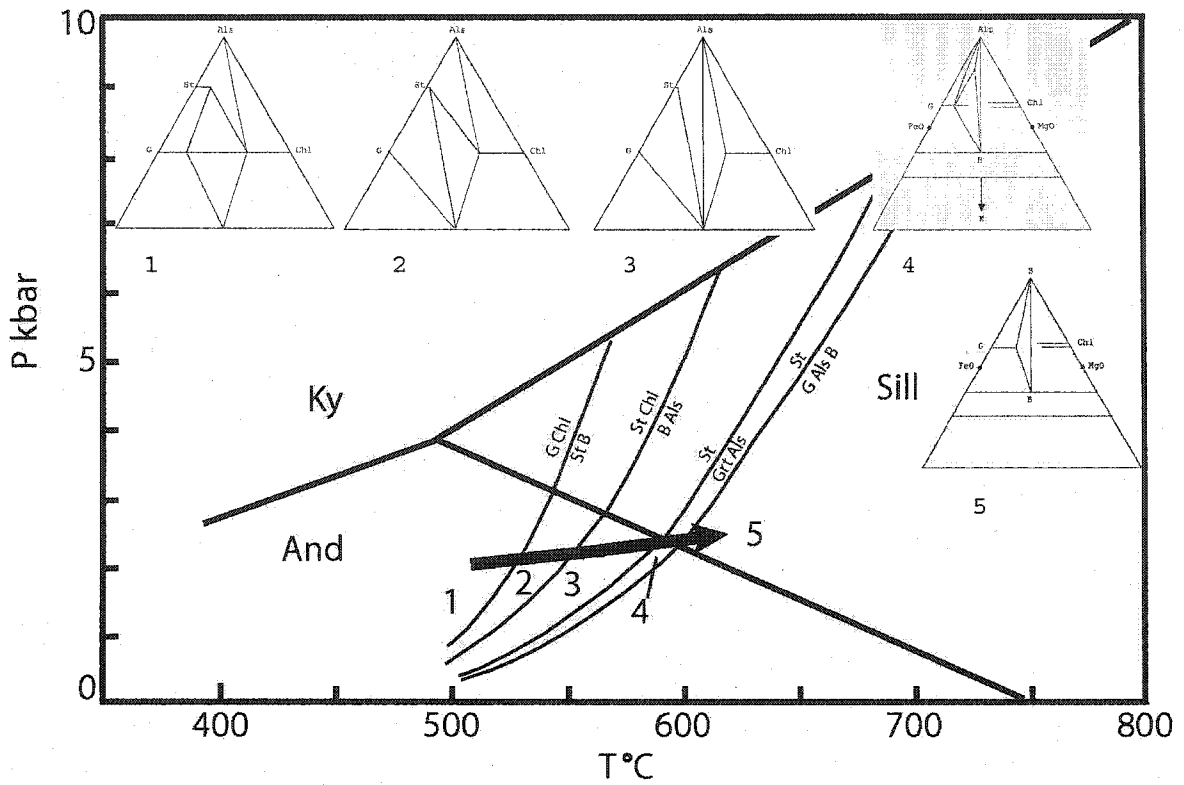


Figure 6.8 - P-T grid showing the metamorphic path of the pelitic rocks in the Golf Course Area of North Hampton New Hampshire. The ternary diagrams on the top of the figure represent the possible mineral assemblages that define the path. 4 and 5 represent Gc-110 and GC-5, respectively. Assemblages illustrated in fields 1 -3 are inferred from the P-T grid. Refer to Table 6.1 for abbreviations, Als represents andalusite in the And field and sillimanite in the Sill field. PT grid adapted from Spear (1993).

CHAPTER VII

INTERPRETATION AND CONCLUSIONS

Introduction

This study evaluated field observations and theoretical tools to achieve the three objectives of this research. These are: 1) Clarify the stratigraphic sequence in the Merrimack Group (MG). 2) Establish the relative chronological order of events, crustal level of deformation, and dynamics of the Portsmouth Fault Zone as a boundary between two blocks, the MG in the west and the Rye Complex (RC) in the east; and 3) establish the stages of deformation of the Great Commons Fault zone within the RC.

In this chapter, the interpretation of results and conclusions are presented in three sections. The first section describes the 1:24 000 scale geologic map of the Exeter and Hampton 7.5-minute quadrangles, a schematic cross section, and a configuration of the bedrock topography (Plate 1).

The second section is devoted to the theoretical aspects of this study. It contains a discussion of the applicability and effectiveness of the Fourier Series Analysis in the solution of geological problems related to folded structures by means of three-dimensional representations and modeling. A discussion regarding the Finite Element Analysis and its relevance in solving geologic problems is included in this section as well.

The third section contemplates the overall geological interpretation of the study area including seven small, but critical, areas which summarize the majority of the field observations. A

tectonic model is presented and discussed in order to contribute to explain the geologic history of the seacoast region of New Hampshire.

Geologic Map

Plate 1 shows the geologic map of the Exeter and Hampton 7.5 minute quadrangles. The files containing the DEM (digital elevation model), roads, and hydrographic information were downloaded directly from the UNH-GRANIT World Wide Web site to construct the topographic base. Geographic Information System (GIS) Arc-View® software was used to compile and re-project the roads and topographic and hydrographic information into the UTM NAD-27 coordinate system.

Based on the findings of this study, the lithologic contacts shown in the State Geologic Map of New Hampshire (Lyons et al., 1997) have been refined. The major changes shown on Plate 1 are the stratigraphic subdivision proposed for the Kittery Formation, the distribution of the minor Exeter-like intrusive bodies, mafic dikes, the contacts between the Breakfast Hill and the Rye Formation in the Rye Complex, and the traces of the Portsmouth and Great Common fault zones.

The present map compiles geologic data collected in this study and by previous authors, e.g. Novotny (1969), Carrigan (1984). No changes have been made in the south portion of the Exeter quadrangle. To give credit and for identification purposes, the map has color coded geologic symbols. Red symbols correspond to Novotny data, blue symbols to Carrigan's data, and black symbols to this study. Field stations are shown as solid circles following the same color code as the symbols. Where only field stations are indicated, neither structural data nor collected samples are available.

The subdivisions of the Kittery Formation are identified in outcrops located in the northwest corner of the Exeter quadrangle, along the trace of the Portsmouth Fault Zone, and in the south portion of

Hampton quadrangle. The traces of the Kittery subunits in the south portion of the Hampton quadrangle are based on the descriptions made by previous authors. At present, most of the outcrops described by these authors have been recently removed by construction. These subunits are represented as folded and following the style recognized in the central area of the Hampton quadrangle. Besides folds, the main structural features in the map are, from east to west, the recently found "Exeter Fault", the continuations of the Nannie Island Fault Zone, the Portsmouth Fault Zone, and the Great Common Fault Zone.

A schematic east-west cross-section is shown at the bottom of Plate 1. The section follows the interpretation in this study: the Exeter Pluton is represented intruding the Kittery and the Eliot Formations, subunits of the Kittery are stratigraphically above of the Eliot Formation, and the contact between the Eliot and the Berwick is a fault.

In the middle part of the section, minor intrusive bodies are represented and one of them has field evidence of reverse faulting (east block up). Such faulting is interpreted as an extension of the Nannie Island Fault Zone (?).

The Merrimack Group is in fault contact with the Rye Complex by the Portsmouth Fault Zone, which is interpreted as a folded thrust. The later Common Fault Zone offsets the Rye complex, the Merrimack Group, and the Portsmouth Fault Zone laterally.

The crosscutting relationships of the structures shown on the map, the cross section, and the suggested chronologic sequence of events in the tectonic model, discussed in a following section, are supported by radiometric ages obtained by previous authors. The radiometric ages are 406 ± 1 Ma (U/Pb, zircon) for the Exeter Diorite and 418 ± 1 Ma (U/Pb, zircon) for the Newburyport Complex (Bothner et al., in Lyons et al.,

1997). Bowring (unpublished data) in an attempt to constrain the age of the Breakfast Hill obtained discordant results and an age of 407 Ma (Pb-Pb) from the most concordant zircon. Boeckeler (1994) obtained a radiometric age of 298 ± 31 Ma from 16 samples of pseudotachyllite veins from the Great Common Fault Zone in the Rye Complex (Rb/Sr systematics). Based on whole rock ages (Ar₄₀/K₄₀) McHone (1978) obtained ages of 158 ± 6 to 191 ± 10 Ma for the several northeast-trending diabase dikes that intrude the Merrimack Group and the Rye Complex.

Additional information regarding the bedrock topography is included in the lower right corner of Plate 1. An attempt was made to determine the bedrock configuration from depth to bedrock data obtained from 220 wells to bedrock provided by the USGS-WRD and NH DES Water Division and outcrop and wellhead elevations. Those data were contoured and failed to identify the extent of metasediments, but showed the presence of Exeter-like minor intrusions that tended to occupy the topographic highs.

The objectives of the configuration were to show areas of potential bedrock outcrops to assist the fieldwork, and to identify geologic structures. Besides the presence of the Exeter-like minor intrusions, that tended to occupy topographic highs, no other units or structures were clearly shown.

Theoretical Aspects

Fourier Series Analysis - The variant of the Fourier series analysis discussed in Chapter II presents the basics for the calculation of a mathematical expression of a curve that resembles the cross-section of a folded surface in the field. The elements of the equation are given from the first three harmonics of the series, calculated from an image of the profile of the fold.

The use of commercial software (e.g. Mathematica® or Matlab®) facilitates the representation of the curve in three dimensions. The procedure consists of three main steps. 1) The curve that represents the fold is expressed as a parametric equation. 2) The ranges of the equation are chosen in order to plot a fold and its many cycles. 3) To represent a second folding stage, another expression is added to the plot as in 1) and 2).

The Mathematica® software permits the calculation of the contours as projected on any given plane. With this software, the user can change the settings in order to reproduce an interference pattern as seen in the field, regardless of the orientation of the plane of projection (fig. 7.1). Hence, the complicated interference patterns can be studied by using these detailed projections (fig 7.2).

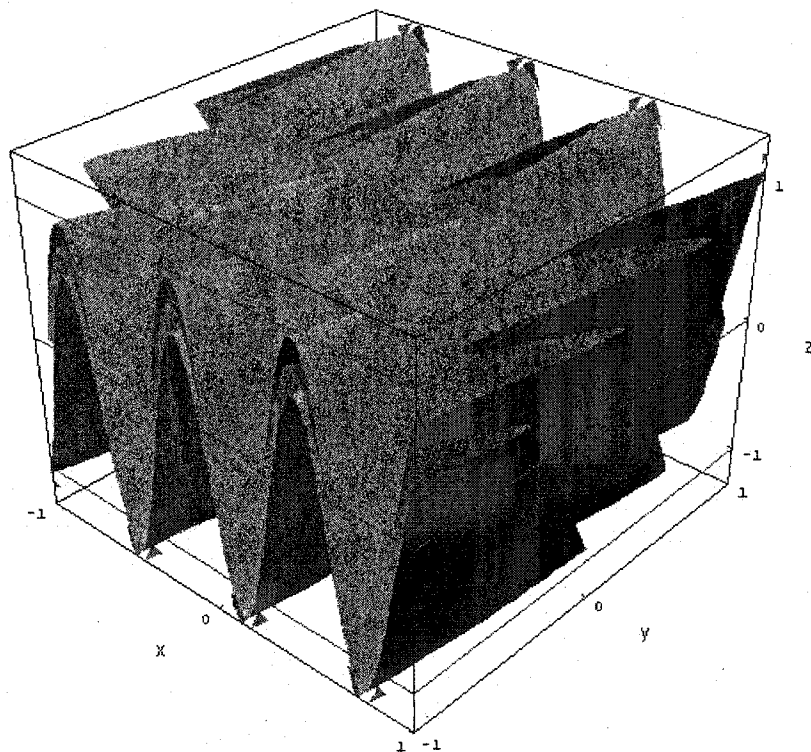


Figure 7.1 - Three dimensional representation of chevron refolded folds.

The Matlab® software allows the rotation of the 3-D graph along either of the two perpendicular axes that define the plane of projection that in turn facilitates visualization of folded surfaces. By rotating the 3D graph, the recalculation of the parametric functions is avoided and comparisons among projections are made easily.

This method opens a wide range of applications and motivates further investigation regarding three dimensional modeling of folded structures. Besides the application of the method to solve geologic problems and the representation of a folding style, the variant of the Fourier series analysis presented in this study and the graphing procedure have proven their effectiveness as a teaching tool.

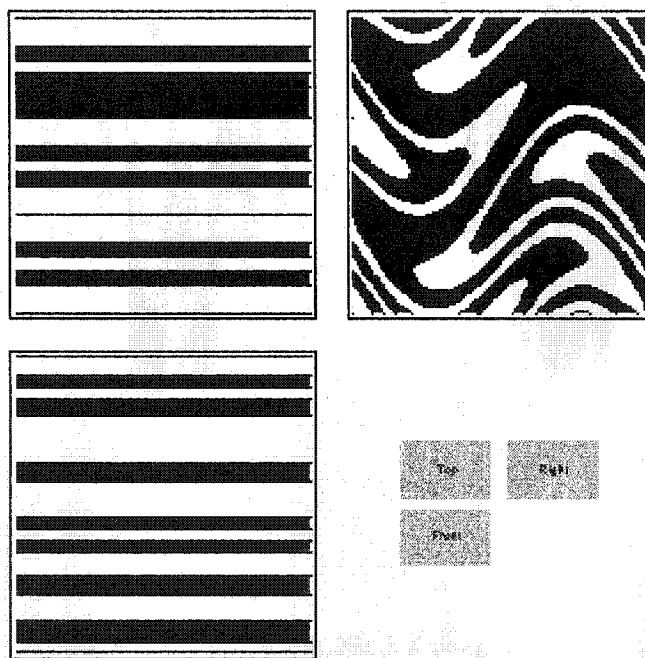


Figure 7.2 - Projection of a Type 3 interference pattern as projected in three mutual orthogonal planes.

Finite Element Analysis - Finite element models of pyrite crystals were used to test the two working hypotheses discussed in Chapter III. Numerical simulations permitted the retrodeformation of pyrite crystals,

considered as deformed quadrilateral shapes, into almost regular squares. The results in Chapter III support the hypothesis that the deformation of the crystals is associated with folding of the rock units that contain them.

The investigation of the deformation history of the crystals led to the implementation of statistical tests to evaluate the results. The "squareness" and eccentricity were chosen as parameters for geometrical evaluation.

The applicability of this method has been tested before by other authors to solve geological problems from a theoretical perspective (e.g. Ramsay and Lisle, 2000; Treagus and Lan, 2003). But in this research, Finite Element Analysis was applied to obtain information from rocks and crystals that are critical to the interpretation of the deformation history of the seacoast region of New Hampshire as discussed below.

Further study and applications of the method to geologic problems will provide information regarding the deformation of objects of known geometry embedded in rocks of different material properties. The Finite Element Analysis will lead to a better understanding of deformation of rocks at microscopic and regional scales.

Geologic interpretation

Stratigraphy - The Kittery, Eliot, and Berwick Formations constitute the stratigraphic subdivision of the Merrimack Group. Nevertheless, the stratigraphic order of these formations remained ambiguous (Katz, 1917, Billings, 1956; Hussey, 1968; Bothner et al., 1984, Lyons, et al., 1997). The clarification of the stratigraphic order in the Merrimack Group constitutes one of the problems that motivated this study. The Kittery Formation has sedimentological characteristics that can be used as criteria to subdivide it. The sedimentary style,

primary sedimentary structures, bed thicknesses, and the relative proportion of metasandstone with respect to metashale, constitute the basis of the subdivision presented in Chapter V. The subdivisions are mapped in the northwest portion of the Exeter quadrangle and across the Hampton quadrangle (Plate 1).

Rickerich (1993, 1984) interpreted the sedimentary section in the Kittery Formation as deposited by turbiditic currents of low and high density, from an "eastern" source (present coordinates). Walker (1993) states that in order to preserve deposits as turbidites, the sediments must not be reworked into different-looking deposits by other currents, and he concludes that the turbidites are placed below the storm wave base (probably at minimum depths of 76-100 ft, 25-30m).

The subunit that contains these well preserved primary sedimentary structures, denoting a strong influence of the turbidity current on the deposition process, is in this case, at the top of the stratigraphic column (S0ka). The stratigraphic tops observed on the outcrops along the Exeter River place S0ka above S0kb. Stratigraphically lower, thicker bedded S0kb and S0kc are interpreted as deeper basinal deposits. Their characteristics reflect lower energy flow currents. The lowermost subunit (S0kc) is interpreted as part of the transition between the Kittery and the Eliot Formations.

The Kittery Formation has been described as a non-fossiliferous unit (Rickerich, 1994 and Bothner et al., 1984). This study documents the presence of a fossil-like object found in a loose block from the east side of Adams Point (Fig. 5.7a and 5.7b in Chapter V). The identification of the well preserved three-dimensional object embedded in a light gray colored metasandstone, is ongoing, but it is likely a fossil of some kind.

Evidence presented in Chapter V indicates that the Kittery Formation is younger than the Eliot Formation: 1) Transition noted above. 2) A piece of core from borehole NR-1, interval 15-19.7ft (4.6-6m), drilled by the USGS at Fabyan Point shows a basal conglomerate of about 1.5cm thick, composed by clasts of the underlying Eliot Formation (ripped-up clasts?). Overlying this conglomerate, there is a light brown metasandstone interlaminated with thin layers of black shale of the Kittery Formation. 3) Detailed mapping and systematic sampling along the Bellamy River, in addition to X-Ray diffraction analysis suggest that this location represents a transition between the two units.

The contact between the Eliot and Berwick Formations is interpreted in this study as a fault contact (Chapter V). In the Coheco River, detailed mapping identified ductile and subsequent brittle faulting separating a northern from a southern block. The northern block, assigned to the Berwick Formation, has thinner layering with less metapelite and more calcsilicate layers than the rocks of the southern block assigned to the Eliot Formation.

This study did not find enough evidence to clarify the stratigraphic order between the Eliot and the Berwick. Nevertheless, the ductile and brittle deformation found in the Coheco River supports two possible interpretations. First, that the Berwick Formation is not part of the Merrimack Group, and that it possibly belongs to a different geologic terrane, tectonically juxtaposed against the Merrimack Group (along Calef Fault ?). The second interpretation is that the Berwick Formation represents a deeper facies in the stratigraphic sequence of the Merrimack Group, and that the Eliot and the Berwick were juxtaposed by a reverse fault.

Interpretation of Folds - A folding style defined by strong topological and structural similarities among folds in the study area was identified and discussed in Chapter II. Results show that the fold shapes vary from chevron to sinusoidal and have an asymmetric "long-short-long" limb pattern in the seacoast region. The degree of asymmetry (DA) ranges from sub-symmetrical to asymmetrical ($0 < DA < 4$ to $4 < DA < 8$, see Table 1.2 in Chapter I).

In the Merrimack Group (MG), the relative proportion of metashale to metasandstone, the n-value of Ramsay and Huber (1987), influences the shape of the folds. Where the proportion ranges from .35 to .25 the folds are chevron; where it ranges from .05 to .085 the folds are sinusoidal.

In the Rye Complex (RC), DA ranges from 4.25 to 4.32 (asymmetrical folds) and have sinusoidal-chevron shape. Folds are smaller and tighter than in the MG, but the long-short-long limb pattern is preserved.

The asymmetric fold pattern is interpreted as the result of a folding mechanism with a shear component with a plane of shear perpendicularly oriented to the fold axis (fig. 7.3). The presence of shear supports a working hypothesis that the principal mechanisms of folding in the study area are a combination of flexural flow and flexural slip. Furthermore, by assuming a relatively large shear component in combination with compression, the resultant fold shape is likely to be asymmetric with a "long-short-long" pattern (fig. 7.3).

In order to understand better the mechanisms of deformation, Finite Element Analysis was applied to pyrite crystals embedded in a limb of one of these folds (Chapter III). The analysis tested two working hypotheses: (1) the deformation imprinted in the pyrite crystals was related to the folded structure where the crystals were

embedded, or (2) the deformation of the crystals was related to the emplacement of a nearby mafic dike(s). The goal of the numerical simulations was to produce regular square shapes from deformed pyrite crystals by applying loads (shear, compression, and a combination of both).

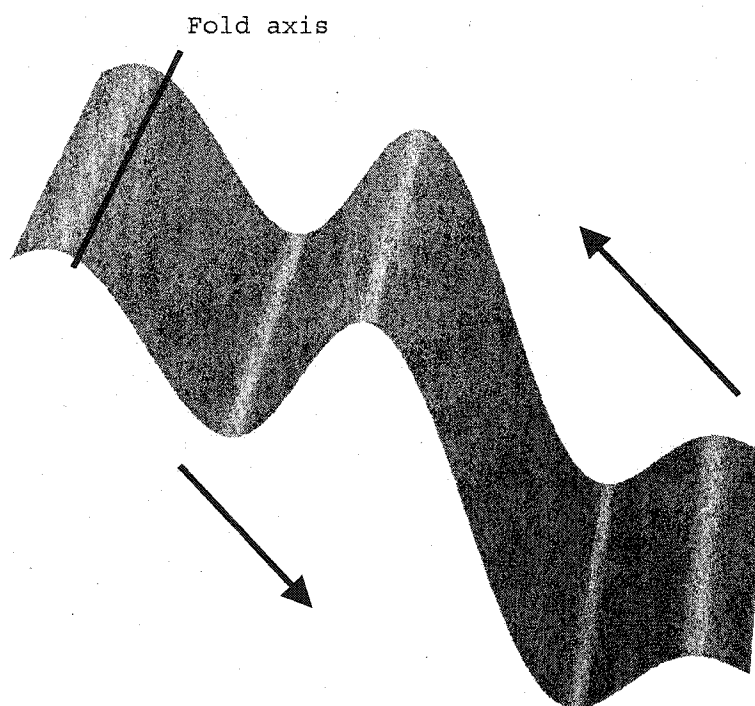


Figure 7.3 - 3-Dimensional representation of the "long-short-long" fold pattern that is pervasive in the study area. Arrows represent the components of the folding mechanism.

Qualitative results show that a combination of compression and sinistral shear were required to reconstruct the crystals to a squared shape. These results indicate that the crystals were subjected to extension perpendicular to the fold axis and dextral shear along a plane parallel to the fold limb.

If the mechanisms of folding include extension and shear along the limbs, then it is likely that the deformation of the crystals occurred during folding. Therefore, the deformation of the crystals is attributed to folding.

The flexural slip and flexural flow have shear and extension components. After buckling, as the folding progressed, the layer that contained the crystals was subjected to extension. The compressional forces acting in the layer at the same time generated perpendicular extension. Therefore, a shear component deformed the layer as well (fig. 7.4)

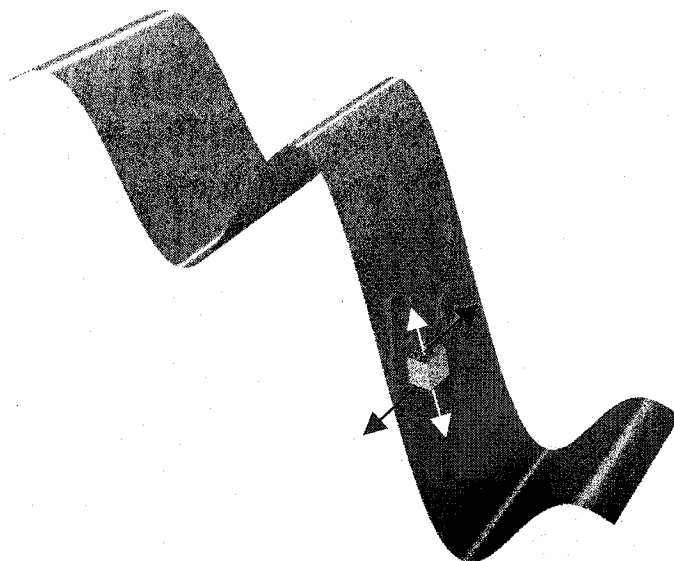


Figure 7.4 - Graphical representation of a fold and a pyrite crystal. White arrows represent extension, black arrows shear.

Results of strain analysis based on the geometrical relationship between folds and cleavages (axial planar and parallel to bedding) observed in MG folds (Willard, 2000) were presented in Chapter II. The interpretation of the strain analysis is that under a heterogeneous

simple shear mechanism, the resultant cleavage is sub-parallel to bedding planes along the limbs of the fold, and that there is no significant strain in the hinge. Additionally, a homogeneous plane strain component in the folding mechanism is needed to generate an axial planar cleavage. In the MG, the two types of cleavages are observed, and it is possible that a combination of heterogeneous simple shear with plane strain constituted the folding mechanism.

The flexural slip and flexural flow mechanism of folding involve both, heterogeneous shear and plane strain. The two cleavages observed in the folds by Willard (2000) and the results from the strain analysis here support the hypothesis that the mechanism of folding is a combination of simple shear and plane strain. Consequently, it is concluded that flexural flow and flexural slip are likely to be the principal mechanisms of folding in the MG prior to emplacement of major plutons.

Variable plunging folds are observed in the study area. According to the interpretation in this study, the effect of anticlastic bending may cause this variation. The anticlastic bending is generated by tangential longitudinal strain during folding, which bends the fold axis along a vertical plane (fig. 7.5). It is associated with the mechanism of folding that generated the fold axis. Because this bending is generated simultaneously with the folds, it is not interpreted as a later folding phase.

In Great Bay, the axial planes of folded rocks of the MG are deflected in map view (fig. 7.6). The apparent clockwise deflection is interpreted as a product of shear deformation produced by the Nannie Island Fault Zone (NIFZ). The interpretation of deformation by shear and shear zones will be discussed later in this chapter.

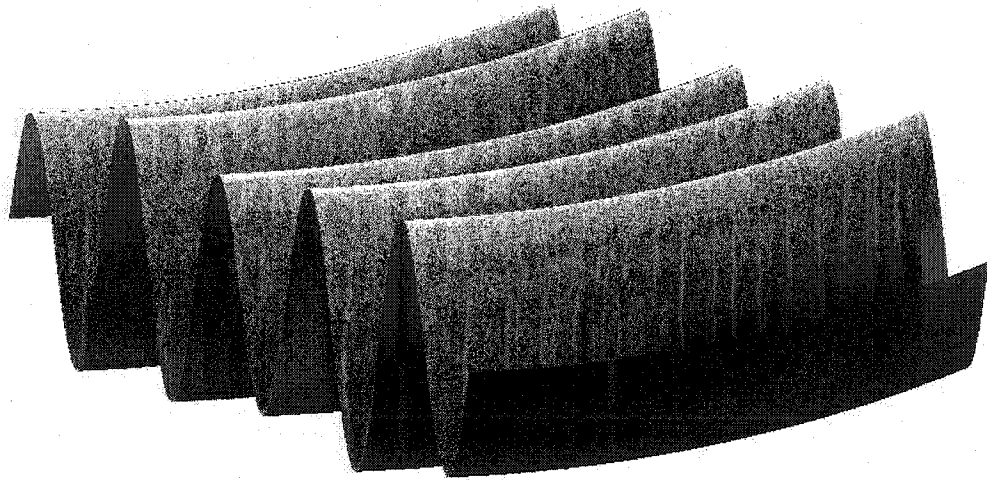


Figure 7.5 - Graphic representation of anticlastic bending. The curvature in the fold axes is generated at the same time as the folds were formed.

In the study area, only three locations of interference patterns of folding were identified at outcrop scale as discussed in Chapter II (Scammel Bridge, Golf Course, and Gerrish Island). For any interference pattern, when there is a large scale difference between the scales of the two generations of folds the pattern cannot be visible in outcrops, it is only observable regionally. Hence, the presence of an interference pattern at outcrop scale implies that there is not a large difference between the scales of the two folding stages.

According to the present interpretation, the three locations are close to fault zones, that are likely to be responsible for the imprinted "re-folding". The observed interference pattern corresponds to a Type 3 of Ramsay's classification. A type 3 is characterized by a "hook" shaped fold pattern formed by coaxial deformation.

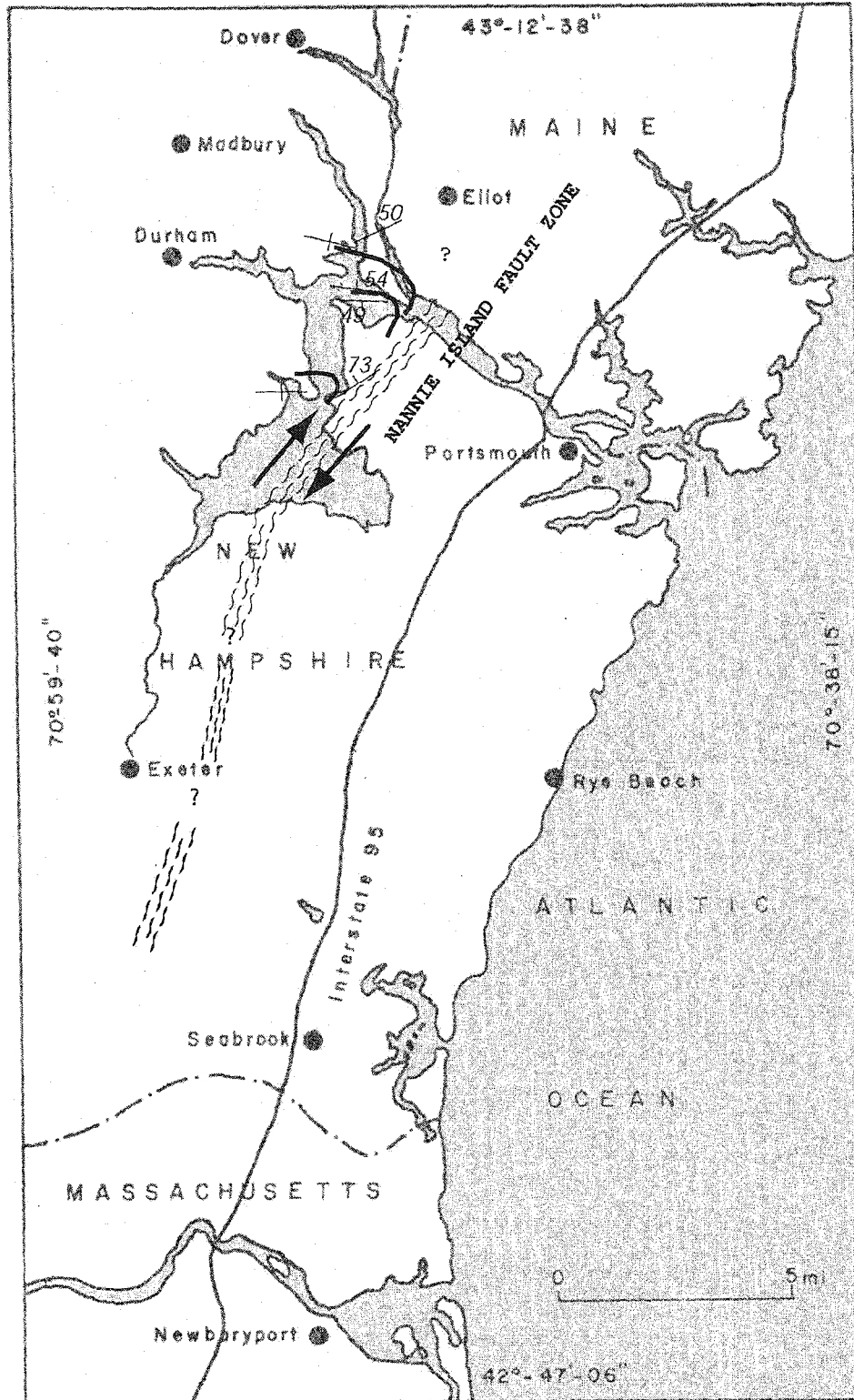


Figure 7.6 Map showing the deflected attitude of the mean direction of the fold planes along the Great Bay and their possible relation with the Nannie Island Fault Zone.

A geometrical example of type 3 interference pattern is shown in Figure 7.7. In a type 3 pattern, the axial planes of the two generations intersect each other, and the intersection between the two sets of axial planes defines the axes of the last generation of folds. Its generation implies the existence of a first generation of folds that is recumbent or nearly recumbent (fig. 7.6). In this pattern, both generations of folds have axes that tend to be parallel to each other. Furthermore, a type 3 interference pattern implies strong changes in the kinematic condition and orientation in the superimposing younger fold generation with respect to the older. In addition, it has to be considered that in order to fold folded rocks in a certain time, either the ductility of the rock has to increase, or the deformational stresses have to increase.

At least three folding phases have been identified in the MG (e.g., Fargo and Bothner, 1995; Hussey et al., 1984; Hussey, 2000). The earliest phase (F_1) consists of recumbent isoclinal folds, F_2 folds are upright open to steeply overturned folds with plunges in the order of 30° . F_3 are relatively open, overturned, and dextral folds. F_1 folds are rarely seen, and most of the time inferred from inverted strata. F_1 and F_3 are observed in Ogunquit, Maine.

However, a single major folding event has been interpreted in this study. After the major folding event, the folds were subsequently deformed by shear and compressional mechanisms related to fault zones (e.g. Nannie Island, Portsmouth, and Great Commons; refer to Plate 1). Figure 7.8 helps to explain graphically the folding sequence in the MG according to the interpretation proposed in this study.

Initially, the major folding event occurred and generated the pervasive fold pattern. As the compression and shear progressed, in

addition to the accommodation of the compressed volumes of rock, a transpressional regime dominated the deformation mechanisms. Because of transpression, fault zones were developed simultaneously, and the strike slip displacements took place.

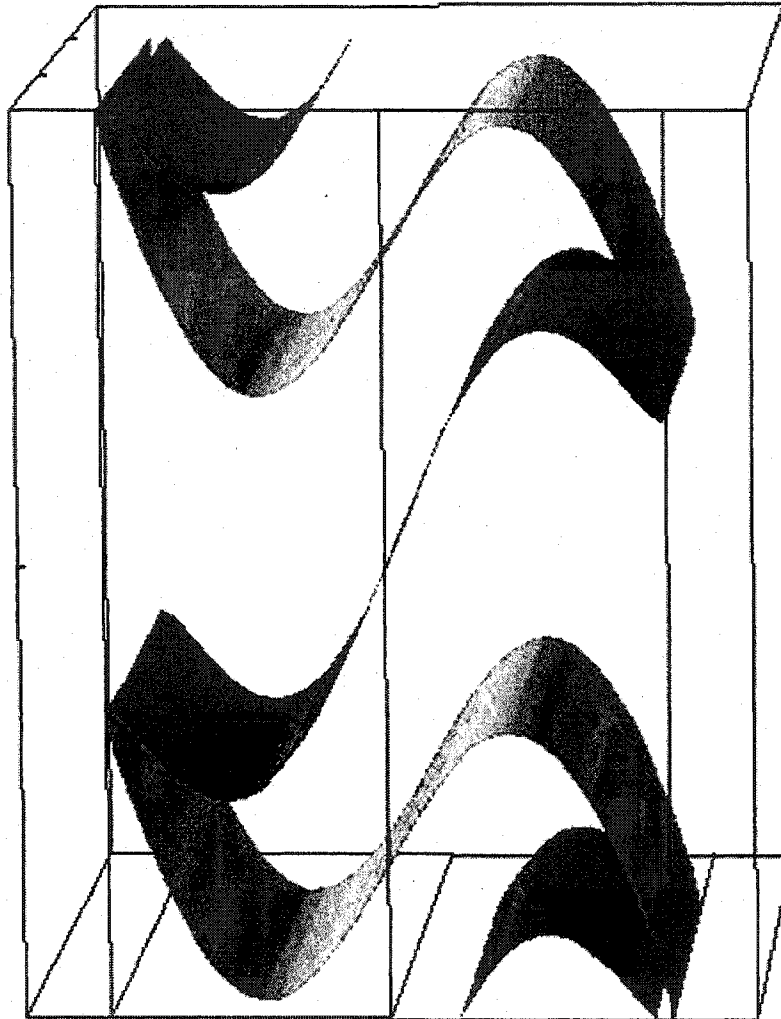


Figure 7.7 - A geometrical 3-D representation of a refolded surface according to a Type 3 interference pattern.

Shear zones are characterized by the concentration of deformation along shear bands. According to the microstructural analysis in

Chapter IV, fault zones in the study area have right lateral sense of movement. As shown in Figure 7.8, if the folded surface is deformed simultaneously by dextral shear in a vertical plane (Y-Z), right lateral horizontal shear (X-Y), and compression (perpendicular to X-Z), then the resultant deformation might generate refolded folds. The refolded shapes observed in the field are represented by the illustration in the center of Figure 7.8. The diagram shows the hinges of the older generation deflected by the younger generation of folds produced by shear.

The method that uses the variant of the Fourier series analysis proposed in Chapter II is applied to generate the 3-dimensional models of the folded surfaces (e.g. fig. 7.8). The effectiveness of this graphing method and further applications were discussed in a previous section of this chapter and in Chapter II.

Interpretation of Faults - In the seacoast region, northeast - southwest trending faults (i.e. Calef, Nannie Island, Great Common, and Portsmouth Fault) are characterized by an early ductile and later brittle fabric (e.g. Carrigan, 1984; Swanson and Carrigan, 1984; and Bothner and Hussey, 1999). In this study, an east west brittle fault has been identified and informally named the "Exeter Fault".

Ductile Deformation - In this study, the ductile deformation in the northeast trending faults is interpreted as a deformation that immediately post-dates the folding event and pre-dates the emplacement of the Exeter Pluton and the Newburyport Complex and the brittle deformation. The presence of refolded folds in the vicinity of fault zones (Calef, Nannie Island, Great Common, and Portsmouth) and the overprinting brittle faults supports this interpretation (Fig. 7.8). Nevertheless, the documentation of the mechanisms of ductile deformation is complicated due to the lack of exposure and the

overprinting brittle deformation. The traces of the faults were refined based on field observations and the use of DEM (fig. 7.9, 7.10, and Plate 1).

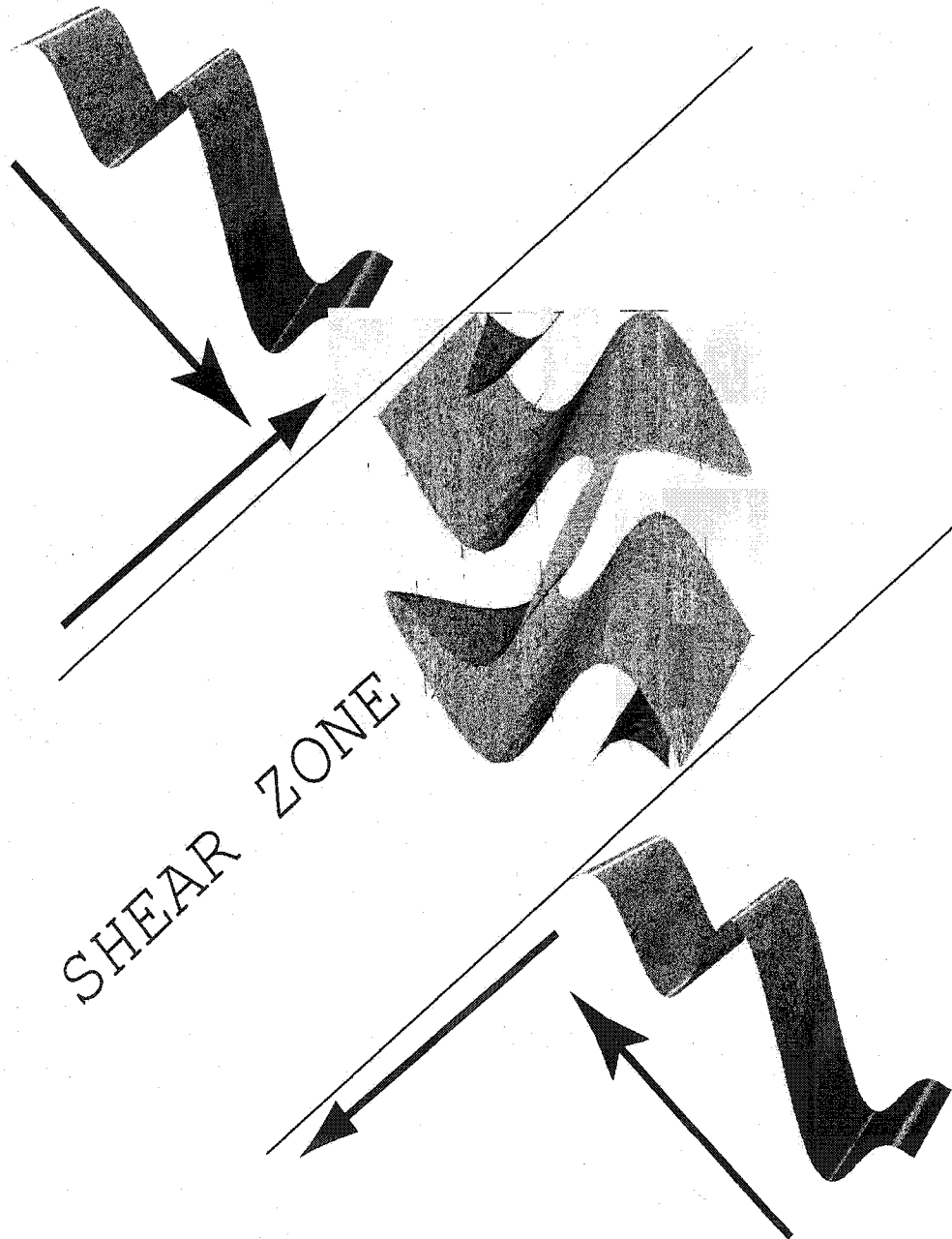


Figure 7.8 - Orthogonal 3-D representation of the folding style observed in the study area and its shape after being refolded during faulting (shear zone).

The Calef fault has been identified in the Coheco River (Chapter V). Among the ductile deformation structures found in this location are attenuated folds with axial planes parallel to the foliation, meter sized dextral kinematic indicators, and boudinage. Based on these structures, a right lateral sense of shear is interpreted in this fault. In this locality, the folds are affected by a subsequent ductile deformation that produced the strong foliation, the boudinage, and the kinematic indicators. A later brittle faulting affected these rocks (Chapter V).

The Nannie Island Fault Zone crops out beneath General Sullivan Bridge, at Woodman Point, and in Nannie Island. The strike of the trace of the fault is approximately 35° to the northeast.

If the strike of the mean direction of the axial planes of the folds in the Great Bay is used as a strain trajectory, then the resultant pattern of deflection represents the strain distribution of this area. The deflection of the mean direction of the axial planes of the folds in the northwest block of the Nannie Island Fault Zone is shown in Figure 7.6.

The deflection defines a hook shaped pattern revealing a right lateral displacement (figs. 7.6 and 2.3 in Chapter II). Therefore, both structures, the deflection of the strain pattern and the shear zone, can be associated.

The hook shaped pattern is a general interpretation. At a larger scale, the pattern might be interrupted and it is probable that several shear bands parallel to the principal shear zone may occur on both sides of the fault. If a fault zone is subdivided into discrete blocks (strain partitioning), the net displacement in the strain trajectories will be distributed among the blocks.

Depending on the horizontal displacement and compression in the shear zone, the strain trajectories in the blocks will show more or less deflection. The geometry of shear zones may vary upon their relative depth with respect to the brittle-ductile boundary, and may develop complicated patterns depending on the mechanisms that generated them. Unfortunately, the southeast block of the Nannie Island Fault Zone is restricted and could not be documented in this study.

In the Rye Complex, the Great Common Fault Zone separates less migmatized rocks to the south from more migmatized rocks to the north. Welch (1993) estimated a temperature of metamorphism in the north block of 625 - 675° C (garnet-biotite) and of 700 - 725° C (amphibole-plagioclase), and a temperature of 480 - 540° C (garnet-biotite) in the south block.

In the Golf Course area, the interpretations of microstructures in quartz grains preserved in the south block of the Great Common Fault, as discussed in Chapter IV Area #1, are consistent with an increase in temperature of deformation to the west, from 250°C ± 50 (Regime 1, Table 4.1) to 450-500°C (Regime 3, Table 4.1). In this area, refolded folds have been reported (Chapter II).

Outcrops farther to the south, along Lafayette Road are correlated with the Great Commons Fault Zone (Areas #2 and #3 in Chapter IV). For Area #2, the microstructural analysis in these localities indicate a temperature of deformation between 400 ± 50 °C (Regimes 2 and 3), and of 450-500 °C (Regime 3) for Area #3. Temperatures of deformation are consistent with the ranges reported from the south block of the fault (Welch, 1993).

The correlation between areas #1, #2, and #3 is based on the strike continuity, temperature of deformation, and the DEM interpretations. According to the metamorphic path discussed in

Chapter VI the pressure at which the Regime 2 and 3 occurred ranges between 2 - 2.5 kilobars.

To the northeast, based on the results discussed in Chapter VI, lithologies in Area #1 of Chapter IV can be correlated with Zone VII of Carrigan (1984) in New Castle Island. Consequently, the trace of Great Common Fault zone crosses through Gerrish Island, New Castle Island, Portsmouth, and North Hampton.

The Rye Complex and the Merrimack Group are in contact along the Portsmouth Fault Zone (Plate 1). This structure crops out on Gerrish Island, Kittery, Maine, where Hussey (1980) described two ductile deformations the first one is characterized by a blastomylonitic fabric, and the second by two major ductile faults with dark brown ultramylonite. Type 3 refolded folds have been identified in this locality (Chapter II).

The presence of two ductile and one brittle deformation in this fault zone suggests that the Portsmouth Fault Zone has a longer ductile deformation history than the other fault zones in the seacoast region. For interpretation purposes, this study considers the Portsmouth Fault as the first structure of this kind formed during the accretion of the Rye Complex and the Merrimack Group. The accretion of these units is discussed in a following section regarding the tectonic model.

Brittle deformation - The contact between the Eliot and Berwick Formations is interpreted as a fault contact with brittle and ductile fabrics (Chapter V). The ductile structures reveal a right-slip shear sense; the brittle fabrics indicate a dip slip motion, northwest side down with a minor left lateral displacement.

In this study, a brittle fault in the Merrimack Group has been identified along the Exeter River, close to the south end of the Exeter Pluton, and informally named the "Exeter Fault" (Plate 1, and Area #4

in Chapter IV). In the Exeter River, the trace of the fault is predominantly east-west ($259^{\circ} - 40^{\circ}$ NW), and does not follow the regional northeast trend of the majority of the structures in the study area. The net displacement of this fault is not defined, but it may be responsible for truncating Kittery formation outcrops to the south.

In this locality, a pervasive slickenfiber lineation is present along the foliation/layering planes, some of which are crosscut by thin veins of pseudotachyllite (Area #4 in Chapter IV). Based on the presence of slickenfibers and pseudotachyllite veins, the displacement and nature of the fault is interpreted as a north block down combined with and eastwards horizontal movement generated by brittle deformation.

In Hampton Falls, in the Dodge Ponds area, sheared rocks crop out under the bridge along Lafayette Road in the south side. According to the microstructural analysis conducted in this location the shear-sense is dextral (Area #3, Chapter IV). Based on the on strike location with Areas #1 and #2, the three localities are interpreted as outcrops affected by the Great Commons Fault Zone. In this fault zone, Carrigan (1984) identified an early ductile fabric and a latter brittle fabric.

In the Portsmouth Fault Zone, ductile fabrics characterized by mylonitized rocks indicate dextral sense of shear, and the brittle fabrics reveal a dip slip motion, northwest side down (Swanson and Carrigan, 1984; and Hussey and Bothner, 1993, 1995). Bothner and Hussey (1999) described the Nannie Island Fault Zone as a narrow (<200 m) dextral shear zone; at present, no brittle deformation has been reported in this shear zone.

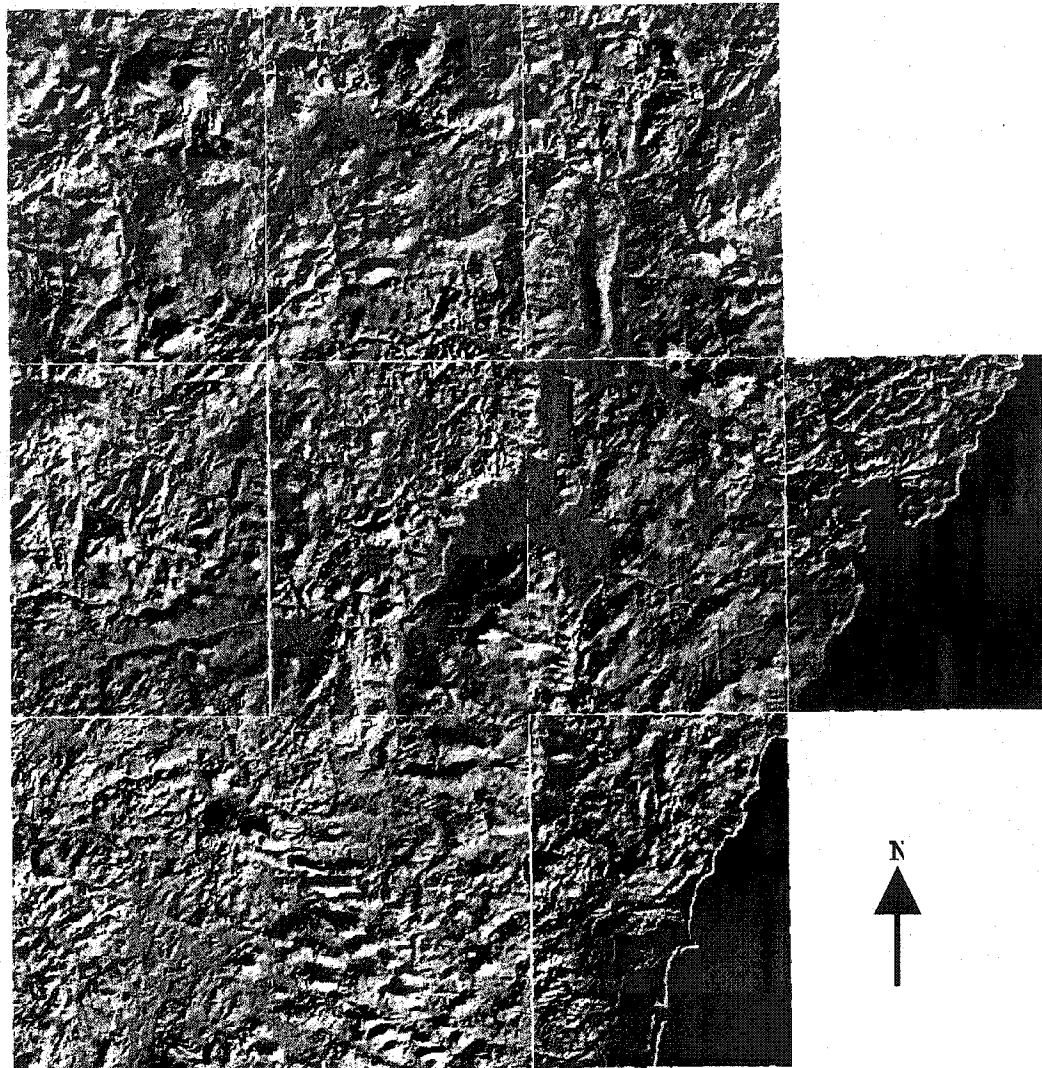
It is virtually impossible to follow the trace of the above-mentioned faults in the field. The access to the outcrops is limited

by the overlying glacial sedimentation, vegetation coverage, and in some places, the access is restricted.

As an attempt to refine the traces of the faults based on the findings made in this study, the Geographic Information System (GIS) Arc-View® software was used to plot digital elevation models (DEM) provided by the UNH-Granit World Wide Web site that covers most of the seacoast region. The topographic features can be enhanced by using the hill-shade tool that allows the setting of the direction of the illumination source. By setting the illumination source at an azimuth of 118° and at a right ascension of 13°, most of the low relief topographic features become observable (Fig 7.9).

Based on field observations and previous mapping, the traces of the faults coincide in most part with the topographic features identified with the aid of the DEM (fig. 7.10). The traces of the faults affected by ductile and later brittle deformation, trend northeast-southwest while the mostly east-west-trending "Exeter Fault" has brittle deformation (pseudotachyllite veins).

By definition, a Riedel system consists of at most 5 elements: 1) principal displacement zone, 2) synthetic shear parallel to the principal displacement, 3) R shears, 4) P shear, and 5) tension fractures. From all five elements, the presence of the R shears is the only mandatory element for a shear zone to be considered a Riedel shear zone (Davis et al., 1999). The geometrical arrangement of the R elements is as follows: the angle between R_1 and R_2 is about 120° while the angle between the R_2 element and the principal displacement zone (long axis of the ellipse) is on the order of 105°.



5 0 5 Miles

Figure 7.9 - Digital Elevation Model from the ten 7.5 min quadrangles that cover most of the seacoast region of New Hampshire (From left to right, top: Barrington, Dover West, Dover East; middle: Epping, New Market, Portsmouth, Kittery; bottom: Kingston, Exeter, Hampton). The azimuth of the illumination source is 118° and the right ascension is 13° .

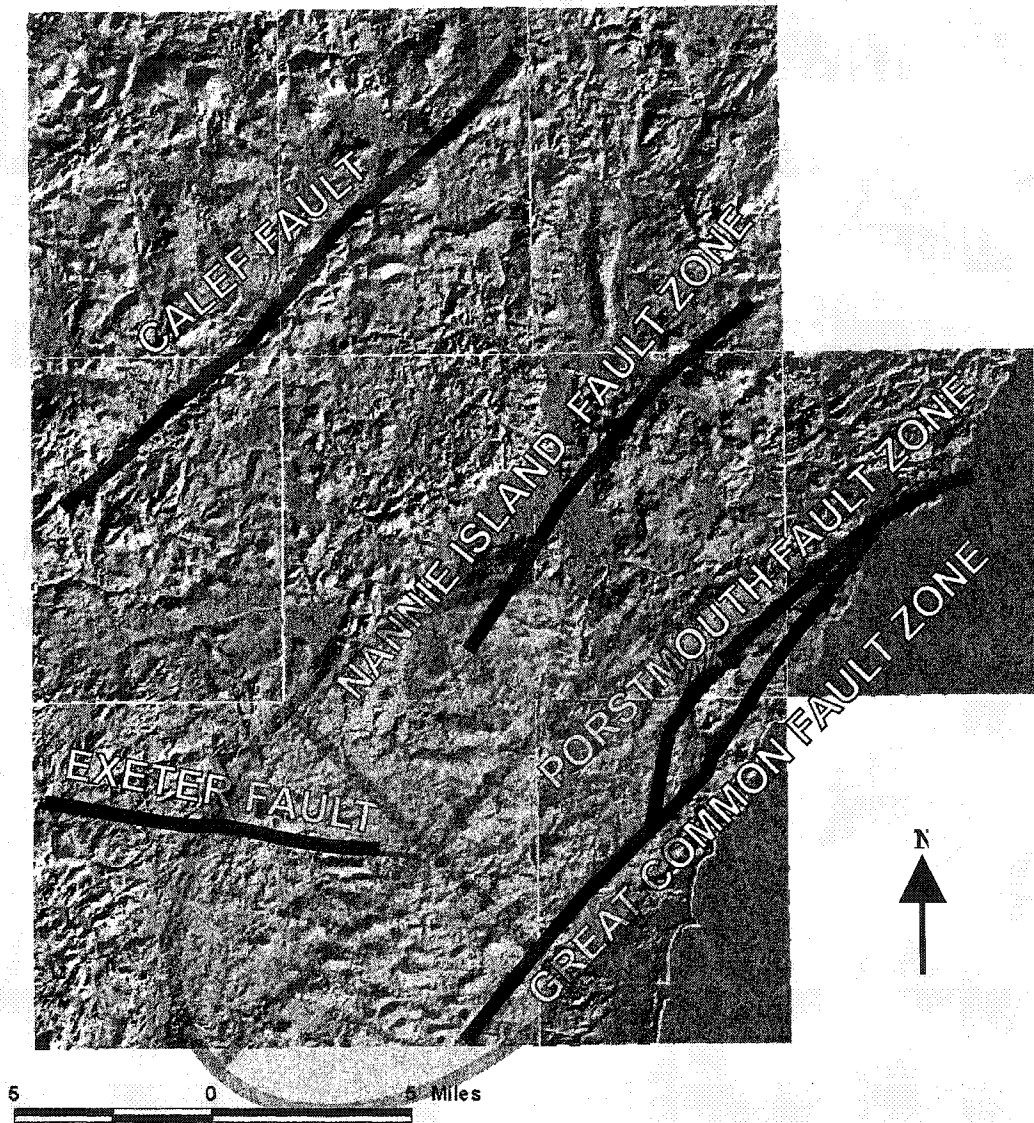


Figure 7.10 - DEM composite map showing the location of faults identified in the study area. The ellipse represents the orientation of the Riedel shear system where R_1 is represented by the brittle component of the northeast trending faults, and R_2 by the brittle "Exeter Fault". See Figure 7.9 for the location of quadrangles and light source settings.

Assuming that the generation of pseudotachyllite in the Great Common Fault Zone is contemporaneous with the emplacement of pseudotachyllite veins in the "Exeter Fault" it can be hypothesized that the two faults form an array of faults that define a Riedel shear system (R elements). The brittle deformation components of the northeast-southwest trending right lateral Great Common Fault Zone represent the R_1 element of the Riedel system, the R_2 left lateral element (antithetic component) is represented by the "Exeter Fault".

In the interpreted system, R elements are present, and the principal displacement zone and the R_1 element are right lateral, while the R_2 element is left lateral. Consequently, based on the geometry and the nature of the displacements in the faults, the brittle deformation in the study area can be interpreted as a Riedel shear zone. According to this interpretation, the principal displacement occurred along the long axis of the ellipse.

In the Great Commons Fault Zone, Boeckeler (1994) obtained Rb/Sr whole rock ages from pseudotachyllite of 298 ± 31 Ma. These ages represent the last stage of movement in this shear zone so far recognized.

If the brittle deformation in the Great Common Fault and the "Exeter Fault" belong to the same Riedel system, then it can be hypothesized that the generation of pseudotachyllite in both localities is contemporaneous, and that it occurred between 298 ± 31 Ma (Carboniferous - Permian age). If this hypothesis can be tested, then it will confirm that the brittle deformation overprinted the ductile deformation in the study area.

The fact that the horizontal component of the brittle faulting in the Cocheco River is left lateral (Chapter V), indicates that it is possible that the Riedel shear occurs as conjugate systems.

Consequently, sinistral and dextral strike slip displacements may occur. Tension fractures constitute another element in the Riedel system, which have not been identified in the study area.

On the DEM, several other topographic features parallel to the "Exeter Fault" can be traced in an echelon array to refine the Riedel system. Field identification of those features and additional east-west brittle-ductile faulting is needed to support this interpretation, otherwise tracing lines on a DEM is mere speculation. Similar bedrock structure investigation has been conducted by the USGS to understand better ground-water-flow paths (e.g. Ferguson, et al., 1997).

Tectonic Model

Based on radiometric data presented in the previous section and results from this study, it is possible to propose a sequence of events that constitute a geologic history of the seacoast region and its role in a regional tectonic frame. Table 7.1 summarizes these data. The tectonic model presented in this study combines some concepts of the models proposed by Van der Pluijm et al., (1993) and by Bradley et al., (2000).

Prior to the Acadian Orogeny (Early Ordovician), sediments of the Rye complex were deposited in a basin associated with the Iapetus Ocean (?). The Iapetus was delimited by the Avalonian micro-continent and the Laurentian craton. During the closure of the Iapetus (produced by the convergence of Avalon and Laurentia by northward subduction), rocks of the Rye Complex were deformed and metamorphosed, Middle Ordovician (?). The sediments of the MG probably were deposited in another basin. Rickerich (1984) interpreted the source of these sediments as derived from a separate micro-continent located to the east (in present coordinates).

As the convergence continued, Rye Complex rocks started to collide

against rocks of the Merrimack Group, probably along a decollement surface (fig. 7.11a). As the collision progressed, a transpressional regime was established and caused (?) the juxtaposition of the Merrimack Group next to the Rye Complex. This juxtaposition was followed by the beginning of the main folding event that deformed these rocks simultaneously in the early stages of the Acadian Orogeny (Early Silurian?). Probably, the folding event that generated the pervasive shape of "long-short-limb" (documented in Chapters II and III) initiated at this time, and the first ductile deformation observed in the Portsmouth Fault occurred. Subsequently, the Merrimack group thrust over the Rye Complex and the main folding event reached its maximum intensity (fig.11b).

EVENT	AGE (Ma)	PERIOD
Diabase Dikes (McHone, 1978)	158 ± 6 191 ± 10	Jurassic
Pseudotahcyllite From the Great Common Fault Zone (Boeckeler, 1994)	298 ± 31	Carboniferous - Permian
Exeter Pluton (Lyons, et al., 1997)	406 ± 1	Devonian
Breakfast Hill Granite (Bowring, S., unpublished)	407 (?)	Devonian
Newburyport Complex (Lyons, et al., 1997)	418 ± 1	Late Silurian

Table 7.1 - Summary of radiometric ages in the seacoast region of New Hampshire.

The mechanisms of transpression in ductile rocks include the displacement of rocks situated at a deeper depth towards a shallower

level in the crust (Fossen and Tikoff, 1998). It is possible that similar mechanisms contributed to the generation and emplacement of migmatites in Rye Complex rocks.

Later, the strike slip component of the transpressional regime foliated the RC, faulted rocks along the Great Common Fault Zone, and produced the second ductile deformation in the Portsmouth Fault Zone. In the Merrimack Group block, shear zones were then developed (e.g. Nannie Island and Calef) due to progressive transpression (fig. 11c).

The development of faults in the MG and RC is related to the Norumbega Fault System, (Bothner and Hussey, 1999), and the earliest reported age of deformation in the Norumbega Fault Zone occurred ca. 380 Ma (West, 1999). At this stage, the main folding event in the seacoast region was completed.

According to Bradley et al. (2000), the deformation front of the Acadian Orogeny migrated from southeast to northwest (Late Silurian to Middle Devonian). At that time, the emplacement of the Newburyport Complex occurred (418 ± 1 Ma; Lyons, et al., 1997) followed by the emplacement of the Breakfast Hill (about 407 Ma; Bowring, unpublished data), and the intrusion of the Exeter Pluton (406 ± 1 Ma Lyons, et al., 1997).

A later brittle deformation event imprinted the already existing fault zones ca. 298 ± 31 Ma (Boeckeler, 1994). Such deformation involved sudden displacements of rocks, in order to generate pseudotachyllite veining (Swanson, 1988). Among others, Passchier and Trouw (1996) attribute the generation of pseudotachyllite to local melting along a brittle fault plane. It is likely that such brittle deformation might be associated with right lateral displacements along the northeast trending normal faults and included the east-west trending "Exeter Fault" to integrate a Riedel shear system, discussed in a

previous section. This extensional faulting may represent a period of relaxation in the crust.

The results of this study are consistent with recent proposals that middle to late Paleozoic tectonism in New England is better treated as a "punctuated continuum" than discrete orogenic events (Robinson, et al., 1998; Bradley et al., 2000; and Robinson, 2003). The latest tectonic event recorded by the Merrimack Group and the Rye Complex is the Mesozoic emplacement of mafic dikes crosscutting all the structures. The extension of the crust at this time is related to the opening of the Atlantic Ocean (McHone, 1978).

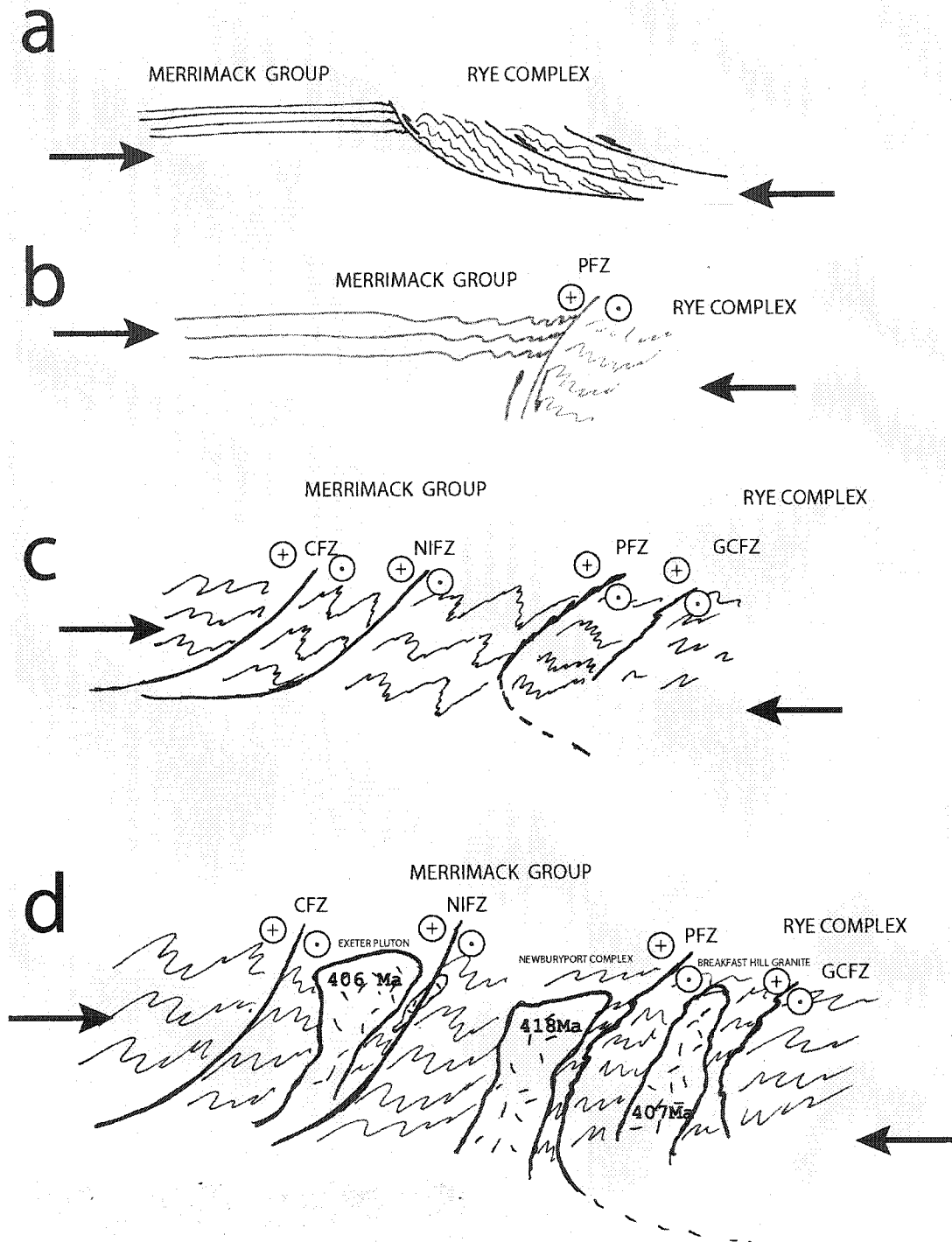


Figure 7.11 - Schematic representation of the tectonic evolution of the seacoast region of New Hampshire for the interval <420 to >300 Ma. CFZ, Calef Fault Zone; NIFZ, Nannie island Fault Zone; PFZ, Portsmouth Fault Zone; GCFZ, Great Common Fault Zone. Arrows represent the compressional component of the transpressional regime and the circles the shear component (away from the observer, circles with a cross; towards the observer, circles with a dot).

REFERENCES CITED

- Aleinikoff, J. N., and Walter, M., 1995, U Pb Ages of Zircon, Monazite, and Sphene from rocks of the Massabesic Gneiss Complex and Berwick Formation, New Hampshire and Massachusetts: Geological Society of America Abstracts with Programs, Northeastern Section, 27 (1), p.26.
- Allard, S. T., 1998, Metamorphic Petrology, and Bedrock Geology of the Berwick Formation within the Mt. Pawtuckaway 7.5 Minute Quadrangle; Raymond and Nottingham, NH: unpublished M. S. Thesis. University of New Hampshire, 125 p.
- Allard, S.T., Laird, J. and Bothner, W.A., 1998, Geothermobarometry of the pelitic members of the Upper Berwick Fm. near the Flint Hill Fault Zone, Raymond NH: Geological Society of America Abstracts with Programs, Northeast Section, Vol. 30, p.1.
- Bates, R. L., and Jackson, J. A., 1984, Dictionary of Geological Terms. Third Edition, Prepared under the direction of the American Geological Institute. Anchor Books. Doubleday, New York.
- Birch, F., 1966, Compressibility; Elastic Constants, Section 7; in Clark, S. P., Jr. editor, Handbook of Physical Constants Revised Edition, Geological society of America, Memoir 97, p. 97-173.
- Blenkinsop, T. G., 2000, Deformation Microstructures and Mechanisms in Minerals and Rocks, Kluwer Academic Publishers, 150 p.
- Boeckeler, A. J., 1994, Isotopic ages of pseudotachylite veins from coastal New Hampshire and SW Maine, evidence for post Acadian strike slip motion: Geological Society of America Abstracts with Programs, Vol. 26, p.7.
- Bothner, W. A., 1974, Gravity Study of the Exeter Pluton, Southeastern New Hampshire: Geological Society of America Bulletin, 85, p. 51-56.
- Bothner, W. A., Boudette, E. L., Fagan, T. J., Gaudette, H. E., Laird, Jo, and Olzewski, W. J., 1984, Geologic framework of the Massabesic anticlinorium and the Merrimack trough, southeastern New Hampshire: in Hanson L., ed., New England Intercollegiate Geological Conference Guidebook, p. 186-206.
- Bothner, W. A., Gaudette, H. E., Fargo, T. G., Bowring, S. A., and Isachsen, C. E. 1993, Zircon and sphene U/Pb ages of the Exeter pluton, constraints on the Merrimack Group and part of the Avalon composite terrane: Geological Society of America Abstracts with Programs, Vol. 25, p. 485.

- Bothner, W. A. and Hussey, A. M., II, 1999, Norumbega connections; Casco Bay, Maine, to Massachusetts? Ludman, A., and West, D. P., Jr. eds., Norumbega Fault System of the Northern Appalachians: Geological Society of America Special Paper No. 331, p.59-72.
- Bouma, A. H., 1963, Sedimentary facies model of turbidites: Bulletin of the American Association of Petroleum Geologists, Vol. 47, No. 2, p. 351.
- Bradley, D. C., Tucker, R. D., Lux, D. R., Harris, A. G., and McGregor, D. C., 2000, Migration of the Acadian Orogen and foreland basin across the Northern Appalachians of Maine and adjacent areas: U. S. Geological Survey Professional Paper 1624, 55 p.
- Bucher, K., and Frey, M., 1994, Petrogenesis of Metamorphic Rocks, 6th edition, Complete Revision of Winkler's Textbook. Springer Verlag, 318 p.
- Billings, M. P., 1956, The Geology of New Hampshire; Part 2, Bedrock Geology, New Hampshire State Planning and Development Commission. Concord, N. H., 203 p.
- Boeckeler, A. J., 1994, Isotopic ages of pseudotachylite veins from coastal New Hampshire and SW Maine, evidence for post Acadian strike slip motion: Geological Society of America Abstracts with Programs, Vol. 26, p.7.
- Carrigan, J. A., 1984, Geology of the Rye Formation, New Castle Island and adjacent areas of Portsmouth Harbor, New Hampshire and Maine: M. S. Thesis, University of New Hampshire, Durham, 128 p.
- Chandrupatla, T. R. and Belegundu, A. D., 1977, Introduction to Finite Elements in Engineering, 2nd edition. Prentice Hall, Englewoods Cliffs, NJ.
- Davis, G. H., Bump, A. P., Garcia, P. E., Ahlgren, S. G., 1999, Conjugate Riedel deformation band shear zones: Journal of Structural Geology, Vol. 22, p. 169-190.
- Donath, F. A. and Parker, R. B., 1964, Folds and Folding: Geological Society of America Bulletin, Vol. 75, p. 45-62.
- Dunlap, W. J., Hirth, G., and Teyssier, C., 1997, Thermomechanical evolution of a ductile duplex: Tectonophysics, Vol. 16, p. 983-1000.
- Escamilla Casas, J. C., 2001, Geology of the Exeter and Hampton 7 12" quadrangles, SE New Hampshire: Geological Society of America Abstracts with Programs, Vol. 33, p.30.
- Escamilla Casas, J. C., 2002, Style and Timing of folds in Seacoast New Hampshire, An Application of Fourier Series analysis, Geological Society of America Abstracts with Programs, Vol. 34, p. 28.
- Fargo, T. R., and Bothner W. A., 1995, Polydeformation in the Merrimack Group, southeastern New Hampshire and southwestern Maine: in Hussey, A. M. II; and Johnston, R. A., eds., Guidebook of field

- trips in southern Maine and adjacent New Hampshire, New England Intercollegiate Geological conference Guidebook, p. 15-28.
- Ferguson, E. W., Clark, S. F., Jr., Picard, M. Z., and Moore, R. B., 1997, Lineament Map of Area 3 of the New Hampshire Bedrock Aquifer Assessment, Eastern New Hampshire: U. S. Geological Survey Open File Report 97-762.
- Fossen H. and Tikoff, B., 1998, Extended models of transpression and transtension, and application to tectonic settings: in, Holdsworth, R. E., Stratchan, R. A., and Dewey, J. F., eds., Continental transpressional and transtensional tectonics, Geological Society of London Special Publication, 135, pp. 15-33.
- Freedman, J., 1950, Stratigraphy and structure of the Mt. Pawtuckaway quadrangle, southeastern New Hampshire: Geological Society of America Bulletin, 61, p. 449-492.
- Gosh, S. K. and Ramberg, H., 1976, Reorientation of Inclusions by Combination of Pure Shear and Simple Shear: Tectonophysics, Vol. 34, p. 1-70.
- GRANIT Complex Systems Research Center, Institute for the Study of Earth, Oceans, and Space, University of New Hampshire.
- Greenberg, M. D., 1978 Foundations of Applied Mathematics: Prentice Hall, p. 80-130.
- Hirth, G., and Tullis, J., 1992, Dislocation creep regimes in quartz aggregates: Journal of Structural Geology, Vol. 14, p. 145-159.
- Holcombe, Rod, 2001, Computer program GEORient V.9.0. Department of Earth Sciences, The University of Queensland, Australia.
- Hudleston, P. J., 1972, Fold morphology and some geometrical implications of theories of fold development: Tectonophysics, Vol. 16, p. 1-46.
- Hudleston, P. J. and Lan Labao, 1993, Information from fold shapes: Journal of Structural Geology, Vol. 15, p. 253-264.
- Hussey, A. M., II, 1968, Stratigraphy and structure of southwestern Maine: in Zen E an, White, W. S., Hadley, J. B., and Thompson, J. B., ed., Studies in Appalachian Geology Northern and Maritime: Interscience, NY, p.291-301.
- Hussey, A. M., II, 1980, The Rye Formation of Gerrish Island, Kittery, Maine, a reinterpretation: The Maine Geologist, Vol. 7, p. 2-3.
- Hussey, A. M., II, 1985, The bedrock geology of Bath and Portland 2 degree map sheets, Maine: Maine Geological Survey, Open File Report No. 85-87, 82 p.
- Hussey, A. M., II, and Bothner, W. A., 1993, Geology of the coastal lithotectonic belt, SW Maine and SE New Hampshire: in Cheney, J. T. and Hepburn, J C., eds., Field Trip Guidebook for the

- Northeastern United States, Boston: Geological Society of America. Vol. 1, p. K1-K19.
- Jasiul, I., 1995, Cavities vis à vis Rigid Inclusions, Elastic Moduli of Materials With Polygonal Inclusions: International Journal of Structures, Vol. 32, p. 407-422.
- Katz, F. J., 1917, Stratigraphy in southwestern Maine and southern New Hampshire: U. S. Geological Survey Professional Paper 108, p.165-177.
- Keppie, D., 1985, The Appalachian Collage: in Gee, D. G., and Sturt, B. A., eds., The Caledonide Orogen, Part 2, Scandinavia and Related Areas, Chichester, United Kingdom, John Wiley & Sons, p. 1217-1226.
- Keppie, D., 1989, Northern Appalachian Terranes and Their Accretionary History: in Dallmeyer, R. D., ed., Terranes in the Circum Atlantic Paleozoic Orogens, Geological Society of America Special Paper, p. 159-192.
- Laird, J., 1988, Chlorites, Metamorphic Petrology: Rev. Mineral. Vol. 19, p. 405-454.
- Loveless, J. P., and Schulz, J. E., 2002, Mapping the Merrimack Group in the Epping 7.5 minute quadrangle, new findings: Geological Society of America Abstracts with Programs, Vol. 34, p. A30.
- Lyons, J. B., Jr., and Bothner, W. A., 1989, A Transect Through New England Appalachians, American Geophysical Union, 28th International Geological Congress, Field Trip Guidebook, T162, 163 p.
- Lyons, J. B., Bothner, W. A., Moench, R. H. and Thompson, J. B., Jr., 1997, Bedrock geologic map of New Hampshire: US Geological Survey map, scale 1:250,000.
- Ludman, A., and West, D. P., 1999, Norumbega Fault System of the Northern Appalachians: Geological Society of America Special Paper, 202 p.
- Mandal, N., Chakraborty, Ch., Chandan, S. K., 2000, Boudinage in multilayered rocks under layer normal compression, a theoretical analysis: Journal of Structural Geology, Vol.22, p. 373-382.
- Mathematica® 4 For Students, Copyright 1998-1999, Version 4.0.1.0.: Wolfram Research, Inc.
- MATLAB6 Student Version, Copyright 1984-2001, Release 12: The MathWorks, Inc.
- McHone, J. G., 1978, Distribution, orientations, and ages of mafic dikes in central New England: Geological Society of America Bulletin, 89, p.1645-1655.

- Novotny, R. F., 1963, Bedrock geology of the Dover-Exeter-Portsmouth region, New Hampshire, Ph.D. unpublished Dissertation. The Ohio State University, Columbus, 181p.
- Novotny, R. F., 1969, The geology of the seacoast region, New Hampshire, New Hampshire Department of Resources and Economic Development, Concord, NH, 46 p.
- Passchier, C. W., and Simpson, C., 1986, Porphyroclast systems as kinematics indicators: *Journal of Structural Geology*, Vol. 8, p. 831-843.
- Passchier, C. W., 1988, Flow Path Analysis in Shear Zones: *Geology Rundschau*, Vol. 71, p. 309-318.
- Passchier, C. W., and Trouw, R. A. J., 1998, *Micro-tectonics*: Springer. 289 p.
- Poirier, J. P., 1985, *Creep of Crystals*: Cambridge University Press, Cambridge, 260 p.
- Ramsay, J. G., 1967, *Folding and Fracturing of Rocks*: McGraw Hill, New York, p. 193-226.
- Ramsay, J. G., and Huber M. I., 1987, *The Techniques of Modern Structural Geology*, Vol. 2, *Folds and Fractures*: Academic Press, p. 309-332.
- Ramsay, J. G. and Lisle R., 2000, *The Techniques of Modern Structural Geology*, Vol. 3, *Applications of Continuum Mechanics in Structural Geology*: Academic Press, p. 737-783.
- Rickerich, S. F., 1983, Sedimentology, stratigraphy, and structure of the Kittery Formation in the Portsmouth, New Hampshire region: M. S. Thesis, University of New Hampshire, 115 p.
- Rickerich, S. F., 1984, Sedimentology and stratigraphy of the Kittery formation near Portsmouth, New Hampshire, *Geological Society of America - Abstracts with Programs*, Vol. 16, No.1, p. 59.
- Robinson, P., Tucker, R. D., Bradley, D., and Berry, H. I VOL., 1998, Paleozoic orogens in New England, USA: *GFF*, Vol. 120, p. 119-148.
- Robinson, P., 2003, Tectonic stratigraphic metamorphic perspective of the New England Caledonides, west central Massachusetts: in Brady, J. B. and Cheney, J. T. eds., *Guidebook*. New England Intercollegiate Geological Conference, p. A1-A54.
- Simpson, C., 1986, Movement Sense Determination in Sheared Rocks: *Journal of Geological Education*, 34, p. 246-261.
- Simpson, C., and Schmidt, S. M., 1983, An evaluation of criteria to determine the sense of movement in sheared rocks: *Geological Society of America Bulletin*, Vol. 94, p.1281-1288.

- Siramadas, A., 1966, The geology of the Manchester quadrangle, New Hampshire: New Hampshire Department of Economic Development, Bulletin 2, Concord, NH, 78 p.
- Spear F. S., 2003, Metamorphic Phase Equilibria and Pressure Temperature Time Paths: Mineralogical Society of America, Monograph 1, 799 p.
- Spjeldnaes, N., 1967, Acanthodians from the Siluro-Devonian of Ellesmere Island: in International Symposium on the Devonian System, Calgary, Vol. 2, p.807-813.
- Stabler, C. L., 1968, Simplified Fourier analysis of fold shapes: Tectonophysics, Vol. 6, p. 343-350.
- Stallard, A., and Hickey, K., 2001, Fold mechanisms in the Canton schist, constraints on the contribution of flexural flow: Journal of Structural Geology, 23, p. 1865-1881.
- Stewart, D. B., and Wones, D. R., 1974, Bedrock Geology of the Northern Penobscot Bay Area: in Osberg, P. H., ed., Geology of East Central and Northern Central Maine, New England Intercollegiate Geological Conference Guidebook, 66th meeting, p. 223-239.
- Swanson, M. T., 1988. Pseudotachyllite bearing strike slip duplex structures in the Fort Foster brittle zone, S. Maine: Journal of Structural Geology, Vol. 10, p. 813-828.
- Swanson, M. T., 1992. Structural sequence and tectonic significance of Mesozoic dikes in southern coastal Maine: in Puffer, J. H., and Ragland, P. C. eds., Eastern North American Mesozoic Magmatism, Geological Society of America Special Paper 268, p. 37-62.
- Swanson, M. T., and Carrigan, J. A., 1984, Ductile and brittle structures within the Rye Formation of southern coastal Maine and New Hampshire: in Hanson, L. S. ed., New England Intercollegiate Geologic Conference Guidebook for 1984, p. 165-185.
- Schulz, J. E. and Loveless, J. P., 2001, Implications of the Calef Member of the Eliot Formation, Epping Quadrangle, southeast New Hampshire: Geological Society of America Abstracts with Programs, Vol. 33, p.
- Stipp, M., Stünitz, H., Heilbronner, R., and Schmid, S. M., 2002, The eastern Tonale fault zone, a "natural laboratory" for crystal plastic deformation of quartz over a temperature range from 250° 700° C: Journal of Structural Geology, Vol. 24, p. 1861-1884.
- Thiessen, R. L., and Means, W. D., 1980, Classification of fold interference patterns, a reexamination: Journal of Structural Geology, Vol. 2, p. 311-316.
- Thompson, J. B. Jr., 1957, The Graphical Analysis of Mineral Assemblages in Pelitic Schists: American Mineralogist, Vol. 42, p. 842-858.

- Tsukrov, I., and Novak, J., 2002, Effective elastic properties of solids defects of irregular shapes: *International Journal of Solids and Structures*, Vol. 39, p. 1539-1555.
- Urai, J. L., Means, W. D., Lister, G. S., 1986, Dynamic Recrystallization of Minerals: in Hobbs, B. E. Heard, H. C., eds., *Mineral and Rock Deformation, Laboratory Studies. Geophysical Monograph 36*, p. 161-199.
- Van der Pluijm, B. A., Johnson, R. J. E., and Van der Voo, R., 1993, Paleogeography, Accretionary History, and Tectonic Scenario, A Working Hypothesis for the Ordovician and Silurian Evolution of the Northern Appalachians: *Geological Society of America Special Paper 275*, p. 27-40.
- Walker, R. G., 1993. Turbidites and submarine fans: in Walker, R. G. and James, N. P., eds., *Facies Models Response to Sea Level Change, GeoText 1*, Geological Association of Canada, p. 125-132.
- Welch, P., 1993, Petrology and Fabric Analysis Across the Great Common Fault Zone (GCFZ) Within the Rye Formation, New Castle, New Hampshire: *Geological Society of America Abstracts with Programs*, Vol. 25, p. 265.
- Willard, G. D., 2000, Bedrock Geology and Ground Magnetic Study of Adams Point, Durham, NH: M. S. Thesis, University of New Hampshire, Durham, 2000, 111 p.
- Williams, H., and Hatcher, R. D., Jr., 1983, Appalachian Suspect Terranes: in Hatcher, R. D., Jr., Williams, H., and Zietz, I., eds., *Contributions to the Tectonics and Geophysics of Mountain Chains*, Geological Society of America Memoir 158, p. 33-53.
- White, S., 1976, The Effects of Strain of the Microstructures, Fabrics, and Deformation Mechanisms in Quartz: *Philosophical Transactions of the Royal Society of London*, A 283, p. 69-86.
- White, S., 1979, Grain and Sub Grain Size Variations Across a Mylonite Zone: *Contributions to Mineralogy and Petrology*, Vol. 70, p. 193-202.
- Whitmeyer, S. J., Allen, R. and Allard, S., 1999, Estimating mode by powder X Ray diffraction; an analysis of granitic sills in southern New Hampshire: *Geological Society of America Abstracts with Programs*, Vol. 31, p.79.
- Yardley, B. W. D., 1989, *An Introduction to Metamorphic Petrology*: Longman, Harlow, England, 248 p.
- Zartman, R. E., and Naylor, R. S., 1984, Structural implications of some radiometric ages of igneous rocks in southeastern New England: *Geological Society of America Bulletin*, 95, p.522-539.

APPENDIX 1

Derivation of Formulas and Program in BASIC

DERIVATION OF FORMULAS

A Fourier series is the summation of an infinite number of harmonics of sine and cosine waves of decreasing amplitudes which maybe used to describe any periodical repeating shape, from a series of circular arcs to a saw tooth. Represented mathematically the series is:

$$f(x,y) = a_0 + a_1\sin\theta + b_1\cos\theta + a_2\sin2\theta + b_2\cos2\theta + \dots + a_n\sin(n\theta) + b_n\cos(n\theta)$$

Where a_0 = constant of position

$a_1, a_2, \text{ etc.},$ and $b_1, b_2, b_3, \text{ etc.},$ are amplitudes and $\theta = 2\pi x/\lambda$ in which λ is the wavelength and x is a distance.

Applied to folded surfaces, for the quarter wavelength unit of a symmetrical anticline placed with its inflection point at the origin of the curve, all cosine terms, even numbered sine terms, and the constant, are zero. Thus, the simplified series:

$$f(x,y) = a_1\sin\theta + a_3\sin3\theta + \dots + a_{2n-1}\sin(2n-1)\theta$$

This series represents a general curve, which will describe any shape between a point of zero curvature (inflection point), and a point of maximum curvature (hinge point). This general curve constitutes the basis for the analysis of geological folded surfaces.

Three distances $D_1, D_2,$ and D_3 were measured at 30° intervals and multiplied by $D_n(\pi/2W)$ to obtain:

$$Y_n = D_n\pi/2W$$

and used to form three simultaneous equations from the first three terms of the series in equation (2). The simultaneous equations are:

$$Y_1 = a_1 \sin 30^\circ + a_3 \sin 90^\circ + a_5 \sin 150^\circ \quad (1a)$$

$$Y_2 = a_1 \sin 60^\circ + a_3 \sin 180^\circ + a_5 \sin 300^\circ \quad (2a)$$

$$Y_3 = a_1 \sin 90^\circ + a_3 \sin 270^\circ + a_5 \sin 90^\circ \quad (3a)$$

Solving for a_1 , a_2 , and a_5 :

Solving for a_3

From equation (1a):

$$Y_1 = 0.5 a_1 + a_3 + 0.5 a_5$$

From equation (3a):

$$a_1 = Y_3 + a_3 - a_5$$

$$Y_1 = 0.5(Y_3 + a_3 - a_5) + a_3 = 0.5 a_5$$

$$Y_1 = 0.5 Y_3 + 0.5 a_3 - 0.5 a_5 + a_3 + 0.5 a_5$$

$$Y_1 = 0.5 Y_3 + 0.5 a_3 + a_3$$

$$Y_1 = 0.5 Y_3 + 3/2 a_3$$

$$3/2 a_3 = Y_1 - 0.5 Y_3$$

$$a_3 = 2/3 (Y_1 - 0.5 Y_3)$$

$$a_3 = \frac{2Y_1 - Y_3}{3} \quad (4a)$$

solving for a_5 :

From equation (2a)

$$Y_2 = a_1 \sin 60^\circ - a_5 \sin 60^\circ$$

$$a_1 = \frac{Y_2 + a_5 \sin 60^\circ}{\sin 60^\circ} \quad (5a)$$

From equation (3a)

$$Y_3 = a_1 - a_3 + a_5$$

$$a_1 = Y_3 + a_3 - a_5$$

From equation (4a) and substituting for (a3):

$$a_1 = Y_3 + \frac{2Y_1 - Y_3}{3} - a_5$$

$$a_1 = Y_3 + \frac{2Y_1}{3} - \frac{Y_3}{3} - a_5$$

Making this equation equal to (5a):

$$a_1 = \frac{Y_2 + a_5 \sin 60^\circ}{\sin 60^\circ} = Y_3 + \frac{2Y_1}{3} - \frac{Y_3}{3} - a_5$$

$$a_5 = \frac{Y_3 + Y_1}{3} - \frac{Y_2}{2 \sin 60} \quad (6a)$$

Solving for a1

From equation (5a)

$$a_1 = \frac{y_2 + a_5 \sin 60^\circ}{\sin 60^\circ}$$

$$a_1 = \frac{y_2}{\sin 60^\circ} + a_5$$

Substituting a5

$$a_1 = \frac{y_2}{\sin 60^\circ} + \frac{y_3 + y_1}{3} - \frac{y_2}{2 \sin 60^\circ}$$

$$a_1 = \frac{y_3 + y_1}{3} + \frac{y_2}{2 \sin 60^\circ} \quad (7a)$$

```

'FOURIER.BAS - PROGRAM IN BASIC

'Jose C. Escamilla-Casas. Fall 2000

DEFDBL A-Z

CLS

PRINT "ENTER OUTPUT DEVICE"

PRINT "(Console, Printer, File)"

DO

  DO

    outdev$ = INKEY$

  LOOP UNTIL LEN(outdev$)

  outdev$ = UCASE$(outdev$)

LOOP UNTIL outdev$ = "F" OR outdev$ = "C" OR outdev$ = "P"

SELECT CASE outdev$

  CASE "C"

    dev$ = "con"

  CASE "P"

    dev$ = "lpt1"

  CASE "F"

    INPUT "File Name: "; filsp$

    dev$ = filsp$

CASE ELSE

END SELECT

OPEN dev$ FOR APPEND AS #2

10

```

```

1 = 1

INPUT "Fourier Data File Name: "; fil$

OPEN fil$ FOR INPUT AS #1

INPUT #1, d$

IF NOT d$ = "FOURIER" THEN

PRINT " Incorrect File Format"

GOTO 10

END IF

CLS

PRINT #2, "File Name:"

PRINT #2, UCASE$(fil$)

PRINT #2, "-----"
-----"

PRINT #2, "Surf. No.      a      b      d      A1      A2      Dsze      Dshp
DA      b3/b1      b3/b1"

PRINT #2, "-----"
-----"

DO WHILE NOT EOF(1)

INPUT #1, snoa$, d1, d2, d3, wa

YA1 = (d1 * 3.142857) / (2 * wa)
YA2 = (d2 * 3.142857) / (2 * wa)
YA3 = (d3 * 3.142857) / (2 * wa)
b1a = ((YA3 + YA1) / 3) + (YA2 / .57735)
b3a = ((2 * YA1) - YA3) / 3
b5a = ((YA3 + YA1) / 3) - (YA2 / (2 * .8660254037#))

INPUT #1, snob$: IF EOF(1) THEN EXIT DO

INPUT #1, d1, d2, d3, wb

YA1 = (d1 * 3.142857) / (2 * wb)

```

```

YA2 = (d2 * 3.142857) / (2 * wb)
YA3 = (d3 * 3.142857) / (2 * wb)
b1b = ((YA3 + YA1) / 3) + (YA2 / .57735)
b3b = ((2 * YA1) - YA3) / 3
b5b = ((YA3 + YA1) / 3) - (YA2 / (2 * .8660254037#))
a = SQR((b1a * b1a) + (b3a * b3a) + (b5a * b5a))
B = SQR((b1b * b1b) + (b3b * b3b) + (b5b * b5b))
d1 = (b1a - b1b) ^ 2
d2 = (b3a - b3b) ^ 2
d3 = (b5a - b5b) ^ 2
d = SQR(d1 + d2 + d3)
Dsize = ABS((d / a) - (d / B))
IF SGN(b3a) = 1 THEN
alpha1 = 57.29578 * (ATN(b1a / ABS(b3a)))
ELSEIF SGN(b3a) = 0 THEN
alpha1 = 90
ELSE
alpha1 = 90 + (57.29578 * ATN((ABS(b3a)) / b1a))
END IF
IF SGN(b3b) = 1 THEN
alpha2 = 57.29578 * (ATN(b1b / ABS(b3b)))
ELSEIF SGN(b3b) = 0 THEN
alpha2 = 90
ELSE
alpha2 = 90 + (57.29578 * ATN((ABS(b3b)) / b1b))
END IF
IF SGN(b3a) = 1 THEN
beta1 = 57.29578 * (ATN(b5a / ABS(b3a)))
ELSEIF SGN(b3a) = 0 THEN

```

```

beta1 = 90
ELSE
beta1 = 90 + (57.29578 * ATN((ABS(b3a)) / b5a))
END IF

IF SGN(b3b) = 1 THEN
beta2 = 57.29578 * (ATN(b5b / ABS(b3b)))
ELSEIF SGN(b3b) = 0 THEN
beta2 = 90
ELSE
beta2 = 90 + (57.29578 * ATN((ABS(b3b)) / b5b))
END IF

IF SGN(b1a) = 1 THEN
gamma1 = 57.29578 * (ATN(b5a / ABS(b1a)))
ELSEIF SGN(b1a) = 0 THEN
gamma1 = 90
ELSE
gamma1 = 90 + (57.29578 * ATN((ABS(b1a)) / b5a))
END IF

IF SGN(b1b) = 1 THEN
gamma2 = 57.29578 * (ATN(b5b / ABS(b1b)))
ELSEIF SGN(b1b) = 0 THEN
gamma2 = 90
ELSE
gamma2 = 90 + (57.29578 * ATN((ABS(b1b)) / b5b))
END IF

shape = ABS(alpha1 - alpha2) + ABS(beta1 - beta2) + ABS(gamma1 -
gamma2)

dshape = shape / 3
DA = dshape + Dsize

```

```
j = b3a / b1a
k = b3b / b1b

PRINT #2, snoa$; "-"; snob$;

PRINT #2, USING "####.##"; a; B; d; alpha1; alpha2; Dsize; dshape; DA;
j; k

PRINT #2, "b5a="; b5a; "b3a="; b3a; "b1a="; b1a
PRINT #2, "b5b="; b5b; "b3b="; b3b; "b1b="; b1b

LOOP

CLOSE

END
```

APPENDIX II

Anticlastic Bending

ANTICLASTIC BENDING

The definition of curvature at a point on a curve is as the rate of change at that point of the slope angle with respect to the distance along the curve (fig. A2-1):

$$\text{Curvature} = k = \frac{d\theta}{ds} = \lim_{ds \rightarrow 0} \frac{d\theta}{ds} = \frac{1}{O'D} = \frac{1}{OC} \quad (1)$$

The radius of curvature at point c is the reciprocal of the curvature:

$$\rho = \frac{1}{k} \text{ (Length)} \quad (2)$$

From fig. A2-2 $\Delta\theta$ is the angle between the normals to the neutral surface passing through points $P_1 R_1$ and $Q_1 S_1$, and where Δs is equal to RS.

$$R_1 S_1 = \rho \Delta\theta = RS = \Delta s \quad (3)$$

PQ experiences a change in length as:

$$P_1 Q_1 = (\rho - y)\Delta\theta \text{ (Assuming no deformation along the "y" direction).}$$

The axial strain ϵ_x of the element PQ, that is, the length divided by the original length, is:

$$\epsilon_x = \frac{P_1 Q_1 - PQ}{PQ} = \text{extension} \quad (4)$$

If $P_1 Q_1 = (\rho - y)\Delta\theta$ and $PQ = \Delta s$, then by substituting:

$$\epsilon_x = \frac{(\rho - y)\Delta\theta - \Delta s}{\Delta s} \quad (5)$$

$$\epsilon_x = \frac{\rho\Delta\theta}{\Delta s} - \frac{y\Delta\theta}{\Delta s} - \frac{\Delta s}{\Delta s} \quad (6)$$

$$\text{As } \rho \Delta\theta = \Delta s \quad (7)$$

$$\epsilon_x = \frac{\Delta s}{\Delta s} - \frac{y\Delta\theta}{\Delta s} - \frac{\Delta s}{\Delta s} = - \frac{y\Delta\theta}{\Delta s} \quad (8)$$

By shrinking ΔS to zero and $k = \frac{1}{\rho} = \frac{d\theta}{ds}$ the extension becomes:

$$\epsilon_x = -\frac{y\Delta\theta}{\Delta s} = -\frac{y}{\rho} \quad (9)$$

Here ρ is the radius of curvature of the neutral axis of the bent layer. The theory of solid mechanics establishes the relation of the normal longitudinal strain and its relation to normal strains in the transverse directions as follows:

$$\epsilon_y = -\nu\epsilon_x \quad (10)$$

$$\epsilon_x = -\nu\epsilon_y \quad (11)$$

The Poisson's ratio is ν . Now, from equation (9), the associated transverse strains are:

$$\epsilon_y = \frac{\nu y}{\rho}$$

$$\epsilon_x = \frac{\nu x}{\rho}$$

The resulting geometry under these conditions generates the anticlastic bending (fig. a2-3).

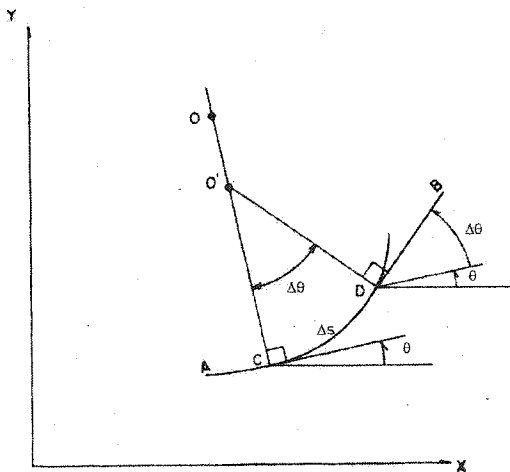


Figure a2-1 - Geometrical representation of the radius of curvature of a plane curve at an arbitrary point "c".

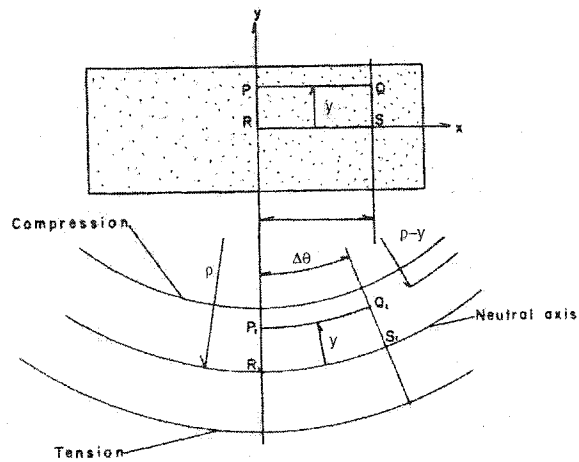


Figure a2-2 - Graphic representation of a rectangular section of a rock as it bends.

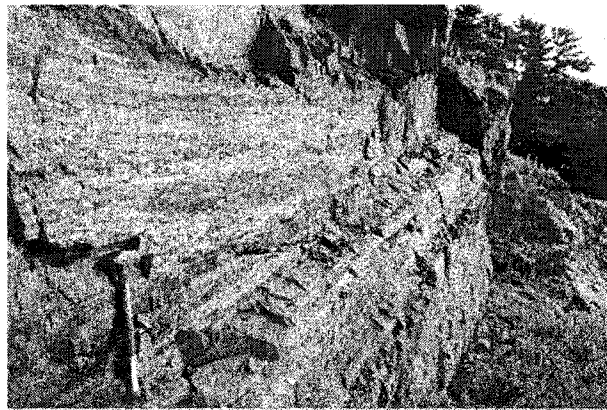
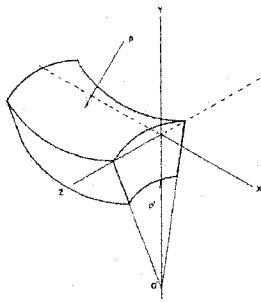


Figure a2-3 - The anticlastic bending represented graphically (left). The same effect as it occurs in naturally deformed rocks (right).

APPENDIX III

Strain Analysis of Cleavages in Folds

Appendix 3

This strain analysis demonstrates that two different folding mechanisms may produce similar types of folds. In both fold-cases, the shape and degree of asymmetry is similar, but the resulting cleavage is different (fig. 17).

The mathematical expression that represents an ideal chevron fold is (Huddleston, 1972):

$$y = 1.25 \sin(x) - .14 \sin(3x) + .05 \sin(5x) \quad (1)$$

Fig. 16 shows ideal chevron folds. The first set of folds, in the upper drawing, is the product of a heterogeneous shearing mechanism that follows a sinusoidal pattern; the second set of folds is the result of heterogeneous shear with a sinusoidal pattern plus homogeneous plain strain. Mathematically, the ellipticity relates the expressions that define the shapes in each case. For this demonstration, the ellipticity is 4 and the relation is, for the second set of folds:

$$n = \sqrt{R}; R = \text{ellipticity} = 4; n = 2 \quad (2)$$

By substituting "n" in the formula of an ideal chevron fold of equation 1, it spans a set of expressions that define folds with the same wavelength, amplitude, degree of asymmetry, and shape. Depending on the value of "R", and consequently on "n" ($n = R^{1/2}$; R = ellipticity) a general formula results as:

$$x' = x / n \quad (3)$$

$$y' = 1.27 \sin(x / n) - .14 \sin(3x / n) + .05 \sin(5x / n) + ny \quad (4)$$

The mathematical expressions that define the upper and lower set of folds are, respectively:

$$y' = 1.27 \sin(x) - .14 \sin(3x) + .05 \sin(5x) + y \quad (5)$$

$$y' = 1.27 \sin(x / 2) - .14 \sin(3x / 2) + .05 \sin(5x / 2) + 2y \quad (6)$$

Following the Lagrange transformation, the displacement equations for each fold-case are:

For the first set of folds:

$$x' = x \quad (7)$$

$$y' = 1.27 \sin(x) - .14 \sin(3x) + .05 \sin(5x) + y \quad (8)$$

For the second set of folds:

$$x' = x / 2 \quad (9)$$

$$y' = 1.27 \sin(x / 2) - .14 \sin(3x / 2) + .05 \sin(5x / 2) + 2y \quad (10)$$

Ramsay (1983) defined the displacement gradient matrix as:

$$M \begin{vmatrix} a & b \\ c & d \end{vmatrix} = \begin{vmatrix} \frac{\partial u}{\partial x} & \frac{\partial u}{\partial y} \\ \frac{\partial v}{\partial x} & \frac{\partial v}{\partial y} \end{vmatrix} \quad (11)$$

Equating $u = x'$ and $v = y'$, M is calculated. The coordinates (x', y') define the new set of coordinates where a point (x, y) moved after the deformation occurred. For the first and second fold-cases the gradient displacement matrices are:

For the first fold-case:

$$M \begin{vmatrix} \frac{\partial u}{\partial x} & \frac{\partial u}{\partial y} \\ \frac{\partial v}{\partial x} & \frac{\partial v}{\partial y} \end{vmatrix} = \begin{vmatrix} 1 & 0 \\ 1.27 \cos(x) - .042 \cos(3x) + .25 \cos(5x) & 1 \end{vmatrix} \quad (12)$$

For the second fold-case:

$$M \begin{vmatrix} \frac{\partial u}{\partial x} & \frac{\partial u}{\partial y} \\ \frac{\partial v}{\partial x} & \frac{\partial v}{\partial y} \end{vmatrix} = \begin{vmatrix} 1 / 2 & 0 \\ 0.635 \cos(x) - .021 \cos(3x) + .125 \cos(2.5x) & 2 \end{vmatrix} \quad (13)$$

In both fold-cases, there is no volume change, as a result, the value of the determinant of M in each case, equals to one. According to Ramsay (1983) the first strain invariant is:

$$I_1 = a^2 + b^2 + c^2 + d^2$$

Substituting the value of I_1 accordingly, the principal strains are:

$$\lambda_1 = \frac{1}{2} \left(I_1 + \left(I_1^2 - 4 \right)^{\frac{1}{2}} \right) \quad (14)$$

$$\lambda_2 = \frac{1}{2} \left(I_1 - \left(I_1^2 - 4 \right)^{\frac{1}{2}} \right) \quad (15)$$

These two values are equal to:

$$\lambda_n = \frac{1}{(1 + e^2)} \quad (16)$$

Hence, equation (16) gives the values for the maximum $(1 + e_1)$ and minimum extension $(1 + e_2)$, respectively.

The calculation of the initial direction (θ) , rotation (ω) , and the directions of the principal strains of the strain ellipse after deformation (θ') result from the following equations:

$$\theta' = \arctan \left(\frac{2(ac + bd)}{a^2 + b^2 - c^2 - d^2} \right) \quad (17)$$

$$\omega = \arctan \left(\frac{c - d}{a + d} \right) \quad (18)$$

$$\theta = \omega - \theta' \quad (19)$$

The columns in tables 1 and 2 show the summary of values for the long $(1 + e_1)$ and short axis $(1 + e_2)$ of the ellipse, the ellipticity (R) , the orientation after (θ') and before the deformation (θ) , rotation (ω) , and the first strain invariant (I_1) . The values for the first set of ideal chevron folds reveal the existence of a cleavage that it is strong at the limbs and it weakens as it approximates to the hinge.

The values of the long and short axes of the "ellipse" at the hinge are unity; therefore, there is no concentration of strain in that position of the folds. At the limbs, the angle of the "cleavage" with

respect to "bedding" varies in the order of $5-2^\circ$. In nature, the resultant structures will look as a strong cleavage almost parallel to bedding in the limbs and no cleavage present in the hinges.

The second fold case defines the presence of a cleavage that it is almost parallel to the axial plane of the folds. The angle between the cleavage and the axial plane is about $0 - 6^\circ$. The cleavage does not have the same inclination along the fold profile; it slightly fans along the ordinate axis. In nature, the cleavage will constitute an axial planar cleavage with no significant attenuation parallel to the fold axial plane.

Conclusively, the shape and degree of asymmetry of a set of folds is independent of the deformation mechanisms implied in the folding event. Furthermore, considering these two examples as end members, there is a whole range of possible geometries of the resultant cleavages. The relative orientation of the cleavages with respect to bedding will change depending on the order and the intensity of the folding mechanisms.

X	$1+e_1$	$1+e_2$	R	θ'	θ	ω	I
0	1.691271221	0.591271221	2.8604	-30.5946	-59.405397	28.8108	3.21
15	1.614017631	0.619571918	2.60505	-31.7812	-58.218807	26.4376	2.9889
30	1.534867815	0.651521903	2.35582	-33.0851	-56.914876	23.8298	2.7803
45	1.631257694	0.613023929	2.661	-31.5093	-58.490706	26.9814	3.0368
60	1.751077086	0.571077086	3.06627	-29.7297	-60.270302	30.5406	3.3924
75	1.523534819	0.656368327	2.32116	-33.2796	-56.720373	23.4407	2.752
90	1	1	1	#DIV/0!	#DIV/0!	6.6E-15	2
105	1.523534819	0.656368327	2.32116	33.27963	56.720373	-23.441	2.752
120	1.751077086	0.571077086	3.06627	29.7297	60.270302	-30.541	3.3924
135	1.631257694	0.613023929	2.661	31.50929	58.490706	-26.981	3.0368
150	1.534867815	0.651521903	2.35582	33.08512	56.914876	-23.83	2.7803
165	1.614017631	0.619571918	2.60505	31.78119	58.218807	-26.438	2.9889
180	1.691271221	0.591271221	2.8604	30.5946	59.405397	-28.811	3.21

Table 1 - Values of the orientations of the elements of the strain ellipse that define a strong strain concentration close to the inflection point and decreases towards the maximum curvature.

x	$1+e_1$	$1+e_2$	R	θ'	θ	ω	h
0	2.295704	0.435596	5.270256	-6.25217	-30.0017	23.74949	5.46
15	2.28067	0.438468	5.201456	-6.16365	-29.3238	23.16015	5.39371
30	2.245113	0.445412	5.04053	-5.92567	-27.6173	21.69159	5.238922
45	2.210452	0.452396	4.886097	-5.64763	-25.7892	20.14161	5.090759
60	2.196123	0.455348	4.822958	-5.51672	-24.977	19.46027	5.0303
75	2.211967	0.452086	4.892799	-5.66089	-25.8731	20.21218	5.097181
90	2.25618	0.443227	5.09035	-6.0044	-28.1651	22.16075	5.2868
105	2.310015	0.432898	5.336168	-6.33054	-30.6254	24.29489	5.523568
120	2.336498	0.427991	5.459224	-6.46182	-31.7291	25.26731	5.6424
135	2.298197	0.435124	5.281708	-6.26622	-30.1118	23.84557	5.471041
150	2.189373	0.456752	4.793356	-5.45136	-24.5813	19.12995	5.001978
165	2.059972	0.485443	4.243485	-3.42982	-14.2693	10.83947	4.47914
180	2	0.5	4	-1.8E-15	-7.1E-15	5.31E-15	4.25

Table 2 - the axes of the strain ellipses have no significant change and the orientation remains almost the same, therefore the concentration of strain defines parallel planes.

APPENDIX IV

Results From Finite Element Analysis

LOADCASE: COMPRESSION (6.5e8)

CRYSTAL	DISPLACEMENT				CORNER				RESULTS
	1	2	3	4	1	2	3	4	
1	X .00447018	.00469132	.005989	.00588968	e	1.128031			
	Y -.0324246	-.0247573	-.0263982	-.0341466	s	5.631680646			
2	X .0127374	.0111727	.011806	.013141	e	.645725			
	Y -.0792482	-.0689961	-.0659648	-.0749058	s	17.14117935			
3	X .00673819	.00679736	.00946232	.00921379	e	1.377382			
	Y -.0511262	-.0422821	-.0400569	-.0494974	s	2.437321053			
4	X .00407471	.00436448	.00547271	.00528056	e	.72108			
	Y -.0311483	-.0237722	-.0243871	-.0323771	s	5.136909919			
5	X .00616089	.00678003	.00790874	-.00748396	e	1.154116			
	Y -.0462017	-.0371714	-.0373989	-.0472385	s	7.3655200684			
6	X .0128389	.0138472	.0155861	.0144787	e	.84283			
	Y -.0916637	-.0780788	-.0849883	-.0779521	s	4.92342497			
7	X .0112034	.0112273	.014596	.0139932	e	.869643			
	Y -.083162	-.0680197	-.0672714	-.0851223	s	13.1102717			
8	X .0095022	.0110372	.0113777	.0100482	e	1.015592			
	Y -.0624334	-.055682	-.0644749	-.0704639	s	6.138322893			
9	X -.00412371	.00521515	.0190421	.0113633	e	1.175617			
	Y -.0703692	-.0307283	-.0466325	.0840856	s	6.641626836			

LOADCASE: SHEAR 4e8

CRYSTAL	D I S P L A C E M E N T O N E A C H C O R N E R				RESULTS	
	1	2	3	4		
1	X	-.419457	-.40803	-.469504	.483087	E 1.46253
	Y	-.0211833	.03403345	.0440503	-.019482	S 5.778067606
2	X	-.680939	-.650564	-.71453	-.0754884	E .658961
	Y	-.0165342	.0145612	.0445977	.0192547	S 17.19942504
3	X	-.419457	-.40803	-.469504	-.483087	E 1.384218
	Y	-.0211833	.0340345	.0440503	-.019482	S 3.48383584
4	X	-.282051	-.229296	-.237399	-.293023	E .945321
	Y	-.0448982	-.0262031	-.00311269	-.0164397	S 1.23104
5	X	-1.19164	-1.13849	-1.25043	-1.32105	E 1.1443
	Y	-.0289348	.0254821	.078046	.0336957	S 9.29754
6	X	-1.36188	-1.30113	-1.42906	1.50977	E .887633
	Y	-.0330684	-.0291224	.0891953	.0385094	S 1.38813
7	X	-3.4047e-5	-3.25282e-5	-1.60769	-3.77442e-5	E 1.05819
	Y	-8.26709e-7	7.28061e-7	.100345	9.62734e-7	S 8.8207
8	X	-1.53211	-1.44592	-3.57265e-5	-1.69849	E 1.19708
	Y	-.0372019	.0327627	2.22989e-6	.043323	S 4.54294
9	X	-.102141	-.0975846	-1.0718	-1.13233	E 1.11987
	Y	-.0248013	.0218418	.0668966	.028882	S 2.9918

LOADCASE: COMBINATION OF COMPRESSION AND SHEAR.

CRYSTAL	D I S P L A C E M E N T O N E A C H C O R N E R				RESULTS
	1	2	3	4	
1	X -.209729	-.204015	-.234752	-.241544	E 1.02808
	Y -.0105917	.0170172	.0220252	-.00974098	S 3.44087
2	X -.314593	-.306022	.0330377	-.362316	E .860276
	Y -.0158875	.0255259	-.352128	-.0146115	S 10.8405
3	X -.419457	-.40803	-.469504	.483087	E 1.19328
	Y -.0211833	.03403345	.0440503	-.019482	S .96308
4	X -.524322	-.510037	-.58688	-.603859	E .905133
	Y -.0264792	.0425431	.0550629	-.0243525	S 2.08991
5	X -.350612	-.371578	-.447069	-.423311	E .97120
	Y -.00259167	.0361442	.0277523	-.0244921	S 3.00903
6	X -.40947	-.433508	-.521581	-.493862	E .957956
	Y -.0035348	.042497	.0323777	-.0285741	S 1.06284
7	X -.838915	-.816059	-.939008	-.966175	E .892422
	Y -.0423667	.0680689	.0881006	-.0389639	S 8.3786
8	X -1.16871e-5	-1.23859e-5	-1.49023e-5	-1.41104e-5	E 1.00356
	Y -8.63891e-8	1.17856e-6	9.25077e-7	-8.16404e-7	S 2.21453
9	X -.943779	-.918067	.0991132	-1.08695	E 1.10235
	Y -.0476625	.0765776	-1.05638	-.0438344	S 9.0356